Scuola Internazionale Superiore di Studi Avanzati - Trieste

Area of Physics
Ph.D. in Theoretical Particle Physics

Phenomenology of dark matter at present and future experiments

Advisor: Candidate:

Prof. G. Villadoro   **G. Grilli di Cortona**

Thesis submitted in partial fulfilment of the requirements
for the degree of Doctor Philosophiae

Academic Year 2015/2016

SISSA - Via Bonomea 265 - 34136 TRIESTE - ITALY

Acknowledgements

Preface

In this thesis we present a study of two different dark matter candidates. We focus on the neutralino in split supersymmetric models and in models of Dirac gauginos, and on the QCD axion.

In the first part of the thesis we discuss supersymmetric searches at future hadron colliders and dark matter direct detection experiments. We obtain mass reach for several simplified models in split supersymmetry with neutralino or gravitino lightest supersymmetric particle at 14, 33 and 100 TeV collider. In particular, a supersymmetric simplified model of anomaly mediation with long lived Winos has crucial importance in the hunt for dark matter since a Wino lightest supersymmetric particle is expected to thermally saturate the relic density for $m_{\tilde{W}} \sim 3$ TeV. In addition, we consider the discovery reach of a future 100 TeV collider for strongly coupled states in supersymmetric theories with Majorana gluinos, and extend this to the cases with Dirac gluinos.

Furthermore, we discuss the current bounds and future reach from dark matter direct detection experiments for split SUSY models with universal gaugino masses and models of anomaly mediation. We then study the interplay between the collider and dark matter searches for the models considered. Also, we consider the dark matter candidate in Dirac gaugino models and the relation between collider searches and dark matter direct detection experiments.

In the second part of this thesis, we study the properties of the QCD axion at zero and finite temperature. The computation of the relic abundance for QCD axion from the misalignment mechanism dramatically depends on the behaviour of the axion potential at finite temperature. Consequently, we compute the axion potential, and therefore its mass, at temperatures below the crossover ($T_c \sim 170$ MeV) exploiting chiral Lagrangians. Around the critical temperature T_c there is no known reliable perturbative expansion under control and non-perturbative methods, such as lattice QCD, are required. At higher temperatures, when QCD becomes perturbative, the dilute instanton gas approximation is available, which is expected to be reliable at temperatures large enough. We point out however that the bad convergence of the perturbative QCD expansion at finite temperatures makes the instanton result unreliable for temperatures below 10^6 GeV. Therefore, we study the impact of the uncertainty in the computation of the axion relic abundance, providing updated plots for the allowed axion parameter space.

Finally, motivated by the fact that zero temperature properties of the QCD axion are fundamental in case of axion discovery in order to infer its possible UV completion, we perform a NLO computation using chiral Lagrangians. We extract zero temperature axion properties, such as the mass, the potential, the self-coupling, the coupling to photon and the tension of domain walls, at the percent level. Moreover, we show a new strategy to extract couplings to nucleons directly from first principle QCD at the 10% level. Such result can be improved as more lattice QCD simulations become available.

The original results obtained in this thesis have been published in the following series of papers [1–4]:

- G. Grilli di Cortona, "*Hunting electroweakinos at future hadron colliders and direct detection experiments*", **JHEP 05 (2015) 035**, arXiv:1412.5952 [hep-ph], chapters 2-3,

- G. Grilli di Cortona, "*Searching SUSY from below*", PoS **PLANCK2015** (2015), arXiv:1510.07616 [hep-ph], chapters 2-3,

- G. Grilli di Cortona, E. Hardy, J. Pardo Vega, and G. Villadoro, "*The QCD axion, precisely*", **JHEP 01 (2016) 034**, arXiv:1511.02867 [hep-ph], chapters 5-6,

- G. Grilli di Cortona, E. Hardy, A. Powell, "*Dirac vs Majorana gauginos at a 100 TeV collider*", **JHEP 08 (2016) 014**, arXiv:1606.07090 [hep-ph], chapters 2-3.

Contents

CONTENTS

Part I

SUSY searches at future colliders and DM experiments

Chapter 1

Introduction and motivations

The Higgs boson, the last missing piece of the Standard Model (SM) [5–7], was discovered at the Large Hadron Collider (LHC) by the ATLAS and the CMS experiments [8, 9], rewarding decades of intense experimental and theoretical work. The Higgs boson was predicted long ago [10–12], arising as the consequence of a mechanism able to provide masses to all the SM fields (but neutrinos). Tests of the SM were performed initially at tree level, but the extraordinary agreement between the SM predictions and the precision measurements at LEP has established the remarkable importance of the radiative corrections for the agreement with data. The SM is therefore a robust framework that describes and predicts a huge number of physical phenomena over an energy range of several order of magnitude.

The SM is nevertheless an incomplete theory. Both experimental arguments - such as the existence of neutrino oscillations, the presence, dark matter and the baryon asymmetry in the universe - and theoretical considerations - such as the naturalness problem of the Higgs mass, the strong CP problem and the presence of gravity - suggest the existence of physics beyond the SM.

All these arguments point in the direction of physics beyond the SM, and some of them do give a hint on the value of the new physics (NP) scale. In particular, the naturalness problem for the Higgs mass suggests that there should be NP at a scale of $\mathcal{O}(\text{TeV})$. Furthermore, the presence of dark matter point to the same mass scale if interpreted in the framework of the weakly interacting massive particle (WIMP) paradigm. In the following I will review shortly how the TeV scale arise as the NP scale, and what are possible solutions to (some of) the previously mentioned problems.

1. Introduction and motivations

The hierarchy problem

The ratio of the strength of the weak and the gravitational force is

$$\frac{G_F h^2}{G_N c^2} = 1.73859(15) \times 10^{33},$$ (1.1)

that, translated in terms of energy scales, drives the question of why the ratio between the Planck scale M_{Pl} and the electroweak scale v is so huge. [1]

The electroweak scale v can be traded for the Higgs mass parameter m_h, the parameter that enters in the scalar potential. Indeed, the potential of the scalar neutral Higgs boson in the SM contains

$$V \supset -m_h^2 |h|^2 + \lambda |h|^4,$$ (1.2)

where h is the neutral Higgs complex scalar. If $\lambda > 0$ and $m_h^2 > 0$, at the minimum of the potential, the Higgs field acquires a vacuum expectation value (VEV)

$$\langle h \rangle = v/\sqrt{2} = \sqrt{m_h^2/2\lambda}.$$ (1.3)

Experimentally, from measurement of the properties of the weak interactions, $v \sim 246$ GeV and therefore m_h^2 must be of order $(100 \text{ GeV})^2$ for a *natural* value of $\lambda \sim 0.1$. However, the Higgs mass receives quantum corrections from all the virtual particles that couples directly or indirectly with it. These give rise to quadratic corrections

$$\delta m_h^2 \sim \frac{3|\lambda_f|^2}{16\pi^2} m_f^2 \log\left(\frac{\Lambda^2}{m_f^2}\right),$$ (1.4)

where the mass scale Λ is the scale at which the SM ceases to be valid and m_f is the mass of the fermion that runs in the loop. The coefficient λ_f represent the coupling of the Higgs with the fermion, e.g. a lepton or a quark (in this case δm_h^2 should be multiplied by a factor 3 to account for the colour), running in the loop. The Higgs mass is therefore highly sensitive to the states with the largest factor $|\lambda_f|^2 m_f^2$. In the SM, the largest contribution comes from the top quark Yukawa that is $\mathcal{O}(1)$.

If we suppose that the SM is valid at any scale, the hierarchy problem would cease to exist, because the SM is a renormalisable theory and all quadratic corrections can be reabsorbed by unphysical counterterms, in this case the bare Higgs mass. However, the SM is not an ultra-violet (UV) complete theory, because the hypercharge and Higgs quartic coupling become non-perturbative at scales $\mathcal{O}(10^{41} \text{ GeV})$, producing a new mass threshold. A new mass threshold Λ is also motivated, for example, by the existence of

---

[1]For a review on the naturalness problem, see [13].

4

gravity, that may involve some NP around the Planck scale[1], or by the fact that, assuming the WIMP paradigm, the SM requires new states around the TeV to reproduce the dark matter abundance. Moreover, Majorana neutrino masses and unification of the gauge couplings seem to point to new dynamics at scales of order $\sim 10^{14-16}$ GeV.

In order to get a light Higgs mass in a theory where a large scale Λ is present, one has to fine tune the tree level and the quantum corrections. Consider the following toy model [14] with a light scalar ϕ and a heavy fermion ψ:

$$\mathcal{L} = \frac{1}{2}(\partial\phi)^2 - \frac{1}{2}m^2\phi^2 + \bar{\psi}(i\slashed{\partial} - M)\psi - g\phi\bar{\psi}\psi, \tag{1.5}$$

with $m \ll M$. The process can be described at energies $E \ll M$ with an effective theory where the fermion has been integrated out. The physical mass of the light scalar field can be computed in the $\overline{MS}$ scheme, and we obtain

$$m_{\text{phys}}^2 = m^2(\mu) - \frac{4g^2}{16\pi^2}\left(5M^2 + \frac{4}{3}m^2(\mu)\right) + \frac{1}{2}(m^2(\mu) - 6M^2)\log\frac{M^2}{\mu^2}, \tag{1.6}$$

where μ is the renormalisation scale. Choosing $\mu = M$, the mass of the light scalar simplifies leading to

$$m_{\text{phys}}^2 = m^2(M) - \frac{4g^2}{16\pi^2}\left(5M^2 + \frac{4}{3}m^2(M)\right), \tag{1.7}$$

showing that m_{phys}^2 is sensible to the largest parameter in the lagrangian, making the theory unstable. Therefore, if we want the ligh scalar sensibly lighter than the scale M, we must have an extremely small renormalised coupling g in order to have a cancellation between the two terms of the right hand side of equation (1.7). While it is not logically impossible to have such a fantastic cancellation, this is usually thought as the origin of a deeper problem.

The *naturalness* criterion, proposed by 't Hooft [15], states that *natural* parameters are allowed to be much smaller than unity only if a symmetry is restored when such a parameter is set to zero. Therefore, parameters that are zero because of symmetries, will remain zero even after the inclusion of quantum corrections, meaning that small parameters are not a problem if they are protected by symmetries. In the SM, Yukawa interactions are natural because setting them to zero, the SM obtains a chiral symmetry.

---

[1]Were the SM valid up to the Planck scale, the natural ratio of G_F/G_N would be 1, contradicting the experimental value, Eq. (1.1).

1. Introduction and motivations

On the contrary, the Higgs mass is not natural because setting m_h to zero would not restore any symmetry.[1]

On the other hand, if the coefficient g^2 takes the *natural* value of 10^{-2}, we can extrapolate the scale at which new effects start to modify the Higgs mass, finding $\Lambda \sim \mathcal{O}(\text{TeV})$. In this second scenario, the maximum energy up to which the SM can be extrapolated is therefore $\sim$ TeV. New dynamics should appear at this energy scale and these new particles should cancel the quantum corrections to the Higgs mass.[2] The appearance of this scale is extremely exciting because it is precisely the range of energy that is currently probed by the LHC.

Dark matter and the WIMP paradigm

A second argument for the presence of new physics is the experimental evidence of the existence of dark matter [16]. Indeed, there are several observations indicating that most of the matter contained in our Universe is non-baryonic.

The first evidence of DM is due to Zwicky [17]. Measuring the proper motion of galaxies in the Coma cluster, he realised that the total mass of the cluster computed via the virial theorem was about 300 times larger than expected from their luminosity. Furthermore, one of the cleanest evidence for dark matter in the Universe comes from the rotation curves of stars in a galaxy [18–20]. Newton's law implies that the velocity of stars in a galaxy is

$$v(R) = \sqrt{\frac{G_N M(R)}{R}}, \qquad M(R) = 4\pi \int_0^R \rho(r)\, r^2\, dr, \qquad (1.8)$$

where R is the distance from the galactic centre, G_N is the gravitational constant, M is the mass of the system, and $\rho(r)$ is the mass density. Given that the contribution of luminous matter would lead to $v(r) \propto R^{-1/2}$ in the limit of large R, at large radii we would expect a fall down of the velocity curve. However observations show that $v(R) \simeq$ const., therefore requiring a dark halo of mass density $\rho(r) \propto 1/r^2$.

The Planck collaboration measured the angular power spectrum of thermal anisotropies in the cosmic microwave background (CMB) to extract informations about the parameters of the early Universe. The dark matter abundance, expressed in terms of the critical

---

[1]Another example of unnaturally small parameter is the θ_{QCD} angle, that we will discuss in the second part of this thesis.

[2]Unfortunately, the hierarchy problem is not completely solved because now there is a tuning to have the NP scale close to the electroweak one.

energy density, from the Planck collaboration is [21]

$$\Omega_{\mathrm{DM}} h^2 = 0.1198 \pm 0.0015. \tag{1.9}$$

An independent argument in favour of the presence of dark matter in the Universe comes from the structure of the matter distribution at large scales. The formation of structures crucially depends on the nature of the dark matter. For dark matter particles that are relativistic at the matter-radiation equality temperature $T_{eq} \sim 1$ eV, dubbed as hot dark matter (HDM), only very large structures can form, and structures as we see them now form with a top-down approach by fragmentation of the larger objects. Observations of the distribution of galaxies strongly disfavour this paradigm. On the other hand, if dark matter particles are non relativistic at T_{eq}, called cold dark matter (CDM), small objects merge into larger ones, first forming galaxy halos and then larger structures. The intermediate case of warm dark matter, where the length scale of structure formation is formed by the inverse of the mass scale of the dark matter particle below which structures are suppressed, is a disfavoured but still viable scenario.

Some of the evidences for dark matter may be explained by models of modified gravity. However, the lack of a fully consistent theory alternative to general relativity and the huge range of scales of the dark matter evidences disfavour these models. Therefore an important problem is to understand the possible particle physics nature of the dark matter. From all the cosmological and astrophysical observations, it is possible to derive some of its properties. A suitable candidate must have the cosmological abundance of Eq. (1.9), must not be a baryon and must be electrically and colour neutral, because strong and electromagnetic interaction would lead to the formation of anomalously heavy isotopes, while limits on the abundance of nuclear isotopes suggest that a dark matter candidate should be weakly interacting with matter for a wide range of masses.

The only possible candidate in the SM is the neutrino. However, cosmological observations restrict the HDM relic density for neutrinos to be only a fraction of the one required by Eq. (1.9). It is therefore evident that the existence of dark matter requires physics beyond the SM.

The origin of species in the early universe can be successfully explained within the thermal decoupling paradigm (see e.g [22–24]). The evolution of a stable thermal relic DM particle is shown in Figure 1.1. At early times (high temperature), the relevant particle interaction rate Γ is much larger than the Hubble expansion rate H and the dark matter is in equilibrium with the plasma. As the Universe expands, its temperature decreases and at temperatures below the dark matter mass, its number density become Boltzmann suppressed. However, in addition to cooling, the Universe is also expanding and when $\Gamma \sim H$, the dark matter particles are so dilute that they cannot annihilate

1. Introduction and motivations
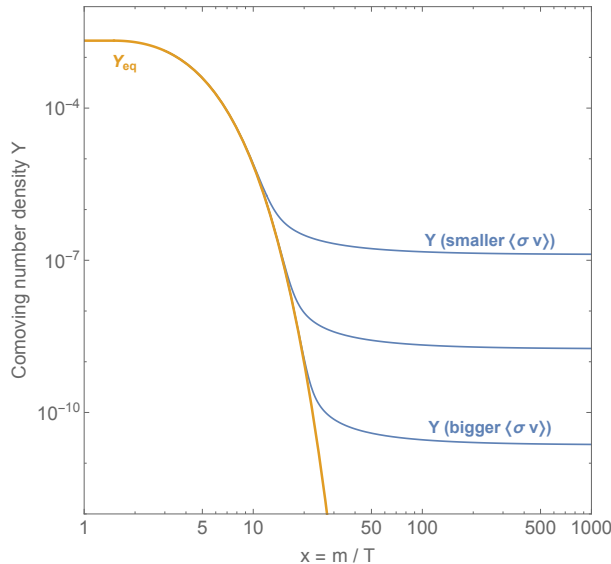
Figure 1.1: The evolution of the DM number density per comoving volume $Y = n_\chi/s$, where s is the entropy.

anymore. At this point the dark matter decouples from the plasma, and its number density become constant (freeze out).

In particular, consider a non relativistic dark matter particle χ, with mass m_χ. Such particle is in equilibrium at temperature $T \gg m_\chi$ by the annihilation processes

$$\chi\,\chi \longleftrightarrow \phi_{\rm SM}\,\phi_{\rm SM}, \tag{1.10}$$

where $\phi_{\rm SM}$ is any Standard Model field. The evolution of the number density of the dark matter particle n_χ is given by the Boltzmann equation

$$\frac{dn_\chi}{dt} + 3Hn_\chi = -\langle\sigma v\rangle \left[n_\chi^2 - (n_\chi^{\rm eq})^2\right], \tag{1.11}$$

where $\langle\sigma v\rangle$ is the zero temperature thermally averaged DM annihilation cross section times velocity, and $n_\chi^{\rm eq}$ is the equilibrium number density of the DM. The dark matter annihilation rate $\Gamma = n_\chi\langle\sigma v\rangle$ is able to keep the dark matter in equilibrium at temperatures for which it is larger than the Hubble expansion. The expansion of the Universe decreases the DM number density, reducing its annihilation rate until is smaller than the Hubble parameter. The process (1.10) can no longer maintain the chemical equilibrium and the dark matter particles decouple from the thermal bath. The freeze out occurs at a temperature $T_{\rm fo}$ given by

$$\Gamma(T_{\rm fo}) = n_\chi(T_{\rm fo})\langle\sigma v\rangle \sim H(T_{\rm fo}), \tag{1.12}$$

8

that, given the Friedmann equations in a radiation dominated era $H \simeq T^2/M_{\mathrm{Pl}}$, yields

$$n_\chi^{\mathrm{fo}} \sim \frac{T_{\mathrm{fo}}^2}{M_{\mathrm{Pl}}\langle\sigma v\rangle}. \tag{1.13}$$

The relic abundance is given by the current dark matter density in terms of the critical density

$$\Omega_\chi = \frac{m_\chi n_\chi^0}{\rho_c}. \tag{1.14}$$

For an isoentropic Universe $R\,T \simeq \mathrm{const}$[1] we have $n_\chi^0/T_0^3 \simeq n_\chi^{\mathrm{fo}}/T_{\mathrm{fo}}^3$, where T_0 denotes the temperature of the universe today, and therefore

$$\Omega_\chi \sim \frac{m_\chi T_0^3}{\rho_{\mathrm{cr}}} \frac{n_\chi^{\mathrm{fo}}}{T_{\mathrm{fo}}^3} \sim \left(\frac{T_0^3}{\rho_c M_{\mathrm{Pl}}}\right) \frac{x_{\mathrm{fo}}}{\langle\sigma v\rangle} \sim 0.2 \frac{x_{\mathrm{fo}}}{20} \left(\frac{3 \times 10^{-26}\,\mathrm{cm}^3/\mathrm{s}}{\langle\sigma v\rangle}\right), \tag{1.15}$$

where $x_{\mathrm{fo}} = m_\chi/T_{\mathrm{fo}} \sim 20$. The equilibrium number density in the non relativistic limit is

$$n \sim (m_\chi T)^{3/2} e^{-m_\chi/T} = \frac{m_\chi^3}{x^{3/2}} e^{-x}. \tag{1.16}$$

Using the freeze out condition $\Gamma \sim H$ we have

$$\sqrt{x_{\mathrm{fo}}}\, e^{-x_{\mathrm{fo}}} = \frac{1}{m_\chi\, M_{\mathrm{Pl}}\, \langle\sigma v\rangle}, \tag{1.17}$$

and replacing the average cross section with the value of an electroweak interacting particle $\langle\sigma v\rangle \sim G_F^2 m_\chi^2$ of mass ~ 100 GeV, we get $x_{\mathrm{fo}} \sim 20$. In Eq. (1.15) notice that the relic abundance is inversely proportional to the annihilation cross section: the larger the annihilation cross section, the longer the dark matter remains coupled to the thermal bath, the equilibrium number density is reached later and the relic density is smaller (see Figure 1.1).

In order to derive (1.15) we used the condition for having a cold dark matter particle, $x_{\mathrm{fo}} \gg 1$[2], and a cross section $\langle\sigma v\rangle = 3 \times 10^{-26}\,\mathrm{cm}^3/\mathrm{s}$. This value is however not peculiar only of the electroweak scale: parametrising the cross section as $\sigma \sim g^4/m_\chi^2$, the two previously mentioned conditions imply that $m_\chi \gg 0.1$ eV. Further, an upper limit can be derived by considering a unitary limit in the partial wave expansion [25], which implies $m_\chi \lesssim 200$ TeV. Although the value of the cross section obtained to get the correct relic density is not specific of the electroweak scale, it points to dark matter masses of order $\sim$ TeV for particles with electroweak couplings.

---

[1]We denote the scale factor with R.
[2]This condition become $m_\chi\langle\sigma v\rangle M_{\mathrm{Pl}} \gg 1$, see Eq. (1.17).

1. Introduction and motivations

It is important to notice that there are three exceptions where the computation of the relic density previously outlined is modified [26]. If another particle lies near in mass to the DM, it must be included in the DM computation because its annihilation can control the relic density. The freeze out of the DM particle and the one of the close states are interconnected if the difference between the two masses is smaller than the freeze out temperature, $m_\chi - m_1 \lesssim T_{\rm fo}$. In this case the relevant cross section $\langle \sigma v \rangle$ is not the DM annihilation cross section, but it is an effective cross section that includes the contribution from the coannihilating particles. Considering N coannihilating particles, the average cross section is modified as

$$\langle \sigma v \rangle \longrightarrow \langle \sigma_{\rm eff} v \rangle = \frac{\sum_{i,j=1}^{N} \sigma_{ij} \exp\left(-\frac{\Delta m_i + \Delta m_j}{T}\right)}{\sum_{i=1}^{N} g_i \exp\left(-\frac{\Delta m_i}{T}\right)}, \tag{1.18}$$

where σ_{ij} is the annihilation between the particle i and j, $\Delta m_i = m_i - m_1$ (m_1 denotes the DM particle) and g_i is the coupling of the particle i (see for example [27, 28]). A second situation occurs when the DM mass is slightly below a mass threshold. Thermal fluctuations may open the kinematically forbidden channel that can dominate the cross section and be important in the determination of the relic density. The last exception occurs if the DM annihilation takes place near a pole in the cross section: the cross section shows a peak near the pole and therefore the relic abundance is suppressed.

The two previously discussed issues of the SM point to the TeV scale as the energy where NP should arise. The naturalness problem for the Higgs can be solved, for example, if its mass breaks some symmetry, so that it is protected from radiative corrections. For example, supersymmetric models [29–32] introduce a new symmetry that relates bosons with fermions, and can solve the hierarchy problem [33]. The Higgs gets a VEV only once SUSY is broken and its quantum corrections are proportional to the SUSY breaking soft terms $\tilde{m}$. As further motivation, supersymmetric models have a viable dark matter candidate and the gauge couplings successfully unify. In the following section the Minimal Supersymmetric Standard Model (MSSM) is reviewed [34].

1.1 The minimal supersymmetric Standard Model

As we have already anticipated, supersymmetry challenges the hierarchy problem through the introduction of new states leading to the cancelation of the quadratic divergencies to the Higgs mass. Consider the existence in the theory of a heavy complex scalar field S

with a mass m_S, that couples to the Higgs via the Lagrangian term $-\lambda_S |h|^2 |S|^2$. Then, the one loop contribution to the Higgs mass with the scalar in the loop gives a correction

$$\delta m_h^2 \sim -\frac{\lambda_S}{16\pi^2} m_S^2 \log(\Lambda^2/m_S^2). \tag{1.19}$$

The cancellation between (1.4) and (1.19) can happen only because of the relative minus sign between fermions and scalars loop. Therefore, the cancellation is possible if every quark and leptons of the SM have two complex scalar superpartner such that $\lambda_S \simeq |\lambda_f|^2$ and $m_S^2 \simeq m_f^2$. The existence of a symmetry that connects fermions and bosons (supersymmetry) leads to the cancellation of the loop contributions to scalar masses, and therefore solve the hierarchy problem.

1.1.1 Structure of the MSSM

States of a SUSY theory belong to superfields, the irreducible representations of the SUSY algebra[1]. Particles in the same superfield must have the same electric charge, weak isospin and colour degrees of freedom. Moreover, a superfield contains both bosons and fermions, that are related to each other by SUSY transformations.

The particle content of the MSSM consists of a superfield associated with each field of the SM. Therefore, the gauge bosons and the fermions of the SM are promoted to gauge and chiral superfields respectively, with gauge quantum numbers exactly as in the SM, while the Higgs sector consists of two Higgs doublets with opposite hypercharge. The model is partially described by the superpotential written as a function of the superfields corresponding to the $SU(2)$ singlet and doublet leptons $(\hat{e}, \hat{l})$, quarks $(\hat{u}, \hat{d}, \hat{q})$ and to the two Higgs doublets $\hat{h}_u$, $\hat{h}_d$ of table 1.1

$$W_{\text{MSSM}} = \lambda_{ij}^u \hat{u}_i^c \hat{q}_j \hat{h}_u + \lambda_{ij}^d \hat{d}_i^c \hat{q}_j \hat{h}_d + \lambda_{ij}^e \hat{e}_i^c \hat{l}_j \hat{h}_d + \mu \hat{h}_u \hat{h}_d, \tag{1.20}$$

where $\lambda^{u,d,e}$ are the dimensionless Yukawa couplings and $i, j = 1, 2, 3$ are family indices (colour indices are neglected). In this notation hatted quantities denote superfields.

Additional renormalisable terms, which violate lepton L or baryon B number and would lead to fast proton decay, are allowed by gauge invariance

$$
\begin{aligned}
W_{\Delta L=1} &= \frac{1}{2} \lambda_0^{ijk} \, \hat{l}_i \, \hat{l}_j \, \hat{e}_k^c + \lambda_1^{ijk} \hat{l}_i \, \hat{q}_j \, \hat{d}_k^c + \mu_0^i \hat{l}_i \, \hat{h}_u \\
W_{\Delta B=1} &= \frac{1}{2} \lambda_2^{ijk} \, \hat{u}_i^c \, \hat{d}_j^c \, \hat{d}_k^c.
\end{aligned}
\tag{1.21}
$$

---

[1]Several reviews and textbook of SUSY exist, see for example [34–39].

Superfields	fermions	scalars	$(SU(3)_C,\ SU(2)_L,\ U(1)_Y)$
$\hat{q}_i$	$(u_i\ d_i)$	$(\tilde{u}_i\ \tilde{d}_i)$	$(\mathbf{3},\ \mathbf{2},\ \mathbf{1/6})$
$\hat{u}_i^c$	u_i^c	$\tilde{u}_i^c$	$(\bar{\mathbf{3}},\ \mathbf{1},\ \mathbf{-2/3})$
$\hat{d}_i$	d_i^c	$\tilde{d}_i^c$	$(\bar{\mathbf{3}},\ \mathbf{1},\ \mathbf{1/3})$
$\hat{l}_i$	$(\nu_i\ e_{Li})$	$(\tilde{\nu}_i\ \tilde{e}_{Li})$	$(\mathbf{1},\ \mathbf{2},\ \mathbf{-1/2})$
$\hat{e}_i^c$	$e_{Ri}^\dagger$	$\tilde{e}_{Ri}^*$	$(\mathbf{1},\ \mathbf{1},\ \mathbf{1})$
$\hat{h}_d$	$(\tilde{h}_d^0\ \tilde{h}_d^-)$	$(h_d^0\ h_d^-)$	$(\mathbf{1},\ \mathbf{2},\ \mathbf{-1/2})$
$\hat{h}_u$	$(\tilde{h}_u^+\ \tilde{h}_u^0)$	$(h_u^+\ h_u^0)$	$(\mathbf{1},\ \mathbf{2},\ \mathbf{1/2})$
$\hat{g}^{X=1,...,8}$	$\tilde{g}^X$	g_μ^X	$(\mathbf{8},\ \mathbf{1},\ \mathbf{0})$
$\hat{W}^{A=1,2,3}$	$\tilde{w}^A$	W_μ^A	$\mathbf{1},\ \mathbf{3},\ \mathbf{0})$
$\hat{B}$	$\tilde{b}$	B_μ	$(\mathbf{1},\ \mathbf{1},\ \mathbf{0})$

Table 1.1: The MSSM particle content.

These dangerous terms are forbidden in the MSSM by the presence of a new symmetry, called R-parity or matter parity. R-parity acts as a multiplicative quantum number defined as

$$P_R = (-1)^{3(B-L)+2s}, \tag{1.22}$$

where s denotes the spin of the particle. All the SM particles and the Higgs feature R-parity $R_P = 1$, while all the supersymmetric partners have $R_P = -1$. The presence of R-parity forbids the terms in Eq. (1.21) and leads to a stable lightest supersymmetric particle (LSP), because sparticles can only decay to an odd number of supersymmetric particles. A stable LSP could therefore be a good dark matter candidate if it is also weakly interacting, and electrically and colour neutral.

Since exact supersymmetry would mean that every superparticle is degenerate in mass with its SM partner, the absence of any evidence of supersymmetry suggests that SUSY must be broken. Moreover, a theoretically appealing supersymmetric model should break supersymmetry spontaneously and analogously to the SM electroweak symmetry breaking, we expect a SUSY invariant Lagrangian, but a vacuum state that is not. Several possible solutions for the mechanism of spontaneous supersymmetry breaking have been proposed [40–65]. It is however possible to hide our ignorance of this mechanism introducing terms that break SUSY explicitly [66]. The breaking must be soft, namely of positive mass dimension, in order to maintain natural the hierarchy between the electroweak and the Planck scale. Therefore, the most general MSSM Lagrangian includes all

possible renormalisable terms which do not introduce quadratic divergence at all order in perturbation theory

$$
\begin{aligned}
\mathcal{L} \supset \ & - \ \frac{1}{2} \left(M_3 \tilde{g}\tilde{g} + M_2 \tilde{W}\tilde{W} + M_1 \tilde{B}\tilde{B} + \text{h.c.} \right) \\
& - \ \left(A^u_{ij} \tilde{u}^c_i \tilde{q}_j h_u + A^d_{ij} \tilde{d}^c_i \tilde{q}_j h_d + A^e_{ij} \tilde{e}^c_i \tilde{l}_j h_d + \text{h.c.} \right) \\
& - \ (B_\mu h_u h_d + \text{h.c.}) - m^2_{h_u} h^\dagger_u h_u - m^2_{h_d} h^\dagger_d h_d \\
& - \ (m^2_{\tilde{q}})_{ij} \tilde{q}^\dagger_i \tilde{q}_j - (m^2_{\tilde{d}})_{ij} \tilde{d}^{c\dagger}_i \tilde{d}_j - (m^2_{\tilde{u}})_{ij} \tilde{u}^{c\dagger}_i \tilde{u}_j - (m^2_{\tilde{l}})_{ij} \tilde{l}^\dagger_i \tilde{l}_j - (m^2_{\tilde{e}})_{ij} \tilde{e}^{c\dagger}_i \tilde{e}_j, \quad (1.23)
\end{aligned}
$$

where the first line correspond to the soft breaking masses for the gluino, the Wino and the Bino respectively, the second to the soft trilinear scalar interactions, the third to the soft bilinear scalar interaction and the soft scalar masses for the Higgs, while the last one to the scalar mass squares of squarks and sleptons.

The supersymmetric spectrum can be computed from the various terms of the soft Lagrangian and of the superpotential. In particular, the composition of the neutralinos in terms of their interaction eigenstates is very important in the context of dark matter studies. The neutralino mass matrix in the basis $(\tilde{B}, \tilde{W}, \tilde{h}^0_d, \tilde{h}^0_u)$ is given by

$$
M_{\tilde{\chi}^0} = \begin{pmatrix}
M_1 & 0 & -g_1 v_d/\sqrt{2} & g_1 v_u/\sqrt{2} \\
0 & M_2 & g_2 v_d/\sqrt{2} & -g_2 v_u/\sqrt{2} \\
-g_1 v_d/\sqrt{2} & g_2 v_d/\sqrt{2} & 0 & -\mu \\
g_1 v_u/\sqrt{2} & -g_2 v_d/\sqrt{2} & -\mu & 0
\end{pmatrix}, \quad (1.24)
$$

where $v_{u,d}$ are the vacuum expectation values of the $H_{u,d}$ Higgs doublets and $g_{1,2}$ are the SM gauge couplings. Diagonalising the neutralino mass matrix, the four neutralinos eigenstates can be expressed as

$$
\tilde{\chi}^0_i = N_{1i}\tilde{B} + N_{2i}\tilde{W} + N_{3i}\tilde{h}_d + N_{4i}\tilde{h}_u, \quad (1.25)
$$

where $i = 1, ..., 4$ and $m_{\chi^0_1} < ... < m_{\chi^0_4}$, providing the Bino $|N_{1i}|$, Wino $|N_{2i}|$ and higgsino $\sqrt{|N_{3i}|^2 + |N_{4i}|^2}$ fraction of each neutralino. Neutralinos get a Majorana mass and the lightest one $\tilde{\chi}^0_1$ is a suitable dark matter candidate, provided it is the lightest supersymmetric particle at low energies.

A second success of supersymmetric models compared to the SM is the prediction of gauge coupling unification. At 1-loop, the renormalisation group (RG) equations for the SM gauge couplings g_1, g_2 and g_3 are

$$
\beta_i \equiv \frac{d}{dt} g_i = \frac{1}{16\pi^2} b_i g_i^3, \quad (1.26)
$$
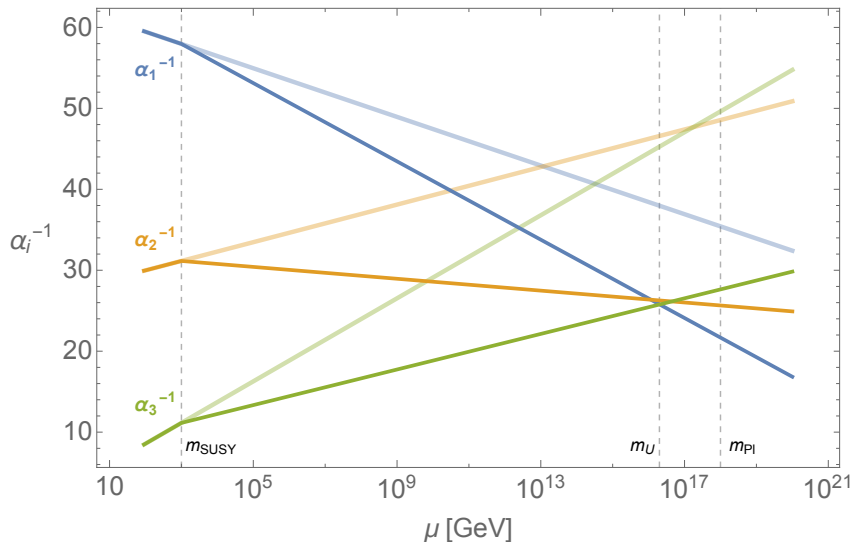
Figure 1.2: RG evolution of the inverse of the gauge couplings $\alpha_i^{-1}(\mu)$ in the Standard Model (light colours) and in the MSSM (darker colour). In the MSSM the sparticle masses are degenerate at $m_{SUSY} \sim 1$ TeV.

where $t = \log(\mu/\mu_0)$, with μ the RG scale, and $b_i = (41/10, -19/6, -7)$ for the SM or $b_i = (33/5, 1, -3)$ for the MSSM. The extra particles in the loop make the MSSM b_i larger than the SM ones. Furthermore, the normalisation of the couplings is chosen as $g_2 = g$ and $g_1 = \sqrt{5/3}g'$. Figure 1.2 compares the evolution of α_i^{-1} in the SM (lighter colours) and in the MSSM, with a SUSY mass scale of $\mathcal{O}(\text{TeV})$. Supersymmetry improves the precision of the unification with respect to the SM, and it pushes the unification scale to higher energies, avoiding the proton decay problem of non-SUSY grand unified theories [67]. However, as the SUSY scale is taken heavier, the precision of the unification becomes worse. Actually, only part of the spectrum has to be near the weak scale in order to improve unification. Indeed, in Split Supersymmetric models [68–70], where the scalar superpartners are heavy and only the supersymmetric fermions are at the weak scale, similar precision is achieved. This is possible because the heavy squarks and sleptons are in complete $SU(5)$ multiplets and do not contribute to the running up to the SUSY scale.

However, supersymmetry has been challenged by the LHC experimental data [72, 73]. The highest mass reach at the LHC has been achieved for strongly interacting particles, such as gluinos and squarks [71]. ATLAS limits on a squark-gluino simplified model, assuming the decays $\tilde{g} \to q\bar{q}\tilde{\chi}$ and $\tilde{q} \to q\tilde{\chi}$, for the first LHC run are shown in Figure 1.3. These results imply that squarks must be heavier than ~ 1.5 TeV for decoupled gluinos, gluinos must be heavier than ~ 1.3 TeV for decoupled squarks, and squarks and
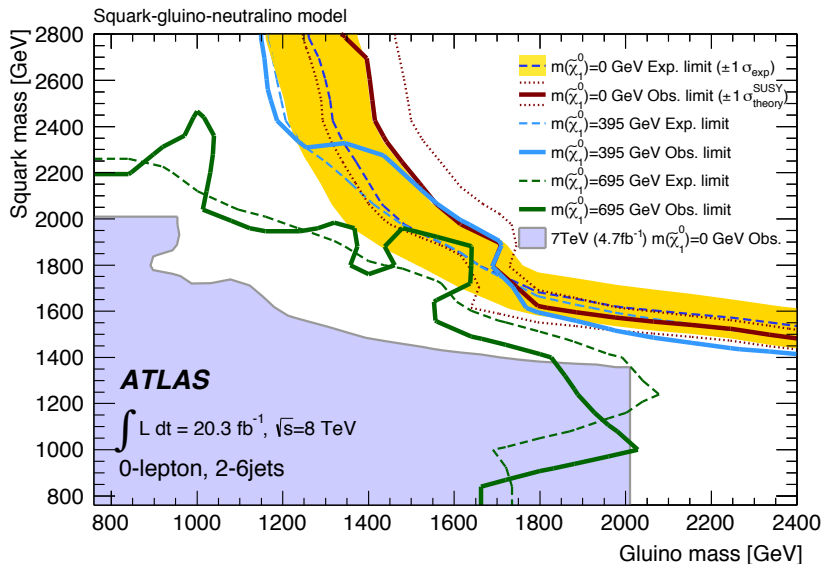
Figure 1.3: Exclusion limits on first and second generation squark and gluino production, with a lightest neutralino mass of 0 GeV (red solid curve), 395 GeV (light blue curve), or 695 GeV (green curve). The Figure is taken from [71].

gluinos must be larger than ~ 1.7 TeV in the degenerate case. This limits are valid for massless neutralino LSP, while increasing the neutralino mass the bounds become weaker. The rest of the supersymmetric spectrum is assumed to be heavy and decoupled. On the other hand, the reaches for uncoloured superpartners, such as neutralino, charginos and sleptons, is weaker [74]. In Figure 1.4 (left), for example, the expected and observed limits for pure Wino $\tilde{\chi}_1^+ \tilde{\chi}_1^-$ and $\tilde{\chi}_1^+ \tilde{\chi}_2^0$ production are shown. The stronger limits come from chargino neutralino associate production decaying into two or three leptons (and missing energy) via SM gauge bosons, bounding a pure Wino to be heavier than ~ 400 GeV for massless Bino LSP. Higgsino production leads to stronger limits than the Wino one if the decays to the final states are mediated by sleptons, as shown in Figure 1.4 (right). For instance, NLSP higgsinos decaying via sleptons, with $m_{\tilde{\chi}_1^0} < m_{\tilde{l}} < m_{\tilde{\chi}_{2,3}^0}$, are excluded up to ~ 700 GeV, a limit that is much weaker than the one for squarks or gluinos.

The existence of a SM-like Higgs with mass 125 GeV and the bounds from the first LHC runs at 7 and 8 TeV are an indirect hint for a small hierarchy between the electroweak and the supersymmetry restoration scale. At tree level, the Higgs mass is

$$m_h^2 \simeq -2(m_{H_u}^2 + |\mu|^2) + \mathcal{O}\left(\frac{1}{\tan\beta}\right), \qquad (1.27)$$
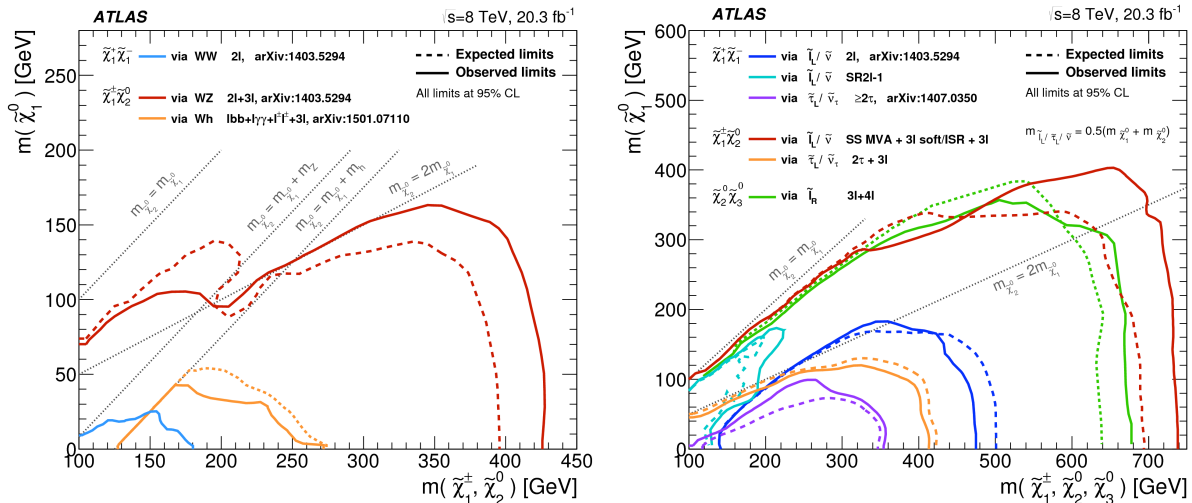
Figure 1.4: Exclusion limits on pure Wino $\tilde{\chi}_1^+ \tilde{\chi}_1^-$ and $\tilde{\chi}_1^+ \tilde{\chi}_2^0$ or pure higgsino $\tilde{\chi}_2^0 \tilde{\chi}_3^0$ production, with SM gauge bosons decays (left) or sleptons mediated decays (right). Figures are taken from [74].

where $\tan\beta$ is the ratio between the VEV of the two Higgs doublets, $\tan\beta = v_u/v_d$. Equation (1.27) implies that a higgsino heavier than the lightest Higgs would induce a tree level tuning. Furthermore, $m_{H_u}^2$ receives corrections from the one loop RG equation proportional to the stop mass

$$\partial_t m_{H_u}^2 = \frac{3|y_t|^2}{8\pi^2} \left(m_{\tilde{t}_L}^2 + m_{\tilde{t}_R}^2 + |A_t|^2 \right) + ...,$$ (1.28)

where $t = \log \mu/\mu_0$. Finally also the stop mass receives corrections from the RG proportional to the gluino mass

$$\partial_t m_{\tilde{t}}^2 = -\frac{8\alpha_s}{3\pi} M_3^2 + ...,$$ (1.29)

showing that the gluino and the stop are the dominant source of tuning. In a weak scale MSSM model with gauginos and first generation squarks above 2 TeV and light higgsinos, the lightest stop mass allowed are about 1.7 TeV, assuming maximal stop mixing [75]. If the A terms are small, large stop masses of about 10 TeV are needed. Such stop masses require some amount of tuning and show therefore a possible tension for SUSY as a natural solution of the hierarchy problem.

There are several ways to ease the tension between the experimental bounds on squarks and gluinos, and the need for light stops and gluinos [76]. One way is to have an LSP that is almost degenerate with the stop, such that the jet produced in the stop decay is soft and it may fail to be detected, or is not visible due to the large background for soft jets (see for

example the green curve of Figure 1.3). However, in this situation there are two unnatural scalars: Eq. (1.29) shows that the less tuned spectra feature $m_{\tilde{t}} \simeq M_3$. Since the largest contribution to the fine tuning comes from the gluino, we should relax its bounds. A possible way to weaken the LHC bounds on gluinos is to hide the collider signature via baryonicc R-parity violating (RPV) couplings. Furthermore, an effective way to keep the stops light is to have first and second generation squarks heavy and the third generation light (split family models). In this way, the constraints on the stops are weakened because the direct production cross section is suppressed by the parton distribution functions and the signal is typically hidden in the large SM background. Nonetheless, for both RPV models and split families, several ATLAS and LHC searches bound the gluino and the squarks to be around the TeV level [77–84], which translates to a few percent tuning.

Finally, it is possible to suppress the squark production cross section by having a Dirac gluino rather than a Majorana one. In this situation, squark pair production via t-channel gluino is suppressed [85]. We will analyse this last scenario further in this thesis.

1.1.2 Split SUSY

The recent discovery of a 125 GeV Higgs boson and the lack of discovery of new coloured states at the LHC raise serious doubts on the MSSM as a solution of the hierarchy problem. If the naturalness problem is not to be taken as a principle to build SUSY models, it is always possible to focus on its other advantages: the existence of a dark matter candidate and the gauge coupling unification.

This is the approach taken in the framework of split SUSY models [68–70]. These models abandon the idea of SUSY as a solution of the hierarchy problem and feature heavy scalars at a mass scale $\tilde{m}$, in the original model ranging from 100 TeV to m_{GUT}. However, the 125 GeV Higgs constrain the mass of the heavy scalars to be about 10^8 GeV for $\tan\beta = 1$ and around 10 TeV for large $\tan\beta$, see Figure 1.5. Such heavy scalars require fine tuning in the light Higgs mass. On the other hand, the higgsinos and the gauginos are light, about 1 TeV, motivated by WIMP dark matter. Moreover gauge coupling unification is not spoiled by the heavy squarks and sleptons that do not contribute anymore to the running between the weak scale and $\tilde{m}$, because they come in complete $SU(5)$ multiplets. As appealing features of Split SUSY models, the heavy scalars strongly suppress flavour changing neutral currents and ameliorates other problems such as CP violation and fast proton decay.
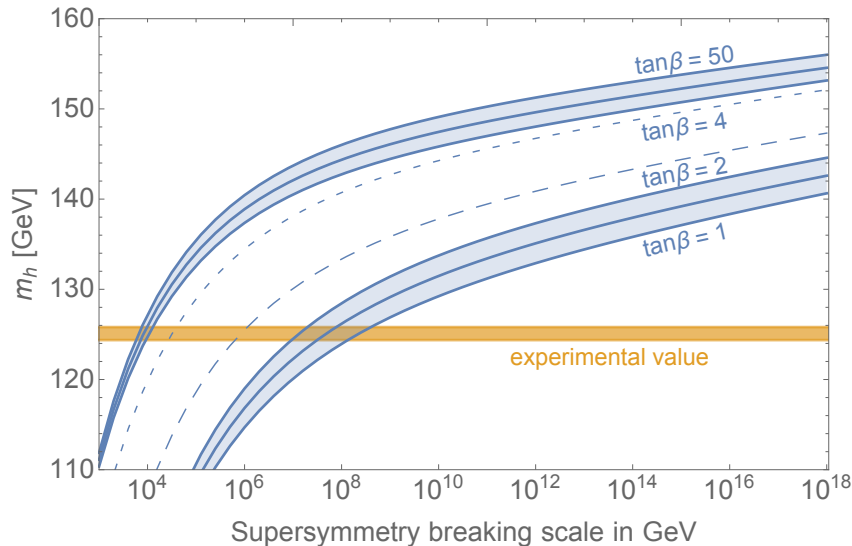
Figure 1.5: Prediction for the Higgs mass m_h in Split Supersymmetry for $\tan\beta = \{1, 2, 4, 50\}$. The thickness of the lower and upper boundary at $\tan\beta = 1$ and $\tan\beta = 50$ shows the uncertainty due to the present 2σ error on the top mass. The plot was done with SUSYHD [75].

1.2 Beyond minimal SUSY: Dirac gauginos

In light of the challenges faced by the MSSM, it is also interesting to consider non-minimal implementations of SUSY. Models with Dirac gaugino masses are an alternative to the MSSM. Such models were considered early in the study of supersymmetric theories [86–88], and have received renewed interest because of potential phenomenologically appealing features [85, 89, 90]. These include possibly weakening collider limits and flavour constraints, and reducing EW fine tuning, compared to Majorana models.

Gauginos can get Dirac masses if extra chiral superfields $\hat{\Phi}_i = \hat{S}, \hat{T}, \hat{O}$, in the adjoint representation of the SM gauge group factors U(1), SU(2), SU(3) respectively, are added to the theory. Then Dirac masses can be generated by the operator

$$\int d^2\theta \ \sqrt{2}\frac{\hat{W}'_\alpha \hat{W}^\alpha_j}{M}\hat{\Phi}_j \ , \tag{1.30}$$

where $\hat{W}'_\alpha$ is a hidden sector U(1)$'$ spurion that gets a D-term D', M is the scale of supersymmetry breaking from the hidden to the visible sector, $\hat{W}^\alpha_i$ is the visible sector gauge superfield for the three gauginos, and $d^2\theta$ is the integration over the Grassmann

variable of the superspace formulation. This leads to terms in the Lagrangian

$$\mathcal{L} \supset -m_{D_j}\lambda_j\tilde{\phi}_j - \sqrt{2}m_{D_j}(\phi_j + \phi_j^*)D_j - \frac{1}{2}D_j^2 \ , \tag{1.31}$$

where λ is the gaugino, ϕ_j is the complex scalar component of $\hat{\Phi}_j$, $\tilde{\phi}_j$ is its fermion partner, and $m_D = D'/M$.

The operator in Eq. (1.30) is supersoft, in contrast to a Majorana gaugino mass, namely it does not give logarithmic divergent contributions to soft parameters. These logarithmic divergences, if only the operator in Eq. (1.30) is present, are canceled by the contribution of the diagram with ϕ and the sfermions in the loop. Therefore there are only threshold contributions to the sfermion masses due to the mass splitting of the Dirac gauginos and the scalar adjoints, given by

$$m_{\tilde{f}}^2 = \sum_i \frac{\alpha_i}{\pi}C_i\left(r\right)m_{D_i}^2\log\left(\frac{m_{\mathrm{Re}\phi_i}^2}{m_{D_i}^2}\right) , \tag{1.32}$$

where m_{D_i} are the gaugino masses, corresponding to the SM groups U(1), SU(2), SU(3) respectively, $C_i(r)$ are the quadratic Casimir of the fermion i under the gauge group r, and $m_{\mathrm{Re}\phi_i}$ is the mass of the real part of the sgauge field. If only the supersoft operator in Eq. (1.30) is present, $m_{\mathrm{Re}\phi_i} = 2m_{D_i}$ and the formula simplifies further. Moreover, the finiteness of Eq. (1.32) allows for a hierarchy between the low scale squark and gluino masses to be maintained during RG flow without tuning.

The scalar adjoints can also have SUSY breaking, R-symmetry preserving, mass terms

$$\mathcal{L} \supset m_{\phi_i}^2\phi_i^\dagger\phi_i + B_{\phi_i}(\phi_i\phi_i + \mathrm{h.c.}) \ . \tag{1.33}$$

The first term of Eq. (1.33) is actually required because otherwise the imaginary part of ϕ_i would be massless. However, the B_{ϕ_i} term splits the real and imaginary components of the adjoint scalar masses, and originates from the operator

$$\int d^2\theta \ \sqrt{2}\frac{\hat{W}'_\alpha\hat{W}^{\alpha'}}{M}\hat{\Phi}_j^2 \ . \tag{1.34}$$

From Eqs. (1.31) and (1.33) we have

$$m_{\mathrm{Re}\phi_i}^2 = 4m_{D_i}^2 + m_{\phi_i}^2 + B_{\phi_i} \ , \qquad m_{\mathrm{Im}\phi_i}^2 = m_{\phi_i}^2 - B_{\phi_i} \ . \tag{1.35}$$

Notably, the first term of Eq. (1.33) is not supersoft, and the non-holomorphic adjoint masses $m_{\phi_i}^2$ contribute at two loops to the β functions for the sfermion masses. This two loop contribution

$$\partial_t m_{\tilde{q}}^2 \simeq \frac{32\alpha_s^2}{(4\pi)^2}m_{\phi_3}^2 + ... \tag{1.36}$$

drives the squarks tachyonic and it can dominate the finite contributions of Eq. (1.32).

In gauge mediated models of Dirac gauginos, couplings of the adjoint fields to messengers in the superpotential lead to the soft masses of Eqs. (1.31) and (1.33) [91–93]. If the messengers are charged under a U(1)$'$, gaugino masses, and B_{ϕ_i} are generated at one loop. Avoiding a tachyonic adjoint scalar therefore requires $m_{\phi_i}^2$ to be large, which is problematic since it is generated at two loops. With many messengers, positive masses for the real and imaginary components of the scalar adjoint are possible [94]. However, the contribution to the sfermion masses from the RG flow may then dominate the finite contribution in Eq. (1.32) leading to problems with tachyonic states, and potentially requiring extra tuning to obtain viable spectra [76]. Additional operators, that give positive contributions to $m_{\mathrm{Re}\phi_i}^2$ and $m_{\mathrm{Im}\phi_i}^2$, may alleviate the problem leading to masses for the real and imaginary components of the scalar adjoint of the same order as the gluino mass [95–97]. Alternatively, it is possible to forbid the operator that produces B_{ϕ_i} if the gauginos themselves are associated to a spontaneously broken global symmetry [98, 99].

The phenomenology of Dirac gaugino models depends on the expected ratios of the scalar masses to gluinos and between the gauginos. If scalar masses are dominantly produced by the supersoft operators of Eq. (1.30), the gluinos are significantly heavier than the squarks, with $m_{D_3} \sim (5 \div 10)\, m_{\tilde{q}}$. However more complete models can alter this minimal picture and lead to squark masses comparable to the gluino mass [92]. Gauge unification is problematic in minimal Dirac models, and if it is not imposed the ratio of gaugino masses depends on the details of the SUSY breaking and mediation sectors. It is also possible that adjoints are present only for the SU(3) group, while the Wino and Bino have Majorana masses, which would allow for large differences in the masses, for example if the theory has an approximate R-symmetry (options include the possibilities that the gluino could have both a Majorana and Dirac mass [100], or that Dirac masses could be generated by an F-term [101]).

Unification is possible, even if difficult to achieve, if additional fields are added, which together with the $\hat{S}$, $\hat{T}$ and $\hat{O}$ adjoints form a complete representation of a unified group: the two simplest choices being SU(5) and SU(3)^3 [89, 102]. The masses of the additional fields have to be above 10^{14} GeV, in order to avoid a Landau pole before the unification scale. This fixes the ratio between the gaugino masses [89], and in many models the Bino and Wino are typically a factor of a few lighter than the gluino, often with a right handed slepton lightest supersymmetric particle (LSP). Another possibility to achieve gauge coupling unification is to add extra states in incomplete GUT multiplets, with masses between the unification and the EW scale.[1] In some scenarios this leads to a ratio

---

[1] These extra fields could even play the role of gauge mediation messengers.

between gaugino masses given by $m_{D_i}/m_{D_j} \sim g_i/g_j$ [93]. In both scenarios, the addition of extra states at intermediate scales quantitatively predict a different gauge coupling unification scale with respect to the MSSM one.

Split family spectra with the first two generation squarks heavy can also be realised in Dirac models. For example, [102] study a model with gauge unification, and stops lighter than the first two generation squarks by a factor of about 5. The low scale gaugino masses are

$$m_{D_1}/m_{D_0} : m_{D_2}/m_{D_0} : m_{D_3}/m_{D_0} \simeq 0.22 : 0.9 : 3.5 \,, \tag{1.37}$$

where m_{D_0} is the common gaugino mass at the GUT scale. The physical stop masses are $m_{\tilde{t}}^2 \simeq 0.2\,m_0^2 + 0.6\,m_{D_0}^2$, where m_0 is a common first two generations squark mass at the GUT scale, while the physical first two generations squark masses are approximately $m_{\tilde{q}_{1,2}}^2 \simeq 0.9\,m_0^2 + 0.6\,m_{D_0}^2$.

Finally, split SUSY models with Dirac gauginos are possible [103]. In these models, sfermions and Dirac gauginos are very heavy and the only phenomenologically viable states are the pseudo-Dirac higgsinos, with mass around 1 TeV. Alternatively, the Bino can be a Majorana fermion, lighter than the other Dirac gauginos, and it can generate a splitting of the pseudo-Dirac higgsino into Majorana states.

To summarise, in their simplest implementations models with Dirac gauginos lead to spectra with relatively heavy gluinos compared to the squarks without tuning, typically with gluino masses about five times larger. Meanwhile Majorana models cannot have gluinos significantly heavier than the squarks without additional tuning. However, minimal theories of Dirac gauginos have problems with tachyonic states, and solving this can lead to squark masses comparable to that of the gluino. Split family models, with the first two generation sfermions heavier than the gluino and the stops are also possible in both Majorana and Dirac models, as are split SUSY models.

1. Introduction and motivations

Chapter 2

SUSY at a 100 TeV collider

Despite negative results from searches at the LHC, supersymmetry remains a well motivated scenario for physics beyond the SM. Supersymmetric theories consistent with observations require a certain amount of fine tuning, but if this is accepted they can explain the remainder of the hierarchy between the electroweak and the Planck scale, and can also lead to viable dark matter candidates and gauge coupling unification. Within this framework the Higgs mass and the lack of discovery of new coloured states hint to a new physics scale higher than the electroweak one. Furthermore, in SUSY models, thermal dark matter candidates might have a mass up to 3 TeV, not accessible at the LHC. The expectation of such heavy spectrum requires a machine more powerful than the LHC. Consequently there has been significant interest in the prospect for discovering supersymmetry at a future hadron collider with a centre of mass energy of about 100 TeV.

In this chapter, we analyse some searches for electroweakinos at current and future colliders (with centre of mass of 14, 33 and 100 TeV) for Split SUSY models. Moreover, in the second part, we carried out a simulation of the collider reach for strongly coupled states in Dirac gaugino models at a future 100 TeV hadron collider.

2.1 Electroweakinos in Split SUSY

In this section we will extrapolate the mass reach for future hadron colliders in several searches of electroweakinos relevant for split SUSY models. In general it is quite difficult to estimate the mass reach for future colliders because cuts, acceptances (a), efficiencies (ϵ) and type of analyses are expected to be different and because of our ignorance on the details of the detector. In the following we will assume that cuts can be rescaled such that efficiencies and acceptances can be kept constant ($\epsilon a \simeq const$). We basically follow

the same strategy outlined in Collider Reach [104, 105]. The energy dependence of the number of signal and background events (S and B respectively) is thus determined by the production cross section. In particular the energy dependence of S and B is the same since the parton level cross section has the same scaling $\sigma \sim 1/E^2$ at high energies and the pdf of both signal and background are evaluated at the same energy.[1] Therefore, requiring that the significance at the new collider is the same as the one setting the current bounds gives

$$\sigma = \frac{S}{\sqrt{B}} = \frac{S'}{\sqrt{B'}} \qquad \Rightarrow \qquad \frac{S}{S'} = 1, \tag{2.1}$$

where S' and B' refer to the number of signal and background events at a future collider.

Given an existing LHC bound, the corresponding mass reach at the new collider can thus be obtained by simply computing the production cross section and requiring the same number of signal events needed to put the original bound. Since in the ratio S'/S the main NLO effects cancel, the number of signal events can be computed using the cross section of electroweakinos at leading order [106] convoluted[2] with the MSTW Parton Distribution Function [107].

We will show in the following that our analysis on electroweakino searches is in agreement with existing studies in the literature when available. Results are shown in figures 2.1–2.5 and in table 2.1 and refer to 95% CL mass reach.

2.1.1 Wino-Bino simplified model

The first search we consider is a Wino-Bino simplified model.[3] Charginos can be produced in association with a neutralino via an s-channel W boson. Production through squarks has been neglected because all the scalar super partners are assumed much heavier. This scenario can be realised both in gravity and in gauge mediation (GMSB) models. When the gaugino masses are universal ($M_1 : M_2 : M_3 = \alpha_1 : \alpha_2 : \alpha_3$), the gluino is only three times heavier than the Wino and we expect direct gluino searches to be stronger than direct Wino searches. However, in non-universal gaugino models the gluino can be much heavier than the Wino and direct electroweak searches would be the best channel to explore this scenario. This channel is also sensitive to GMSB models where the

---

[1]This is true away from the squeezed limit, where most of the background come from softer SM particles. For this reason we will restrict to the case $m_{LSP} \ll m_{NLSP}$.

[2]Computing the signal, the cross section can be factorized out from the convolution with the Parton Distribution Function $S \sim \sigma_\chi \cdot pdf$ because the integral is dominated only by the threshold $\tau_0 \sim 4m^2$. We verified numerically the negligible effects of the tail of the distribution.

[3]The Wino-higgsino simplified model has been recently studied in [110].

Wino in the WZ channel
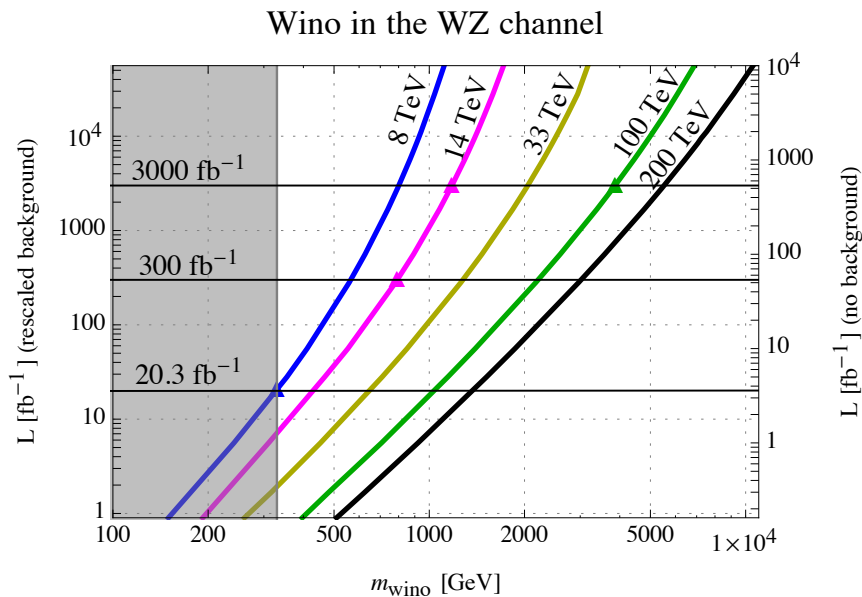
Figure 2.1: Wino-Bino simplified model in the *WZ* channel. The left axis shows the integrated luminosity for the method explained in the text and on the right axis, the same for having 5 events and no background. The grey shaded area is the current bound from [108].

Wino is the lightest neutralino, all the other gauginos are heavy and the gravitino is approximately massless. In this case Winos decay promptly through the same channel $\tilde{W}^{\pm}\tilde{W}^{0} \to W^{\pm} Z \tilde{G}\tilde{G}$.

We consider the two different extreme cases, where the neutral Wino decays with $BR = 1$ either to Z and LSP or to Higgs and LSP. The charged Wino decays always to W and LSP. In the first case the dominant signature is three leptons and missing energy and the main background comes from the SM *WZ* production. A Wino NLSP for $m \lesssim 350$ GeV is excluded for Bino masses less than 100 GeV [108, 111]. In the second case the final states are one charged lepton (electron or muon), missing transverse energy (from the LSP and the neutrino coming from the W decay) and two b-jets (from the Higgs). For a massless Bino, Winos between 125 and 141 GeV and between 166 and 287 GeV are excluded [109].

The mass reaches in the Wino-Bino simplified model are shown in figure 2.1 and figure 2.2 for the *WZ* and the *Wh* channel respectively. In this scenario higgsinos are decoupled and therefore the only relevant parameter in the cross section is M_2 (the cross section is weakly dependent on $\tan\beta$ and M_1, fixed to be less than 100 GeV by the method used).
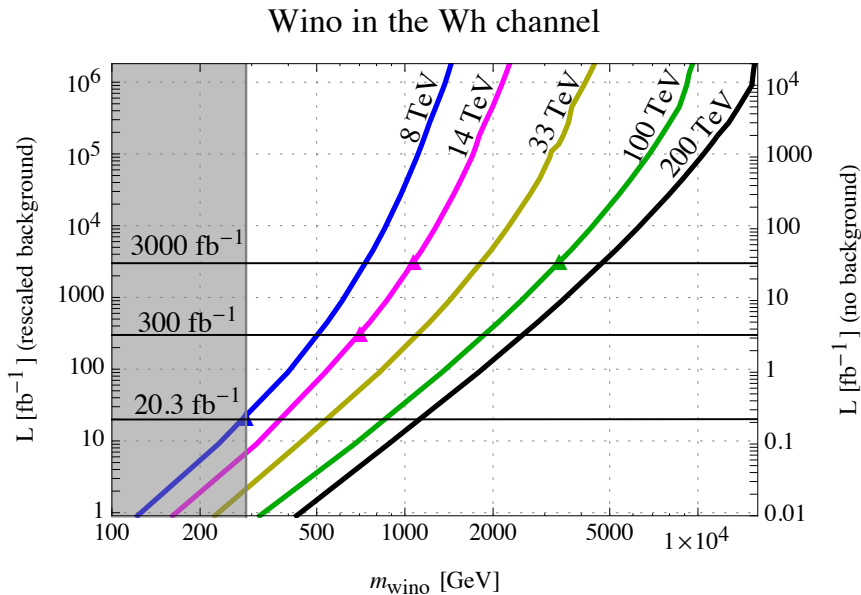
Wino in the Wh channel

Figure 2.2: Wino-Bino simplified model in the $W h$ channel. The left axis shows the integrated luminosity for the method explained in the text and on the right axis, the same for having 5 events and no background. The grey shaded area is the current bound from [109].

In the WZ scenario, we find that the LHC14 may extend the mass reach to 1.2 TeV for a luminosity of 3000 fb^{-1} and it will increase up to ~ 4 TeV at a 100 TeV collider.

The first result is in agreement with the 1.1 TeV mass reach given by ATLAS [112]. The latter can be compared with results by [113], although the two analyses differ for the treatment of the branching ratios: we assume 100% decay in Z or h, while they keep into account the fact that the branching ratios of Winos depend on the choice of $\tan\beta$ and on the choice of the relative sign between gauginos and higgsinos. Moreover, in [113] only the lepton channels have been considered, however the b-jet channel has a higher sensitivity in the Higgs mediated scenario, due to the enhanced branching ratio $\mathrm{BR}(h \to b\bar{b}) \gg \mathrm{BR}(h \to WW/ZZ)$. So we find that a 100 TeV collider with 3000 fb^{-1} of luminosity may reach 3.4 TeV in the b-jets channel as opposed to the only 1.3 TeV reach found in [113] considering only the lepton channel. As a reference point in the right axis of the figures we show how the reach in mass can be extended for a given integrated luminosity assuming that the background can be reduced to zero and the efficiencies and the acceptances can be made 100% (obtained by requiring $S' = 5$). (A more realistic result can be simply obtained by rescaling the required luminosity by ϵ, a and the $\sqrt{B}$.) The

right axis of each figure allows also to derive the cross section for the different searches at different colliders as a function of the suitable gaugino masses. The plots can also be used to compare the performance of different colliders. For example, in figure 2.1 and 2.2, we notice that, for the electroweak (EW) searches described in this section, the sensitivity of the LHC14 with 3000 fb^{-1} is approximately the same as a 33 TeV collider with a luminosity ten times smaller.

2.1.2 Long-lived Wino

Long-lived chargino searches can be used to probe models with Wino LSP such as anomaly mediation models (AMSB) or high scale GMSB with non universal gaugino masses. In these models the neutral Wino states are highly degenerate with the charged Wino and all the other states are decoupled. For heavy higgsino the mass splitting at tree level is suppressed and it is dominated by the radiative generated contribution, which is around 160-170 MeV at one-loop level [114–116]. This small mass splitting implies that the charged Wino has a considerable lifetime (of order $c\tau = \mathcal{O}(10)$ cm) and it decays mainly into the neutral Wino and a soft charged pion.

The signature for this search is one hard jet from initial state radiation (ISR), large missing transverse energy and a disappearing track (the chargino eventually decays to a soft not reconstructed pion). The jet must not be too close to the missing energy direction because it usually implies jet mismeasurement. Chargino pair ($\tilde{\chi}_1^+ \tilde{\chi}_1^-$) and chargino neutralino ($\tilde{\chi}_1^\pm \tilde{\chi}_1^0$) associated production with initial state radiation are the relevant processes for this search. The relevant background originates from unidentified leptons and charged particles with high mis-reconstructed transverse momentum (p_T) as well as charged hadrons interacting with the inner detector. ATLAS excludes charginos with mass below 250 GeV in the AMSB model [117].

We model the relevant cross section through the process $q\bar{q} \to Z\,j \to e^+ e^-\,j$ using the program MCFM [118] and rescaling the partonic cross section with the electroweakino one. This is a good approximation within the method used because the cross section depends only on the energy and on the different pdfs and the process with the exchange of a photon is negligible with respect of the Z exchange diagrams. We derived the mass reach in two ways: by conservatively rescaling the cut on the transverse momentum of the jet with the mass of the final state (solid lines in figure 2.3), in such a way that $p_T/m_{\tilde{W}} = const$, or keeping the cut fixed to the value the ATLAS experiment used in its study ($p_T > 80$ GeV), if feasible (dashed lines in figure 2.3).

This scenario is relevant for dark matter searches. Indeed a Wino LSP is expected to thermally saturate the relic density for a mass $m_\chi \simeq 3.2$ TeV. LHC14 has the potential to
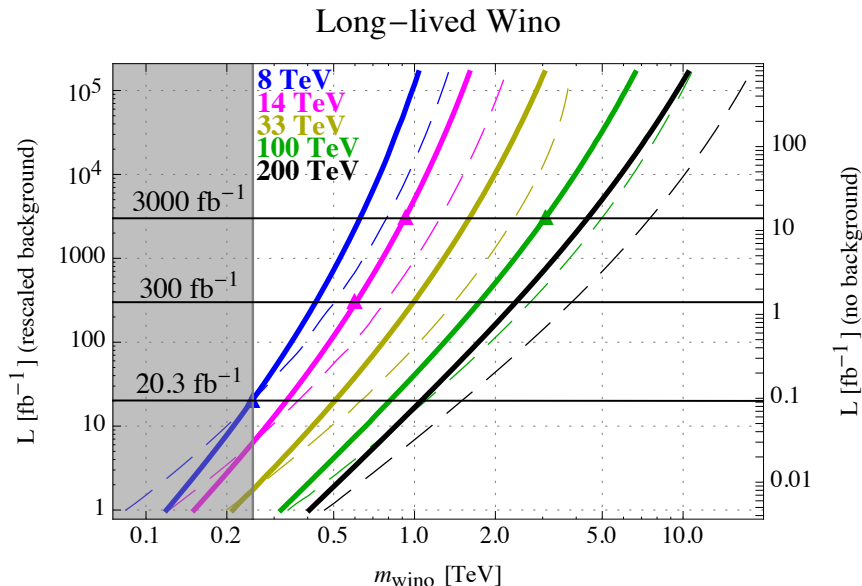
Figure 2.3: Long-lived Wino. The left axis shows the integrated luminosity for the method explained in the text and on the right axis, the same for having 5 events and no background. The grey shaded area is the current bound from [117].

explore long lived chargino scenarios for masses around 600 GeV for a luminosity of 300 fb^{-1}. This result is in agreement with the study in [119]. By exploiting the new tracker installed at ATLAS, the reach for this kind of search may increase up to 800 GeV at the LHC14 with 100 fb^{-1}. We find that a 100 TeV collider would reach a Wino mass around 3.1 TeV for 3000 fb^{-1}.

In the literature there are similar results for the disappearing track of long-lived Wino searches [120, 121]. In order to be sure to reach the thermal dark matter mass range we should either increase the luminosity or the collider energy: for example with a 200 TeV collider and 1000 fb^{-1} of luminosity the Wino reach would comfortably extend to over 3 TeV. In addition it seems that without stronger cuts than the one used by ATLAS the reach could be extended up to 5 TeV for a 100 TeV collider with a luminosity of 3000 fb^{-1}. This channel is particularly important in models such as anomaly mediation, where the ratio between the gluino and the Wino is large ($M_3 \simeq 7 M_2$), because it could be more powerful than the gluino searches [122].
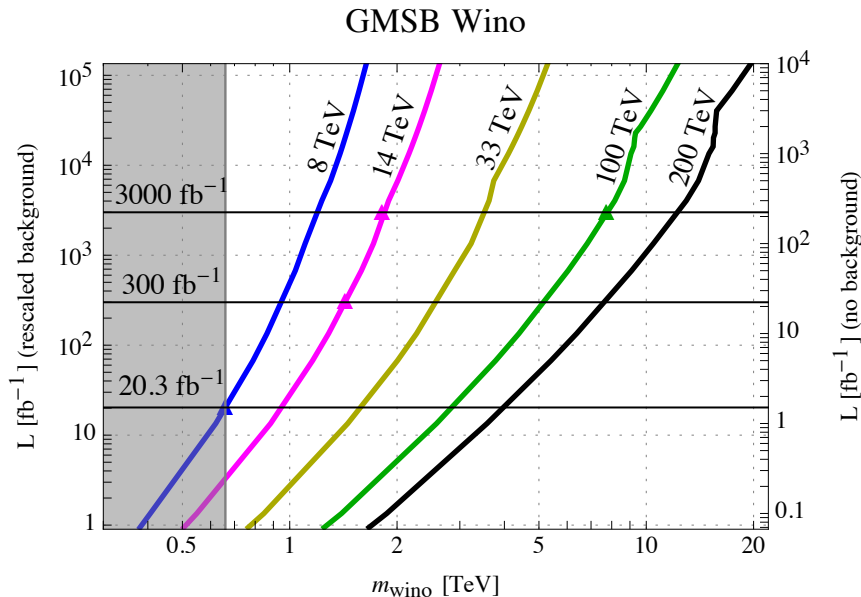
Figure 2.4: GMSB Wino-Bino scenario. The left axis shows the integrated luminosity for the method explained in the text and on the right axis, the same for having 5 events and no background. The grey shaded area is the current bound from [123].

2.1.3 GMSB Wino-Bino simplified model

In gauge mediated supersymmetric models usually the gravitino and the Bino are the LSP and the NLSP respectively and the latter decays to the former via emission of one hard photon. The search discussed in this section describes the production of Winos decaying into Binos that subsequently decay into photons and gravitinos. This channel leads to events with two final state photons, large missing energy and a moderate amount of visible transverse energy. The relevant background is given by QCD processes involving photons and jets, where a photon or a jet is mis-measured, EW processes like $W + X$, where X is mis-reconstructed as a photon, and W and Z production in association with photons. ATLAS set limits on a Wino mass of 570 GeV for any Bino above 50 GeV [123]. For models with universal gaugino masses the limit increases to 660 GeV.

In figure 2.4 we show the reach for the GMSB Wino-Bino scenario with universal gaugino masses. The relevant parameter in the computation of the cross section is the Wino mass, while higgsinos are decoupled (the cross section is weakly dependent $\tan \beta$). Already the LHC14 will probe Winos up to 1.8 TeV with 3000 fb^{-1}, corresponding to a gluino ~ 5.4 TeV. At 100 TeV it is possible to exclude ~ 7.8 TeV Wino. This has a strong impact in GMSB models with universal gaugino masses in which $\tan \beta$ is large. Indeed
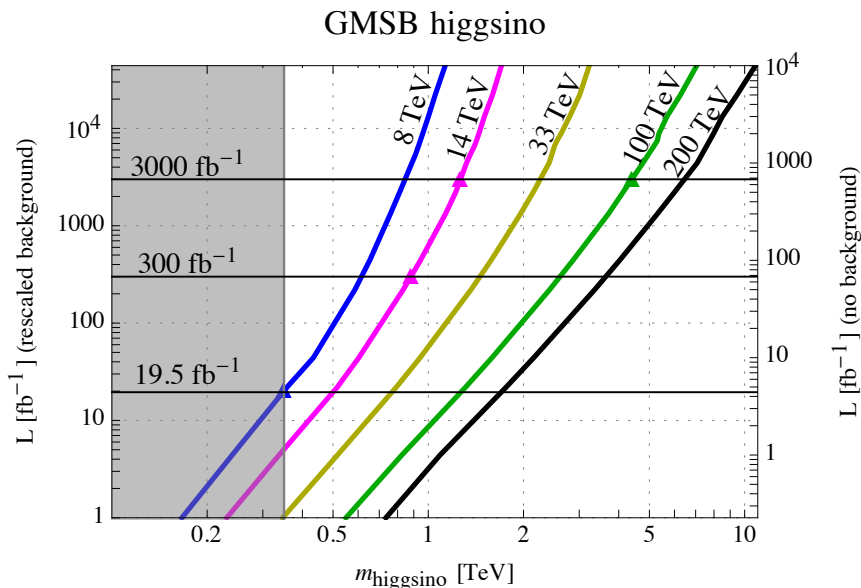
Figure 2.5: GMSB higgsino NLSP scenario. The left axis shows the integrated luminosity for the method explained in the text and on the right axis, the same for having 5 events and no background. The grey shaded area is the current bound from [111].

in these models the ~ 125 GeV Higgs mass fix the squark masses to be around 10 TeV or below. Gluinos are expected at the same scale or below, which means a Wino around ~ 3.3 TeV or below. Such Wino could be probed already at a 33 TeV collider with 3000 fb^{-1}. Like in the previous case also in this scenario the Wino reach is stronger than the gluino one.

2.1.4 GMSB higgsino simplified model

In the last analysis the gravitino is assumed to be the LSP with higgsinos NLSP and all the other states decoupled. This channel is relevant, for example, in lopsided gauge mediation models [124], where scalars and gauginos are in the multi-TeV range and the production of electroweakinos in the cascade of coloured sparticles is suppressed with respect to the direct production of light higgsinos.

Higgsino NLSP decays to gravitino and Z or W bosons. The branching fraction of higgsino to Z can be enhanced (with respect to the decay to Higgs) in the so called Z-enriched GMSB model [125, 126]. The signature for this search is three or four leptons plus missing transverse momentum or two leptons, two jets and missing transverse momentum.

	8 TeV [1]	14 TeV [300(0) fb^{-1}]	33 TeV [300(0) fb^{-1}]	100 TeV [300(0) fb^{-1}]
Wino ($\chi_2^0 \to \chi_1^0 Z$)	330 [108]	790 (1180)	1280 (2050)	2210 (3870)
Wino ($\chi_2^0 \to \chi_1^0 h$)	287 [109]	700 (1080)	1110 (1830)	1890 (3380)
long-lived Wino	250 [117]	600 (930)	990 (1600)	1750 (3080)
GMSB Wino	660 [123]	1430 (1820)	2590 (3510)	5170 (7750)
GMSB higgsino	350 [111]	880 (1260)	1460 (2260)	2610 (4400)

Table 2.1: Current experimental status (LHC8) and results of the analyses with rescaled background for LHC14, 33 and 100 TeV future hadron colliders. All the numbers are in GeV. The models are explained in sections 2.1.1, 2.1.2, 2.1.3, 2.1.4 respectively.

The background is given mainly by the Standard Model *WZ* and *ZZ* production. CMS set a limit of 350 GeV to this type of higgsinos [111]. We consider only the channel with two leptons, two jets and missing transverse momentum since it is the one that dominates the search. In figure 2.5 we show the results. The mass reach of this search is expected to surpass 1 TeV by the end of the LHC lifetime ($\sim$ 2035) and reach 4.4 TeV at a 100 TeV machine with 3000 fb^{-1}.

2.2 Strongly coupled states: Majorana vs Dirac

Hadron colliders are very efficient at producing strongly interacting states, and even though coloured superpartners are often amongst the heaviest they constitute the most important channels for the discovery or exclusion of SUSY theories. For this reason, we also study the production cross sections of coloured states at a 100 TeV proton–proton collider obtaining the expected discovery and exclusion reach for a squark-gluino-neutralino simplified model. The Dirac or Majorana nature of gluino masses leads to significant differences in the production rates in some parts of parameter space [85, 127–129] and we highlight the effects of these. LHC searches already set stringent limits on SUSY models [130, 131] and these can be recast to give significant constraints on models of Dirac gluinos. The bounds on the first two generation squark masses from 8 TeV data are found

---

[1]The limit for GMSB higgsino model was given for 19.5 fb^{-1} of luminosity. All the other limits are given for 20.3 fb^{-1}.

to be roughly in the region of 800 GeV for Dirac gluino masses of around 5 TeV, and are expected to increase up to roughly 1.2 TeV with 14 TeV data [85, 129].

2.2.1 Production cross sections

Motivated by UV theories of Dirac gluinos, discussed in Section 1.2, we consider two benchmark patterns of soft terms, one with $m_{\tilde{q}} = m_{\tilde{g}}$ and the other with $m_{\tilde{g}} = 5m_{\tilde{q}}$ where $m_{\tilde{g}}$ is the gluino mass. Due to the parton content of the proton, the first two generation sfermions are produced far more readily than stops, provided the masses are not very hierarchical. Therefore we take $m_{\tilde{q}}$ to be a degenerate mass for these states, and neglect the production of stops. Our calculations are performed with MadGraph5 [132], and we have not included next to leading order (NLO) K-factors in this section. These are not yet known for Dirac gluinos and we are primarily concerned with the relative sizes of cross sections here. Cross sections for Majorana models at 100 TeV have previously been studied (for example in [133]), while cross sections for Dirac models at an energy of 33 TeV are given in [134], and we find good agreement with these.

In Fig. 2.6 (left) we show the production cross sections for squark pairs for Majorana and Dirac gluinos. This production channel shows the most striking difference between the two cases. For Dirac gluinos only production of $(\tilde{q}_L\tilde{q}_R)$ is possible, with $(\tilde{q}_L\tilde{q}_L)$ forbidden due to the lack of an allowed chirality flip. In contrast, a chirality flip is possible with a Majorana gluino mass, and consequently this cross section is dramatically larger than in Dirac models [134].[1] In Fig. 2.6 (right) the production cross sections for squark-antisquark pairs is plotted. The cross section is only slightly reduced in Dirac models because the dominant production mode is through an s-channel gluon. This production mode is independent of the gluino mass, reflected in the relatively small drop in cross sections between the models with gluino mass equal to the squarks and the models with a heavy gluino.

In Fig. 2.7 (left) we show the gluino-squark production cross section. To a good approximation this is the same for both Dirac and Majorana models. If the squarks are relatively heavy compared to the gluino, gluino pair production is the dominant source of superparticles. The cross section for this is plotted in Fig. 2.7 (right), and here the only difference between the models is the additional degrees of freedom in the Dirac gluino model. This simply enhances the production cross section of gluino pairs by a factor of a few.

---

[1]The difference in the relative production of same chirality and opposite chirality squarks could even be used to distinguish Dirac from Majorana gluinos [128].
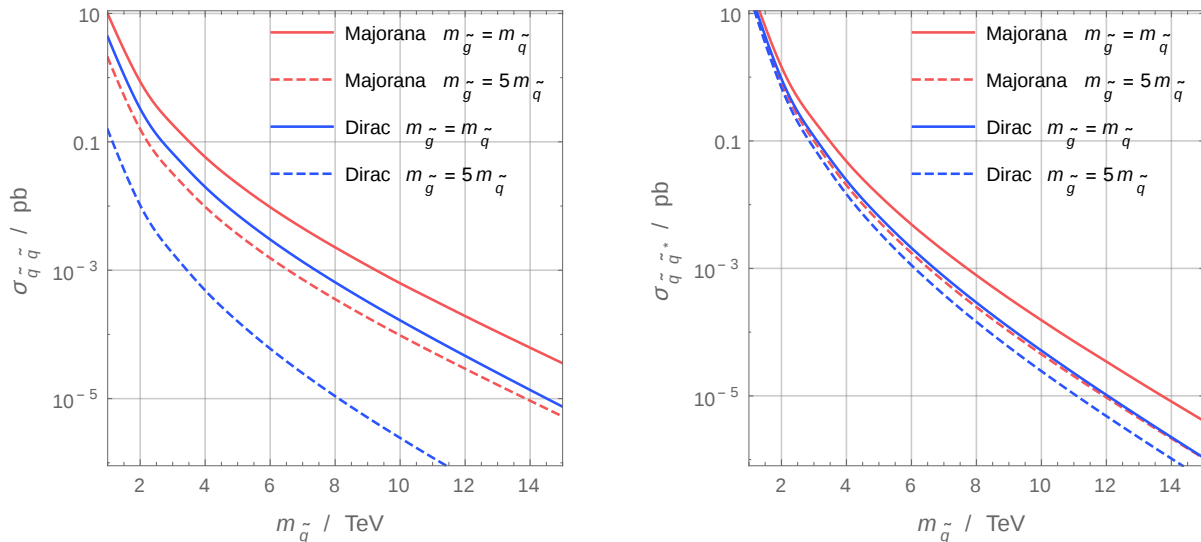
Figure 2.6: *Left:* The squark-squark production cross sections for Dirac (plotted in blue) and Majorana (red) gluinos as a function of the squark mass. We show the production cross sections for two benchmark relations between the soft parameters, $m_{\tilde{g}} = m_{\tilde{q}}$ (solid lines) and $m_{\tilde{g}} = 5m_{\tilde{q}}$ (dashed lines). *Right:* The squark-anti-squark production cross sections for the same models.

Therefore the main differences in exclusion and discovery reach will be in regions of parameter space where gluino pair production, or squark pair production dominates. With relatively heavy squarks, gluino pair production will be most important and the Dirac model will lead to higher potential exclusion.

Comparing the cross sections in Figs. 2.6 and 2.7, we see that when the squark masses are equal to the gluino mass squark-gluino production will be large, and in Majorana models there will be also be a comparable squark-squark production cross section, while this is suppressed in Dirac models. Consequently, the collider reach is expected to be roughly similar in the two cases. For larger gluino masses, the squark-gluino cross section decreases fast, and squark-squark production dominates. In this part of parameter space the exclusion and discovery potential will be drastically reduced in the Dirac model compared to the Majorana model. Eventually, in the decoupling limit where the gluino is so heavy that it is completely removed from the spectrum, squark-anti-squark production is dominant and the two models have the same production cross section.

As well as squarks and gluinos, Dirac gluino models feature another new coloured state. This is the sgluon ϕ, a complex scalar in the adjoint of SU(3). The sgluon mass depends on the UV completion of the theory, but is often comparable in mass to the
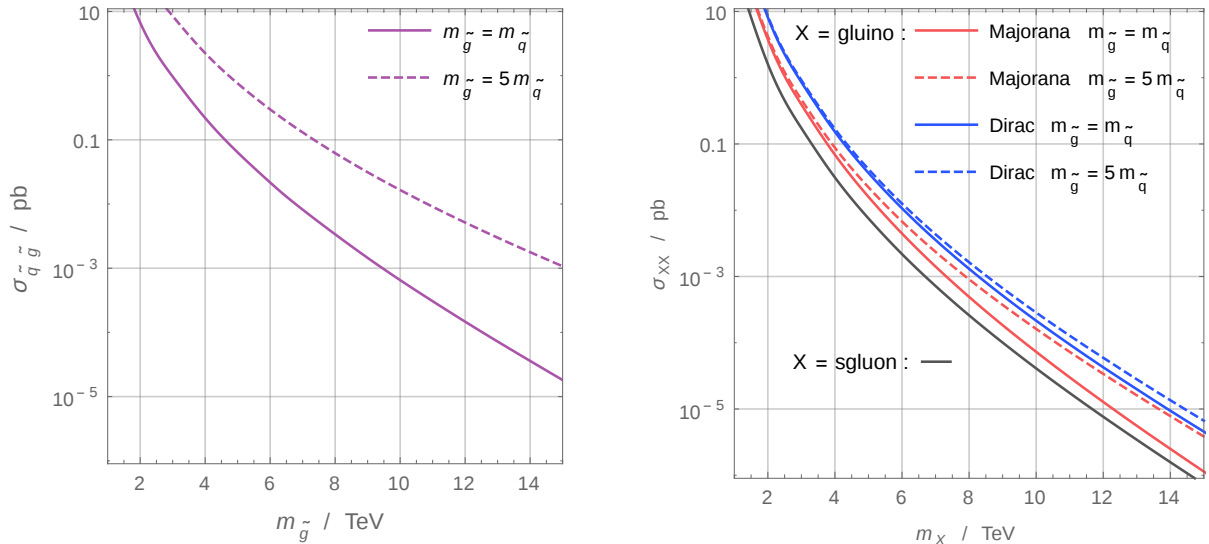
Figure 2.7: *Left:* The gluino-squark production cross section for the two soft mass relations, as a function of the gluino mass. To a good approximation this is identical for the Dirac and Majorana scenarios. For the $m_{\tilde{g}} = 5m_{\tilde{q}}$ curve, the plotted region corresponds to light squarks, and gluino-squark production is entirely negligible for models with such a mass relation if the squarks are heavier than a few TeV. *Right:* The gluino pair production cross sections, for the Dirac (blue) and Majorana (red) benchmark models as a function of the gluino mass. We also show the production cross section for pair production of sgluons (plotted in black), as a function of the sgluon mass, which is approximately independent of the other soft parameters in the model.

gluino. Over most of parameter space sgluons are dominantly pair produced with single production significantly suppressed [135], and to a good approximation the cross section for this is independent of the other soft parameters of the theory. In Fig. 2.7 (right), we therefore show the leading order production cross section for pair production, assuming the scalar and pseudo-scalar components are degenerate in mass (NLO corrections for sgluon production have been obtained in [136], and including these does not qualitatively affect our conclusions). It can be seen that sgluons are pair produced less frequently than gluinos unless they are substantially lighter.

2.2.2 Discovery and exclusion reach

To determine the expected discovery and exclusion reach of a 100 TeV proton–proton collider, we study a simplified squark-gluino-neutralino model. We set the neutralino

mass to 100 GeV, and scan over the masses of the degenerate first and second generation squarks, and the gluinos, with all other superpartners decoupled. The signal of such a model, jets and missing energy, is a classic search for supersymmetry, and the main SM backgrounds to this are W/Z boson + jets, and $t\bar{t}$ + jet production.

Our simulation is performed using the SARAH Dirac Gauginos model [137]. We produce parton level events for the production channels $(\tilde{g}\tilde{g})$, $(\tilde{q}\tilde{g})$, $(\tilde{q}\tilde{q})$, and $(\tilde{q}\tilde{q}^*)$ in MadGraph5 [132]. Decay, showering and hadronisation is carried out with Pythia6.4 [138], and we use the Snowmass detector card [139] in Delphes [140] to perform our detector simulation. Given how rapidly the cross sections fall with increasing superpartner masses the order one uncertainties on the properties of a future detector are expected to lead to relatively small changes to our results. To obtain the SM backgrounds we use the publicly available Snowmass results [141]. We assume that there are 20% systematic uncertainties associated with the SM backgrounds (this may be a fairly cautious estimate and we comment on the effect of altering it). Further, we compute the expected number of events at a 100 TeV collider assuming, somewhat conservatively, 3 ab^{-1} worth of luminosity. Total integrated luminosities of up to 30 ab^{-1} have been suggested as a suitable aim for a 100 TeV collider, and if this is achieved a significant increase in mass reach is possible [142, 143], and we discuss this later.

To determine the discovery reach we first perform a series of preselection cuts to remove the majority of the SM background. For this we follow the choices of the Snowmass study [122], although further optimisation may be possible and could lead to a small improvement in reach. We require all jets have at least 30 GeV transverse momentum, otherwise we ignore that jet. At least four jets with transverse momentum greater than 60 GeV are also required, and we perform a cut on the missing energy $E_{T,\text{miss}}$ and H_t, the scalar sum of the final state jets, of $E_{T,\text{miss}}^2/H_T > 225$ GeV. Further, we also demand there are no leptons in the final state. We then scan over square cuts on $E_{T,\text{miss}}$ and H_T, with the final cuts chosen so as to maximise the signal significance, i.e. maximising, see [144]

$$\sigma = \frac{S}{\sqrt{1 + B + \gamma^2 B^2 + \delta^2 S^2}} \, , \tag{2.2}$$

where S and B are the number of signal and background events, and γ and δ are the assumed systematic uncertainties on the background and signal events.

NLO K-factors $K = \sigma_{\text{NLO}}/\sigma_{\text{LO}}$ are calculated for Majorana gluinos using Prospino2.1 [145]. These factors have not been calculated for the Dirac case. As an estimate of the effect of going to NLO we apply the K-factors calculated with a Majorana gluino to both models. We do not generate events with any additional parton level jets, nor do we include the effects of pile up. Pile up could be a substantial challenge at a 100 TeV
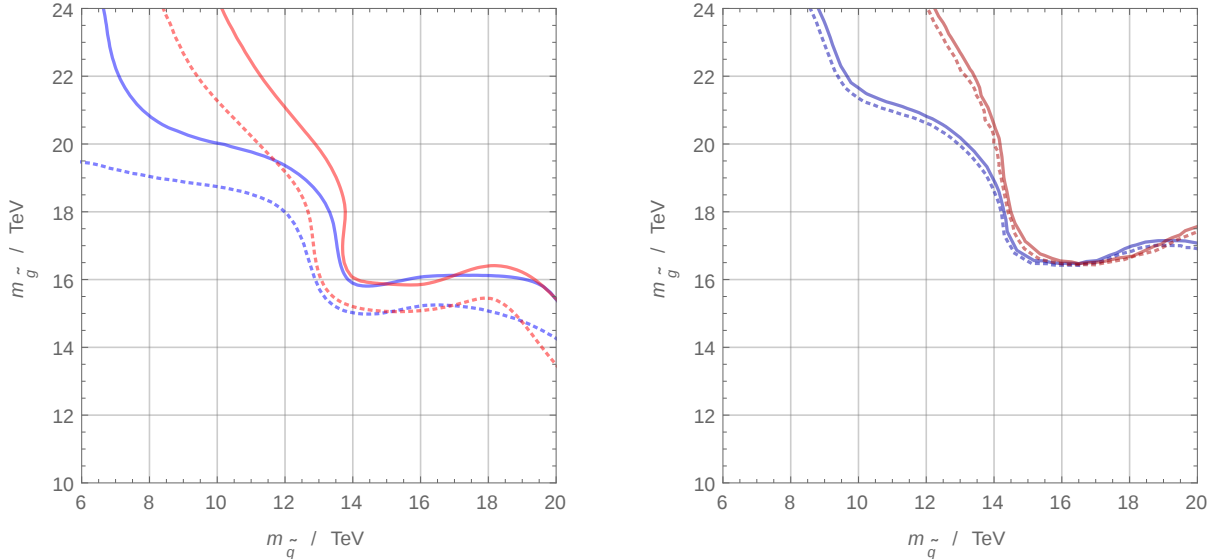
Figure 2.8: *Left:* The 5σ discovery potential of the Dirac (blue) and Majorana (red) gluino-squark-neutralino model including the Majorana K factors for both models at a 100 TeV collider, for 5%, and 15% systematic uncertainty on the signal shown solid and dotted respectively. *Right:* The expected 95% exclusion bounds for the same models.

collider [146, 147], but it has been argued that the present analysis is not likely to be very sensitive to its effects [122].

We study the discovery and exclusion potential in both Majorana and Dirac gluino models, and scan over gluino masses between 8 and 24 TeV, and squark masses between 6 and 20 TeV. For squarks much heavier than the gluino, the main decay mode for the gluino is to a $q\,\bar{q}\,\chi^0$ final state, whilst the squark decays to $\tilde{g}\,\chi^0$. For the opposite case, the squark decays to a $q\,\chi^0$ final state, while the gluino decays to $\tilde{q}\,\bar{q}$.

Of primary interest to us is the difference between the Dirac and Majorana models, and this is plotted in Fig. 2.8. In the region of parameter space where the masses of the gluinos and squarks are comparable, we find both models have the same discovery potential. Similarly, if the squark mass is above the gluino mass then the discovery reach is comparable between the models. For larger still squark masses, much above the gluino mass, gluino pair production will dominate and in this case a Dirac model will have slightly higher exclusion reach. In both models a 100 TeV collider would be able to discover gluinos with masses up to approximately 15 TeV, and exclude gluino masses of approximately 17 TeV.
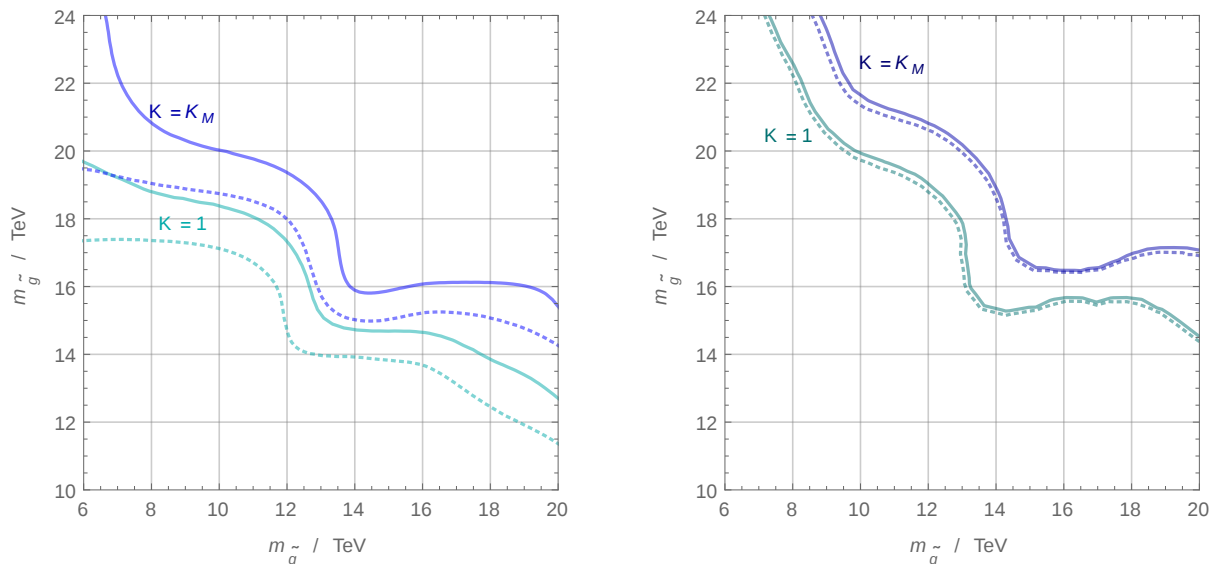
Figure 2.9: *Left:* The 5σ discovery potential of the Dirac gluino-squark-neutralino model including the Majorana k factors, dark blue, and with no K factor, light blue, for 5%, and 15% systematic uncertainty on the signal shown solid and dotted respectively. ***Right:*** The expected 95% exclusion for the same models.

The main difference comes in the region with heavy gluinos, with masses in the range 18 to 24 TeV. In a Majorana model a 100 TeV collider can probe squark masses up to approximately 11 TeV, however a Dirac model only has sensitivity to masses up to 6 TeV. This is expected given the relative sizes of the production cross sections. In this mass region the dominant Majorana production mode is squark-squark pairs, but in a Dirac model this production mode is very suppressed. In theories of Dirac gluinos, the dominant production is instead through squark-anti-squark pairs, which has a smaller cross section leading to reduced sensitivity.

It can be seen from the figures that the systematic uncertainty on the signal leads to reasonable differences in the discovery potential, of order a few TeV, and the range of values shown is plausible given the uncertainties in typical LHC analyses. The effect of this uncertainty on the exclusion potential is relatively minor. Changing the systematic uncertainty on the SM background has little effect on the expected discovery and exclusion regions, with statistical uncertainty being the dominant source of error on the SM background.

General arguments, based on parton distribution functions, suggest that an order of magnitude increase in integrated luminosity from 3 ab^{-1} to 30 ab^{-1} could boost the reach

for heavy particles by several TeV [142, 143]. Repeating our analysis with a luminosity of 30 ab^{-1}, we find that this is indeed the case. In the heavy gluino part of parameter space, squark masses about 4 TeV larger than before are probed, so that in the Dirac model squarks with masses between 8 and 10 TeV could be discovered depending on the signal uncertainty. If the squark and gluino masses are similar the reach is increased by about 2 TeV in both masses.

Let us also note the impact of using NLO K-factors, which is shown in Fig. 2.9. We have computed the K-factors using Prospino2.1 in a model with Majorana gluinos. NLO K-factors have not been calculated for Dirac gluino models to our knowledge. Thus the inclusion of these K-factors in the Dirac model should be thought of purely as an estimate of the impact of going to NLO, rather than a firm prediction. We see that the inclusion of K-factors has a dramatic effect on the discovery and exclusion potential of both models, and thus calculation of K-factors for Dirac gluino models is an important task if accurate predictions are to be made.

A shortcoming of our present work is that we have not included additional parton level jets, which is computationally expensive, in our simulation. The effect of this can be estimated by comparing our Majorana results with the Snowmass study [122], which includes up to two additional jets. Our results match the Snowmass study well in most of the parameter space, while there is some difference in the high gluino mass region. In particular, the Snowmass study finds sensitivity to 14 TeV squarks for gluinos at masses around 20 TeV, falling to 12 TeV squarks for gluino masses of 24 TeV. In comparison we find a maximum discovery reach of 10 to 12 TeV squark masses for these gluino masses. It is likely that in this parameter region the lack of jets results in a signal that is not well separated from the background. However even for such spectra the numerical error introduced is relatively minor compared to, for example, uncertainties from the unknown luminosity a future collider might achieve.

As well as models with close to universal squark masses, it is well motivated to consider theories with stops relatively light compared to the first two generation squarks. In the case where the gluino is decoupled, the discovery potential of this model is no different to that studied in [148]. In a simplified model with a neutralino, it is found that pair production allows 5.5 TeV stops to be discovered, while 8 TeV stops can be excluded.

Differences between Dirac and Majorana models can arise if the gluino mass is not completely decoupled from the spectrum. In Dirac models the stop-anti-stop production cross section is only slightly suppressed compared to a Majorana model due to the main production mode being through an s-channel gluon. Thus if the gluino is out of kinematic reach and the only way to produce stops is through pair production, then we expect only a slight reduction in sensitivity in Dirac models compared to a Majorana model.

However, this could change if stops and gluinos are both kinematically accessible. Since gluino production is larger in Dirac models, stop production through gluino decay would be more important in this case. As the stop masses are varied, it is expected that the bound on gluino masses will be at least as strong as that obtained when all squarks are decoupled, giving us a lower limit on the discoverable parameter space. A dedicated analysis of these scenarios at a 100 TeV collider, along the lines of the study of LHC search carried out in [149], would be worthwhile.

The discovery potential for sgluons depends on details of the pattern of superpartner masses. Decays to a squark-anti-squark pair are typically dominant if they are kinematically allowed, and otherwise decays to a pair of gluinos or a quark-antiquark pair though a loop of squarks can be significant. In the case of decays to quark-antiquark pairs, the rate is suppressed by the mass of the quark, so a substantial proportion of events involve top quarks. This leads to the interesting possibility of searching for events with same sign top quarks [135], which is reasonably easy to distinguish from SM backgrounds. Studies relevant to the LHC have been carried out [150–156], and assuming a model where sgluons decay mostly to tops, LHC searches rule out sgluon masses up to the region of 700 GeV. Since, in most of the parameter space of motivated models, sgluons do not lead to the dominant discovery and exclusion potential we do not consider them further in our present collider simulations. However, if gluinos or squarks were to be discovered they would be a very exciting state to search for, not least because their presence would be a very strong hint that gluino masses were at least partially Dirac.

We stress that our analysis and simplified model nowhere near covers the full range of possible models and signatures. For example, it is plausible that the spectrum could include a number of light higgsinos. These can lead to squarks decaying via a cascade, potentially weakening our search signal, but these can give other signatures involving photons or leptons, as pointed out in [85]. Our assumption of a light LSP may also not hold, and if the LSP mass is instead a significant fraction of the squark or gluino mass the sensitivity could be significantly weakened [85]. Further, many well motivated Dirac gaugino models have a gravitino LSP, and if decays to this are slow on collider timescales the expected signals could be altered dramatically.

2.3 Higgs mass and fine tuning in Dirac gaugino models

2.3.1 Higgs sector

In the MSSM, the tree level mass of the lightest neutral Higgs is constrained to be below the Z boson mass and enhancing it to the observed value [8, 9] requires large radiative

corrections from the stops. In a model with gauginos and first generation squarks above 2 TeV and light higgsinos, the lightest stop masses allowed are about 1.7 TeV assuming maximal stop mixing [75]. However, if the A terms are small, large stop masses of about 10 TeV are needed. Extra contributions to the Higgs quartic self coupling can relax the need for large radiative corrections. This happens in the NMSSM, which has a term $\lambda_S \hat{S} \hat{H}_u \hat{H}_d$ in the superpotential [157]. In this case very light stops are possible. For $\lambda_S > 0.7$ the stops can be as light as 500 GeV, although in some parameter ranges this leads to λ_S running non-perturbative at an intermediate scale [158, 159].

In Dirac gaugino models, if the operator in Eq. (1.30) is the only source of supersymmetry breaking, the equations of motion set the D-terms for the SM gauge interactions $D_i \equiv 0$. Consequently, the tree level Higgs quartic, and its tree level mass, vanish identically. However, this is no longer the case if the terms in Eq. (1.33) are present, and the suppression can be reduced if the soft masses for the singlet S and the triplet T are large enough. The suppression is also ameliorated if the gaugino masses are a mix of Dirac and Majorana. Models with entirely Dirac gaugino masses have an R-symmetry in the gauge sector. This may or may not be respected by the Higgs sector, leading to different ways to raise the Higgs mass to 125 GeV.[1]

If the R-symmetry is broken in the Higgs sector, there can be couplings between the singlet or the triplet adjoint and the Higgs

$$W \supset \lambda_S \hat{S} \hat{H}_u \cdot \hat{H}_d + \lambda_T \hat{H}_d \cdot \hat{T} \hat{H}_u \ . \tag{2.3}$$

These enhance the tree level Higgs mass at small $\tan\beta$ by an NMSSM-like term proportional to the couplings $\lambda_{S,T}$, competing with the suppression of the D-term Higgs quartic [160]. A radiative contribution from the stops is still typically needed, though stop masses below 1 TeV may be sufficient depending on the value of the other parameters. Dirac gluino and Wino masses can be large without disrupting this conclusion, but the Dirac Bino is bounded to be below a few hundred GeV because it mixes dangerously with the lightest Higgs, reducing its mass. As a side effect, this mixing will lead to a Majorana neutralino.

On the other hand, if the R-symmetry is preserved in the Higgs sector, extra inert Higgs-like doublets $R_{u,d}$ must be introduced to obtain a viable model, since the standard

---

[1] In both the cases with preserved or broken R-symmetry in the Higgs sector, the new couplings break custodial symmetry, potentially leading to large contributions to the EW precision observables. In particular the ρ parameter leads an upper bound on the triplet vacuum expectation value of $|v_T| \lesssim 4$ GeV.

μ term is forbidden.[1] The extra doublets can couple through R-symmetric μ-type and trilinear terms

$$
\begin{aligned}
W \; \supset \; & \mu_u \, \hat{R}_u \cdot \hat{H}_u + \mu_d \, \hat{R}_d \cdot \hat{H}_d + \lambda_u \, \hat{S} \, \hat{R}_u \cdot \hat{H}_u \\
& + \; \lambda_d \, \hat{S} \, \hat{R}_d \cdot \hat{H}_d + \Lambda_u \, \hat{R}_u \cdot \hat{T} \, \hat{H}_u + \Lambda_d \, \hat{R}_d \cdot \hat{T} \, \hat{H}_d \; .
\end{aligned}
\tag{2.4}
$$

However, the extra couplings $\lambda_{u,d}$ and $\Lambda_{u,d}$ do not alleviate the depletion of the D-terms. For example, in the limit where $\lambda = \lambda_d = -\lambda_u$, $\Lambda = \Lambda_u = \Lambda_d$, $\mu_u = \mu_d = \mu$, and the vacuum expectation values of the singlet and triplet scalar adjoints $v_S \simeq v_T \simeq 0$, the tree level Higgs mass is

$$
m_{h,\text{tree}}^2 = m_Z^2 \cos^2 2\beta - v^2 \left(\frac{(g_1 m_{D_1} - \sqrt{2}\lambda\mu)^2}{4(m_{D_1})^2 + m_S^2} + \frac{(g_2 m_{D_2} + \Lambda\mu)^2}{4(m_{D_2})^2 + m_T^2} \right) \cos^2 2\beta \; ,
\tag{2.5}
$$

where m_{D_1} and m_{D_2} are the Dirac gaugino masses and m_S and m_T are the masses of the real parts of the scalar adjoints before EW symmetry breaking. Therefore the tree level upper bound is even stronger than in the MSSM, and radiative corrections are vital. At one loop the most relevant corrections come from four powers of the couplings λ and Λ. The leading contribution is [2] (see also [164, 165])

$$
\begin{aligned}
\Delta m_h^2 \; = \; & \frac{2v^2}{16\pi^2} \left[\frac{\Lambda^2 \lambda^2}{2} + \frac{4\lambda^4 + 4\lambda^2\Lambda^2 + 5\Lambda}{8} \log \frac{m_{R_u}^2}{Q^2} \right. \\
& + \left(\frac{\lambda^4}{2} - \frac{\lambda^2\Lambda^2}{2} \frac{m_S^2}{m_T^2 - m_S^2} \right) \log \frac{m_S^2}{Q^2} \\
& + \left(\frac{5}{8}\lambda^4 + \frac{\lambda^2\Lambda^2}{2} \frac{m_T^2}{m_T^2 - m_S^2} \right) \log \frac{m_T^2}{Q^2} \\
& - \left(\frac{5}{4}\lambda^4 - \lambda^2\Lambda^2 \frac{m_{D_2}^2}{m_{D_1}^2 - m_{D_2}^2} \right) \log \frac{m_{D_2}^2}{Q^2} \\
& \left. - \left(\lambda^4 + \lambda^2\Lambda^2 \frac{m_{D_1}^2}{m_{D_1}^2 - m_{D_2}^2} \right) \log \frac{m_{D_1}^2}{Q^2} \right] \; .
\end{aligned}
\tag{2.6}
$$

The form of these is analogous to those from the stop and if $|\lambda| \sim |\Lambda| \sim 1$ the new terms can give a significant contribution.[3] For large couplings, $\Lambda_u = \Lambda_d \sim 1 \sim -\lambda_u = -\lambda_d$, and light higgsinos with mass around 300 GeV, it is possible to obtain the correct Higgs

---

[1]Models of Dirac gaugino without the μ term [161] or where the μ term is generated as in the NMSSM are also possible [162], as are models where SM-like Higgs state is not the lightest scalar, increasing its tree level mass [163].

[2]In the limit where $\lambda = \lambda_d = -\lambda_u$, $\Lambda = \Lambda_u = \Lambda_d$, $\mu_u = \mu_d = \mu$ and $v_S \simeq v_T \simeq 0$.

[3]However the condition $|\lambda| \sim |\Lambda| \sim y_t$ may lead to a loss of perturbativity at low scales [164].

mass for stops as light as 300 GeV (not necessarily ruled out by the LHC if they have a compressed spectrum). A beneficial feature is that the adjoint fields do not reduce the Higgs mass at two loop, as the stop contribution proportional to α_s does.

In conclusion, the physical Higgs mass leads to significant constraints on the form of viable models, especially in theories with Dirac gauginos. However, for all gluino and stop masses not ruled out by the LHC, models exist in which a 125 GeV Higgs is possible. Therefore none of the parameter space of discoverable strongly interacting states studied in Section 2.2 is directly excluded, although in R-symmetric Dirac models with light stops fairly large dimensionless coupling constants are required.

2.3.2 Fine tuning

The fine tuning of a given low energy spectrum is only well defined once a UV complete theory is specified, such that the underlying parameters that can be varied are known. For example, there may be extra tuning hidden in the UV theory, or alternatively the true tuning might be reduced by particular correlations between parameters that from the low energy perspective appear independent.[1] Despite these caveats, it is interesting to make some naive estimates of the tuning in the regions of parameter space probed by the LHC and future colliders.

In the MSSM, at large $\tan\beta$, the EW scale is fixed by the relation

$$M_Z \simeq -2\left(m_{hu}^2 + |\mu|^2\right) \ , \tag{2.7}$$

where m_{hu}^2 is the soft mass squared for the up type Higgs, and the physical Higgs mass m_{h0} is equal to M_Z at tree level, and increased by radiative corrections.

If the mass of the stops is significantly above the EW scale there are large radiative corrections to the soft mass squared of the up type Higgs through a term in the RGEs proportional to the top quark Yukawa. Similarly, a heavy gluino leads to a large contribution to m_{hu}^2 at two loops, through the stop. As a result, obtaining a low EW scale requires an unnatural cancellation of terms in Eq. (2.7), which can be quantified by the fine tuning

$$\Delta^{-1} = \frac{\partial \log m_{h0}^2}{\partial \log p_i} \ , \tag{2.8}$$

where p_i are the UV parameters of the theory that can be varied independently.

Because of the large coupling in the RGE, even for low scale mediation the low scale stop mass typically ends up close to the gluino mass. The LHC has already set strong

---

[1]The latter however raises concerns about whether assuming a UV model with such helpful correlations is itself an additional tuning.

bounds on the gluino mass. Consequently, regions of parameter space with 2 TeV stops, heavy enough to produce a 125 GeV Higgs, are typically no more tuned than those with lighter stops. Models with very light stops in special parts of parameter space that are not excluded by searches, for example close to the top mass, may even be more tuned, due to the extra cancellations needed to keep a second scalar light [166].

In Natural SUSY models the first two generation squarks cannot be made arbitrarily heavy without introducing further tuning. Their soft masses $m_{1,2}^2$ (which are assumed close to degenerate) feed into the RGE for the stop mass squared at two loops, driving it towards tachyonic values through a term in the RGE

$$\frac{dm_{\tilde{t}}^2}{dt} \supset \frac{8\alpha_3^2}{3\pi^2} m_{1,2}^2 \ . \tag{2.9}$$

Depending on the mediation scale it is possible to raise the first two generation squark masses a factor of roughly 10 to 20 above the gluino mass (i.e. the typical mass of the stop) without making the tuning of the theory worse. In extended models, for example the NMSSM, the Higgs potential is modified and Eq. (2.7) does not hold. In some circumstances, for example if there is a large coupling $\lambda \hat{S} \hat{H}_u \hat{H}_d$ to a singlet $\hat{S}$, this can reduce the sensitivity of the EW scale to the Higgs soft mass squared parameter. However, in this case the model involves extra tuning from the requirement that the Higgs properties closely resemble those of the SM Higgs [167].

In models of Dirac gauginos, the dependence of the EW scale on the up type Higgs mass remains close to that of Eq. (2.7) [164]. There is a tuning from the gluino mass associated to the finite contribution to the stop mass of Eq. (1.32), which feeds into the up type Higgs mass. However, this contribution is enhanced only by two relatively small logarithms $\log m_{Re(A)}^2/m_{\tilde{g}}^2 \times \log m_{\tilde{g}}^2/m_{\tilde{t}}^2$, unlike the MSSM where the gluino tuning varies with the mediation scale as $\log^2 m_{med}^2/m_{\tilde{t}}^2$. This raises the hopes that relatively heavy gluinos may be possible without introducing excessive tuning.[1] There is also a finite contribution to the Higgs soft mass from the Wino and Bino (assuming that these also have dominantly Dirac masses). For ratios of Dirac gaugino masses coming from typical models this leads to less tuning than that from the gluino.

Additionally, a soft mass for the imaginary part of the adjoint from Eq. (1.33) contributes to the running of the squark masses at two loops

$$\frac{dm_{\tilde{t}}^2}{dt} \supset \frac{2\alpha_3^2}{\pi^2} m_{\phi 3}^2 \ . \tag{2.10}$$

---

[1]Models based on Scherk-Schwarz SUSY breaking, which can have very small EW tuning, also feature Dirac gauginos [168, 169].

For large sgluon masses this can be important, especially since the additional matter in Dirac models results α_3 being larger at high scales than in the MSSM.

To study the fine tuning as a function of the gluino and stop masses in models with a viable low energy spectrum, we fix $m_{\phi 3}$ at the mediation scale such that the low scale mass of the imaginary part of the sgluon is equal to the gluino mass. There may be additional tuning to achieve this in an actual SUSY breaking and mediation mechanism, since as discussed it is often a loop factor too large. However we do not attempt to quantify this in our measure of tuning. While it is possible that the stop mass is determined solely by the gluino mass and the negative RG contribution from the sgluon, such a setup does not allow for squark masses comparable to the gluino mass at a low scale (even allowing the mediation scale to vary). Instead we allow an extra stop soft mass generated directly at the mediation scale, opening up the low energy parameter space. Such a mass is not supersoft and gives a logarithmically divergent contribution to the Higgs mass squared parameter. However, in parameter ranges where the stop mass is dominantly generated by the gluino multiplet the direct stop soft mass is small by construction, so does not make the tuning significantly worse.

Under these assumptions we plot the fine tuning for Majorana and Dirac models in Fig. 2.10 as a function of the low scale gluino stop masses. We add the individual tunings in quadrature,

$$\Delta = \sqrt{\Delta_{\tilde{t}}^2 + \Delta_{\tilde{g}}^2} \, , \tag{2.11}$$

where $\Delta_{\tilde{t}}$ and $\Delta_{\tilde{g}}$ are the tunings from the stop and gluino parameters respectively. We also distinguish between regions of parameter space where the stop mass squared parameter at the mediation scale is negative (assuming the stop mass is degenerate with the other squarks at the mediation scale). In these parts of parameter space there are possible concerns about whether the universe could be trapped in a colour-breaking vacuum at early times (although this may not be the case [170]). Because of the sgluon and stop soft masses the tuning depends on the mediation scale even in the Dirac scenario.

Comparing with the projected collider reach studied in Fig. 2.8, we see that in scenarios with approximately universal squarks masses of the same order as the gluino mass, a 100 TeV collider can exclude models with tuning of one part in 10,000 for both Dirac and Majorana gluinos assuming low scale mediation and up to one part in 100,000 for high scale mediation. Under our assumptions about the tuning, in this region there is a slight improvement in tuning in Dirac gluino models, but given the possible extra model building tunings required this is certainly not significant.

In parts of parameter space where the gluino is much heavier than the stops, Dirac models are less tuned than Majorana models especially if the mediation scale is high. This
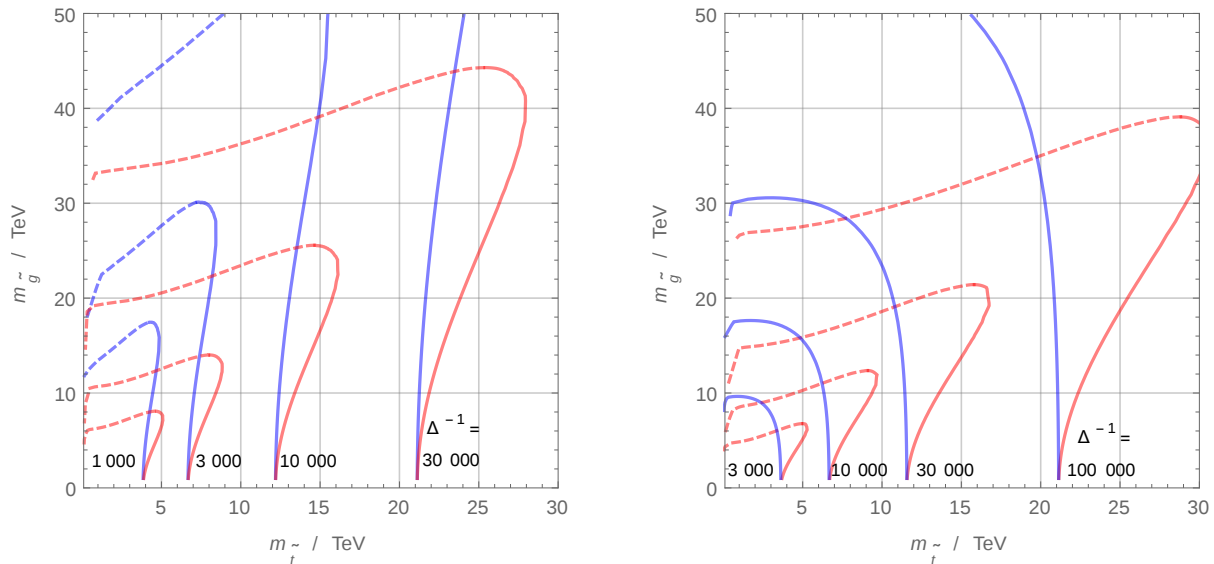
Figure 2.10: *Left:* Contours of fine tuning for Dirac gluino models (blue) and Majorana models (red) assuming a mediation scale of 10^6 GeV. The contour labels apply to both the Dirac and Majorana models, whose tuning coincides in the limit of small gluino mass. In regions with a dashed line the stop mass at the mediation scale must be tachyonic (assuming universal squark masses). *Right:* The same plot for a mediation scale of 10^{16} GeV.

reflects the supersoftness of the gluino contribution to squark masses. The boundary between dashed and solid lines for the Dirac contours in Fig. 2.10 corresponds to the stops being massless at the mediation scale. If the mediation scale is low and the squark masses are approximately universal, along this line in parameter space Dirac models with tuning of approximately one part in 1,000 will be excluded. The same low scale soft masses correspond to a tuning of almost one part in 10,000 in Majorana models. Further, the collider reach is significantly stronger for Majorana models in this parameter regime allowing models that are even more tuned to be discovered or excluded.

Natural SUSY models, with squarks far heavier than the stops, can lead to weaker discovery and exclusion potential in the gluino-stop mass plane than models with universal squark masses. Such models might therefore escape being observed with a 100 TeV collider while still having not enormous tuning. However, comparing our discussion in Section 2.2 with Fig. 2.10, we see that relatively strong searches for a gluino even in the case of decoupled squarks leads to significant constraints. For low scale mediation, Majorana Natural SUSY models will be probed up to a tuning of one part in 3,000 and Dirac models up to similar levels depending on the efficiency of searches for stops. For high

scale mediation, the longer RG flow means a Majorana gaugino has even more impact. Models with tunings of one part in approximately $30,000$ will be constrained in this case, while Dirac models with tuning of one part in 10,000 will be probed.

Chapter 3

SUSY from DM direct detection experiments

Dark matter direct detection experiments are based on the idea of [171] that exploits the recoil energy from dark matter particles scattering on nuclei. If the dark matter has interactions with the SM quarks or gluons, these interactions imply the possibility of the scattering on nuclei and the release of a certain amount of energy, which is measured through the ionisation produced by the collisions with electrons. This recoil energy is given by

$$E_R = \frac{|\vec{q}|^2}{2m_A}, \tag{3.1}$$

where $|\vec{q}|^2 = 2\mu_{\chi A}^2 v^2 (1 - \cos\theta)$, v is the DM velocity with respect to the target nucleus, θ is the scattering angle in the centre of mass frame, and $\mu_{\chi A} = m_\chi m_A / (m_\chi + m_A)$ is the reduced mass of the system of the DM and the nucleon mass m_A. Therefore, the measure of the recoil energy can signal the occurrence of a DM particle scattering on nuclei. The differential event rate R per recoil energy is

$$\frac{dR}{dE_R} = N_T \int_{|\vec{v}| > v_{\min}} |\vec{v}| \frac{d\sigma_{\chi A}}{dE_R} dn_{DM}, \tag{3.2}$$

where N_T is the target nuclei number density, $\sigma_{\chi A}$ is the scattering cross section of the DM with a nucleon A and n_{DM} is the DM density. It is possible to determine the scattering cross section from the interaction between the DM and the quarks and gluons, and the nuclear matrix elements. For typical Majorana WIMP candidates, such as the MSSM neutralino, the interaction can be spin-independent or spin-dependent, corresponding to interactions mediated by scalar or pseudo-vector, respectively. Spin dependent interactions are usually subdominant, because the DM scatters only on unpaired nucleon in the

3. SUSY from DM direct detection experiments
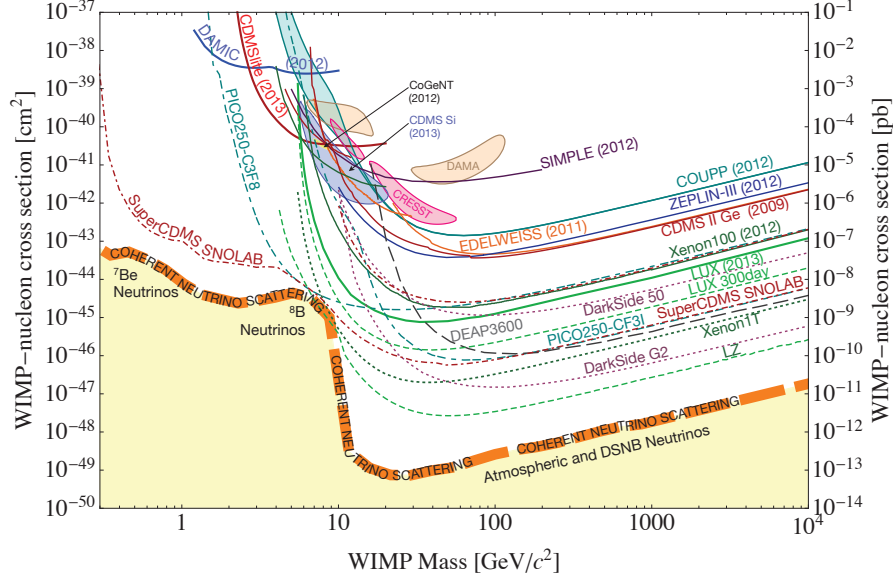
Figure 3.1: Current bounds (solid lines), hints for a DM signal (shaded closed contours) and future experimental reach (dashed lines) for DM-nucleon spin independent cross section in direct detection experiments. The approximate region, where neutrino coherent scattering from solar, atmospheric and supernova neutrinos will dominate, is also shown [172]. Figure taken from [173].

nucleus. On the other hand, spin independent scattering happen coherently for all the nucleons in the target, giving more stringent experimental bounds.

The total event rate turns out to be proportional to $\propto \lambda \mu_{\chi A}^2 / m_\chi$, where λ is the coupling between the DM and the quarks or gluons, such that the total number of observed events translates in a limit on the coupling

$$\lambda \propto m_\chi / \mu_{\chi A}^2. \tag{3.3}$$

In Figure (3.1) current bounds (solid lines), hints for a DM signal (closed contours) and future reach (dashed lines) of several dark matter direct detection experiments are shown. The dependence of λ in Eq. (3.3) explains the exclusion curves of Figure 3.1: for DM much lighter than the nucleus mass, the excluded coupling is proportional to m_χ^{-1}, while if the DM is heavier than m_A, the excluded coupling goes as the DM mass m_χ. Therefore

the exclusion is stronger for a dark matter particle with mass $m_\chi \simeq m_A$. Moreover, the presence of multiple experiments with different target mass may provide better constraints on the DM.

From Figure 3.1 we also notice that direct detection experiments are highly sensitive to DM mass between 10 GeV and few TeV. However, if the WIMP nucleon cross section is too small, the neutrino background would dominate over the dark matter signal [172].

In the following sections, we will show the interplay between DM direct detection experiments and collider searches for models of split SUSY (section 3.1) and models of Dirac gauginos (section 3.2).

3.1 Split SUSY

In split SUSY, dark matter searches depend on the low energy electroweakino spectrum. We focus on two representative scenarios: models with universal gaugino masses and models of anomaly mediated SUSY breaking. These scenarios cover all the relevant dark matter candidates in split SUSY, i.e. pure higgsino, pure Wino, $\tilde{h}/\tilde{W}$, $\tilde{h}/\tilde{B}$ and $\tilde{B}/\tilde{W}$.

The scattering cross section of the neutralino with nucleons is calculated using the effective Lagrangian describing the interaction among neutralinos, quarks and gluons in the limit of low relative velocity [174–176]. The spin independent scattering cross section of the neutralino with a nucleon N can be expressed in a simple way as

$$\sigma_N^{SI} = |\text{Higgs} + \text{gluon} + \text{twist-2}|^2. \tag{3.4}$$

Higgs, twist-2 and gluon refer to the diagrams in figure 3.2. The Higgs diagrams (figure 3.2(a)) are generated by the scalar-type effective operators $\overline{\tilde{\chi}^0}\,\tilde{\chi}^0\bar{q}q$ and $\overline{\tilde{\chi}^0}\,\tilde{\chi}^0 G_{\mu\nu}^a G^{a\mu\nu}$ and their contribution to the amplitude is proportional to the $\tilde{\chi}^0\tilde{\chi}^0 h$ coupling:

$$c_{h\tilde{\chi}\tilde{\chi}} = (N_{12} - N_{11}\tan\theta_W)(N_{13}\cos\beta - N_{14}\sin\beta), \tag{3.5}$$

where N_{1i} are the elements of the matrix that diagonalise the neutralino mass matrix. The first subscript of N_{1i} is an index in the mass basis (ordered from the lightest to the heaviest), while the second in the interaction basis ($\tilde{B}, \tilde{W}, H_u, H_d$). The twist-2 diagram (figure 3.2(b)) plays an important role in the computation of the cross section because it contributes to the amplitude with opposite sign with respect to the other diagrams. This will lead to some accidental cancellation. The gluon contributions (figure 3.2(c)) are of the same order of the one-loop diagrams because of the presence of a factor $1/\alpha_s$ that comes from the calculation of the gluon matrix element.

(a) Higgs.   (b) Twist-2.

(c) Gluon.
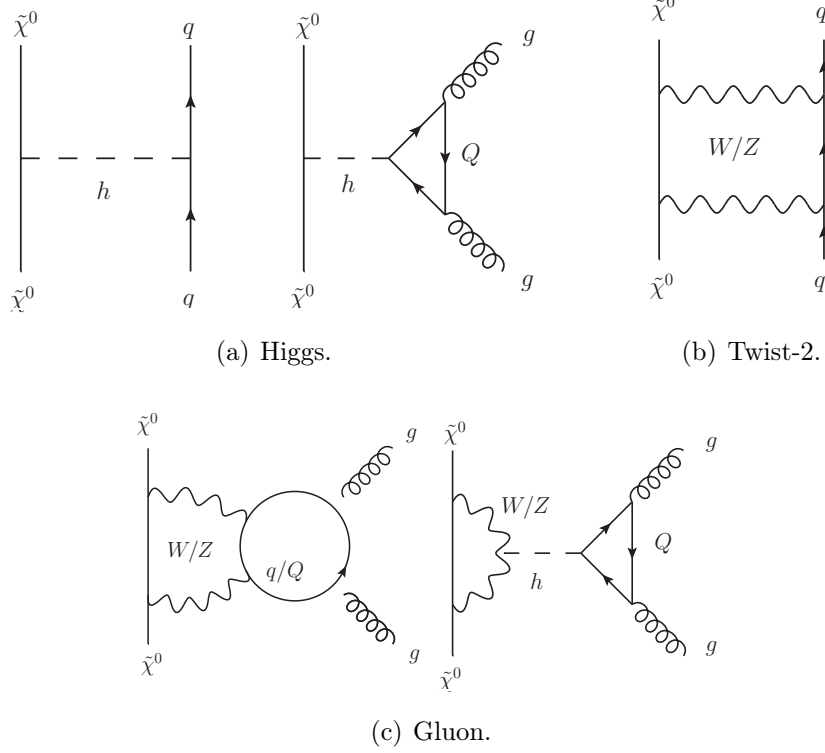
Figure 3.2: Diagrams that contribute to the neutralino nucleon cross section. The diagrams with Z exchange are relevant only for the Spin Dependent cross section.

For the computation of the cross section we used leading order formulae [174–176]. The uncertainty has been estimated by taking into account the uncertainties from hadronic matrix elements and those from known 1-loop QCD corrections. The order of magnitude of the latter is comparable with [177–180].

In the rest of the section we only focus on neutralino dark matter that is thermally produced. The relic density was computed with DarkSusy [181, 182] and the package DarkSE [183] to compute the Sommerfeld effect. For the value of the relic density we used the Planck result, $\Omega h^2 = 0.1196 \pm 0.0031$ [184].

3.1.1   Models with universal gaugino masses

The first scenario we consider is split SUSY with universal gaugino masses. Higgsinos can be either light or heavy and are left as free parameters. In general we have two free parameters, μ and M_0 ($M_i \propto \alpha_i M_0$) which are further constrained to one by requiring
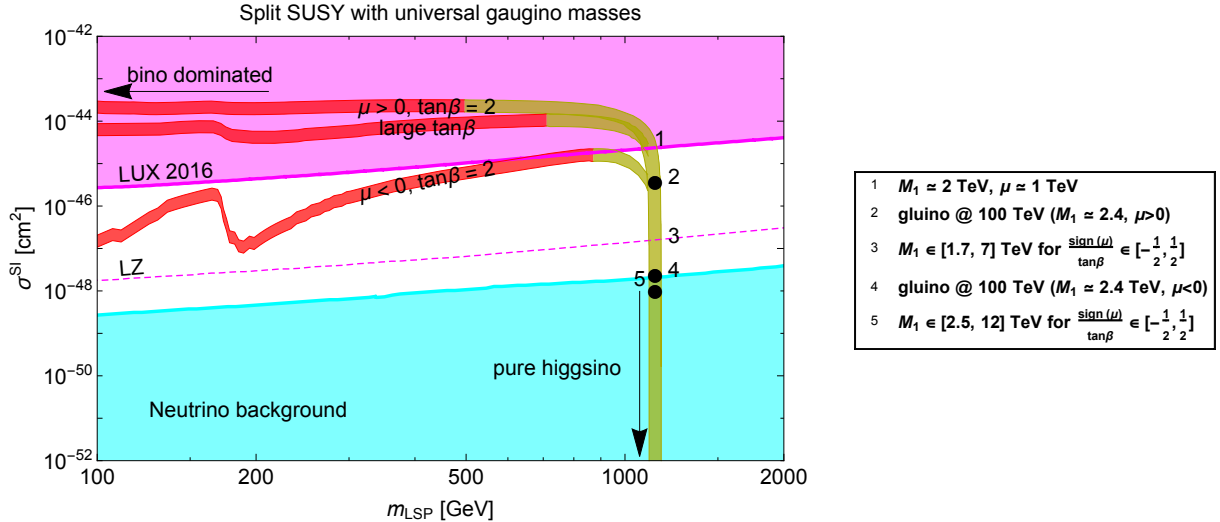
Figure 3.3: Spin independent neutralino-nucleon scattering cross section (σ^{SI}) requiring $\Omega h^2 = 0.1196 \pm 0.0031$ in the universal gaugino masses model (red is Bino-like, yellow is higgsino-like LSP). The magenta area is the current bound by LUX, the dashed magenta line is the projected reach of LZ. The neutrino background, where direct detection experiments lose sensitivity, is shaded in light blue. The numbers are explained in the legend on the right panel.

$\Omega_{DM} = \Omega_{\exp}$. This leads to a phenomenology in which the LSP can be either the higgsino (when $|\mu| < M_1$) or the Bino (when $|\mu| > M_1$).

In figure 3.3 we show the spin independent cross section for the scattering of neutralinos on nucleons. The magenta shaded area shows the region excluded by LUX [185]. The dashed magenta curve set the projected reach for LZ [186, 187]. The light blue area represents the irreducible neutrino background [172]. The three red/yellow curves represent the spin independent cross section requiring the correct relic density for $\mu > 0$, large $\tan\beta$ and $\mu < 0$ from top to bottom respectively (in the following we set the gaugino masses positive). For large $\tan\beta$ the sign of μ is irrelevant: the curve in the middle is the limit for both positive and negative scenario. The red colour of each curve represents a Bino-like LSP, while the yellow a higgsino-like LSP. A Bino needs to mix with an higgsino in order to have sizeable annihilation cross section and therefore the correct relic density. In this region the cross section is dominated by the Higgs diagrams. The relic density constraint gives a relation between μ and M_1, depending on $\tan\beta$ and on the sign of μ (as it is shown in figures 3.4). In particular for $\mu < 0$ the two states are close enough and therefore coannihilation effects become relevant. At low LSP masses in the negative

51

branch, the mixing is not maximal and it is given by

$$
\begin{aligned}
N_{11} &\simeq 1 - \frac{N_{13}^2}{2} - \frac{N_{14}^2}{2} \\
N_{13} &\simeq -\frac{\sin\theta_{\mathrm{w}} M_Z}{M_1^2 - \mu^2}(\mu\sin\beta + M_1\cos\beta) \\
N_{14} &\simeq \frac{\sin\theta_{\mathrm{w}} M_Z}{M_1^2 - \mu^2}(\mu\cos\beta + M_1\sin\beta),
\end{aligned}
\tag{3.6}
$$

while the cross section is proportional to $|M_Z(M_1 + \mu\sin 2\beta)/(\mu^2 - M_1^2)|^2$. As the LSP mass increases, the relic density constraint needs more mixing and more coannihilation, the two states become more degenerate and the cross section increases (figure 3.3). Also for $\mu > 0$ at small LSP mass there is small mixing between the Bino and the higgsino. In this region coannihilation is not present. The relic density constraint gives a relation between the parameter μ and M_1 such that the nucleon-neutralino scattering cross section is constant.

Continuing the description of figure 3.3, the $t\bar{t}$ threshold is visible only for $\mu < 0$ because for positive μ there is no coannihilation and the dominant annihilation channel is into gauge bosons. For $m_{LSP} > m_t$ (also the annihilation in $t\bar{t}$ is present), in order to get the correct relic density the two states have to become less degenerate such that the new annihilation channel is balanced by the weaker coannihilation effect.

Once the region of maximal mixing is reached, the $m_{LSP} \simeq 500$ (900) GeV for positive (negative) μ respectively, we have $(N_{11}, N_{12}, N_{13}, N_{14}) \simeq (1/\sqrt{2}, 0, 1/2, \mp 1/2)$, where the $\mp$ sign refers to the cases $\mu \simeq \pm M_1$. Thus the cross section is proportional to $|\cos\beta + \mathrm{sign}(\mu)\sin\beta|^2$ and it is constant for both signs of μ. The suppression in the negative μ branch is again due to the sign of μ and the value of $\tan\beta$.

Recent results by LUX [185] already exclude the region with positive μ independently on the value of $\tan\beta$. The only available parameter space is for negative μ and small $\tan\beta$. When the higgsino becomes the LSP and $m_{\tilde{B}}$ become heavier and heavier, the Higgs exchange become suppressed and the twist-2 and gluon diagrams will eventually dominate. However, their contribution is suppressed by a factor 10 due to a cancellation between the gluon and twist-2 diagrams. When the scale of the LSP is such that coannihilation does not help anymore to maintain the correct relic density, the mixing is

$$
N_{11} \simeq \frac{(\sin\beta \pm \cos\beta)\sin\theta_{\mathrm{w}} M_Z}{\mp M_1\sqrt{2}} \qquad N_{13} \simeq \pm\frac{1}{\sqrt{2}} \qquad N_{14} \simeq \frac{1}{\sqrt{2}},
\tag{3.7}
$$

the Higgs diagrams are suppressed by M_1 and the cross section decreases. Figure 3.3 shows also the indirect reach from gluino searches: a 16 TeV gluino corresponds to $M_1 \simeq 2.4$

Split SUSY with universal gaugino masses
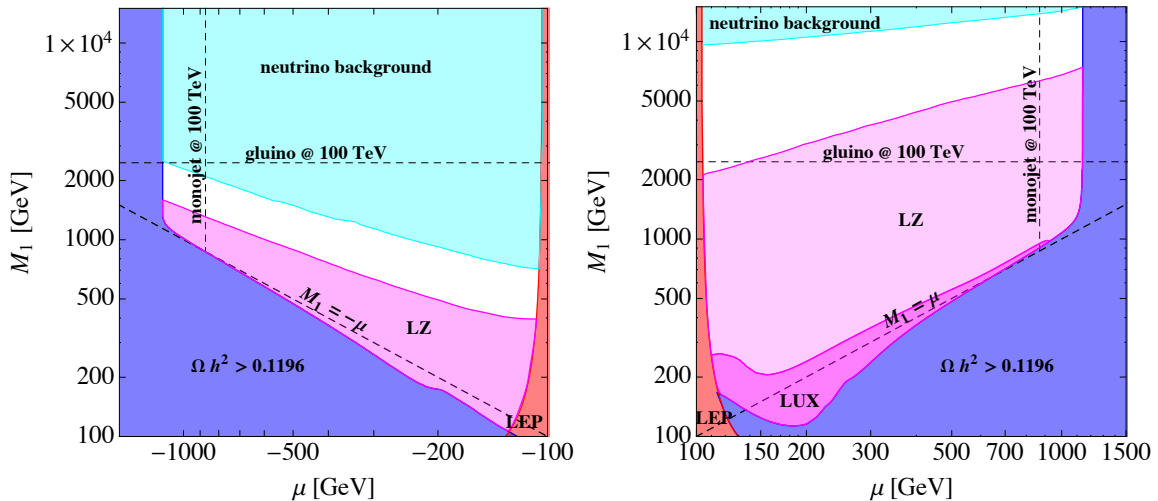
Figure 3.4: Region in the (μ, M_1) allowed by direct chargino searches at LEP (excluded in red) and by the requirement that the neutralino does not exceed the CDM relic density (excluded in blue). The left (right) panel are for negative (positive) μ, respectively. The colour shading for actual bounds, future reach and background for direct detection are the same as in the previous figure.

TeV. This is the reach for a 100 TeV collider in the (m_{LSP}, σ^{SI}) plane. However, direct detection is stronger for $\mu > 0$: indeed LZ can reach $M_1 \simeq 7$ TeV corresponding to gluinos around 42 TeV. On the other hand the curve for negative μ is not bounded by LUX and LZ will explore pure higgsino states with $M_1 \lesssim 1.7$ TeV. The gluino reach for a 100 TeV collider is stronger in this scenario. Continuing along the yellow curve, there is a value of M_1 such that the Higgs contribution is of the same order of the gluon and twist-2 diagrams and the cross section vanishes. Due to the cancellation uncertainty becomes $\mathcal{O}(1)$ and we cannot tell where exactly the cancellation happens. While the Bino completely decouples ($m_{\tilde{B}} = \mathcal{O}(100 \text{ TeV})$), the Higgs amplitude vanishes and the cross section reaches the value of the pure higgsino case given by the gluon+twist-2 diagrams:

$$\sigma_N^{SI} \lesssim 10^{-48} \text{ cm}^2. \tag{3.8}$$

When the LSP does not contribute to the whole DM abundance, the interplay between collider and direct dark matter searches is better shown in figure 3.4. The dark blue area describes the region where the relic abundance exceeds the experimental value. The dark

Split SUSY with universal gaugino masses
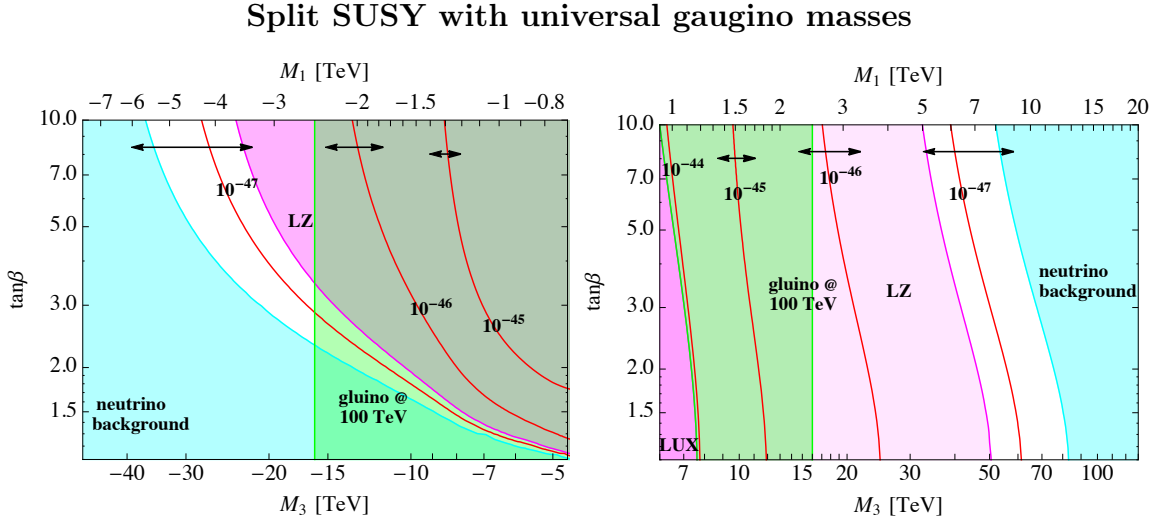
Figure 3.5: Contours of SI neutralino-nucleon cross section in [cm^2] for higgsino dark matter (red curves). The black arrows shows the uncertainty on the cross section. The parameter μ is fixed such that the lightest neutralino has the correct relic density. The colour shading for actual bounds, future reach and background for direct detection are the same as in the previous figure. The green shaded area shows the expected reach at a 100 TeV collider for gluino searches.

magenta is the bound by LUX, the light magenta region shows the reach of LZ and the light blue is the neutrino background. In red is the bound on charginos from LEP [188]. In the plot are shown also future reach from mono-jet searches ($m_{\chi_1^0} \simeq 870$ GeV, [120]) and the indirect reach coming from gluinos at a 100 TeV collider ($m_{\tilde{g}} \simeq 16$ TeV). According to the left panel of figure 3.4, for $\mu < 0$ thermal Bino-higgsino DM is not constrained by Direct Detection searches. Future experiments can however explore scenarios where $\mu \simeq -1.1$ TeV and $M_1 < 1.7$ TeV. Nonetheless the strongest reach in this kind of models would come from a 100 TeV collider: gluino pair searches have the potential to explore a large area of the parameter space, while mono-jet searches will not have enough sensitivity to explore pure thermal higgsinos. The right panel shows how the Direct Detection reach is stronger for $\mu > 0$.

The pure higgsino region is shown in figure 3.5 and it is interesting because it does not require the coincidence $|\mu - M_1| \ll |\mu|$ in order to explain the WIMP miracle. Figure 3.5 shows the dependence of $\tan\beta$ as a function of the gluino mass (and thus $M_1 = \alpha_1/\alpha_3 M_3$), for a dark matter particle with the correct relic density for $M_3 < 0$ and $M_3 > 0$ in the left and right panel respectively (now we fixed μ to be positive and the sign of M_3 can vary).
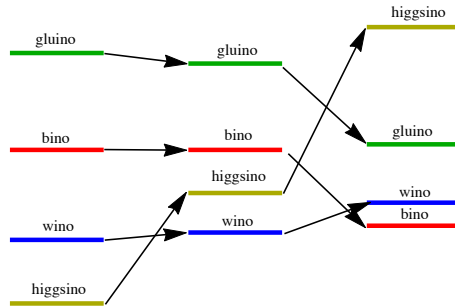
Figure 3.6: Spectrum of gauginos and higgsinos in Anomaly Mediation.

The value of the parameter μ has been fixed by requiring the correct relic density and it is approximately 1.1 TeV across the whole plot. The colour labelling is the same as in the previous figures except for the green region that denotes the reach for gluinos at a 100 TeV collider. The red curves represent the SI cross section, while the black arrows show the uncertainties on the cross section. We notice that the collider reach is weaker than the direct detection experiments for $M_3 > 0$, while in the other case it can be competitive.

3.1.2 Anomaly Mediation

In split SUSY with Anomaly Mediation [64, 65, 70] the physical gaugino masses are predicted in terms of the gravitino mass. The leading contributions to Bino and Wino masses come from one-loop anomaly mediation and threshold effects

$$M_{1,2} = \frac{\beta_{1,2}}{g_{1,2}} m_{3/2} + \frac{\alpha_{1,2}}{2\pi} \frac{(\tilde{m}^2 + \mu^2)\mu \tan\beta}{(\tan^2\beta + 1)\tilde{m}^2 + \mu^2} \ln\left[(1 + \tan^{-2}\beta)\left(1 + \frac{\tilde{m}^2}{\mu^2}\right) \right], \qquad (3.9)$$

where g_i is the corresponding gauge coupling, β_i its beta function, $m_{3/2}$ is the gravitino mass and $\tilde{m}$ is the scalar mass-scale. The gluino mass receives contributions only from anomaly mediation. In this scenario the scalars (except the SM-like Higgs) are heavy and close to the gravitino mass, while the gauginos are light. Higgsinos are not constrained.

Figure 3.6 shows the spectrum of split SUSY with anomaly mediation. Depending on the contribution of the higgsinos the nature of the LSP changes. Light higgsinos lead to a spectrum in which the higgsino is the LSP and the ratio between gauginos is $M_1 : M_2 : M_3 \simeq 3 : 1 : 9$. Scenarios in which the Wino is the LSP are allowed if the higgsino is heavier than the Wino. For very heavy higgsinos the threshold corrections in (3.9) dominate and the Bino become the LSP.
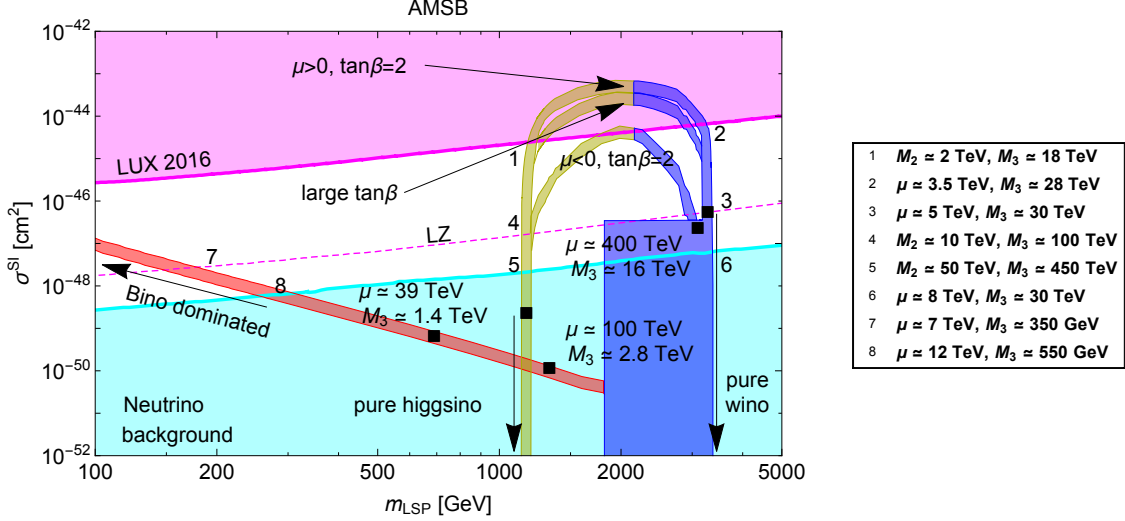
Figure 3.7: Spin independent nucleon-neutralino cross section in a split SUSY with anomaly mediation model (the red curve describe a Bino-like LSP, the yellow curve a higgsino-like and the blue one a Wino-like dark matter candidate). The magenta area is the actual bound by LUX, the dashed magenta line is the projected reach of LZ. The neutrino background is shaded in light blue. The numbers are explained in the legend on the right panel.

The model is entirely described in terms of four parameters: $m_{3/2}$, μ, $\tan\beta$ and $\tilde{m}$. However, the value of the Higgs mass gives a relation between $\tan\beta$ and $\tilde{m}$. In order to have heavy scalars compatible with the Higgs mass we choose $\tan\beta = 2$. We also discuss how the results change in the large $\tan\beta$ scenario.

In figure 3.7 we show the spin independent cross section that satisfies the relic density constraint. We start with the case $\mu < M_2$ and discuss the behaviour of the cross section and the bounds as the higgsino mass is increased. The yellow curve describes a mostly higgsino LSP state. At $m_{LSP} \simeq 1.1$ TeV the cross section behaviour is the same explained for the Universal Gaugino masses scenario. The neutrino background makes it difficult for future direct detection experiments to probe this region of the parameter space, while LZ will probe only anomaly mediated spectra with higgsino LSP and $M_2 \lesssim 10$ TeV. As M_2 approaches μ the coupling increases and so does the cross section. A 100 TeV collider may explore a very small region where $1.2 \lesssim |\mu| \lesssim 1.7$ TeV (see for example the gluino reaches of the top panels of figure 3.8). Continuing along the yellow curve of figure 3.7, when $\mu \sim M_2$ the mixing is maximal, the tree level Higgs exchange dominate and the LUX bounds apply. The recent LUX results [185] already exclude maximal Wino-higgsino mixing for positive μ. Moreover, for small $\tan\beta$ higgsino dark matter with $M_2 < 2$ TeV or Wino dark matter with $\mu < 3.5$ TeV are ruled out. On the other hand, Wino-higgsino

mixing for negative μ and small $\tan\beta$ will be probed by LZ. In this region the cross section is constant and the Higgs coupling is proportional to

$$(\cos\beta + \text{sign}(\mu)\sin\beta). \tag{3.10}$$

The lower curve represents the cross section for $\mu < 0$ which is suppressed by the sign of μ. At large $\tan\beta$ the sign of μ becomes irrelevant. Analogously to what happens for the pure higgsino case, the cross section decreases when $\mu \gg M_2$ and the LSP approaches the pure Wino state. Indeed now the mixing is given by $N_{12} \sim 1$,

$$N_{13} \simeq \frac{\cos\theta_{\mathrm{w}} M_Z}{|\mu|^2}(M_2\cos\beta + \mu\sin\beta) \qquad N_{14} \simeq \frac{\cos\theta_{\mathrm{w}} M_Z}{|\mu|^2}(M_2\sin\beta + \mu\cos\beta), \tag{3.11}$$

and the Higgs coupling becomes

$$-\frac{\cos\theta_{\mathrm{w}} M_Z}{|\mu|^2}(M_2 + \mu\sin 2\beta). \tag{3.12}$$

The cross section therefore decreases as the higgsino decouples from the Wino. In this regime the gluon and the twist-2 diagrams are also important. However, as for the higgsino case the gluon and the twist-2 amplitudes accidentally cancel suppressing their contribution by a factor 5. Going down along the blue curve there is a value of μ for which the cross section vanish because the Higgs diagrams cancel the gluon+twist-2 contributions. Due to $\mathcal{O}(1)$ uncertainties it is not possible to define exactly for which value of μ this cancellation happens. When the higgsino and the Bino are both decoupled, the cross section is estimated to be

$$\sigma_N^{SI} \lesssim 10^{-47}\ \mathrm{cm}^2. \tag{3.13}$$

If one keeps increasing the value of μ, with $M_2 \sim 3$ TeV in order to reproduce the correct relic density that provide a Wino dark matter candidate, the mass of the Bino-like neutralino decreases (see (3.9)). While the splitting between Wino and Bino decreases, the cross section increases because the Higgs diagrams become negligible with respect to the other contributions (N_{11} is negligible with respect to N_{12} and N_{13} and N_{14} are given by equation (3.11)). This is the top flat edge of the blue rectangle. In this region the LSP neutralino is a pure Wino, with M_1 closer and closer and μ decoupled. From the top right to the top left part of the blue rectangle, the value of M_1 ranges between 10 and 1.8 TeV, while the higgsino is decoupled and the LSP mass is given by the value of M_2. The mixing between Bino and Wino is always negligible for mass splitting larger than a GeV. Once $M_1 < M_2$ the Higgs diagrams, the only contributions to the cross section, become

AMSB
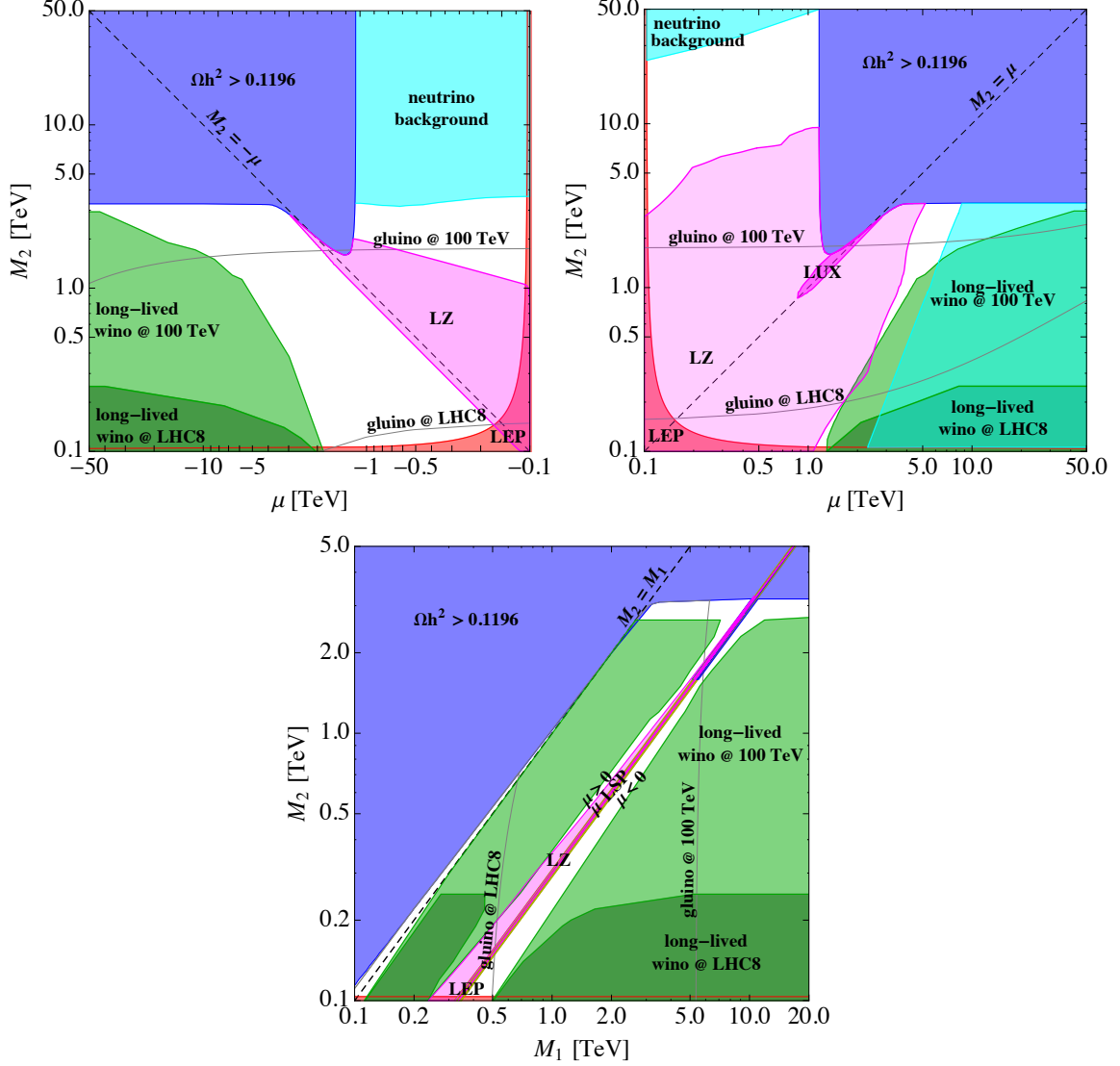
Figure 3.8: The parameter space region allowed by the requirement that the neutralino relic abundance does not exceed the relic density in the plane (μ, M_2) for $\mu < 0$ ($\mu > 0$) in the left (right) panel. The bottom panel shows the plane (M_1, M_2). Direct Detection and collider constraints and future reach are also shown.

suppressed by the large value of μ. In this region the neutralino is almost a pure Bino with the mixing given by (3.6). In this case in order to have the correct relic, the Bino must coannihilate with the Wino and therefore the splitting must be $\lesssim 30$ GeV. In order

to decrease the gaugino mass scale and maintain such splitting, μ has to decrease and thus the cross section increases, being the Higgs coupling given by

$$M_W \tan \theta_{\mathrm{w}} \frac{M_1 + \mu \sin 2\beta}{|\mu|^2}. \tag{3.14}$$

There is no top threshold in this case because the annihilation into $t\bar{t}$ is not the dominant contribution. A 100 TeV collider could be able to explore the whole region where the LSP is a mixed Bino/higgsino and Bino/Wino state from the LEP bound to $M_{LSP} \sim 3.1$ TeV (those reaches are better shown in the figure 3.8). Given the large value of μ, at large $\tan \beta$ the cross section is further suppressed.

The (μ, M_2) and the (M_1, M_2) planes are shown in figure 3.8. The upper panels show the (μ, M_2) planes for $\mu < 0$ (left) and $\mu > 0$ (right). The blue region is excluded by the requirement on the relic density. The dark and light green areas describe the constraints from long lived Winos at LHC8 and the future reach for a 100 TeV collider. The grey lines shows the bounds and reach on gluino pair searches. It is interesting to note that the direct detection reach is limited in the left panel, due to the suppression of the cross section for $\mu < 0$. On the right panel the two different searches are complementary. The bottom panel shows the plane (M_1, M_2), for both positive and negative μ. The colour coding is the same as in the upper plots. The yellow line that cuts the panel in two represents the area in which the higgsino is the LSP and it cuts the plane in a region with $\mu > 0$ (left) and $\mu < 0$ (right). The yellow region is strongly connected with the upper plots. The blue stripe overlapping the yellow line is a region in which M_1 is decoupled and it shows the crossing between the Wino LSP parameter space and the higgsino one. A large region of the parameter space could be probed at a 100 TeV collider, leaving unexplored just the narrow region corresponding to the pure Wino and higgsino cases.

3.2 Dirac gauginos

The viable dark matter candidates can change dramatically if gauginos have Dirac masses. In models of gauge mediation the gravitino can be a suitable dark matter candidate. However, similarly to the MSSM the possible collider signatures are highly model dependent, so we focus on the high mediation scale case where a neutralino is the LSP.

If there are additional chiral adjoints only for the SU(3) gauge group, while the other gauginos are Majorana and the Higgs sector is unchanged from the MSSM, viable dark matter candidates are the same as for the MSSM. For the purpose of a 100 TeV collider, such models simply change the relations between gluino searches and dark matter. It is

interesting that large hierarchies between the gluino and other gaugino masses can easily occur in this scenario, for example due to an approximately conserved R-symmetry. Such a spectrum relaxes the links between collider searches for coloured states and dark matter, which we discuss shortly. Similarly, if chiral adjoints are present for the $SU(2)$ and $U(1)$ groups, but the mediation is such that these gauginos are dominantly Majorana, the dark matter candidates are similar to the MSSM, with the extra possibility that the LSP could have a significant adjoint fermion component. New dark matter scenarios occur when the LSP is a combination of the MSSM-like gaugino and the adjoint fermion, and when the Bino and Wino in the MSSM are replaced with the corresponding adjoint fermion, leading to dark matter candidate with either Majorana or Dirac masses [93, 94, 102, 160, 189–193].

On the other hand, if the theory has an unbroken R-symmetry, neutralinos are a linear combination of the Bino/adjoint singlet (Dirac Bino), Wino/adjoint triplet (Dirac Wino), up and down higgsinos, and extra so-called R-higgsinos that must be introduced [85]. We take this scenario, called Minimal R-symmetric Supersymmetric SM (MRSSM), as a representative example to study Dirac gaugino masses and it is reviewed in Appendix A. Another motivated possibility is that the mediation mechanism is such that all the gaugino masses are dominantly Dirac, but the Higgs sector is that of the MSSM. The phenomenology of this case qualitatively follows that of the MRSSM. In these cases the Dirac nature of the gauginos has a large effect on direct detection searches.

In the following we study the relationship between DM direct and indirect detection experiments, relic density and collider reach for Dirac gaugino models. For our numerical results we get model inputs from the CalcHEP [194] output of SARAH [195], the mass spectrum and couplings are computed at one-loop with SPheno [196], and finally the relic density and direct and indirect detection rates are computed with MicrOMEGAs [197].

3.2.1 Direct detection and relic density

Direct and indirect dark matter detection experiments can be used to place bounds on the dark matter mass. The Dirac or Majorana nature of the lightest neutralino dramatically changes the interactions probed by direct detection experiments. For Majorana particles the vector interaction with quarks vanishes and the neutralino–nucleon cross section is suppressed. Therefore in the MSSM the dominant process for the spin independent cross section are Higgs and squark exchange, while Z exchange contributes only to the spin dependent cross section. Combining the relic density constraint [198] and bounds from direct detection experiments, in most models a significant part of the parameter space is ruled out already for Bino/higgsino and higgsino/Wino LSP, although there are still viable regions (Section 3.1 and Refs. [1, 199]). Moreover, indirect detection may set limits

on Wino dark matter with masses between 500 GeV and 3 TeV [200], although there are large astrophysical uncertainties.

In contrast, in models of Dirac gauginos the vector interaction of the Z exchange can lead to a large contribution to the spin independent cross section if the dark matter has a significant higgsino content [201]. In general the spin independent cross section with protons can be written as

$$\sigma_{SI} = \left(\frac{m_\chi m_p}{m_\chi + m_p}\right)^2 \frac{1}{16\pi \, m_\chi^2 m_p^2} \left(\frac{1}{4}\sum_{\text{spins}} |\mathcal{M}|^2\right) , \qquad (3.15)$$

where m_χ is the DM mass and m_p is the proton mass. The Z-exchange spin independent cross section with protons is given by

$$\begin{aligned}
\sigma_{SI}^p &\simeq \left(\frac{m_\chi m_p}{m_\chi + m_p}\right)^2 \frac{1}{\pi \, m_Z^4} c_{\chi\chi Z}^2 \left(\sum_{q=u,d} c_{q\bar{q}Z} B_{qZ}^p\right)^2 \\
&\simeq \left(\frac{m_\chi m_p}{m_\chi + m_p}\right)^2 \frac{g^4 \left(\frac{1}{2} - 2s_W^2\right)^2}{\pi c_W^4 m_Z^4} \left(|N_{13}^{(1)}|^2 - |N_{14}^{(1)}|^2 + |N_{13}^{(2)}|^2 - |N_{14}^{(2)}|^2\right)^2 \quad (3.16)
\end{aligned}$$

where s_W (c_W) is the sine (cosine) of the weak mixing angle, $c_{\chi\chi Z}$ is the coupling between two DM particles and the Z boson, g is the SU(2) coupling and $N_{ij}^{(1)}, N_{ij}^{(2)}$ are the unitary mixing matrices that diagonalise the neutralino mass matrix, in a basis where N_{13} and N_{14} corresponds to the higgsino content of the dark matter (complete definitions are in Appendix A).[1] The squark-exchange spin independent cross section with protons, for Bino dark matter, is given by

$$\sigma_{SI}^p \simeq \left(\frac{m_\chi m_p}{m_\chi + m_p}\right)^2 \frac{g_1^4}{4\,\pi\, m_{\tilde{q}}^4} \left(Y_{u_L}^2 + Y_{u_R}^2 + \frac{Y_{d_L}^2}{2} + \frac{Y_{d_R}^2}{2}\right) , \qquad (3.17)$$

where $m_{\tilde{q}}$ is the squark mass and Y_i are the hypercharges of the different quarks.[2] Finally the Higgs-exchange spin independent cross section with protons is given by

$$\sigma_{SI}^p = \left(\frac{m_\chi m_p}{m_\chi + m_p}\right)^2 \frac{c_{\chi\chi h}}{\pi \, m_h^4} \left(\sum_q c_{q\bar{q}h} B_{q\bar{q}h}^p\right)^2 , \qquad (3.18)$$

where $c_{\chi\chi h}$ is the coupling between DM and the Higgs boson and $c_{q\bar{q}h}$ is the coupling of the Higgs with the quarks. The Yukawa suppression in the Higgs contribution makes the

---

[1]Depending on the different values of the parameters characterising the mass matrix, $N_{1j}^{(1,2)} \lesssim 1$. If the dark matter is a pure state, the corresponding element is $\mathcal{O}(1)$, while the others vanish.

[2]In the Wino dark matter case, we have to replace $g_1 \to g_2$.
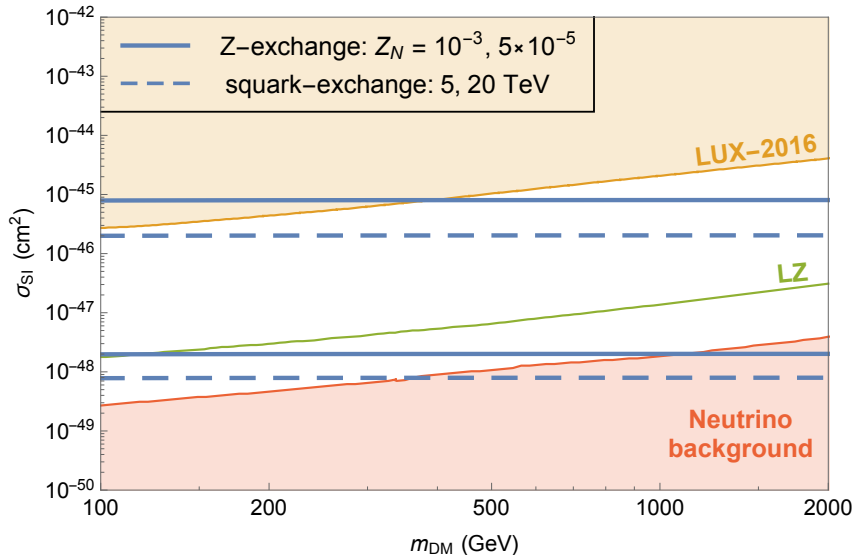
Figure 3.9: The proton elastic scattering cross section due to Z and squark exchange processes. The two blue solid lines show the cross section for the Z-exchange for LSP higgsino contents of $Z_N \simeq 10^{-3}$ (upper curve) and $Z_N \simeq 5 \times 10^{-5}$ (lower curve). In the limit of Eq. (3.23) these correspond to higgsino masses of 1.3 TeV and 6 TeV respectively. The blue dashed lines show the cross section for squark-exchange for squark masses of 5 TeV (upper) and 20 TeV (lower), assuming a dominantly Bino dark matter candidate. The orange shaded region is the actual bound from LUX, while the green curve is the projected reach of LZ. The red area denotes the neutrino background.

Higgs-exchange diagram subdominant to the Z- and squark-exchange, while interference between these is only important if their amplitudes are comparable. Defining

$$Z_N = |N_{13}^{(1)}|^2 - |N_{14}^{(1)}|^2 + |N_{13}^{(2)}|^2 - |N_{14}^{(2)}|^2 \,, \tag{3.19}$$

we have that

$$
\begin{aligned}
\sigma_{SI}^{p,Z} &\simeq 8 \times 10^{-46} \left(\frac{Z_N}{10^{-3}} \right)^2 \text{cm}^2, \\
\sigma_{SI}^{p,\tilde{q}} &\simeq 8 \times 10^{-46} \left(\frac{3.5 \,\text{TeV}}{m_{\tilde{q}}} \right)^4 \text{cm}^2 \,.
\end{aligned}
\tag{3.20}
$$

In Fig. 3.9 we plot the different contributions to the spin independent elastic scattering cross section. The spin independent cross section for Z-exchange is shown for two benchmark values of the higgsino content of the LSP: the upper curve has $Z_N \sim 10^{-3}$,

while the lower curve has $Z_N \sim 5 \times 10^{-5}$. The dashed lines give the spin independent cross section for squark-exchange with squark masses 5 TeV and 20 TeV, assuming Bino dark matter. Therefore to avoid the bound from LUX [185], the neutralino needs a small higgsino content[1] and the squarks must be heavier than roughly 3 TeV. The LZ experiment [186, 187] will be able to probe a higgsino content of the LSP as small as 5×10^{-5} TeV and squarks around 20 TeV. In the plot we show also the neutrino background, where direct detection experiments lose sensitivity [172].

A small higgsino content typically requires a heavy higgsino. For example, in the limit where $M_D^B < \mu = \mu_u = \mu_d \ll M_D^W$, with $\lambda = \lambda_u = \lambda_d = \Lambda_u = \Lambda_d \sim 0$ and large $\tan\beta$ we have

$$N_{11}^{(1)} \simeq 1 - \left(\frac{g_1 v M_D^B}{4(\mu^2 - (M_D^B)^2)} \right)^2 , \qquad N_{12}^{(1)} \simeq N_{13}^{(1)} \simeq 0, \qquad N_{14}^{(1)} \simeq \frac{g_1 v M_D^B}{2(\mu^2 - (M_D^B)^2)} ,$$

(3.21)

and

$$N_{11}^{(2)} \simeq 1 - \left(\frac{g_1 v \mu}{4(\mu^2 - (M_D^B)^2)} \right)^2 , \qquad N_{12}^{(2)} \simeq N_{13}^{(2)} \simeq 0, \qquad N_{14}^{(2)} \simeq \frac{g_1 v \mu}{2(\mu^2 - (M_D^B)^2)} .$$

(3.22)

Inserting Eqs. (3.21) and (3.22) into (3.19) gives

$$Z_N \simeq \frac{g_1^2 v^2}{4} \frac{\mu^2 + (M_D^B)^2}{(\mu^2 - (M_D^B)^2)^2} ,$$

(3.23)

and therefore higgsinos heavier than 1 TeV are needed for Bino masses around 100 GeV to avoid the bound from LUX. LZ may explore parameter regions corresponding to higgsinos lighter than 4.5 TeV for 100 GeV Dirac Bino dark matter.

With light higgsino scenarios excluded, the Wino or the Bino remain as possible dark matter candidates. A Wino LSP is hard to achieve from a model building perspective, since it turns out that in most of the parameter space the lightest Wino is a chargino [202]. Consider, for example, the limit where $\Lambda \simeq \lambda \simeq 0$, $\tan\beta \gg 1$ and $M_D^B \gg \mu_d, \mu_u, M_D^W$. After the Bino has been integrated out, the mass matrices for the neutralinos and the charginos are[2]

$$M_\chi = \begin{pmatrix} m_D^W & -m_W & 0 \\ 0 & \mu & 0 \\ 0 & 0 & \mu \end{pmatrix} , \qquad \text{and} \qquad m_{\tilde\rho^-} = \begin{pmatrix} m_D^W & \sqrt{2} m_W \\ 0 & \mu \end{pmatrix} . \quad (3.24)$$

---

[1]There are however blind spots, where a tuning of the parameters may lead to $N_{13}^{(1)} = N_{14}^{(1)}$ and $N_{13}^{(2)} = N_{14}^{(2)}$, giving rise to a vanishing vector current and suppressing the spin independent cross section.

[2]The neutralino mass matrix is in the basis $\left(\tilde{W}^0, R_d^0, R_u^0 \right), \left(\tilde{T}^0, \tilde{H}_d^0, \tilde{H}_u^0 \right)$, while the chargino mass matrix is in the basis $\left(\tilde{W}^-, R_u^- \right), \left(\tilde{T}^+, \tilde{H}_u^+ \right)$.
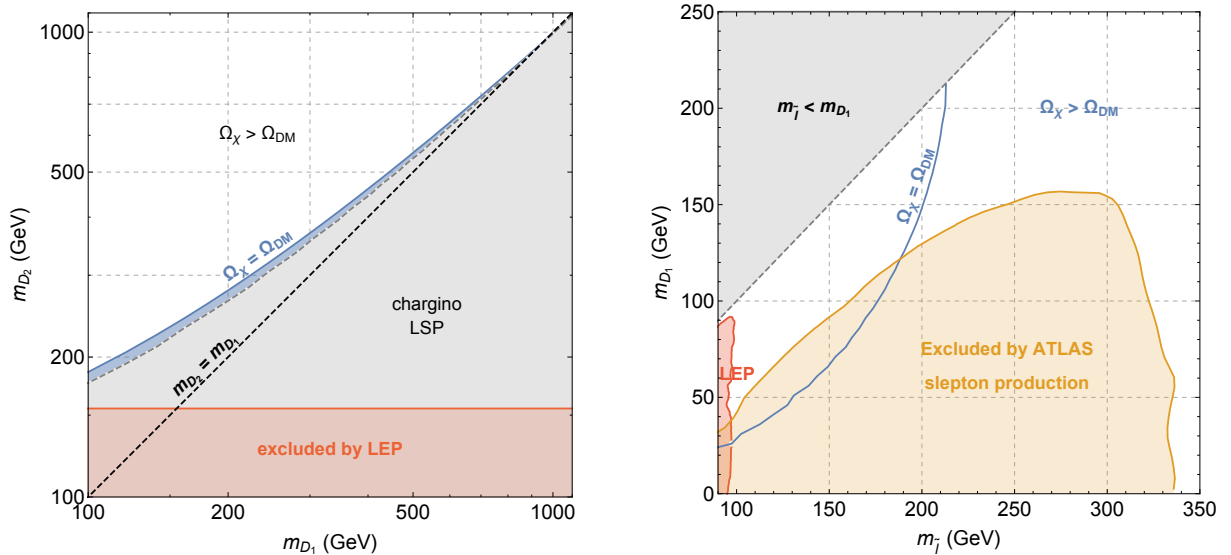
Figure 3.10: *Left:* The constraints on Dirac Bino-Wino dark matter parameter space as a function of their soft masses m_{D_1} and m_{D_2}. Models in the thin blue strip can give the correct dark matter relic density, while the relic density is too large in the white region. In the grey region the theories have a chargino LSP, and we also show the LEP constraint on light charginos [203]. *Right:* The constraints on Dirac Bino dark matter annihilating through sleptons, as a function of the Bino mass m_{D_1}, and the common first two generation slepton soft mass $m_{\tilde{l}_{1,2}}$. The correct relic density is obtained along the blue contour, and the relic density is too large to the right of this. The ATLAS search for sleptons is shown in yellow and excludes a significant part of parameter space, while the constraints from LEP are shown in red.

The neutralino mass matrix is simplified by the higgsino (in the third row) not mixing with the other states. The upper left 2×2 block has the same form as the chargino mass matrix $m_{\tilde{\rho}^-}$, but the off-diagonal element is smaller. This means that the lightest chargino is lighter than the lightest neutralino both in the higgsino-like limit ($\mu < m_D^B, m_D^W$) and the Wino limit ($m_D^W < m_D^B, \mu$), preventing a pure Wino being a viable dark matter candidate. This feature of the MRSSM appears in large portions of parameter space for arbitrary values of Λ, λ away from the limit considered here [202].

A small part of parameter space remains in which a mostly Bino LSP can coannihilate with the Winos to give the correct relic density. In Fig. 3.10 we plot the parameter space for a Bino-Wino dark matter candidate, where squarks, sleptons and higgsinos are decoupled with masses of order 10 TeV. The singlet and triplet vacuum expectaction values

are $v_S \simeq 0.1$ GeV and $v_T \simeq 0.02$ GeV, evading bounds from EW precision observables [164, 165]. We take large $\tan\beta$ to enhance the tree level Higgs mass, and the couplings $\lambda_d = -\lambda_u = \lambda \simeq -0.1$ and $\Lambda = \Lambda_d = \Lambda_u \simeq 0.5$ giving a Higgs mass of approximately 125 GeV over the whole parameter space.[1] Over a large part of parameter space the LSP is a chargino, and the only viable models are in a thin strip, where a mainly Bino neutralino can be the dark matter candidate. In this region the mass splitting between the Bino dark matter and the mostly Wino NLSP is around 20 GeV, similar to the MSSM Bino-Wino scenario. However, in Dirac models the expected signal from indirect detection searches is reduced with respect to the MSSM.

In the pure Bino case annihilation must proceed through sleptons to give the correct relic density, while avoiding direct detection constraints on squarks and higgsinos. For pure Dirac states Bino annihilation is dominated by the t-channel sfermion exchange, and the largest contribution is from right handed sleptons due to the their large hypercharge. The annihilation is relatively slow, $\sigma_{\mathrm{ann}} \propto m_{\chi^0}^2/m_{\tilde{l}_R}^4$, therefore the Bino and the sleptons need to be close to the LEP limit and have similar masses to reduce the relic density sufficiently. In this case the dominant annihilation mechanism is $\chi_1^0 \bar{\chi}_1^0 \to l_i^+ l_i^-$, and there is also coannihilation with sleptons mainly via $\tilde{l}_i \chi_1^0 \to \gamma\, l_i$ or $Z\, l_i$, and $\tilde{l}_i \tilde{l}_j^* \to \gamma\,\gamma$, γZ or ZZ.

In Fig. 3.10 (right) we plot the contour with the correct relic density for a Bino-slepton scenario. The model parameters are the same as in the left panel, but now the first two generation of sleptons are light (we keep the stau heavy) and the Wino is decoupled with a mass of order 10 TeV. With lighter staus it is possible to have Bino dark matter with a mass up to about 300 GeV. Fig. 3.10 (right) also shows the constraints from LEP [204] and from ATLAS [205]. Although the viable parameter space is relatively small, it is easier to obtain the correct relic density than in such a scenario in the MSSM. This is because in the MSSM the dominant annihilation process is P-wave suppressed and a large enough annihilation cross section is only possible with close to degenerate Bino and slepton masses. In contrast, in Dirac models with an unbroken R-symmetry the annihilation cross section into a fermion and an anti-fermion pair has a non-vanishing S-wave contribution even in the limit of vanishing fermion masses.[2]

---

[1]There are other possibilities for reaching a 125 GeV Higgs mass. However, varying the values of Λ and λ, keeping $v_{S,T}$ fixed to have the right Higgs mass we did not find any appreciable difference in the relic density, while the spin independent cross sections vary slightly but remain below the reach of LZ everywhere.

[2]If the R-symmetry is broken the self annihilation cross section for the processes $\chi_1^0 \chi_1^0 \to l_i^+ l_i^-$ and $\chi_2^0 \chi_2^0 \to l_i^+ l_i^-$ are P-wave suppressed (analogously to the MSSM), while the process $\chi_1^0 \chi_2^0 \to l_i^+ l_i^-$ has a non vanishing S-wave contribution (as in the MRSSM).

The large annihilation of Dirac Binos into charged lepton pairs leads to different indirect detection signatures with respect to the MSSM. Dark matter annihilation to leptonic channels does not contribute to the signal of cosmic ray antiprotons, yielding a very weak constraint. The strongest indirect detection constraints come from the annihilation to e^+e^-, leading to a bound $m_\chi \gtrsim 60$ GeV for an annihilation cross section of order 10^{-26} cm^3/s [206].

Finally, small Majorana mass terms can slightly break the R-symmetry and change the behaviour of the dark matter. For example, in Split Dirac Supersymmetry models [103], the relic abundance is as it is in the usual Dirac scenario, while direct and indirect detection signals may or may not be, depending on the splitting between the two Majorana states. In particular, for splittings larger than a few keV the neutralino scattering through Z-exchange is suppressed, as in Majorana models. In this framework it is then possible to have a pseudo-Dirac higgsino LSP as a dark matter candidate with a mass around 1 TeV.

3.2.2 MRSSM dark matter at colliders

A Dirac Bino LSP coannihilating with first and second generation sleptons is a viable dark matter candidate for masses up to about 300 GeV. The correct relic density is possible for larger mass splittings between a Dirac Bino and sleptons than in the Majorana case, and as a result searches for slepton pair production can probe this scenario unlike in the MSSM. Because sleptons are directly produced in Drell Yann processes, the collider limits in the slepton–neutralino parameter space obtained by ATLAS and CMS analyses apply to Dirac Binos [111, 205], and the ATLAS bound is plotted in Fig. 3.10 right. Slepton NLSPs are directly pair produced and subsequently decay into two same flavour leptons and two LSPs (giving rise to missing energy). As a result, in this scenario the ATLAS and CMS experiments exclude a Bino dark matter lighter than 120 GeV, leaving unexplored regions of small neutralino-slepton mass splitting. New colliders will be able to improve the reach for sleptons with light LSP mass, but the sensitivity in the interesting region, where $m_{\tilde{l}} - m_{\chi_1^0} < m_W$, is limited by the large background.

The Dirac Bino-Wino dark matter scenario is complicated to search for at hadron colliders, because the small mass splitting, comparable with the one of the Majorana Bino-Wino dark matter case, creates issues in background rejection and triggering. However interesting opportunities arise in boosted electroweakino searches [199]. In particular, searches for $pp \to \tilde{\chi}_1^\pm \tilde{\chi}_2^0 \to l^\pm \tilde{\chi}_1^0 \gamma \tilde{\chi}_1^0 j$ are very effective in probing models with Bino-Wino coannihilation. This search has the advantage that the smaller the splitting between the two neutralinos, the greater the branching fraction to photons compared to off-shell Z bosons. The cross section for this process is suppressed at the LHC, but studies for the

MSSM at a 100 TeV collider indicate that this search could probe dark matter masses up to 2 TeV for a luminosity of 20 ab^{-1}. The production cross section for charged and neutral Dirac Winos is a few times the one in the MSSM, while the splitting between the Bino LSP and the Wino NLSP is comparable to in the MSSM. Therefore boosted electroweakino studies at a future hadron collider are expected to probe the whole Dirac Bino-Wino dark matter parameter space after a few ab^{-1} of luminosity.

Similarly to the MSSM, if the gaugino mass ratios are fixed, searches for coloured particles can be relevant. If squarks are light compared to a Dirac gluino, LHC searches constrain the gluino mass to be heavier than 1.5 TeV. Therefore, since a Dirac Bino must have mass less than about 300 GeV to be a suitable dark matter candidate, this is only a viable scenario in models with a ratio of gaugino masses $M_{D_3}/M_{D_1} \gtrsim 5$. As seen in Fig. 2.9, for light squarks a 100 TeV collider can probe up to 20 TeV Dirac gluinos. Consequently, models with Dirac Bino dark matter and $M_{D_3}/M_{D_1} \lesssim 70$ will either be discovered or excluded. Given the typical ratios of gaugino masses from UV models (discussed in Section 1.2), for large classes of theories this probes the entire Bino dark matter parameter space, surpassing the sensitivity of searches for sleptons. In the Bino-Wino scenario, M_{D_2} and M_{D_1} must be close to degenerate. This is not naively the case in any of the simple UV completions considered and therefore the impact of searches for gluinos is unclear.

Finally, searches for squarks and gluinos at 100 TeV colliders can have an interesting interplay with direct detection. In models where the higgsinos are decoupled, the spin independent cross section is mediated only by squarks. Therefore, LZ can effectively exclude squark masses up to 15 TeV in models with a Dirac Bino LSP. On the other hand, a 100 TeV collider can be sensitive to comparable mass squarks. The discovery of squarks would therefore lead to an expected minimum direct detection cross section in models with Bino dark matter, close to the experimentally accessible values. Meanwhile the exclusion of squarks with similar masses would mean that Dirac Bino dark matter would have to scatter via a higgsino component if it was to be visible at LZ.

Part II

Axion dark matter

Chapter 4

Introduction and motivation

Many models for dark matter have been proposed so far, and can be classified in two categories with different production mechanisms. On one hand, dark matter can be thermally produced and such mechanism selects a dark matter with mass close to the electroweak scale. Dark matter candidates with masses around the TeV are also motivated by possible solutions to the hierarchy problem, that point at NP at the same scale. In the first part of this thesis (chapters 1-3) we analysed one of the most popular WIMP candidate, the neutralino.

On the other hand, dark matter particles can be produced via non-thermal mechanisms. In this case, the dark matter mass scale is arbitrary. In particular, motivated models contain light pseudo-scalar particles, as the QCD axion [207–214]. The QCD axion provides a robust solution to the strong CP problem, and the hypothesis that the axion is the dark matter has been analysed in several papers [215–227].

In the second part of this thesis we analyse the QCD axion properties at high precision and the consequences for cosmology and axion searches. In particular, in section 4.1 we outline the strong CP problem, and in section 4.2 we present the QCD axion solution.[1] In chapter 5 we discuss the axion as a DM candidate, we give results for the temperature dependence of the axion mass and potential at increasing temperatures and the implications for the axion dark matter abundance. Finally, in chapter 6 we review current and future axion searches and we present our new computations and numerical estimates for the various properties of the axion at zero temperature.

---

[1]Numerous reviews of the QCD axion exists. See for example [228, 229].

4.1 The $U(1)_A$ and the strong CP problem

The QCD Lagrangian in the limit of vanishing quark masses is invariant under a global $U(n_f)_V \times U(n_f)_A$, where n_f is the number of families. However, such symmetry would imply that hadrons come in doublets [230], which is not observed experimentally. In fact, quark condensates spontaneously break the axial symmetry $SU(n_f)_A \times U(1)_A$. Pseudo-Goldstone bosons arise as a consequence of this breaking and are identified with the pions, the kaons and the η meson. On the other hand, there is no candidate for the pseudo-Goldstone from the breaking of the $U(1)_A$. Such particle should have a mass $\lesssim \sqrt{3} m_\pi$, which excludes the η' meson as a possible candidate. The absence of this particle is known as the $U(1)_A$ problem [231].

The addition of a term in the QCD Lagrangian that explicitly breaks the $U(1)_A$ symmetry is a possible solution of the $U(1)_A$ problem [232, 233]. Indeed, the QCD Lagrangian allows a topological term of the form

$$\mathcal{L}_{QCD} \supset \theta_0 \frac{g_s^2}{32\pi^2} \text{Tr}\, G_{\mu\nu} \tilde{G}^{\mu\nu}, \tag{4.1}$$

where g_s is the strong gauge coupling, $G_{\mu\nu}$ is the gluon field strength tensor, $\tilde{G}_{\mu\nu} = \epsilon_{\mu\nu\rho\sigma} G^{\rho\sigma}/2$ is its dual and the trace is over the adjoint representation of $SU(3)$. This term is allowed by symmetries, but it violates CP [212]. Moreover, it is a total divergence [234]

$$G_{a\,\mu\nu} \tilde{G}_a^{\mu\nu} = \partial_\mu \epsilon^{\mu\alpha\beta\gamma}(A_{a\alpha} G_{a\,\beta\gamma} - \frac{g_s}{3} f_{abc} A_{a\alpha} A_{b\beta} A_{c\gamma}), \tag{4.2}$$

where A is the gluon vector potential. At any order in perturbation theory this term does not modify the equation of motion, and it contributes to the action only as a surface term. However, it was shown that already at the classical level there are gauge configuration, called instantons,[1] with non trivial $G_{a\,\mu\nu} \tilde{G}_a^{\mu\nu}$ and finite action [232, 233]. At infinity $A_{a\mu}$ is a pure gauge field and the field strength vanishes. At infinity the second term on the right hand side of Eq. (4.2) does not vanish and it gives a finite contribution to the classical action

$$\int d^3x\, G_{a\,\mu\nu} \tilde{G}_a^{\mu\nu} = 32\pi^2\, n, \tag{4.3}$$

where n is the winding number. The contribution of configurations with non vanishing winding number to the Euclidean path integral is suppressed at small coupling by a factor

$$e^{-S_{\text{inst}}} = e^{-\int \frac{1}{4g_s^2} G_{a\,\mu\nu} \tilde{G}_a^{\mu\nu} d^4x} = e^{-\frac{8\pi^2 |n|}{g_s^2}}. \tag{4.4}$$

---

[1] Instantons are solutions of the condition $G_{a\,\mu\nu} = \pm \tilde{G}_{a\,\mu\nu}$.

In QCD configuration with $n \neq 0$ however are not small. The QCD coupling $g_s = g_s(\mu)$ is a function of an energy scale μ and become larger at low energies. The relevant scale of this configuration is set by the size of the instanton ρ, where the energy density is enclosed, leading to $\mu = 1/\rho$. At one loop, the QCD running coupling is given by

$$g(\mu)^2 = \frac{8\pi^2}{\beta_0 \log{(\mu/\Lambda)}}, \tag{4.5}$$

where $\beta_0 = 11 - 2\,n_f/3$, with n_f the number of active flavours at the renormalisation scale μ, and $\Lambda \sim 150$ MeV is the QCD non perturbative scale. Equation (4.4) therefore becomes

$$e^{-\frac{8\pi^2 n}{g_s^2(1/\rho)}} = (\rho\Lambda)^{\beta_0}. \tag{4.6}$$

The path integral is the sum over all gauge configurations, in particular over instantons of any size. This shows that for large instanton configurations, the one with $\rho\Lambda \simeq 1$, instanton effects are non perturbative. On the other hand, for small instantons, the QCD coupling constant is small, the instanton configuration is perturbative and contribute with exponentially small factors. Unfortunately, the contribution from instantons to the QCD action is dominated by large non perturbative instanton configurations that are not calculable. The existence of configurations for which Eq. (4.4) does not vanish provide a solution to the $U(1)_A$ problem.

To understand better the consequences of the θ_0-term in Eq. (4.1), consider the effect of the axial symmetry on quarks

$$q \to e^{i\gamma_5\alpha}q, \tag{4.7}$$

where q are the quark fields and α is a phase. Under this transformation the path integral is not invariant. In particular, the measure in the path integral transforms non trivially

$$\delta q\,\delta\bar{q} \to \exp\left\{-\frac{i}{16\pi^2}\alpha\int d^4x\, G_{\mu\nu}\tilde{G}^{\mu\nu}\right\}\delta q\,\delta\bar{q}. \tag{4.8}$$

This is equivalent to shift θ_0

$$\theta_0 \to \theta_0 + 2\alpha, \tag{4.9}$$

showing that θ_0 is non physical, because under a field redefinition it is shifted by a phase. The same field redefinition will change also the quark mass term

$$\bar{q}_L\, M\, q_R + \text{h.c} \to \bar{q}_L\, M\, e^{2i\alpha}\, q_R, \tag{4.10}$$

leading to

$$\arg \det M \to \arg \det M + 2\alpha. \tag{4.11}$$

4. Introduction and motivation

Therefore, θ_0 and $\arg \det M$ are separately non physical, but

$$\theta = \theta_0 - \arg \det M \tag{4.12}$$

is physical, because it is invariant under a field redefinition. Notice that individually θ_0 and $\arg \det M$ violate parity and time inversion (and therefore CP) and a non vanishing θ breaks CP.

In particular the θ term induces a neutron electric dipole moment of order [235, 236]

$$d_n \simeq \frac{e|\theta|m_\pi^2}{m_N^3} \simeq 10^{-16} |\theta| \, \mathrm{e \, cm}, \tag{4.13}$$

and therefore the experimental bound on the electric dipole moment of the neutron $d_n \lesssim 3 \cdot 10^{-26}$ e cm [237] implies $\theta \lesssim 10^{-10}$.

Since experimentally no CP violation has been observed in the strong interactions, either θ_0 and $\arg \det M$ should be both tiny individually or there must be a cancellation between the two. However, θ_0 comes just from gluon dynamics, while the phase in the mass matrix of the quarks comes from the electroweak sector, in particular from the Yukawa sector and the coupling to the Higgs. Therefore, we expect them to be unrelated. On top of this we know that off- diagonal phases in the mass matrix, the CKM phases, are of order one, such that in order to have a cancellation we would expect $\theta_0 \sim \mathcal{O}(1)$. A solution to this problem would exist if any of the quarks were massless. In this situation the θ angle would not be physical and there would be no CP violation in QCD. Lattice computations show, however, that the light quark masses are non zero [238–240]. The strong CP problem is therefore driven by the question of why strong interactions do not violate CP symmetry even if CP violation is not forbidden by the theory.

There are two known families of solutions to the theta problem. One uses CP invariance in the UV, the other uses the so called Peccei-Quinn symmetry. Requiring CP to be a fundamental symmetry of the theory, will not allow the contributions to the θ term from both the $G\tilde{G}$ term and the quark mass term. However CP is broken in nature by the CKM phases. Therefore, the new theory needs some mechanism that breaks CP producing the CKM angles and possibly also extra CP for baryogenesis, without introducing a contribution to the θ term. There are various implementation of this idea [241–243]. For example in the Barr-Nelson model [244–247], CP is a symmetry of the UV theory and needs to be broken. Heavy singlet quarks, with a vacuum expectation value much above the electroweak scale, are introduced and after symmetry breaking they mix with the SM quarks. At low energy the heavy quarks can be integrated out and the SM quarks acquire the required amount of CP violation through the CKM mixing. The $\arg \det M$ vanishes at tree level and it is different from zero only at loop level, being therefore able

to evade the bound from the neutron electric dipole moment if small coupling are chosen. However, this model needs some sort of tuning between its parameters to reproduce $\mathcal{O}(1)$ CKM phases and it is very sensitive to extra NP contributions that may spoil the CP breaking mechanism.

On the other hand, the introduction of an additional chiral symmetry is one of the most robust solutions of the strong CP problem. The description of the properties of this solution is the main subject of this chapter.

4.2   The QCD axion

The axion solution may be considered the most robust solution to the strong CP problem because it is insensitive to any extra source of CP violation generated at higher energies. The model is based on the idea of making θ a dynamical field [207, 208], achieved introducing a new global chiral symmetry $U(1)_{PQ}$, which is spontaneously broken at a scale f_a. The axion is the pseudo-Goldstone resulting from the symmetry breaking.

The SM Lagrangian is made $U(1)_{PQ}$ invariant adding the axion kinetic term and the interaction of the axion with gluons

$$\mathcal{L} \supset -\frac{1}{2}\partial_\mu a\,\partial^\mu a + \frac{\alpha_s}{8\pi}\frac{a}{f_a}G_{\mu\nu}\tilde{G}^{\mu\nu}\,, \tag{4.14}$$

where a is the axion field. Since the axion is the pseudo-Goldstone boson of the broken symmetry, it is invariant under a shift symmetry

$$a(x) \to a(x) + \alpha. \tag{4.15}$$

The shift symmetry is broken only by the coupling to $G\tilde{G}$. Furthermore, the axion can couple to photons, quarks and leptons in ways that do not break the shift symmetry. Even if these couplings are not present, the gluon will generate them from quark loops.

In the SM Lagrangian with the θ term and the axion, the θ term can be reabsorbed by the axion. The axion then acquires a potential, whose minimum is reached when $\langle a(x) + \theta f_a \rangle = 0$. This has been proven in [248]. Consider $E(\theta)$, the vacuum energy of QCD, as a function of θ in a volume V. Then, the path integral formula for the ground state energy is

$$e^{-V\,E(\theta)} = \int \delta[\phi]\,e^{-S_0 + i\theta Q}, \tag{4.16}$$

where ϕ denotes all the possible fields, S_0 is the SM action, $\theta = a/f_a$ and $Q = \frac{\alpha_s}{8\pi}\int d^4x\, G_{\mu\nu}\tilde{G}_{\mu\nu}$ is the topological charge. The integrand is positive definite and using the Schwartz inequality we obtain

$$
\begin{aligned}
e^{-V\,E(\theta)} &= \int \delta[\phi]\, e^{-S_0 + i\theta Q} = \left| \int \delta[\phi]\, e^{-S_0 + i\theta Q} \right| \\
&\leq \int \delta[\phi]\, \left| e^{-S_0 + i\theta Q} \right| = e^{-V\,E(0)}
\end{aligned}
\tag{4.17}
$$

In the last equality, the theta term appears only as a phase to the topological charge and therefore the modulus is the same as the argument of the path integral at $\theta = 0$. It is then possible to prove that $\theta = 0$ is always an absolute minimum of the QCD energy and that the axion has always a global minimum at $\theta = 0$, thus solving the strong CP problem.

In the following subsections I will discuss feature of specific axion models, starting with the Peccei-Quinn-Weinberg-Wilczek (PQWW) model, also dubbed *visible* axion, and continuing with the Kim-Shifman-Vainshtein-Zakharov (KSVZ) and the Dine-Fishler-Srednicki-Zhitnitsky (DFSZ) axion models. Finally, I will summarise the properties of the QCD axion.

4.2.1 The visible axion

In the PQWW model [207–210], the axion is embedded in the phase of the Higgs field in the usual SM. One Higgs doublet is not enough to give rise to the axion because three Goldstones are absorbed by the longitudinal degrees of the SM gauge bosons and the remaining Higgs boson has a potential. The Lagrangian contains two Higgs doublets H_u and H_d, where H_u gives a mass to the up-type quarks and H_d give a mass to the down-type quarks and the charged leptons

$$
\mathcal{L} \supset -y^{(u)}\bar{q}_L H_u u_R - y^{(d)}\bar{q}_L H_d d_R - V(H_u, H_d) + \text{h.c.} \,.
\tag{4.18}
$$

The potential $V(H_u, H_d)$ has two mexican hat like potential, one for each Higgs doublet, so that they both take a VEV $v_{u,d}$

$$
V = \frac{\lambda_u}{4}\left(|H_u|^2 - \frac{v_u^2}{2} \right)^2 + \frac{\lambda_d}{4}\left(|H_d|^2 - \frac{v_d^2}{2} \right)^2 + \dots
\tag{4.19}
$$

The symmetries of the lagrangian shows that we have a $U(1)$ phase for each Higgs doublet. One of the two phases is the hypercharge, absorbed by the Z boson, while the other, after

giving a VEV to the Higgs doublets, is spontaneously broken and gives a Goldstone boson. The axion content of H_u and H_d, that is orthogonal to the hypercharge, is therefore

$$H_u = \frac{v_u}{\sqrt{2}} \begin{pmatrix} 0 \\ 1 \end{pmatrix} e^{\frac{ia\tan\beta}{v}}, \qquad\qquad H_d = \frac{v_d}{\sqrt{2}} \begin{pmatrix} 1 \\ 0 \end{pmatrix} e^{\frac{ia}{\tan\beta\, v}}, \qquad (4.20)$$

where $\tan\beta = v_u/v_d$ and $v^2 = v_u^2 + v_d^2$.

The axion couplings to the SM fields are in the Yukawa terms

$$\mathcal{L} \supset -y_u \bar{q}_L H_u u_R - y_d \bar{q}_L H_d d_R - y_e \bar{L} H_d e_R + \text{h.c.} \qquad (4.21)$$

and replacing the Higgs doublets with the expressions in Eq. (4.20) we get

$$\mathcal{L} \supset -y_u \frac{v_u}{\sqrt{2}} e^{\frac{ia\tan\beta}{v}} \bar{u}_L u_R - y_d \frac{v_d}{\sqrt{2}} e^{\frac{ia}{\tan\beta\, v}} \bar{d}_L d_R - y_e \frac{v_d}{\sqrt{2}} e^{\frac{ia}{\tan\beta\, v}} \bar{e}_L e_R + \text{h.c.} \qquad (4.22)$$

These terms contain therefore the couplings between the SM fermions and the axion. Expanding the exponents, one finds that the generic coupling of the axion to SM fermions is suppressed by a factor m_q/v. Moreover, the Yukawa terms are invariant under chiral transformations of the fermion fields

$$u_R \to e^{-i\frac{a\tan\beta}{v}} u_R, \qquad\qquad d_R \to e^{-i\frac{\alpha}{v\tan\beta}} d_R. \qquad (4.23)$$

Using these transformations we see that the couplings of the axion to the SM fermions disappear from the term of the lagrangian in equation (4.22), giving rise to the $G\tilde{G}$ term that is needed to solve the strong CP problem. After performing the transformation of the quarks, the couplings between the axion and the quarks will appear from the quarks kinetic terms.

The original PQWW model, with weak scale visible axions where $f_a \simeq v$, has been ruled out experimentally. Indeed, for such models the axion is lighter than the electron and it is long lived, since the only possible decay is into photons. Such an axion model has been ruled out by the non observation, for example, of the process $K^+ \to \pi^+ a$. Indeed, the branching ratio for this process is estimated to be [249]

$$BR(K^+ \to \pi^+ a) \simeq 3 \times 10^{-5} \left(\tan\beta + \frac{1}{\tan\beta} \right)^2, \qquad (4.24)$$

which is larger than the bound from KEK, $BR(K^+ \to \pi^+ + \text{nothing}) < 3.8 \times 10^{-8}$ [250].

On the other hand, models where the axion decay constant is much larger than the electroweak scale are still viable. As we will see shortly, if $f_a \gg v$, the axion is very light, very weakly coupled and long lived.[1] It is in general possible to classify invisible axion models depending on whether the axion couples directly or not with the SM fermions.

---

[1]Such models are often called *invisible* axion models.

4.2.2 The KSVZ model

In 1979, Kim [211] and independently Shifman, Vainshtein and Zakharov [212] proposed a model where the axion does not couple to Standard Model fermions at tree level. Suppose to add to the Standard Model lagrangian a heavy quark Q in the fundamental of $SU(3)_C$ and a complex scalar field ϕ

$$\mathcal{L} \supset \partial_\mu \phi \, \partial^\mu \phi + i \, \bar{Q} \, \slashed{D} \, Q + \lambda \, \phi \, \bar{Q}_L Q_R + \text{h.c.} - V(|\phi|^2), \tag{4.25}$$

where $V(|\phi|^2)$ is a mexican hat like potential that breaks the global $U(1)$ symmetry associated to ϕ. These terms of the lagrangian, except $\lambda \phi \bar{Q}_L Q_R$, respect a global $U(1)$ symmetry such that

$$\phi \to e^{i\alpha}\phi. \tag{4.26}$$

Also the term $\lambda \phi \bar{Q}_L Q_R$ is invariant if Q is allowed to transform in the same way

$$Q \to e^{-\frac{\alpha}{2}\gamma_5}Q, \tag{4.27}$$

such that the absence of bare mass terms for the heavy quark, that would spoil the realisation of the PQ symmetry, is guaranteed.

If ϕ gets a vacuum expectation value, the symmetry is spontaneously broken and

$$\phi = \frac{v_{PQ}}{\sqrt{2}} e^{i\frac{a}{v_{PQ}}}. \tag{4.28}$$

After the spontaneous breaking of the symmetry, the heavy quark gets a mass term

$$\frac{\lambda v_{PQ}}{\sqrt{2}} e^{i\frac{a}{v_{PQ}}} \bar{Q}_L Q_R + h.c., \tag{4.29}$$

that also generates a coupling to the axion. Exploiting the PQ symmetry and Eqs. (4.26) and (4.27), we can redefine the heavy quarks

$$Q \longrightarrow Q' = e^{\frac{ia}{2v_{PQ}}\gamma_5}Q, \tag{4.30}$$

such that Eq. (4.29) becomes

$$\frac{\lambda v_{PQ}}{\sqrt{2}} \bar{Q}'_L Q'_R + \text{h.c.} \, . \tag{4.31}$$

The shift in the action is just

$$\delta S = \int \frac{a}{v_{PQ}} \frac{1}{32\pi^2} G_{\mu\nu} \tilde{G}^{\mu\nu}. \tag{4.32}$$

Now the field Q' has only a mass term and not anymore an interaction with the axion and it is possible to integrate it out. The only non derivative coupling that remains is the coupling to the gluon. Furthermore, if the heavy quark Q was charged under $U(1)_Y$, we would have also analogous couplings to photons and Z.

It is possible to do the same procedure in the case of a number N of heavy quark fields $Q_{i=1,...,N}$. In this situation, we would get

$$\delta S = \int \frac{a}{v_{PQ}} \frac{N}{32\pi^2} G_{\mu\nu}\tilde{G}^{\mu\nu} = \int \frac{a}{f_a} \frac{1}{32\pi^2} G_{\mu\nu}\tilde{G}^{\mu\nu}, \tag{4.33}$$

by defining $f_a = v_{PQ}/N$, where N is the colour anomaly coefficient of having N fundamental heavy quarks.

At low energy, this model has only the coupling with gluons and the axion do not couple with quarks or leptons at tree level. However, at energies where the QCD is strongly coupled, the axion coupling to gluons will produce couplings to pions and nucleons.

4.2.3 The DFSZ model

This class of models, due to Zhitnitsky [213] and independently Dine, Fishler and Srednicki [214], employs two Higgs doublets H_u and H_d, one giving mass to the up quarks, the other to the down quarks and the charged leptons, and a scalar field ϕ. The scalar potential is

$$\begin{aligned} V &= \frac{\lambda_u}{4}\left(|H_u|^2 - \frac{v_u^2}{2}\right)^2 + \frac{\lambda_d}{4}\left(|H_d|^2 - \frac{v_d^2}{2}\right)^2 + \frac{\lambda_\phi}{2}\left(|\phi|^2 - \frac{v_\phi^2}{2}\right)^2 \\ &+ \tilde{f}\left(|H_u|^2|\phi|^2, |H_d|^2|\phi|^2, H_u^T H_d \phi^2, |H_u^T H_d|^2, |H_d^\dagger H_u|^2\right), \end{aligned} \tag{4.34}$$

where $\tilde{f}$ is a function of the terms $|H_u|^2|\phi|^2, |H_d|^2|\phi|^2, H_u^T H_d \phi^2, |H_u^T H_d|^2, |H_d^\dagger H_u|^2$. The $H_u^T H_d \phi^2$ terms make the Higgs doublets charged under PQ. Out of the three different $U(1)$ phases for H_u, H_d and ϕ, the potential only preserves two, the hypercharge and the PQ symmetry, which, after giving a VEV to all the scalar fields, is spontaneously broken and give rise to a Goldstone boson. Writing the three scalar fields around the vacuum, we have

$$H_u = \frac{v_u}{\sqrt{2}}e^{i\frac{a}{v_{PQ}}q_u}, \qquad H_d = \frac{v_d}{\sqrt{2}}e^{i\frac{a}{v_{PQ}}q_d}, \qquad \phi = \frac{v_\phi}{\sqrt{2}}e^{i\frac{a}{v_{PQ}}q_\phi}. \tag{4.35}$$

The axion a, the linear combination of the three phases, is the generator that it is not broken by the $H_u^T H_d \phi^2$ term in the potential and which is not the hypercharge. The

constants q_u, q_d, and q_ϕ are determined by preserving the $H_u^T H_d \phi^2$ term and writing the generator orthogonal to the hypercharge. The $H_u^T H_d \phi^2$ term is preserved if

$$q_u + q_d + 2q_\phi = 0. \tag{4.36}$$

On the other hand, writing the kinetic terms for the Higgs doublets and the complex scalar, we find the cross term between the axion and the Z boson, that must vanish. This gives the following condition:

$$q_u v_u^2 - q_d v_d^2 = 0. \tag{4.37}$$

We can solve this equations up to an overall constant, that anyway can be reabsorbed in v_{PQ}. The solution is

$$q_u = \frac{2v_d^2}{v^2}, \qquad q_d = \frac{2v_u^2}{v^2}, \qquad q_\phi = -1. \tag{4.38}$$

Both the VEVs of the two Higgs doublets break the electroweak symmetry and the total breaking is $v^2 = v_u^2 + v_d^2$. However, v_ϕ can be arbitrary large because it does not break any SM symmetry. The PQ scale can be fixed requiring that the kinetic term for the axion is canonically normalised

$$v_{PQ}^2 = v_\phi^2 + v^2 \sin 2\beta, \tag{4.39}$$

where, as in the visible axion models, $\tan\beta = v_u/v_d$. We notice that if v_ϕ is very large, v_{PQ} is dominated by v_ϕ and the axion is mostly the component associated to the new scalar field.

As in the PQWW model, the coupling of the axion to the SM fermions arise in the Yukawa terms. Again, if we replace the Higgs doublets with Eqs. (4.35) we get

$$\mathcal{L} \supset -y_u \frac{v_u}{\sqrt{2}} \bar{u}_L e^{2i\sin^2\beta \frac{a}{v_{PQ}}} u_R - y_d \frac{v_d}{\sqrt{2}} \bar{d}_L e^{2i\cos^2\beta \frac{a}{v_{PQ}}} d_R - y_e \frac{v_d}{\sqrt{2}} \bar{e}_L e^{2i\cos^2\beta \frac{a}{v_{PQ}}} e_R. \tag{4.40}$$

Since part of the Higgs doublets is made of axions, now we have direct couplings between the axion and the charged fermions of the SM, which are suppressed by m_f/v_{PQ}.

How does this model solve the strong CP problem? As we did previously, we can rotate the phase away by redefining the quarks with the chiral rotation. At this point the axion-fermion couplings disappear from the terms of the lagrangian in equation (4.40) and the term

$$\delta\mathcal{L} = \frac{6}{32\pi^2 v_{PQ}} a G\tilde{G} = \frac{1}{32\pi^2 f_a} a G\tilde{G}, \tag{4.41}$$

appears, where in the second equality we defined $f_a = v_{PQ}/6$. The factor 6 is the anomaly coefficient associated with the 6 standard model quarks. The SM fermion kinetic terms generate axion fermion couplings

$$\bar{q}_L \slashed{D} q_L \rightarrow c_q \frac{\partial_\mu a}{v_{PQ}} \bar{q} \gamma^\mu \gamma_5 q, \tag{4.42}$$

where c_q is a coefficient depending on whether the quark is up or down type.

4.3 Leading order axion properties

In this section we summarise the leading order axion properties and the notation that is used in the following chapters. At energies below the Peccei Quinn (PQ) and the electroweak (EW) breaking scales the axion dependent part of the Lagrangian, at leading order in $1/f_a$ and the weak couplings can be written, without loss of generality, as

$$\mathcal{L}_a = \frac{1}{2}(\partial_\mu a)^2 + \frac{a}{f_a}\frac{\alpha_s}{8\pi} G_{\mu\nu}\tilde{G}^{\mu\nu} + \frac{1}{4}a\, g_{a\gamma\gamma}^0 F_{\mu\nu}\tilde{F}^{\mu\nu} + \frac{\partial_\mu a}{2f_a}\, j_{a,0}^\mu\,, \tag{4.43}$$

where the second term defines f_a, the dual gluon field strength $\tilde{G}_{\mu\nu} = \frac{1}{2}\epsilon_{\mu\nu\rho\sigma}G^{\rho\sigma}$, color indices are implicit, and the coupling to the photon field strength $F_{\mu\nu}$ is

$$g_{a\gamma\gamma}^0 = \frac{\alpha_{em}}{2\pi f_a}\frac{E}{N}\,, \tag{4.44}$$

where E/N is the ratio of the Electromagnetic (EM) and the color anomaly ($=8/3$ for complete SU(5) representations). Finally in the last term of eq. (4.43) $j_{a,0}^\mu = c_q^0 \bar{q}\gamma^\mu\gamma_5 q$ is a model dependent axial current made of SM matter fields. The axionic pseudo shift-symmetry, equation (4.15), has been used to remove the QCD θ angle.

The only non-derivative coupling to QCD can be conveniently reshuffled by a quark field redefinition. In particular performing a change of field variables on the up and down quarks

$$q = \begin{pmatrix} u \\ d \end{pmatrix} \rightarrow e^{i\gamma_5 \frac{a}{2f_a} Q_a} \begin{pmatrix} u \\ d \end{pmatrix}\,, \qquad \mathrm{tr}\,Q_a = 1\,, \tag{4.45}$$

eq. (4.43) becomes

$$\mathcal{L}_a = \frac{1}{2}(\partial_\mu a)^2 + \frac{1}{4}a\, g_{a\gamma\gamma} F_{\mu\nu}\tilde{F}^{\mu\nu} + \frac{\partial_\mu a}{2f_a}\, j_a^\mu - \bar{q}_L M_a q_R + h.c.\,, \tag{4.46}$$

where

$$g_{a\gamma\gamma} = \frac{\alpha_{em}}{2\pi f_a}\left[\frac{E}{N} - 6\,\mathrm{tr}\left(Q_a Q^2\right)\right]\,, \qquad j_a^\mu = j_{a,0}^\mu - \bar{q}\gamma^\mu\gamma_5 Q_a q\,, \tag{4.47}$$

$$M_a = e^{i\frac{a}{2f_a}Q_a} M_q \, e^{i\frac{a}{2f_a}Q_a} \,, \qquad M_q = \begin{pmatrix} m_u & 0 \\ 0 & m_d \end{pmatrix} \,, \qquad Q = \begin{pmatrix} \frac{2}{3} & 0 \\ 0 & -\frac{1}{3} \end{pmatrix} \,.$$

The advantage of this basis of axion couplings is twofold. First the axion coupling to the axial current only renormalizes multiplicatively unlike the coupling to the gluon operator, which mixes with the axial current divergence at one-loop. Second the only non-derivative couplings of the axion appear through the quark mass terms.

At leading order in $1/f_a$ the axion can be treated as an external source, the effects from virtual axions being further suppressed by the tiny coupling. The non derivative couplings to QCD are encoded in the phase dependence of the dressed quark mass matrix M_a, while in the derivative couplings the axion enters as an external axial current. The low energy behaviour of correlators involving such external sources is completely captured by chiral Lagrangians, whose *raison d'être* is exactly to provide a consistent perturbative expansion for such quantities.

Notice that the choice of field redefinition (4.45) allowed us to move the non-derivative couplings entirely into the lightest two quarks. In this way we can integrate out all the other quarks and directly work in the 2-flavor effective theory, with M_a capturing the whole axion dependence, at least for observables that do not depend on the derivative couplings.

At the leading order in the chiral expansion all the non-derivative dependence on the axion is thus contained in the pion mass terms:

$$\mathcal{L}_{p^2} \supset 2B_0 \frac{f_\pi^2}{4} \langle U M_a^\dagger + M_a U^\dagger \rangle \,, \tag{4.48}$$

where

$$U = e^{i\Pi/f_\pi} \,, \quad \Pi = \begin{pmatrix} \pi^0 & \sqrt{2}\pi^+ \\ \sqrt{2}\pi^- & -\pi^0 \end{pmatrix} \,, \tag{4.49}$$

$\langle \cdots \rangle$ is the trace over flavor indices, B_0 is related to the chiral condensate and determined by the pion mass in term of the quark masses, and the pion decay constant is normalized such that $f_\pi \simeq 92$ MeV.

In order to derive the leading order effective axion potential we need only consider the neutral pion sector. Choosing Q_a proportional to the identity we have

$$V(a, \pi^0) = -B_0 f_\pi^2 \left[m_u \cos\left(\frac{\pi^0}{f_\pi} - \frac{a}{2f_a}\right) + m_d \cos\left(\frac{\pi^0}{f_\pi} + \frac{a}{2f_a}\right) \right]$$

$$= -m_\pi^2 f_\pi^2 \sqrt{1 - \frac{4m_u m_d}{(m_u + m_d)^2} \sin^2\left(\frac{a}{2f_a}\right)} \cos\left(\frac{\pi^0}{f_\pi} - \phi_a\right) \tag{4.50}$$
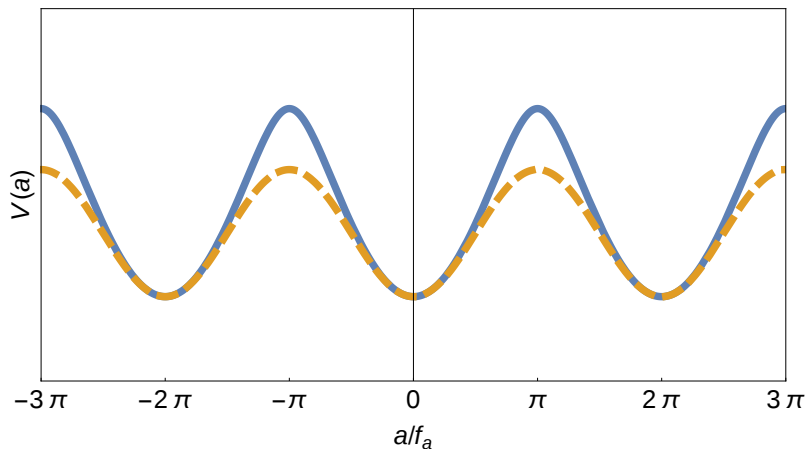
Figure 4.1: Comparison between the axion potential predicted by chiral Lagrangians, eq. (4.52) (continuous line) and the single cosine instanton one, $V^{inst}(a) = -m_a^2 f_a^2 \cos(a/f_a)$ (dashed line).

where

$$\tan \phi_a \equiv \frac{m_u - m_d}{m_d + m_u} \tan\left(\frac{a}{2f_a}\right) . \tag{4.51}$$

On the vacuum π^0 gets a vacuum expectation value (VEV) proportional to ϕ_a to minimize the potential, the last cosine in eq. (4.50) is 1 on the vacuum, and π^0 can be trivially integrated out leaving the axion effective potential

$$V(a) = -m_\pi^2 f_\pi^2 \sqrt{1 - \frac{4 m_u m_d}{(m_u + m_d)^2} \sin^2\left(\frac{a}{2f_a}\right)} . \tag{4.52}$$

As expected the minimum is at $\langle a \rangle = 0$ (thus solving the strong CP problem). Expanding to quadratic order we get the well-known [210] formula for the axion mass

$$m_a^2 = \frac{m_u m_d}{(m_u + m_d)^2} \frac{m_\pi^2 f_\pi^2}{f_a^2} . \tag{4.53}$$

Although the expression for the potential (4.52) was derived long ago [251], we would like to stress some points often under-emphasized in the literature.

The axion potential (4.52) is nowhere close to the single cosine suggested by the instanton calculation (see fig. 4.1). This is not surprising given that the latter relies on a semiclassical approximation, which is not under control in this regime. Indeed the shape of the potential is $\mathcal{O}(1)$ different from that of a single cosine, and its dependence on the

quark masses is non-analytic, as a consequence of the presence of light Goldstone modes. The axion self coupling, which is extracted from the fourth derivative of the potential

$$\lambda_a \equiv \left. \frac{\partial^4 V(a)}{\partial a^4} \right|_{a=0} = -\frac{m_u^2 - m_u m_d + m_d^2}{(m_u + m_d)^2} \frac{m_a^2}{f_a^2}, \tag{4.54}$$

is roughly a factor of 3 smaller than $\lambda_a^{(inst)} = -m_a^2/f_a^2$, the one extracted from the single cosine potential $V^{inst}(a) = -m_a^2 f_a^2 \cos(a/f_a)$. The six-axion couplings differ in sign as well.

The VEV for the neutral pion, $\langle \pi^0 \rangle = \phi_a f_\pi$ can be shifted away by a non-singlet chiral rotation. Its presence is due to the π^0-a mass mixing induced by isospin breaking effects in eq. (4.48), but can be avoided by a different choice for Q_a, which is indeed fixed up to a non-singlet chiral rotation. As noticed in [252], expanding eq. (4.48) to quadratic order in the fields we find the term

$$\mathcal{L}_{p^2} \supset 2B_0 \frac{f_\pi}{4f_a} a \langle \Pi \{Q_a, M_q\} \rangle, \tag{4.55}$$

which is responsible for the mixing. It is then enough to choose

$$Q_a = \frac{M_q^{-1}}{\langle M_q^{-1} \rangle}, \tag{4.56}$$

to avoid the tree-level mixing between the axion and pions and the VEV for the latter. Such a choice only works at tree level, the mixing reappears at the loop level, but this contribution is small and can be treated as a perturbation.

The non-trivial potential (4.52) allows for domain wall solutions. These have width $\mathcal{O}(m_a^{-1})$ and tension given by

$$\sigma = 8 m_a f_a^2 \, \mathcal{E}\left[\frac{4 m_u m_d}{(m_u + m_d)^2} \right], \qquad \mathcal{E}[q] \equiv \int_0^1 \frac{dy}{\sqrt{2(1-y)(1+\sqrt{1-qy})}}. \tag{4.57}$$

The function $\mathcal{E}[q]$ can be written in terms of elliptic functions but the integral form is more compact. Note that changing the quark masses over the whole possible range, $q \in [0, 1]$, only varies $\mathcal{E}[q]$ between $\mathcal{E}[0] = 1$ (cosine-like potential limit) and $\mathcal{E}[1] = 4 - 2\sqrt{2} \simeq 1.17$ (for degenerate quarks). For physical quark masses $\mathcal{E}[q_{phys}] \simeq 1.12$, only 12% off the cosine potential prediction, and $\sigma \simeq 9 m_a f_a^2$.

In a non vanishing axion field background, such as inside the domain wall or to a much lesser extent in the axion dark matter halo, QCD properties are different than in

the vacuum. This can easily be seen expanding eq. (4.50) at the quadratic order in the pion field. For $\langle a \rangle = \theta f_a \neq 0$ the pion mass becomes

$$m_\pi^2(\theta) = m_\pi^2 \sqrt{1 - \frac{4 m_u m_d}{(m_u + m_d)^2} \sin^2\left(\frac{\theta}{2}\right)} , \qquad (4.58)$$

and for $\theta = \pi$ the pion mass is reduced by a factor $\sqrt{(m_d + m_u)/(m_d - m_u)} \simeq \sqrt{3}$. Even more drastic effects are expected to occur in nuclear physics (see e.g. [253]).

The axion coupling to photons can also be reliably extracted from the chiral Lagrangian. Indeed at leading order it can simply be read out of eqs. (4.46), (4.47) and (4.56)[1]:

$$g_{a\gamma\gamma} = \frac{\alpha_{em}}{2\pi f_a}\left[\frac{E}{N} - \frac{2}{3}\frac{4 m_d + m_u}{m_d + m_u}\right] , \qquad (4.59)$$

where the first term is the model dependent contribution proportional to the EM anomaly of the PQ symmetry, while the second is the model independent one coming from the minimal coupling to QCD at the non-perturbative level.

The other axion couplings to matter are either more model dependent (as the derivative couplings) or theoretically more challenging to study (as the coupling to EDM operators), or both.

---

[1]The result can also be obtained using a different choice of Q_a, but in this case the non-vanishing a-π^0 mixing would require the inclusion of an extra contribution from the $\pi^0\gamma\gamma$ coupling.

Chapter 5

Axion dark matter

Due to the large value of the symmetry breaking scale f_a, axions have many properties required by dark matter: they are stable on cosmological scales and interact weakly with matter. Moreover, they are non-baryonic and massive. Depending on the production mechanism, the axion can be either hot or cold dark matter. The requirement that the axion has the correct relic density gives constraints on the value of the scale f_a (and therefore on its mass and interactions). Furthermore, as we will see in chapter 6, the dark matter properties of the axion are a necessary feature for several experiments.

It is therefore very important to study the mechanisms of axion production and the properties of the axion that give the correct relic density. In section 5.1, the cosmology of the axion will be reviewed, describing its production mechanisms and assessing the importance of studying axion properties at high temperatures. Then, in section 5.2, the properties of the axion at finite temperature are reviewed and their implication for dark matter are outlined.

5.1   Axion cosmology

Relic axions are produced both through thermal and non-termal mechanisms. They can arise due to the usual freeze out process, via the coherent production from the initial misalignment of the axion field, or through topological defects. These three mechanisms can be the dominant process for the production of relic axions, depending on the time of the breaking of the PQ symmetry relative to inflation, and on the effective value of the axion mass.

5.1.1 Thermal production

Axions can be produced in the early universe from the coupling to the thermal bath. Initially, the thermal equilibrium is kept by collisions with the SM particles and annihilation, and the axion number density follows the Boltzmann equation

$$\frac{dn_a}{dt} + 3H(T)n_a = \Gamma_{\text{ann}} \left(n_a^{\text{eq}} - n_a \right), \tag{5.1}$$

where the number density of axion in thermal equilibrium is

$$n_a^{\text{eq}} = \frac{\zeta(3)}{\pi^2} T^3. \tag{5.2}$$

The axion annihilation rate in the hot bath is

$$\Gamma_{\text{ann}} = \sum_i n_i \langle \sigma_i v \rangle, \tag{5.3}$$

where n_i is the number density for the particle species i, and v is the relative velocity between the particle species i and the axion. The cross section σ_i for the process $a + i \leftrightarrow SM\,SM$ is averaged over the momentum distributions of the particles involved.

As long as the annihilation rate is faster than the Hubble expansion, $\Gamma_{\text{ann}}(T) > H(T)$, the axion is in thermal equilibrium with the bath. Therefore, the temperature at which the axion decouples from the thermal bath is set by

$$\Gamma_{\text{ann}}(T_{\text{fo}}) = H(T_{\text{fo}}) = \sqrt{\frac{8\pi^2 g_*}{90}} \frac{T_{\text{fo}}^2}{M_{\text{Pl}}}, \tag{5.4}$$

where g_* is the number of degrees of freedom at the decoupling temperature T_{fo} and M_{Pl} is the Planck mass. In order to solve this equation we have to compute the annihilation rate $\Gamma_{\text{ann}}(T)$.

In the thermal bath, the axion couples mainly with gluons and quarks (if it directly couples to that, depending on the model) [223, 227].[1] The cross section of the conversion of two gluons in axions is

$$\sigma \sim \frac{\alpha_s^3}{f_a^2}. \tag{5.5}$$

For this process, the annihilation rate become

$$\Gamma_{\text{ann}}(T) \sim \frac{\alpha_s^3}{f_a^2} T^3 \sim \frac{10^{-5}}{f_a^2}. \tag{5.6}$$

---

[1]Thermal axions were first studied in [219], where Primakoff (conversion of an axion into a photon in presence of an external electromagnetic field) and photoproduction processes were considered.

From this last Equation, we can derive the decoupling temperature[1]

$$T_{\text{fo}} \sim 2 \cdot 10^{11} \text{ GeV} \sqrt{\frac{g_*}{100}} \left(\frac{f_a}{10^{12} \text{ GeV}} \right)^2.$$ (5.7)

After decoupling, the number density is

$$n_a(T) \propto n_a(T_{\text{fo}}) \left(\frac{R(T_{\text{fo}})}{R(T)} \right)^3,$$ (5.8)

and the current abundance from thermal production can be estimated to be

$$\Omega_a = 10^{-8} \left(\frac{100}{g_*} \right) \frac{10^{12} \text{ GeV}}{f_a}.$$ (5.9)

The axion production from thermal processes is not efficient for $f_a \sim 10^{12}$ GeV. If f_a is smaller, the coupling of the axion increases and the axion decouples later, helping to get more relic abundance. It is possible to get the correct relic abundance for $f_a \sim 10^6$ GeV. As we will see in the next chapter, this value is normally excluded by astrophysics bounds. However, the astrophysical bounds do not apply if the axion has an anomalously small coupling to photons. In this scenario the axion forms a hot dark matter candidate, but bounds from Planck already exclude the axion as hot dark matter [254].

5.1.2 Misalignment mechanism

The most efficient mechanism for axion production is non-thermal and it is called the misalignment mechanism [215–217]. The axion abundance today depends on whether inflation happened and on the value of the reheating temperature. Therefore there are two possible scenarios:

1) the breaking of the PQ symmetry happens before inflation, and the reheating phase happens at a temperature such that it cannot restore the PQ symmetry, $v_{PQ} \gtrsim \max(T_R, H_I)$;

2) the breaking of the PQ scale happens after inflation or at smaller scales with respect to the reheating temperature, $v_{PQ} \lesssim \max(T_R, H_I)$.

---

[1]There is another window of temperature that makes the axion to be in thermal equilibrium, $T \simeq f_\pi$. At this temperature it matters only the coupling of the axion to pions, that is larger than the perturbative α_s, and the process is more efficient. At this temperature the axion would have been in thermal equilibrium for $f_a \lesssim 10^7$ GeV.

5. Axion dark matter

In the first case, the PQ symmetry is broken at some very high scale, and then inflation happens. During inflation all modes are inflated: whatever was the configuration of the axion before inflation, because of the exponential expansion, all the modes get stretched and effectively in our universe the axion will end up to be a constant. During inflation the value of the axion is flattened within each Hubble patch, up to small fluctuation induced by the inflationary phase itself, which are of order $\delta a \sim H_I/2\pi$. When inflation ends, the universe starts to reheat. If the reheating temperature is below the PQ breaking scale, reheating cannot restore the PQ phase and there is a constant axion at low energy. After reheating, the universe will evolve as in the Standard Cosmology.

In the second case, either the inflation scale H_I or the reheating temperature T_R are larger than the PQ breaking scale. If $T_R > v_{PQ}$, independently on when inflation happens, the reheating phase will restore the PQ phase. As the temperature drops, there is a phase transition and the axion gets a potential. Once the potential is formed, the axion will start falling towards the minimum. After the restoration, in our observable patch there are regions where the axion has a different random initial value. If $H_I > v_{PQ}$, independently of T_R, the axion field assumes any value between $(0, 2\pi)$ because of the quantum fluctuation of inflation, that are of order $\langle \delta a \delta a \rangle \simeq H_I^2/(2\pi)^2$. When the modes reenter the horizon, they would populate all the values of the axion potential. Independently of whether T_R or H_I is larger than v_{PQ}, the axion has an effective initial condition assuming all the values in the range $(0, 2\pi)$.

In the first scenario, the axion is a constant up to small fluctuation of order H_I, which are negligible at the moment. The equation of motion of the axion are

$$\ddot{a} + 3H\dot{a} + m_a^2(T)f_a \sin\left(\frac{a}{f_a}\right) = 0, \tag{5.10}$$

where we assumed a cosine-like potential.

In the early universe, the mass is basically zero and a is a constant.[1] After inflation, during radiation or matter domination, H decreases in time. On the other hand, $m_a = 0$ at high temperature and as T drops, it starts increasing. There will be a time (temperature) when H and m_a are comparable. At that time the axion mass will pull the axion towards the minimum, and at lower temperature the pull will become stronger than the Hubble friction. As a consequence, the term $3H\dot{a}$ can be neglected. The axion then starts oscillating towards the minimum with a frequency m_a. When it starts oscillating it is possible to build an adiabatic invariant. The energy density is

$$\rho = \frac{1}{2}\dot{a}^2 + \frac{m^2}{2}a^2, \tag{5.11}$$

---

[1]Even if a would not be a constant, it would be driven to a constant by the Hubble friction: if $H \gg a$, $a = $ const.

where $\dot{a}$ denotes the derivative of a with respect to time, and the time derivative of ρ is

$$\dot{\rho} = \dot{a}\ddot{a} + m^2\dot{a}a + m\dot{m}a^2. \tag{5.12}$$

Using the equation of motion (5.10), I can rewrite the previous equation as

$$\dot{\rho} = \dot{a}(-3H\dot{a}) + \frac{\dot{m}}{m}m^2a^2, \tag{5.13}$$

assuming that the axion already started oscillating, and the term $3Ha$ is sufficiently smaller than m_a. Averaging over one oscillation we have

$$\langle\dot{\rho}\rangle = \langle m^2a^2\rangle\left(-3H + \frac{\dot{m}}{m}\right). \tag{5.14}$$

Replacing Equation (5.11) in the expression for $\langle\dot{\rho}\rangle$, we get

$$\frac{\dot{\rho}}{\rho} = \frac{\dot{m}}{m} - 3\frac{\dot{R}}{R}, \tag{5.15}$$

and integrating this equation

$$\frac{\langle\rho\rangle R^3}{m} = \text{const}, \tag{5.16}$$

one gets the number density

$$\langle n\rangle = \frac{\langle\rho\rangle}{m} = \frac{\text{const}}{R^3}, \tag{5.17}$$

showing that the number of axions in a comoving volume is conserved over time and the energy density behaves as cold dark matter. It is then possible to use this conservation law to extrapolate the energy density stored in the axion field today. In order to do so, we need to estimate the temperature at which the axion starts to oscillate. The axion starts oscillating when $m_a(T_*) \simeq 3\,H(T_*)$.[1] Assuming we are in radiation domination,

$$3\,H(T_*) = 3\left(\frac{8\pi^3 g_*(T_*)}{90 M_{\text{Pl}}^2}\right)^{1/2} T_*^2 \simeq m_a(T_*) \tag{5.18}$$

where g_* is the number of degrees of freedom of the standard model at the temperature when the axion start oscillating, T_*. A crucial point of the extraction of the temperature at which the axion starts oscillating is the understanding of the behaviour of the temperature dependence of the axion mass.

---

[1]There will be a region where both terms are important, but the transition is very fast.

5. Axion dark matter

The current axion abundance from misalignment, assuming standard cosmological evolution, is given by

$$\Omega_a = \frac{86}{33} \frac{\Omega_\gamma}{T_\gamma} \frac{n_a^\star}{s^\star} m_a \, , \tag{5.19}$$

where Ω_γ and T_γ are the current photon abundance and temperature respectively and $s^\star$ and $n_a^\star$ are the entropy density and the average axion number density computed at any moment in time $t_\star$ sufficiently after the axion starts oscillating such that $n_a^\star/s^\star$ is constant. The latter quantity can be obtained by solving eq. (5.10) and depends on 1) the QCD energy and entropy density around T_c, 2) the initial condition for the axion field θ_0, and 3) the temperature dependence of the axion mass and potential. The first is reasonably well known from perturbative methods and lattice simulations (see e.g. [255, 256]). The initial value θ_0 is a free parameter in the first scenario, where the PQ transition happens before inflation—since in this case θ_0 can be chosen in the whole interval $[0, 2\pi]$ only an upper bound to Ω_a can be obtained in this case. In the scenario where the PQ phase is instead restored after inflation $n_a^\star$ is obtained by averaging over all θ_0, which numerically corresponds to choosing[1] $\theta_0 \simeq 2.1$. Since θ_0 is fixed, Ω_a is completely determined as a function of f_a in this case. At the moment the biggest uncertainty on the misalignment contribution to Ω_a comes from our knowledge of $m_a(T)$.

In the computation of the axion relic density, we assumed that the axion is constant everywhere. However, this is not true, because during inflation the axion is subject to non adiabatic quantum fluctuations, called isocurvature fluctuations.

Isocurvature fluctuations

In the first scenario, where the PQ symmetry breaks before inflation and the reheating temperature T_R is smaller than the PQ breaking scale, the axion modes that enter the horizon feels quantum fluctuations

$$\langle |\delta a(x)|^2 \rangle = \left(\frac{H_I}{2\pi} \right)^2 \qquad \Rightarrow \qquad \sigma_\theta^2 = \left(\frac{H_I}{2\pi f_a} \right)^2 . \tag{5.20}$$

The perturbations are non adiabatic because the axion is massless during inflation and the fluctuation in the axion field do not change the energy density. If $H_I < v_{PQ}$ the fluctuation do not restore the PQ phase and the heavy modes are not excited. Thus, inflationary axion fluctuations leads to

$$\delta\rho = 0 = \delta\rho_a + \sum_{i \neq a} \delta\rho_i + \delta\rho_r, \tag{5.21}$$

---

[1]The effective θ_0 corresponding to the average is somewhat bigger than $\langle \theta^2 \rangle = \pi^2/3$ because of anharmonicities of the axion potential.

where ρ_i represents the energy density of matter and ρ_r the one of radiation. Assuming that all the fields but the axion have adiabatic perturbations

$$\frac{\delta\rho_i}{\rho_i} = \frac{3}{4}\frac{\delta\rho_r}{\rho_r} = 3\frac{\delta T}{T}, \tag{5.22}$$

one gets

$$\frac{\delta T}{T} = -\frac{\delta\rho_a}{\rho_a}\frac{\rho_a}{3\sum_i \rho_i + 4\rho_r}. \tag{5.23}$$

Since the biggest contributions come from modes that reentered the universe the latest, we can neglect the radiation contribution and the temperature fluctuations coming from isocurvature fluctuations are

$$\frac{\delta T}{T} = -\frac{\delta n_a}{n_a}\frac{\Omega_a}{3\Omega_{\mathrm{m}}}. \tag{5.24}$$

There are strong bounds on this type of fluctuations from the CMB. The fraction of isocurvature to total temperature fluctuations has been constrained by the Planck Collaboration to be [198]

$$\alpha_a = \frac{\langle(\delta T/T)^2\rangle_{\mathrm{iso}}}{\langle(\delta T/T)^2\rangle_{\mathrm{tot}}} < 0.02, \tag{5.25}$$

where $(\delta T/T)_{\mathrm{tot}} \simeq 10^{-5}$.

Assuming a gaussian distribution for θ, we find

$$\left\langle\left(\frac{\delta n_a}{n_a}\right)^2\right\rangle = \left\langle\left(\frac{\theta^2 - \langle\theta^2\rangle}{\langle\theta^2\rangle}\right)^2\right\rangle = 2\,\sigma_\theta^2\,\frac{2\langle\theta^2\rangle - \sigma_\theta^2}{\langle\theta^2\rangle^2}. \tag{5.26}$$

It follows then that

$$\alpha_a = \left(\frac{\Omega_a}{\Omega_{\mathrm{m}}}\right)^2 \frac{2\,\sigma_\theta^2}{\langle(\delta T/T)^2\rangle_{\mathrm{tot}}}\frac{2\langle\theta^2\rangle - \sigma_\theta^2}{\langle\theta^2\rangle^2}. \tag{5.27}$$

The solution of this equation leads to an upper bound on the scale of inflation [257]

$$H_I \lesssim k10^7 \text{ GeV } \left(\frac{f_a}{10^{12}\,\mathrm{GeV}}\right)^{1/2}\left(\frac{\alpha_a}{0.02}\right)^{1/2}\left(\frac{0.24}{\Omega_a}\right)^{1/2}, \tag{5.28}$$

where k is a constant that depends on the temperature dependence of m_a and can vary of about one order of magnitude.[1] Equation (5.28) shows that high scale inflation is not compatible with this type of scenario. Requiring that the axion does not give the whole dark matter could relax the constraint on H_I, allowing larger value. However, Ω_a cannot be too small because θ_0 is bounded to be at least σ_θ. If Ω_a is the smallest possible compatible with the bound on θ_0 and $f_a \sim M_{\mathrm{Pl}}$, the scale of inflation will still be too small to be compatible with high scale inflation models.

---

[1]In the following of this thesis we will discuss the impact of this constant depending on $m_a(T)$.

5.1.3 Topological defects

In the scenario where the PQ symmetry happens after inflation the physics of axion production goes beyond the misalignment mechanism. After inflation, when the temperature drops below the scale v_{PQ}, the PQ symmetry breaks spontaneously, and the axion field rolls down the potential randomly. Therefore, in different patches of the universe, the value of the axion may be different. In particular, there could be configurations where the axion in the minimum of the PQ potential forms a loop, spanning all the values from $\theta_0 = 0$ to 2π. In such configurations, inside the loop, there is a value of the field that is on the maximum of the potential, with an energy stored of order f_a^2. Considering a family of surfaces, there must be a line of points in the maximum of the potential, called cosmic string [258].

The energy stored in the string is measured as a tension μ (an energy per unit length)

$$\mu = \frac{E}{l} \simeq \pi f_a^2 \log \frac{f_a}{m_a}, \qquad (5.29)$$

where the logarithm comes form the fact that the axion must lie between 0 and 2π as we go around the string. Therefore, there is a gradient of energies associated to the axion $(\delta a \neq 0)$ around the cosmic string. The energy stored in the gradient is logarithmic divergent, exactly like the potential induced by a charged wire. Cosmic strings, therefore, may give rise to extra contributions to the axion energy density, that have to be taken into account in the computation of the relic abundance. Moreover, since the mass of the axion is much lighter than the scale f_a, the logarithm can be as big as ~ 70.

Such cosmic strings may evolve, cross each other and form loops.[1] Loops shrink because they have to minimise the energy, and by shrinking emit axions. At first, the Hubble expansion stretch the strings, that are stuck in the primordial plasma. Due to the Hubble expansion, the density of strings increases and it may be larger than one string per horizon. However, the expansion dilutes the plasma and at some point strings start to move freely at a relativistic speed. At this point, collapsing string loops and wiggles on long strings radiate axions. Moreover, strings move and intersect each other. After strings may intersect, may form loops that collapse and may emit axions. Given such efficient mechanism, the density of long strings is expected to reach a scaling solution [277] where the universe, in average, is filled up with a few strings per horizon.

At temperatures around the QCD phase transition, when $H(T) \sim m_a(T)$, the axion gets a mass and around each string the QCD potential develops with different initial conditions. The periodicity of the potential is $2\pi v_{PQ}$, where $v_{PQ} = N f_a$ and N is the number

---

[1]Cosmic string evolution has been discussed in several papers, see for example [259–276].

of charged representations that were inducing the anomaly. Therefore, the potential of the axion is periodic in f_a. The axion starts to oscillate towards the minimum and there are N different minima. At this point, each string become the edge of N domain walls.[1] The presence of domain walls may be dangerous because the process of axion radiation by strings stops [259], unless there is inflation after the PQ phase transition, such that the axion field is homogenised and there are no strings or domain walls, or unless $N = 1$ [258, 278, 279].

If $N = 1$ the period of the QCD potential is the same as the one of the PQ. Therefore, when the axion goes from 0 to 2π, there is only one vacuum and one domain wall for each string. Each domain wall starts from one string and ends to another, such that each string is a boundary of a domain wall. Strings attached to a domain wall are pulled by the domain wall tension and they annihilate into axions. In this case every string annihilates giving rise to a new population of axions that may significantly change the computation of the relic abundance.

Alternatively, in the scenario where $N > 1$, strings are connected by domain walls and form a stable network. As the universe expands, domain walls dilute slower than any other relativistic or non-relativistic particle and their energy density dominates at late times. This fact changes the history of the universe and this scenario is completely excluded. In principle it is possible to solve this problem by a small breaking of the PQ symmetry [259]: an extra term that breaks PQ tilts the potential and makes distinguishable the N vacua because they have different energy density. If the energy density of two close minima are different, the domain walls may accelerate towards each other in order to minimise the energy and the whole system may collapse, recovering the $N = 1$ scenario. Unfortunately, the PQ breaking must be small in order not to spoil the solution of the θ problem. With such a small PQ breaking, the process of domain wall collapse would be too slow, the annihilation would happen at late times and axions would be overproduced. It appears, then, that the scenario $N > 1$ is almost excluded.

In general, due to the large logarithmic factor, the final abundance of axions coming from this configuration may dominate over the misalignment mechanism [258, 259, 261, 264, 277, 280, 281].

5.2 The hot axion at NLO: finite temperature results

We now turn to discuss the properties of the QCD axion at finite temperature. The temperature dependence of the axion potential and its mass are important in the early

---

[1]Domain walls are two dimensional objects that interpolate between two close vacua.

5. Axion dark matter

Universe because they control the relic abundance of axions today (for a review see e.g. [282]). The most model independent mechanism of axion production in the early universe, the misalignment mechanism [215–217], is almost completely determined by the shape of the axion potential at finite temperature and its zero temperature mass. Additionally, extra contributions, such as string and domain walls can also be present if the PQ preserving phase is restored after inflation, and might be the dominant source of dark matter [258, 259, 261, 264, 277, 280, 281]. Their contribution also depends on the finite temperature behavior of the axion potential, although there are larger uncertainties in this case coming from the details of their evolution (for a recent numerical study see e.g. [274]).[1]

One may naively think that, as the temperature is raised, our knowledge of axion properties gets better and better—after all the higher the temperature the more perturbative QCD gets. The opposite is instead true. In this section we show that, at the moment, the precision with which we know the axion potential worsens as the temperature is increased!

At low temperature this is simple to understand. Our high precision estimates at zero temperature rely on chiral Lagrangians whose convergence degrades as the temperature approaches the critical temperature $T_c \simeq$ 160-170 MeV where QCD starts deconfining. At T_c the chiral approach is already out of control. Fortunately around the QCD cross-over region lattice computations are possible. The current precision is not yet competitive with our low temperature results but they are expected to improve soon. At higher temperatures several lattice computations are available [283–286], although with different results. For $T \gg T_c$ the dilute instanton gas approximation, being a perturbative computation, is believed to give a reliable estimate of the axion potential. It is known however that finite temperature QCD converges fast only for very large temperatures, above $\mathcal{O}(10^6)$ GeV (see e.g. [287]). The situation is particularly bad for the instanton computation. The screening of QCD charge causes an exponential sensitivity to quantum thermal loop effects. The resulting uncertainty on the axion mass and potential can easily be one order of magnitude or more! This is compatible with a recent lattice computation [288], performed without quarks, which found a high temperature axion mass differing from the instanton prediction at $T = 1$ GeV by a factor ~ 10. Recent results from simulations with physical quark masses [283] seem to show an even bigger disagreement, suggesting that at these temperatures even the form of the action is very different from the instanton prediction. However, other recent results from lattice simulations show a better agreement with the instanton computation [284–286], but still a factor ~ 10 larger.

---

[1]Axion could also be produced thermally in the early universe, this population would be sub-dominant for the allowed values of f_a [221, 223, 226, 227] but might leave a trace as dark radiation.

5.2.1   Low temperatures

For temperatures T below T_c axion properties can be reliably computed within finite temperature chiral Lagrangians [289, 290]. Given the QCD mass gap in this regime temperature effects are exponentially suppressed.

The computation of the axion mass is straightforward. Note that the temperature dependence can only come from the non local contributions that can feel the finite temperature. At one loop the axion mass only receives contribution from the local NLO couplings once rewritten in terms of the physical m_π and f_π [291]. This means that the leading temperature dependence is completely determined by the temperature dependence of m_π and f_π, and in particular is the same as that of the chiral condensate [289–291]

$$\frac{m_a^2(T)}{m_a^2} = \frac{\chi_{top}(T)}{\chi_{top}} \stackrel{\text{NLO}}{=} \frac{m_\pi^2(T)f_\pi^2(T)}{m_\pi^2 f_\pi^2} = \frac{\langle \bar{q}q \rangle_T}{\langle \bar{q}q \rangle} = 1 - \frac{3}{2}\frac{T^2}{f_\pi^2} J_1\left[\frac{m_\pi^2}{T^2}\right] , \qquad (5.30)$$

where

$$J_n[\xi] = \frac{1}{(n-1)!}\left(-\frac{\partial}{\partial \xi}\right)^n J_0[\xi] , \qquad J_0[\xi] \equiv -\frac{1}{\pi^2}\int_0^\infty dq\, q^2 \log\left(1 - e^{-\sqrt{q^2+\xi}}\right) . \quad (5.31)$$

The function $J_1(\xi)$ asymptotes to $\xi^{1/4}e^{-\sqrt{\xi}}/(2\pi)^{3/2}$ at large ξ and to $1/12$ at small ξ. Note that in the ratio $m_a^2(T)/m_a^2$ the dependence on the quark masses and the NLO couplings cancel out. This means that, at $T \ll T_c$, this ratio is known at a even better precision than the axion mass at zero temperature itself.

Higher order corrections are small for all values of T below T_c. There are also contributions from the heavier states that are not captured by the low energy Lagrangian. In principle these are exponentially suppressed by $e^{-m/T}$, where m is the mass of the heavy state. However, because the ratio m/T_c is not very large and a large number of states appear above T_c there is a large effect at around T_c, where the chiral expansion ceases to reliably describe QCD physics. An in depth discussion of such effects appears in [292] for the similar case of the chiral condensate.

The bottom line is that for $T \lesssim T_c$ eq. (5.30) is a very good approximation for the temperature dependence of the axion mass. At some temperature close to T_c eq. (5.30) suddenly ceases to be a good approximation and full non-perturbative QCD computations are required.

The leading finite temperature dependence of the full potential can easily be derived as well,

$$\frac{V(a;T)}{V(a)} = 1 + \frac{3}{2}\frac{T^4}{f_\pi^2 m_\pi^2\left(\frac{a}{f_a}\right)} J_0\left[\frac{m_\pi^2\left(\frac{a}{f_a}\right)}{T^2}\right] . \qquad (5.32)$$

The temperature dependent axion mass, eq. (5.30), can also be derived from eq. (5.32) by taking the second derivative with respect to the axion. The fourth derivative provides the temperature correction to the self-coupling,

$$\frac{\lambda_a(T)}{\lambda_a} = 1 - \frac{3}{2}\frac{T^2}{f_\pi^2}J_1\left[\frac{m_\pi^2}{T^2}\right] + \frac{9}{2}\frac{m_\pi^2}{f_\pi^2}\frac{m_u m_d}{m_u^2 - m_u m_d + m_d^2}J_2\left[\frac{m_\pi^2}{T^2}\right] . \tag{5.33}$$

5.2.2 High temperatures

While the region around T_c is clearly in the non-perturbative regime, for $T \gg T_c$ QCD is expected to become perturbative. At large temperatures the axion potential can thus be computed in perturbation theory, around the dilute instanton gas background, as described in [293]. The point is that, at high temperatures large gauge configurations, which would dominate at zero temperature because of the larger gauge coupling, are exponentially suppressed because of Debye screening. This makes the instanton computation a sensible one.

The prediction for the axion potential is of the form $V^{inst}(a; T) = -f_a^2 m_a^2(T)\cos(a/f_a)$ where

$$f_a^2 m_a^2(T) \simeq 2\int d\rho\, n(\rho, 0)e^{-\frac{2\pi^2}{g_s^2}m_{D1}^2\rho^2 + \cdots}, \tag{5.34}$$

the integral is over the instanton size ρ, $n(\rho, 0) \propto m_u m_d e^{-8\pi^2/g_s^2}$ is the zero temperature instanton density, $m_{D1}^2 = g_s^2 T^2(1 + n_f/6)$ is the Debye mass squared at LO, n_f is the number of flavor degrees of freedom active at the temperature T, and the dots stand for smaller corrections (see appendix B and [293] for more details). The functional dependence of eq. (5.34) on temperature is approximately a power law $T^{-\alpha}$ where $\alpha \approx 7 + n_f/3 + \ldots$ is fixed by the QCD beta function.

There is however a serious problem with this type of computation. The dilute instanton gas approximation relies on finite temperature perturbative QCD. The latter really becomes perturbative only at very high temperatures $T \gtrsim 10^6$ GeV due to IR divergences of the thermal bath [294]. Further, due to the exponential dependence on quantum corrections, the axion mass convergence is even worse than many other observables. In fact the LO estimate of the Debye mass m_{D1}^2 receives $\mathcal{O}(1)$ corrections at the NLO for temperatures around few GeV [295, 296]. Non-perturbative computations from lattice simulations [297–299] confirm the unreliability of the LO estimate.

Both lattice [299] and NLO [295] results give a Debye mass $m_D \simeq 1.5\, m_{D1}$ where m_{D1} is the leading perturbative result. Since the Debye mass enters the exponent of eq. (5.34) higher order effects can easily shift the axion mass at a given temperature by an order of magnitude or more.

Given the failure of perturbation theory in this regime of temperatures even the actual form of eq. (5.34) may be questioned and the full answer could differ from the semiclassical instanton computation even in the temperature dependence and in the shape of the potential. Because of this, direct computations from non-perturbative methods such as lattice QCD are highly welcome and have been performed lately [283–286].

Recently several computations of the temperature dependence of the topological susceptibility for pure SU(3) Yang-Mills appeared [288, 300]. While computations in this theory cannot be used for the QCD axion[1], they are useful to test the instanton result. In particular in [288] an explicit comparison was made in the interval of temperatures $T/T_c \in [0.9, 4.0]$. The results for the temperature dependence and the quartic derivative of the potential are compatible with those predicted by the instanton approximation, however the overall size of the topological susceptibility was found one order of magnitude bigger. While the size of the discrepancy seem to be compatible with a simple rescaling of the Debye mass, it goes in the opposite direction with respect to the one suggested by higher order effects, preferring a smaller value for $m_D \simeq 0.5 m_{D1}$. This fact betrays a deeper modification of eq. (5.34) than a simple renormalization of m_D.

Several full studies for real QCD are now available in the same range of temperatures. Results for $T \in [150, 600]$ are available in [283], for $2 + 1$ flavour QCD with physical quark masses. Fig. 5.1 compares these results with the ChPT ones, with nice agreement around $T \sim 140$ MeV. The plot is in terms of the ratio $m_a^2(T)/m_a^2$, which at low temperatures weakens the quark mass dependence, as manifest in the ChPT computation. However, at high temperature this may not be true anymore. For example the dilute instanton computation suggests $m_a^2(T)/m_a^2 \propto (m_u + m_d) \propto m_\pi^2$, which implies that the slope across the crossover region may be very sensitive to the value of the light quark masses. It is therefore very important to use the physical quark masses in lattice computations. These results suggest that $\chi(T)$ decreases with temperature much more slowly than in the quarkless case, in contradiction to the instanton computation. The result for the temperature slope in [283] imply a temperature dependence for the topological susceptibility $(\chi(T) \sim T^{-3})$ departing strongly from the one predicted by instanton computations. As we will see in the next section this could have dramatic consequences in the computation of the axionic relic abundance.

More recently lattice results appeared in [286], for temperatures between 100 MeV and 3 GeV. The analysis was performed with $2 + 1 + 1$ flavours (therefore including the charm quark) and physical quark masses. These results are also shown in figure 5.1, and

---

[1]Note that quarkless QCD differs from real QCD both quantitatively (e.g. $\chi(0)^{1/4} = 181$ MeV *vs* $\chi(0)^{1/4} = 75.5$ MeV, $T_c \simeq 300$ MeV *vs* $T_c \simeq 160$ MeV) and qualitatively (the former undergoes a first order phase transition across T_c while the latter only a crossover).
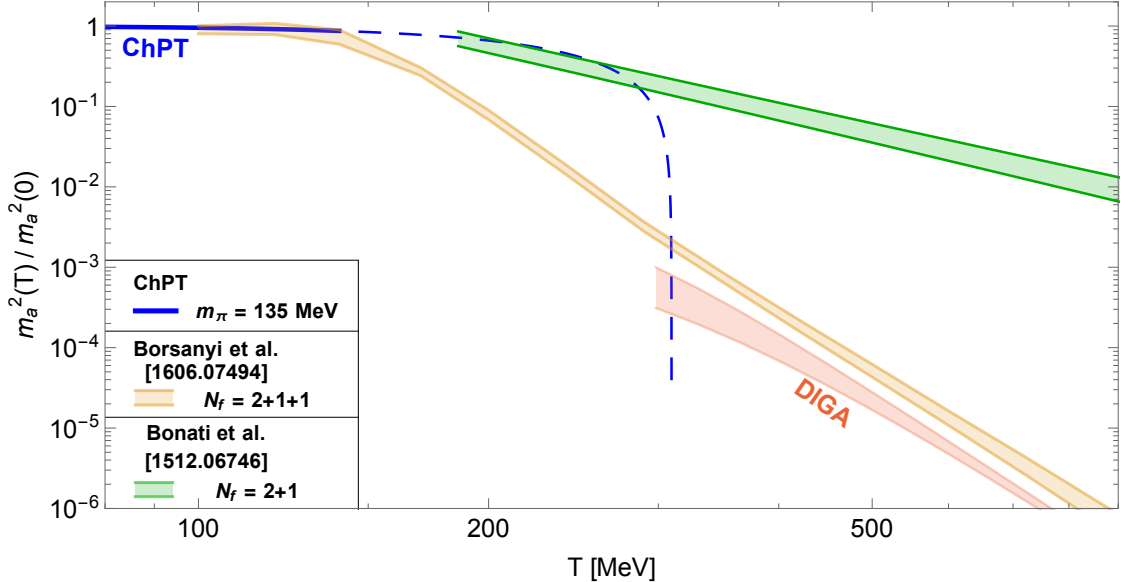
Figure 5.1: The temperature dependent axion mass squared normalized to the zero temperature value squared. In blue the prediction from chiral Lagrangians. In green the continuum extrapolation from the lattice data from ref. [283], and in yellow the lattice data from [286]. The red shaded curve shows the results from the instanton computation, varying the renormalisation scale μ between ρ^{-1} and $2\rho^{-1}$.

suggest that the topological susceptibility $\chi(T)$ has a slope in agreement with the one in the instanton computation. For completeness, in figure 5.1 we also show the instanton computation result, for details see appendix B.

5.2.3 Implications for dark matter

As we saw in section 5.1.2, the biggest uncertainty on the misalignment contribution to Ω_a comes from our knowledge of $m_a(T)$. Assuming that $m_a(T)$ can be approximated by the power law

$$m_a^2(T) = m_a^2(1\text{ GeV})\left(\frac{\text{GeV}}{T}\right)^\alpha = m_a^2 \frac{\chi(1\text{ GeV})}{\chi(0)}\left(\frac{\text{GeV}}{T}\right)^\alpha,$$

around the temperatures where the axion starts oscillating, eq. (5.10) can easily be integrated numerically. In fig. 5.2 we plot the values of f_a that would reproduce the correct dark matter abundance for different choices of $\chi(T)/\chi(0)$ and α in the scenario where θ_0 is integrated over. We also show three representative points, two of them with parameters
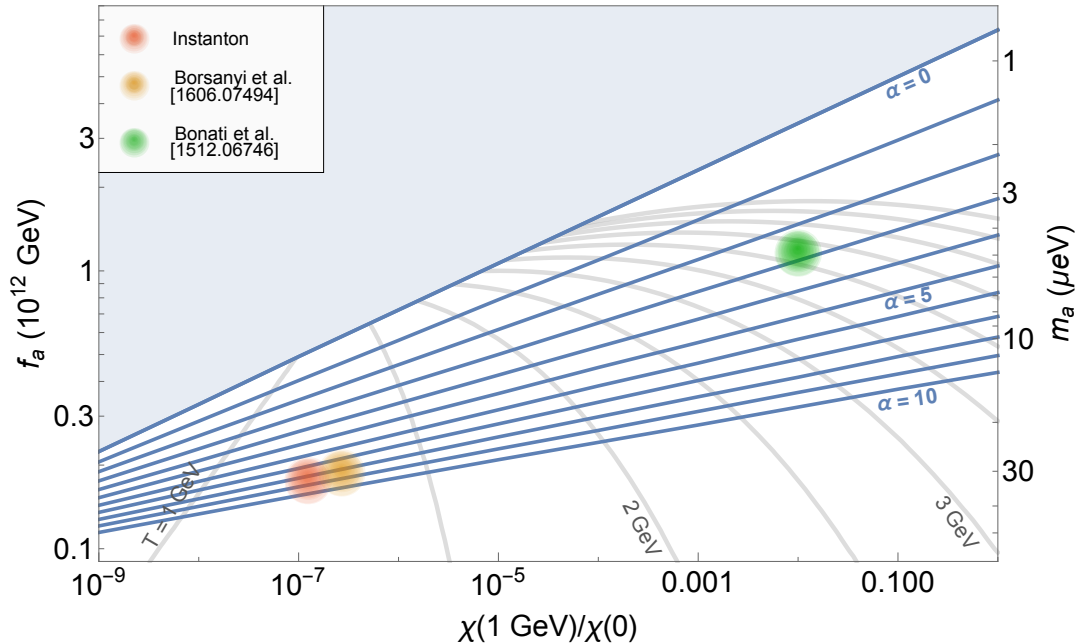
Figure 5.2: Values of f_a such that the misalignment contribution to the axion abundance matches the observed dark matter one for different choices of the parameters of the axion mass dependence on temperature. For definiteness the plot refers to the case where the PQ phase is restored after the end of inflation (corresponding approximately to the choice $\theta_0 = 2.15$). The temperatures where the axion starts oscillating, i.e. satisfying the relation $m_a(T) = 3H(T)$, are also shown. The three points corresponding to the dilute instanton gas prediction, lattice data by [286] and lattice data by [283] are shown for reference.

$(\alpha \approx 8, \chi(1 \text{ GeV})/\chi(0) \approx \text{few } 10^{-7})$, corresponding respectively to the expected behaviour from instanton computations and the lattice results [284–286], and one with parameters $(\alpha \approx 3, \chi(1 \text{ GeV})/\chi(0) \approx 10^{-2})$ from the lattice data in [283]. The figure also shows the corresponding temperature at which the axion starts oscillating, here defined by the condition $m_a(T) = 3H(T)$.

Notice that for large values of α, as predicted by instanton computations, the sensitivity to the overall size of the axion mass at fixed temperature ($\chi(1 \text{ GeV})/\chi(0)$) is weak. However if the slope of the axion mass with the temperature is much smaller, as claimed by the results in [283], then the corresponding value of f_a required to give the correct relic abundance can even be larger by an order of magnitude (note also that in this case the temperature at which the axion starts oscillating would be higher, around $4 \div 5$ GeV). The difference between the three cases could be taken as an estimate of the current uncertainty
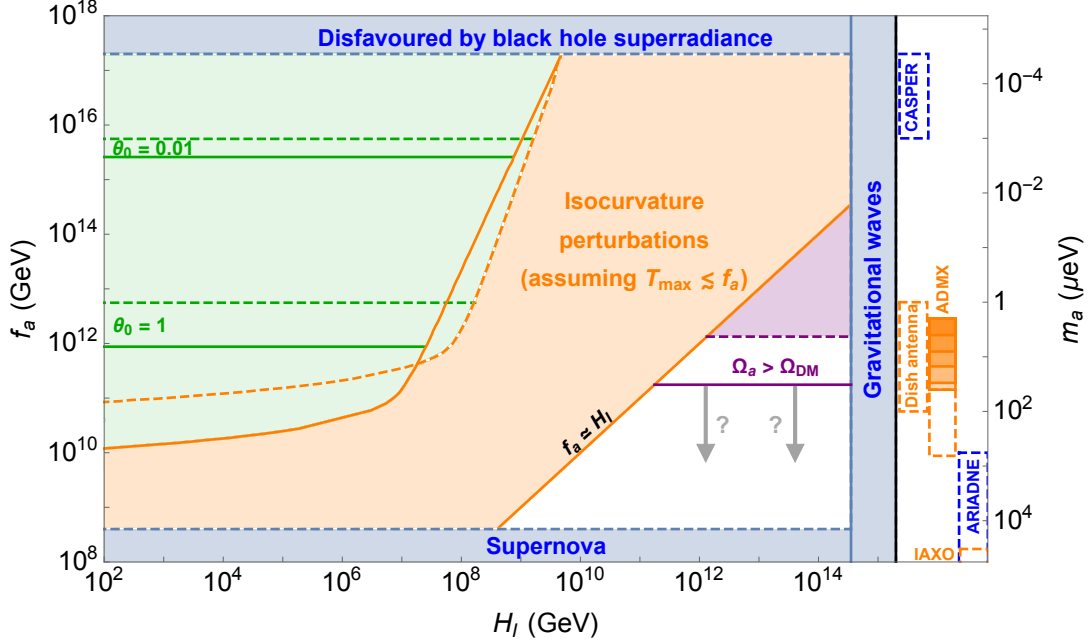
Figure 5.3: The axion parameter space as a function of the axion decay constant and the Hubble parameter during inflation. The bounds are shown for the two choices for the axion mass parametrization suggested by the instanton computations and the lattice simulation by [286] (continuous lines), and by the lattice results by [283] (dashed lines), corresponding to the labeled points in fig. 5.2. In the green shaded region the misalignment axion relic density can make up the entire dark matter abundance, and the isocurvature limits are obtained assuming that this is the case. In the white region the axion misalignment population can only be a sub-dominant component of dark matter. The region where PQ symmetry is restored after inflation does not include the contributions from topological defects, the lines thus only represent conservative upper bounds to the value of f_a. Ongoing (solid) and proposed (dashed empty) experiments testing the available axion parameter space are represented on the right side (see chapter 6).

on this type of computation. More accurate lattice results are needed to assess the actual temperature dependence of the axion mass and potential.

To show the impact of this uncertainty on the viable axion parameter space and the experiments probing it, in fig. 5.3 we plot the various constraints as a function of the Hubble scale during inflation and the axion decay constant. Limits that depend on the temperature dependence of the axion mass are shown for the instanton and lattice inspired forms (solid and dashed lines respectively), corresponding to the red and green labeled

points in fig. 5.2. On the right side of the plot we also show the values of f_a that will be probed by ongoing experiments (solid) and those that could be probed by proposed experiments (dashed empty). Orange colors are used for experiments using the axion coupling to photons, blue for the others. Experiments in the last column (IAXO and ARIADNE) do not rely on the axion being dark matter. The boundary of the allowed axion parameter space is constrained by the CMB limits on tensor modes [21], supernova SN1985 and other astrophysical bounds including black-hole superradiance.

When the PQ preserving phase is not restored after inflation (i.e. when both the Hubble parameter during inflation H_I and the maximum temperature after inflation T_{max} are smaller than the PQ scale) the axion abundance can match the observed dark matter one for a large range of values of f_a and H_I by varying the initial axion value θ_0. In this case isocurvature bounds [301] (see e.g. [302] for a recent discussion) constrain H_I from above. At small f_a obtaining the correct relic abundance requires θ_0 to be close to π, where the potential is flat, so the the axion begins oscillating at relatively late times. In the limit $\theta_0 \to \pi$ the axion energy density diverges. Given the sensitivity of Ω_a to θ_0 in this regime, isocurvatures are enhanced by $1/(\pi - \theta_0)$ and the bound on H_I is thus strengthened by a factor $\pi - \theta_0$.[1] Meanwhile, the axion decay constant is bounded from above by black-hole superradiance. For smaller values of f_a axion misalignment can only explain part of the dark matter abundance. In fig. 5.3 we show the value of f_a required to explain Ω_{DM} when $\theta_0 = 1$ and $\theta_0 = 0.01$ for the two reference values of the axion mass temperature parameters.

If the PQ phase is instead restored after inflation, e.g. for high scale inflation models, θ_0 is not a free parameter anymore. In this case only one value of f_a will reproduce the correct dark matter abundance. Given our ignorance about the contributions from topological defect we can use the misalignment computation to give an upper bound on f_a. This is shown on the bottom-right side of the plot, again for the two reference models, as before. Contributions from higher-modes and topological defects are likely to make such bound stronger by shifting the forbidden region downwards. Note that while the instanton behavior for the temperature dependence of the axion mass would point to axion masses outside the range which will be probed by ADMX (at least in the current version of the experiment), if the lattice behavior will be confirmed the mass window which will be probed would look much more promising.

---

[1]This constraint guarantees that we are consistently working in a regime where quantum fluctuations during inflation are much smaller than the distance of the average value of θ_0 from the top of the potential.

Chapter 6

Axion searches

The feeble couplings to photons and matter make the axion very challenging to search for. However, despite its elusive nature, excellent progress has been done in proposing new ways to detect it (see for example the following reviews [303–306]). The first proposal for axion detection [307] showed that axions can be directly searched in laboratories using the conversion of an axion into a photon in the presence of an external electromagnetic field.[1] Other proposals exploit axion telescopes (helioscopes) [309, 310] or new techniques as Nuclear Magnetic Resonance [311, 312].

   Alternatively, axions can be produced in the hot plasma that constitutes astrophysical objects like stars, opening up additional channels for the occurrence of astrophysical processes and altering star evolution. As a consequence, it would be possible to observe a modification of the solar sound-speed profile, an increase in the solar neutrino flux, a reduction of the helium-burning life time of globular cluster stars, an accelerated white dwarfs cooling, and a reduction of the supernova SN 1987A neutrino burst duration (see [313] for a review).

   Some of the proposed laboratory experiments to detect the QCD axion are reviewed in section 6.1, while the astrophysical bounds are described in section 6.2. Finally, the precision axion properties at $T = 0$ are presented in section 6.3.

6.1   Laboratory searches

Exploiting the coupling of the axion with photons

$$\mathcal{L} = \frac{1}{4}\, a\, g_{a\gamma\gamma} F_{\mu\nu} \tilde{F}^{\mu\nu} = -g_{a\gamma\gamma}\, \boldsymbol{E} \cdot \boldsymbol{B}\, a, \qquad (6.1)$$

---

[1]This process is called Primakoff effect [308].

where $\boldsymbol{E}$ and $\boldsymbol{B}$ are respectively the standard electric and magnetic field of the coupling photons respectively, it is possible to detect the axion [307]. Indeed, axions passing through an electromagnetic cavity, where a strong electromagnetic field with a frequency related to the size of the cavity is produced, could resonantly convert into photons when the cavity resonant frequency ω_a matches with the axion mass m_a.

Relic axions from the Big Bang are gravitationally bound to the Milky Way with a non relativistic velocity v and dispersion[1] $\Delta v \simeq 10^{-3}$. Consequently, the predicted axion mean energy would be

$$E \simeq m_a \left(1 + \frac{\Delta v^2}{2} \right), \tag{6.2}$$

with energy dispersion $\Delta E = \frac{1}{2} m_a \Delta v^2 \simeq 10^{-6}$.

The power of axions converting into photons in an electromagnetic cavity is given by

$$P_a = C g_{a\gamma\gamma}^2 V B_0^2 \frac{\rho_a}{m_a} Q_{\text{eff}}, \tag{6.3}$$

where C is a constant that depends on the transverse magnetic cavity modes, V is the volume of the cavity, B_0 is the magnetic field, and Q_{eff} is an effective quality factor that is smaller or equal than the cavity's quality factor Q_L and the quality factor for the axion signal $Q_a \simeq 1/\Delta v^2 \sim 10^6$. Three physical parameters that are extremely important are the axion-photon coupling $g_{a\gamma\gamma}$, the axion mass m_a and the local axion density ρ_a. Such an experiment would lead to measurements of the axion-photon coupling and its mass, once the local axion DM density is fixed to its value [314, 315]. The resonant condition requires that the frequency of the cavity must be equal to the axion mass $\nu = m_a(1 + \Delta v^2/2)$. Therefore, should the axion be discovered by such experiments, its mass would be known with a precision comparable to the suppressed line width of the resonance, $\delta m_a/m_a \sim \mathcal{O}(10^{-6})$.

The drawback of cavity microwave experiments is that the cavity frequency has to be equal to the energy of the axion, which is essentially given by its mass. Since the axion mass is not known and it may be in a wide range, these experiments require a slow scan over large numbers of frequencies.

The first experiments of this kind were performed at the Brookhaven National Laboratory [316, 317] and at the University of Florida [318], and excluded an axion mass in the range $[4.5, 16.3]$ μeV, without reaching the photon coupling characteristic of the QCD axion. The best sensitivity is currently achieved by the Axion Dark Matter eXperiment (ADMX) [319]. Currently, ADMX excludes the region between 1.9 and 3.65 μeV, for an axion photon coupling larger than $\sim 10^{-15}$ GeV^{-1}, on the edge of the KSVZ QCD axion

---

[1]We use natural units where $c = \hbar = 1$.
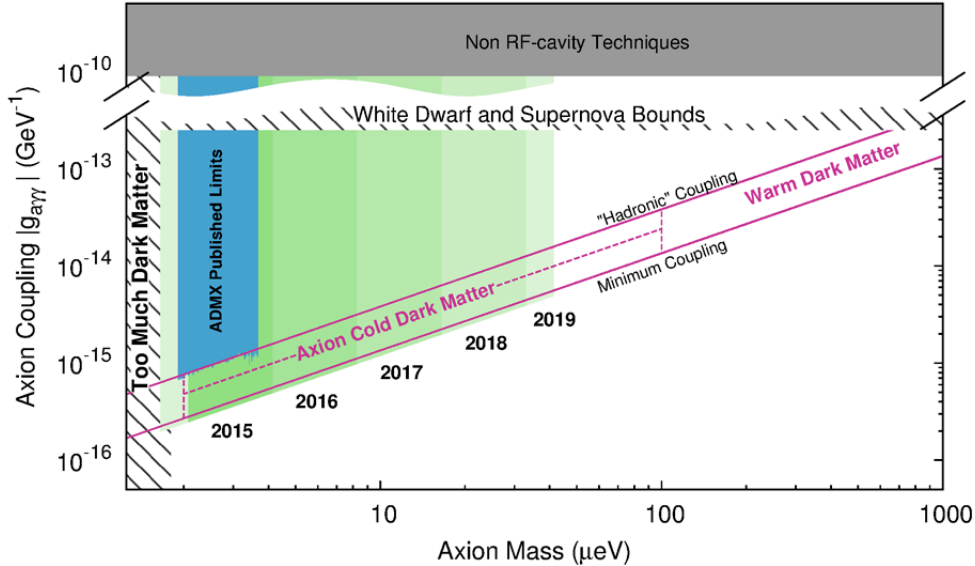
Figure 6.1: Search reach of ADMX and ADMX-HF over the next years in the m_a-$|g_{a\gamma\gamma}|$ plane. The blue shaded area denotes the current limits from ADMX. The shaded green regions are the reach of the future stages of ADMX. The red curves show the QCD axion parameter space.

model, see figure 6.1. In the figure it is also shown the possible future reach of the high frequency version of ADMX (ADMX-HF), that may cover along the years the QCD axion parameter space for $m_a \in [2, 40]$ μeV.

Future experiments

New search concepts for the detection of dark matter axions have been proposed in the last years. The authors of [320] proposed a microwave resonator structure sensitive to dark matter axions with an expected sensitivity to dark matter axion mass between 40 and 600 μeV for axion photon couplings below 10^{-14} GeV^{-1}.

Alternatively, the oscillating axion field induces oscillating electric dipole moments that cause a precession of nuclear spins in spin polarised nucleon in presence of an electric field. Consequently, it is possible to search for the resulting transverse magnetisation exploiting nuclear magnetic resonance techniques. The Cosmic Axion Spin Precession Experiment (CASPEr) searches for two different couplings of the axion [311]. On one hand, CASPER-Wind searches for the axion wind effect which causes a precession of the nuclear spin, probing the pseudo-scalar coupling g_{aNN}. On the other hand, CASPER-Electric exploits the time varying nucleon electric dipole moment g_d caused by the axion.

This experiment may reach large values of f_a corresponding to masses of the order of the neV but, at least with the current technology, it is not able to reach the parameter space of the QCD axion.

The search for axion can be extended by combining nuclear magnetic resonance techniques and short distance tests of gravity. The proposals by [312] (ARIADNE) is based on resonant couplings between the rotational frequency of a source mass and a nuclear magnetic resonance sample with matching spin precession frequency. ARIADNE may be able to probe CP-violating axion couplings to matter for QCD axion masses below 10^{-3} eV.

The authors of [321] proposed a new technique to search for axions with dish antennas. Cold dark matter axions mixing with photons are converted into monochromatic photons emitted from the surface of a spherical antenna and focused in the centre, where a broadband detector is placed. The proposed experiment would be both directional and broadband in frequency, overcoming some of the drawbacks of the resonant cavity experiments. The lack of resonant enhancement can be compensated by increasing the area of the dish surface. Such experiment may be sensitive to QCD axion with masses between 1 and 100 μeV.

6.2 Astrophysical bounds

Solar axions

The existence of axion produced in the hot plasma of astrophysical objects would open up additional channels for the occurrence of astrophysical process and would alter the star evolution. Consequently, the sun would be a powerful axion source. Particles with a two-photon vertex, like the axion, transform into photons in an electric or magnetic field. Thus, the axion can be produced from thermal photons in the electromagnetic fields of the stellar plasma [322]. This new process can in principle shorten the lifetime of the sun. Requiring that the axion does not spoil the standard solar model constrain the axion photon coupling to be $g_{a\gamma\gamma} \lesssim 1.1 \times 10^{-9}$ GeV^{-1} [323]. A similar bound can be derived by the fact that the axion affect the sound speed profile of the sun. Moreover, solar models with axion losses would dramatically increase the solar ^8B neutrino flux [323], while the measured value implies $g_{a\gamma\gamma} \lesssim 5 \times 10^{-10}$ GeV^{-1} [324–326].

Additionally, the inverted Primakoff effect can be exploited to search for axion conversion in a magnetic field. The CERN Axion Solar Telescope (CAST) consists in a telescope pointed at the Sun, with a strong magnetic field and an X-ray detector at the end. An axion passing through the magnetic field may convert to a low energy photon that can

be detected at the end of the telescope. CAST has already been able to constrain the axion photon coupling to lie below $g_{a\gamma\gamma} \lesssim 8.8 \times 10^{-11}$ GeV^{-1} for $m_a < 0.02$ eV and $g_{a\gamma\gamma} \lesssim 2.2 \times 10^{-10}$ GeV $^{-1}$ for $0.02 < m_a < 0.4$ eV [327].

Furthermore, it is possible to reach an increased sensitivity with stronger magnets, the basis for the International Axion Observatory (IAXO) [310]. After few years of data taking, IAXO may be able to reach $g_{a\gamma\gamma} \sim 5 \times 10^{-12}$ GeV^{-1} for $m_a \lesssim 0.02$ eV and $g_{a\gamma\gamma} \sim 1 \times 10^{-11}$ GeV^{-1} for $0.02 \lesssim m_a \lesssim 0.2$ eV.

Supernova SN1987A

One of the strongest bounds on the axion mass comes from the observations of neutrinos originating from the supernova SN1987A [328]. The relevant process consists of a core collapse of a massive star which subsequently leads to a proto neutron star. Axion can therefore be produced through nucleon nucleon axion bremsstrahlung $N+N \to N+N+a$, involving the axion nucleon coupling.

The cooling time of the supernova can be affected by such a process and the duration of the burst can therefore be reduced. As a consequence, the associated neutrino flux may be reduced. If the axion nucleon coupling g_{aNN} is very small, the axion emission does not change the cooling time. As g_{aNN} increases, the emission of bremsstrahlung axions increase and therefore the burst duration shortens. A minimum in the cooling time is reached when the axion mean free path corresponds to the geometric size of the supernova core. For even larger couplings, axions are trapped in the medium and their emission decreases reaching a point where the cooling time is unaffected by their presence.

The Kamiokande-II and the Irvine-Michigan-Brookhaven experiments measured the flux of electron antineutrinos coming from the SN1987A, allowing comparison of the data with theoretical expectations. Such measurements allowed to exclude axions for $3 \times 10^{-10} \lesssim g_{aNN}/\,\mathrm{GeV}^{-1} \lesssim 3 \times 10^{-7}$ [313], implying that QCD axion masses heavier than $\mathcal{O}(10)$ meV are excluded. This bound corresponds to $f_a \gtrsim 2 \times 10^8$ GeV.

White dwarf cooling

After helium burning stars reach the latest stages of their helium consumption, they evolve to the asymptotic giant branch (AGB) in the Hertzsprung-Russell diagram. An AGB star may then evolve into a white dwarf star by cooling down because of neutrino emission and surface photon emission. The existence of axions would open up an additional channel for the cooling of AGN into white dwarfs via the process

$$e + Ze \to e + Ze + a, \tag{6.4}$$

where Z is the atomic number. It is then possible to derive constraints on the axion mass and the axion-electron coupling comparing the theoretical luminosity function, including the above process, and the observed cooling rate derived from the decrease of the rotational period. The constraint on the axion-electron coupling obtained is [329, 330]

$$g_{aee} \lesssim 1.3 \times 10^{-13}. \tag{6.5}$$

Globular cluster stars

Gravitationally bound systems of stars that formed at the same time are called globular clusters. Globular clusters are particularly useful for testing models of stellar evolution because their stars formed at the same time. If axions exist, they would change the evolution of helium burning stars accelerating the helium consumption via the axion production channel. This effect would reduce the lifetime of the horizontal branch stars by a factor proportional to the axion-photon coupling

$$\left[1 + \frac{3}{8} \left(\frac{g_{a\gamma\gamma}}{10^{-10} \, \text{GeV}^{-1}} \right)^2 \right]^{-1} . \tag{6.6}$$

A reasonably conservative estimate from the analysis of a statistically significant set of helium burning stars implies [331]

$$g_{a\gamma\gamma} \lesssim 6.6 \times 10^{-11} \, \text{GeV}^{-1}, \tag{6.7}$$

a limit comparable to the one of CAST, but applying for higher masses. This limit excludes QCD axions heavier than $\mathcal{O}(10)$ eV.

Black hole superradiance

Very light axions have a Compton wavelength comparable to the size of black holes and thus form an approximately hydrogenic spectrum of bound states with different energy levels. The occupation number of the bound states grows exponentially, fed by the energy and the angular momentum of the black hole. While the occupation number of the bound states grows forming a condensate around the black hole, axions can superradiate extracting angular momentum and rotational energy from the black hole. Furthermore, axions can emit gravitational waves resulting in a regular extraction of angular momentum from the black hole. As a consequence, the black hole spins down. Current black hole spin measurements imply an upper bound on the QCD axion decay constant of 2×10^{17} GeV [332, 333].

6.3 The cool axion, precisely: $T = 0$ properties

Axion searches set bounds on the axion mass and on its couplings. Furthermore, the discovery of the axion by ADMX, for example, would lead to a very accurate measurement of its mass. Depending on the experiment, different axion couplings may also be extracted with a different accuracy. It is therefore important to understand what we could learn from these measurements and if it is possible to exploit such high precision in the axion mass and maybe couplings.

At this point the natural question is, how good are the estimates obtained so far using leading order chiral Lagrangians? In the 3-flavor chiral Lagrangian NLO corrections are typically around 20-30%. The 2-flavor theory enjoys a much better perturbative expansion given the larger hierarchy between pions and the other mass thresholds. To get a quantitative answer the only option is to perform a complete NLO computation. Given the better behaviour of the 2-flavor expansion we perform all our computation with the strange quark integrated out. The price we pay is the reduced number of physical observables that can be used to extract the higher order couplings. When needed we will use the 3-flavor theory to extract the values of the 2-flavor ones. This will produce intrinsic uncertainties $\mathcal{O}(30\%)$ in the extraction of the 2-flavor couplings. Such uncertainties however will only have a small impact on the final result whose dependence on the higher order 2-flavor couplings is suppressed by the light quark masses.

6.3.1 The mass

The first quantity we compute is the axion mass. As mentioned before at leading order in $1/f_a$ the axion can be treated as an external source. Its mass is thus defined as

$$m_a^2 = \frac{\delta^2}{\delta a^2} \log \mathcal{Z}\big(\tfrac{a}{f_a}\big)\Big|_{a=0} = \frac{1}{f_a^2} \frac{d^2}{d\theta^2} \log \mathcal{Z}(\theta)\Big|_{\theta=0} = \frac{\chi_{top}}{f_a^2}\,, \tag{6.8}$$

where $\mathcal{Z}(\theta)$ is the QCD generating functional in the presence of a theta term and χ_{top} is the topological susceptibility.

A partial computation of the axion mass at one loop was first attempted in [334]. More recently the full NLO corrections to χ_{top} has been computed in [335]. We recomputed this quantity independently and present the result for the axion mass directly in terms of observable renormalized quantities[1].

---

[1]The results in [335] are instead presented in terms of the unphysical masses and couplings in the chiral limit. Retaining the full explicit dependence on the quark masses those formula are more suitable for lattice simulations.

The computation is very simple but the result has interesting properties:

$$m_a^2 = \frac{m_u m_d}{(m_u + m_d)^2} \frac{m_\pi^2 f_\pi^2}{f_a^2} \left[1 + 2\frac{m_\pi^2}{f_\pi^2} \left(h_1^r - h_3^r - l_4^r + \frac{m_u^2 - 6m_u m_d + m_d^2}{(m_u + m_d)^2} l_7^r \right) \right], \qquad (6.9)$$

where h_1^r, h_3^r, l_4^r and l_7^r are the renormalized NLO couplings of [336] and m_π and f_π are the physical (neutral) pion mass and decay constant (which include NLO corrections). There is no contribution from loop diagrams at this order (this is true only after having reabsorbed the one loop corrections of the tree-level factor $m_\pi^2 f_\pi^2$). In particular l_7^r and the combinations $h_1^r - h_3^r - l_4^r$ are separately scale invariant. Similar properties are also present in the 3-flavor computation, in particular there are no $\mathcal{O}(m_s)$ corrections (after renormalization of the tree-level result), as noticed already in [334].

To get a numerical estimate of the axion mass and the size of the corrections we need the values of the NLO couplings. In principle l_7^r could be extracted from the QCD contribution to the π^+-π^0 mass splitting. While lattice simulations have started to become sensitive to EM and isospin breaking effects, at the moment there are no reliable estimates of this quantity from first principle QCD. Even less is known about $h_1^r - h_3^r$, which does not enter other measured observables. The only hope would be to use lattice QCD computation to extract such coupling by studying the quark mass dependence of observables such as the topological susceptibility. Since these studies are not yet available we employ a small trick: we use the relations in [337] between the 2- and 3-flavor couplings to circumvent the problem. In particular we have

$$\begin{aligned}
l_7^r &= \frac{m_u + m_d}{m_s} \frac{f_\pi^2}{8m_\pi^2} - 36L_7 - 12L_8^r + \frac{\log(m_\eta^2/\mu^2) + 1}{64\pi^2} + \frac{3\log(m_K^2/\mu^2)}{128\pi^2} \\
&= 7(4) \cdot 10^{-3}, \\
h_1^r - h_3^r - l_4^r &= -8L_8^r + \frac{\log(m_\eta^2/\mu^2)}{96\pi^2} + \frac{\log(m_K^2/\mu^2) + 1}{64\pi^2} = (4.8 \pm 1.4) \cdot 10^{-3}. \qquad (6.10)
\end{aligned}$$

The first term in l_7^r is due to the tree-level contribution to the π^+-π^0 mass splitting due to the π^0-η mixing from isospin breaking effects. The rest of the contribution, formally NLO, includes the effect of the η-η' mixing and numerically is as important as the tree-level piece [337]. We thus only need the values of the 3-flavor couplings L_7 and L_8^r, which can be extracted from chiral fits [338] and lattice QCD [339], we refer to appendix C for more details on the values used. An important point is that by using 3-flavor couplings the precision of the estimates of the 2-flavor ones will be limited to the convergence of the 3-flavor Lagrangian. However, given the small size of such corrections even an $\mathcal{O}(1)$ uncertainty will still translate into a small overall error.

The final numerical ingredient needed is the actual up and down quark masses, in particular their ratio. Since this quantity already appears in the tree level formula of the axion mass we need a precise estimate for it, however, because of the Kaplan-Manohar (KM) ambiguity [340], it cannot be extracted within the meson Lagrangian. Fortunately recent lattice QCD simulations have dramatically improved our knowledge of this quantity. Considering the latest results we take

$$z \equiv \frac{m_u^{\overline{\mathrm{MS}}}(2 \text{ GeV})}{m_d^{\overline{\mathrm{MS}}}(2 \text{ GeV})} = 0.48(3) \,, \tag{6.11}$$

where we have conservatively taken a larger error than the one coming from simply averaging the results in [238–240] (see the appendix C for more details). Note that z is scale independent up to α_{em} and Yukawa suppressed corrections. Note also that since lattice QCD simulations allow us to relate physical observables directly to the high-energy $\overline{\mathrm{MS}}$ Yukawa couplings, in principle[1], they do not suffer from the KM ambiguity, which is a feature of chiral Lagrangians. It is reasonable to expect that the precision on the ratio z will increase further in the near future.

Combining everything together we get the following numerical estimate for the axion mass

$$m_a = 5.70(6)(4) \ \mu\mathrm{eV} \left(\frac{10^{12}\mathrm{GeV}}{f_a} \right) = 5.70(7) \ \mu\mathrm{eV} \left(\frac{10^{12}\mathrm{GeV}}{f_a} \right) \,, \tag{6.12}$$

where the first error comes from the up-down quark mass ratio uncertainties (6.11) while the second comes from the uncertainties in the low energy constants (6.10). The total error of $\sim 1\%$ is much smaller than the relative errors in the quark mass ratio ($\sim 6\%$) and in the NLO couplings ($\sim 30 \div 60\%$) because of the weaker dependence of the axion mass on these quantities

$$m_a = \left[5.70 + 0.06 \, \frac{z - 0.48}{0.03} - 0.04 \, \frac{10^3 l_7^r - 7}{4} \right.$$
$$\left. + 0.017 \, \frac{10^3 (h_1^r - h_3^r - l_4^r) - 4.8}{1.4} \right] \mu\mathrm{eV} \, \frac{10^{12} \text{ GeV}}{f_a} \,. \tag{6.13}$$

Note that the full NLO correction is numerically smaller than the quark mass error and its uncertainty is dominated by l_7^r. The error on the latter is particularly large because of a partial cancellation between L_7^r and L_8^r in eq. (6.10). The numerical irrelevance of the other NLO couplings leaves a lot of room for improvement should l_7^r be extracted directly from Lattice QCD.

---

[1]Modulo well-known effects present when chiral non-preserving fermions are used.

The value of the pion decay constant we used ($f_\pi = 92.21(14)$ MeV) [341] is extracted from π^+ decays and includes the leading QED corrections, other $\mathcal{O}(\alpha_{em})$ corrections to m_a are expected to be sub-percent. Further reduction of the error on the axion mass may require a dedicated study of this source of uncertainty as well.

As a by-product we also provide a comparably high precision estimate of the topological susceptibility itself

$$\chi_{top}^{1/4} = \sqrt{m_a f_a} = 75.5(5)\,\text{MeV}\,, \tag{6.14}$$

against which lattice simulations can be calibrated.

6.3.2 The potential: self-coupling and domain-wall tension

Analogously to the mass, the full axion potential can be straightforwardly computed at NLO. There are three contributions: the pure Coleman-Weinberg 1-loop potential from pion loops, the tree-level contribution from the NLO Lagrangian, and the corrections from the renormalization of the tree-level result, when rewritten in terms of physical quantities (m_π and f_π). The full result is

$$
\begin{aligned}
V(a)^{\text{NLO}} = & -m_\pi^2\!\left(\tfrac{a}{f_a}\right) f_\pi^2 \left\{ 1 - 2\frac{m_\pi^2}{f_\pi^2}\left[l_3^r + l_4^r - \frac{(m_d - m_u)^2}{(m_d + m_u)^2}l_7^r - \frac{3}{64\pi^2}\log\left(\frac{m_\pi^2}{\mu^2}\right)\right] \right. \\
& + \frac{m_\pi^2\!\left(\tfrac{a}{f_a}\right)}{f_\pi^2}\left[h_1^r - h_3^r + l_3^r + \frac{4m_u^2 m_d^2}{(m_u + m_d)^4}\frac{m_\pi^8 \sin^2\!\left(\tfrac{a}{f_a}\right)}{m_\pi^8\!\left(\tfrac{a}{f_a}\right)}l_7^r \right. \\
& \left.\left. - \frac{3}{64\pi^2}\left(\log\left(\frac{m_\pi^2\!\left(\tfrac{a}{f_a}\right)}{\mu^2}\right) - \frac{1}{2}\right)\right]\right\}
\end{aligned}
\tag{6.15}
$$

where $m_\pi^2(\theta)$ is the function defined in eq. (4.58), and all quantities have been rewritten in terms of the physical NLO quantities[1]. In particular the first line comes from the NLO corrections of the tree-level potential while the second line is the pure NLO correction to the effective potential.

The dependence on the axion is highly non-trivial, however the NLO corrections account for only up to few percent change in the shape of the potential (for example the difference in vacuum energy between the minimum and the maximum of the potential changes by 3.5% when NLO corrections are included). The numerical values for the additional low-energy constants $l_{3,4}^r$ are reported in appendix C. We thus know the full QCD axion potential at the percent level!

---

[1]See also [342] for a related result computed in terms of the LO quantities.

It is now easy to extract the self-coupling of the axion at NLO by expanding the effective potential (6.15) around the origin

$$V(a) = V_0 + \frac{1}{2} m_a^2 a^2 + \frac{\lambda_a}{4!} a^4 + \dots \tag{6.16}$$

We find

$$\lambda_a = -\frac{m_a^2}{f_a^2} \left\{ \frac{m_u^2 - m_u m_d + m_d^2}{(m_u + m_d)^2} \right. \tag{6.17}$$

$$\left. +6\frac{m_\pi^2}{f_\pi^2} \frac{m_u m_d}{(m_u + m_d)^2} \left[h_1^r - h_3^r - l_4^r + \frac{4\bar{l}_4 - \bar{l}_3 - 3}{64\pi^2} - 4\frac{m_u^2 - m_u m_d + m_d^2}{(m_u + m_d)^2} l_7^r \right] \right\}, \tag{6.18}$$

where m_a is the physical one-loop corrected axion mass of eq. (6.9). Numerically we have

$$\lambda_a = -0.346(22) \cdot \frac{m_a^2}{f_a^2}, \tag{6.19}$$

the error on this quantity amounts to roughly 6% and is dominated by the uncertainty on l_7^r.

Finally the NLO result for the domain wall tensions can be simply extracted from the definition

$$\sigma = 2 f_a \int_0^\pi d\theta \sqrt{2[V(\theta) - V(0)]}, \tag{6.20}$$

using the NLO expression (6.15) for the axion potential. The numerical result is

$$\sigma = 8.97(5) \, m_a f_a^2, \tag{6.21}$$

the error is sub percent and it receives comparable contributions from the errors on l_7^r and the quark masses.

As a by-product we also provide a precision estimate of the topological quartic moment of the topological charge Q_{top}

$$b_2 \equiv -\frac{\langle Q_{top}^4 \rangle - 3\langle Q_{top}^2 \rangle^2}{12\langle Q_{top}^2 \rangle} = \frac{f_a^2 V''''(0)}{12 V''(0)} = \frac{\lambda_a f_a^2}{12 m_a^2} = -0.029(2), \tag{6.22}$$

to be compared to the cosine-like potential $b_2^{inst} = -1/12 \simeq -0.083$.

6.3.3 Coupling to photons

Similarly to the axion potential, the coupling to photons (4.59) also gets QCD corrections at NLO, which are completely model independent. Indeed derivative couplings only produce m_a suppressed corrections which are negligible, thus the only model dependence lies in the anomaly coefficient E/N.

For physical quark masses the QCD contribution (the second term in eq. (4.59)) is accidentally close to -2. This implies that models with $E/N = 2$ can have anomalously small coupling to photons, relaxing astrophysical bounds. The degree of this cancellation is very sensitive to the uncertainties from the quark mass and the higher order corrections, which we compute here for the first time.

At NLO new couplings appear from higher-dimensional operators correcting the WZW Lagrangian. Using the basis of [343], the result reads

$$g_{a\gamma\gamma} = \frac{\alpha_{em}}{2\pi f_a} \left\{ \frac{E}{N} - \frac{2}{3} \frac{4m_d + m_u}{m_d + m_u} \right.$$
$$\left. + \frac{m_\pi^2}{f_\pi^2} \frac{8m_u m_d}{(m_u + m_d)^2} \left[\frac{8}{9} \left(5\tilde{c}_3^W + \tilde{c}_7^W + 2\tilde{c}_8^W \right) - \frac{m_d - m_u}{m_d + m_u} l_7^r \right] \right\} . \quad (6.23)$$

The NLO corrections in the square brackets come from tree-level diagrams with insertions of NLO WZW operators (the terms proportional to the $\tilde{c}_i^W$ couplings[1]) and from a-π^0 mixing diagrams (the term proportional to l_7^r). One loop diagrams exactly cancel similarly to what happens for $\pi \to \gamma\gamma$ and $\eta \to \gamma\gamma$ [344]. Notice that the l_7^r term includes the m_u/m_s contributions which one obtains from the 3-flavor tree-level computation.

Unlike the NLO couplings entering the axion mass and potential little is known about the couplings $\tilde{c}_i^W$, so we describe the way to extract them here.

The first obvious observable we can use is the $\pi^0 \to \gamma\gamma$ width. Calling δ_i the relative correction at NLO to the amplitude for the i process, i.e.

$$\Gamma_i^{\text{NLO}} \equiv \Gamma_i^{\text{tree}} (1 + \delta_i)^2 , \quad (6.24)$$

the expressions for $\Gamma_{\pi\gamma\gamma}^{\text{tree}}$ and $\delta_{\pi\gamma\gamma}$ read

$$\Gamma_{\pi\gamma\gamma}^{\text{tree}} = \frac{\alpha_{em}^2}{(4\pi)^3} \frac{m_\pi^3}{f_\pi^2} ,$$
$$\delta_{\pi\gamma\gamma} = \frac{16}{9} \frac{m_\pi^2}{f_\pi^2} \left[\frac{m_d - m_u}{m_d + m_u} \left(5\tilde{c}_3^W + \tilde{c}_7^W + 2\tilde{c}_8^W \right) - 3 \left(\tilde{c}_3^W + \tilde{c}_7^W + \frac{\tilde{c}_{11}^W}{4} \right) \right] . \quad (6.25)$$

Once again the loop corrections are reabsorbed by the renormalization of the tree-level parameters and the only contributions come from the NLO WZW terms. While the isospin breaking correction involves exactly the same combination of couplings entering the axion width, the isospin preserving one does not. This means that we cannot extract the required NLO couplings from the pion width alone. However in the absence of large cancellations between the isospin breaking and the isospin preserving contributions we

---

[1]For simplicity we have rescaled the original couplings c_i^W of [343] into $\tilde{c}_i^W \equiv c_i^W (4\pi f_\pi)^2$.

can use the experimental value for the pion decay rate to estimate the order of magnitude of the corresponding corrections to the axion case. Given the small difference between the experimental and the tree-level prediction for $\Gamma_{\pi \to \gamma\gamma}$ the NLO axion correction is expected of order few percent.

To obtain numerical values for the unknown couplings we can try to use the 3-flavor theory, in analogy with the axion mass computation. In fact at NLO in the 3-flavor theory the decay rates $\pi \to \gamma\gamma$ and $\eta \to \gamma\gamma$ only depend on two low-energy couplings that can thus be determined. Matching these couplings to the 2-flavor theory ones we are able to extract the required combination entering in the axion coupling. Because the $\tilde{c}_i^W$ couplings enter eq. (6.23) only at NLO in the light quark mass expansion we only need to determine them at LO in the $m_{u,d}$ expansion.

The $\eta \to \gamma\gamma$ decay rate at NLO is

$$\Gamma^{\text{tree}}_{\eta \to \gamma\gamma} = \frac{\alpha_{em}^2}{3(4\pi)^3} \frac{m_\eta^3}{f_\eta^2},$$

$$\delta_{\eta\gamma\gamma}^{(3)} = \frac{32}{9} \frac{m_\pi^2}{f_\pi^2} \left[\frac{2m_s - 4m_u - m_d}{m_u + m_d} \tilde{C}_7^W + 6 \frac{2m_s - m_u - m_d}{m_u + m_d} \tilde{C}_8^W \right]$$

$$\simeq \frac{64}{9} \frac{m_K^2}{f_\pi^2} \left(\tilde{C}_7^W + 6 \tilde{C}_8^W \right), \tag{6.26}$$

where in the last step we consistently neglected higher order corrections $\mathcal{O}(m_{u,d}/m_s)$. The 3-flavor couplings $\tilde{C}_i^W \equiv (4\pi f_\pi)^2 C_i^W$ are defined in [343]. The expression for the correction to the $\pi \to \gamma\gamma$ amplitude with 3 flavors also receives important corrections from the π-η mixing ϵ_2,

$$\delta_{\pi\gamma\gamma}^{(3)} = \frac{32}{9} \frac{m_\pi^2}{f_\pi^2} \left[\frac{m_d - 4m_u}{m_u + m_d} \tilde{C}_7^W + 6 \frac{m_d - m_u}{m_u + m_d} \tilde{C}_8^W \right] + \frac{f_\pi}{f_\eta} \frac{\epsilon_2}{\sqrt{3}} (1 + \delta_{\eta\gamma\gamma}), \tag{6.27}$$

where the π-η mixing derived in [337] can be conveniently rewritten as

$$\frac{\epsilon_2}{\sqrt{3}} \simeq \frac{m_d - m_u}{6m_s} \left[1 + \frac{4m_K^2}{f_\pi^2} \left(l_7^r - \frac{1}{64\pi^2} \right) \right], \tag{6.28}$$

at leading order in $m_{u,d}$. In both decay rates the loop corrections are reabsorbed in the renormalization of the tree-level amplitude[1].

---

[1]NLO corrections to π and η decay rates to photons including isospin breaking effects were also computed in [345]. For the $\eta \to \gamma\gamma$ rate we disagree in the expression of the terms $\mathcal{O}(m_{u,d}/m_s)$, which are however subleading. For the $\pi \to \gamma\gamma$ rate we also included the mixed term coming from the product of the NLO corrections to ϵ_2 and to $\Gamma_{\eta\gamma\gamma}$. Formally this term is NNLO but given that the NLO corrections to both ϵ_2 and $\Gamma_{\eta\gamma\gamma}$ are of the same size as the corresponding LO contributions such terms cannot be neglected.
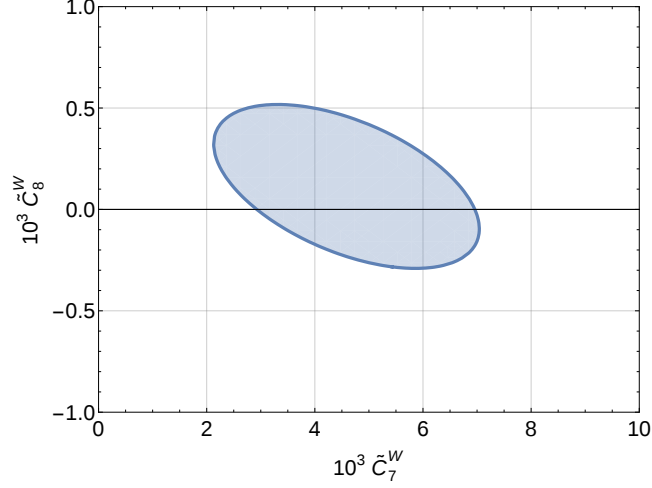
Figure 6.2: Result of the fit of the 3-flavor couplings $\tilde{C}^W_{7,8}$ from the decay width of $\pi \to \gamma\gamma$ and $\eta \to \gamma\gamma$, which include the experimental uncertainties and a 30% systematic uncertainty from higher order corrections.

By comparing the light quark mass dependence in eqs. (6.25) and (6.27) we can match the 2 and 3 flavor couplings as follows

$$\tilde{c}^W_3 + \tilde{c}^W_7 + \frac{\tilde{c}^W_{11}}{4} = \tilde{C}^W_7 \,,$$

$$5\tilde{c}^W_3 + \tilde{c}^W_7 + 2\tilde{c}^W_8 = 5\tilde{C}^W_7 + 12\tilde{C}^W_8$$
$$+ \frac{3}{32}\frac{f_\pi^2}{m_K^2}\left[1 + 4\frac{m_K^2}{f_\pi f_\eta}\left(l_7^r - \frac{1}{64\pi^2}\right)\right](1 + \delta_{\eta\gamma\gamma}) \,. \tag{6.29}$$

Notice that the second combination of couplings is exactly the one needed for the axion-photon coupling. By using the experimental results for the decay rates (reported in appendix C), we can extract $C^W_{7,8}$. The result is shown in fig. 6.2, the precision is low for two reasons: 1) $\tilde{C}^W_{7,8}$ are 3 flavor couplings so they suffer from an intrinsic $\mathcal{O}(30\%)$ uncertainty from higher order corrections[1], 2) for $\pi \to \gamma\gamma$ the experimental uncertainty is not smaller than the NLO corrections we want to fit.

For the combination $5\tilde{c}^W_3 + \tilde{c}^W_7 + 2\tilde{c}^W_8$ we are interested in, the final result reads

$$5\tilde{c}^W_3 + \tilde{c}^W_7 + 2\tilde{c}^W_8 = \frac{3f_\pi^2}{64m_K^2}\frac{m_u + m_d}{m_u}\left\{\left[1 + 4\frac{m_K^2}{f_\pi^2}\left(l_7^r - \frac{1}{64\pi^2}\right)\right]\frac{f_\pi}{f_\eta}(1 + \delta_{\eta\gamma\gamma})\right.$$

---

[1]We implement these uncertainties by adding a 30% error on the experimental input values of $\delta_{\pi\gamma\gamma}$ and $\delta_{\eta\gamma\gamma}$.
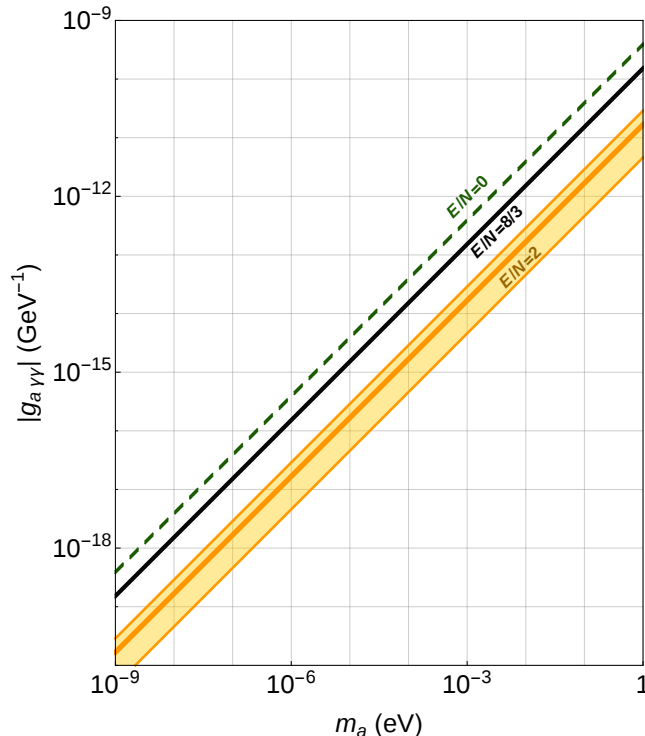
Figure 6.3: The relation between the axion mass and its coupling to photons for the three reference models with $E/N = 0$, 8/3 and 2. Notice the larger relative uncertainty in the latter model due to the cancellation between the UV and IR contributions to the anomaly (the band corresponds to 2σ errors.). Values below the lower band require a higher degree of cancellation.

$$+3\delta_{\eta\gamma\gamma} - 6\frac{m_K^2}{m_\pi^2}\delta_{\pi\gamma\gamma}\bigg\} = 0.033(6)\,. \tag{6.30}$$

When combined with eq. (6.23) we finally get

$$g_{a\gamma\gamma} = \frac{\alpha_{em}}{2\pi f_a}\left[\frac{E}{N} - 1.92(4)\right] = \left[0.203(3)\frac{E}{N} - 0.39(1)\right]\frac{m_a}{\text{GeV}^2}\,. \tag{6.31}$$

Note that despite the rather large uncertainties of the NLO couplings we are able to extract the model independent contribution to $a \to \gamma\gamma$ at the percent level. This is due to the fact that, analogously to the computation of the axion mass, the NLO corrections are suppressed by the light quark mass values. Modulo experimental uncertainties eq. (6.31) would allow the parameter E/N to be extracted from a measurement of $g_{a\gamma\gamma}$ at the percent level.

For the three reference models with respectively $E/N = 0$ (such as hadronic or KSVZ-like models [211, 212] with electrically neutral heavy fermions), $E/N = 8/3$ (as in DFSZ models [213, 214] or KSVZ models with heavy fermions in complete SU(5) representations) and $E/N = 2$ (as in some KSVZ "unificaxion" models [346]) the coupling reads

$$
g_{a\gamma\gamma} = \begin{cases} -2.227(44) \cdot 10^{-3}/f_a & E/N = 0 \\ 0.870(44) \cdot 10^{-3}/f_a & E/N = 8/3 \\ 0.095(44) \cdot 10^{-3}/f_a & E/N = 2 \end{cases} . \tag{6.32}
$$

Even after the inclusion of NLO corrections the coupling to photons in $E/N = 2$ models is still suppressed. The current uncertainties are not yet small enough to completely rule out a higher degree of cancellation, but a suppression bigger than $\mathcal{O}(20)$ with respect to $E/N = 0$ models is highly disfavored. Therefore the result for $g_{a\gamma\gamma}^{E/N=2}$ of eq. (6.32) can now be taken as a lower bound to the axion coupling to photons, below which tuning is required. The result is shown in fig. 6.3.

6.3.4 Coupling to matter

Axion couplings to matter are more model dependent as they depend on all the UV couplings defining the effective axial current (the constants c_q^0 in the last term of eq. (4.43)). In particular, there is a model independent contribution coming from the axion coupling to gluons (and to a lesser extent to the other gauge bosons) and a model dependent part contained in the fermionic axial couplings.

The couplings to leptons can be read off directly from the UV Lagrangian up to the one loop effects coming from the coupling to the EW gauge bosons. The couplings to hadrons are more delicate because they involve matching hadronic to elementary quark physics. Phenomenologically the most interesting ones are the axion couplings to nucleons, which could in principle be tested from long range force experiments, or from dark-matter direct-detection like experiments.

In principle we could attempt to follow a similar procedure to the one used in the previous section, namely to employ chiral Lagrangians with baryons and use known experimental data to extract the necessary low energy couplings. Unfortunately effective Lagrangians involving baryons are on much less solid ground—there are no parametrically large energy gaps in the hadronic spectrum to justify the use of low energy expansions.

A much safer thing to do is to use an effective theory valid at energies much lower than the QCD mass gaps $\Delta \sim \mathcal{O}(100 \text{ MeV})$. In this regime nucleons are non-relativistic, their number is conserved and they can be treated as external fermionic currents. For exchanged momenta q parametrically smaller than Δ, heavier modes are not excited and

the effective field theory is under control. The axion, as well as the electro-weak gauge bosons, enters as classical sources in the effective Lagrangian, which would otherwise be a free non-relativistic Lagrangian at leading order. At energies much smaller than the QCD mass gap the only active flavor symmetry we can use is isospin, which is explicitly broken only by the small quark masses (and QED effects). The leading order effective Lagrangian for the 1-nucleon sector reads

$$\mathcal{L}_N = \bar{N}v^\mu D_\mu N + 2g_A A^i_\mu \bar{N}S^\mu\sigma^i N + 2g^q_0 \hat{A}^q_\mu \bar{N}S^\mu N + \sigma\langle M_a\rangle\bar{N}N + b\bar{N}M_a N + \dots \quad (6.33)$$

where $N = (p, n)$ is the isospin doublet nucleon field, v^μ is the four-velocity of the non-relativistic nucleons, $D_\mu = \partial_\mu - V_\mu$, V_μ is the vector external current, σ^i are the Pauli matrices, the index $q = (\frac{u+d}{2}, s, c, b, t)$ runs over isoscalar quark combinations, $2\bar{N}S^\mu N = \bar{N}\gamma^\mu\gamma_5 N$ is the nucleon axial current, $M_a = \cos(Q_a a/f_a)\mathrm{diag}(m_u, m_d)$, and A^i_μ and $\hat{A}^q_\mu$ are the axial isovector and isoscalar external currents respectively. Neglecting SM gauge bosons, the external currents only depend on the axion field as follows

$$\hat{A}^q_\mu = c_q\frac{\partial_\mu a}{2f_a}, \qquad A^3_\mu = c_{(u-d)/2}\frac{\partial_\mu a}{2f_a}, \qquad A^{1,2}_\mu = V_\mu = 0, \qquad (6.34)$$

where we used the short-hand notation $c_{(u\pm d)/2} \equiv \frac{c_u\pm c_d}{2}$. The couplings $c_q = c_q(Q)$ computed at the scale Q will in general differ from the high scale ones because of the running of the anomalous axial current [347]. In particular under RG evolution the couplings $c_q(Q)$ mix, so that in general they will all be different from zero at low energy. We explain the details of this effect in appendix D.

Note that the linear axion couplings to nucleons are all contained in the derivative interactions through A_μ while there are no linear interactions[1] coming from the non derivative terms contained in M_a. In Eq. (6.33) dots stand for higher order terms involving higher powers of the external sources V_μ, A_μ, and M_a. Among these the leading effects to the axion-nucleon coupling will come from isospin breaking terms $\mathcal{O}(M_a A_\mu)$.[2] These corrections are small $\mathcal{O}(\frac{m_d - m_u}{\Delta})$, below the uncertainties associated to our determination of the effective coupling g^q_0, which are extracted from lattice simulations performed in the isospin limit.

Eq. (6.33) should not be confused with the usual heavy baryon chiral Lagrangian [348] because here pions have been integrated out. The advantage of using this Lagrangian is clear: for axion physics the relevant scale is of order m_a, so higher order terms are

---

[1]This is no longer true in the presence of extra CP violating operators such as those coming from the CKM phase or new physics. The former are known to be very small, while the latter are more model dependent and we will not discuss them in the current work.

[2]Axion couplings to EDM operators also appear at this order.

negligibly small $\mathcal{O}(m_a/\Delta)$. The price to pay is that the couplings g_A and g_0^q can only be extracted from very low-energy experiments or lattice QCD simulations. Fortunately the combination of the two will be enough for our purposes.

In fact, at the leading order in the isospin breaking expansion, g_A and g_0^q can simply be extracted by matching single nucleon matrix elements computed with the QCD+axion Lagrangian (4.46) and with the effective axion-nucleon theory (6.33). The result is simply:

$$g_A = \Delta u - \Delta d, \quad g_0^q = (\Delta u + \Delta d, \Delta s, \Delta c, \Delta b, \Delta t), \quad s^\mu \Delta q \equiv \langle p|\bar{q}\gamma^\mu \gamma_5 q|p\rangle, \quad (6.35)$$

where $|p\rangle$ is a proton state at rest, s^μ its spin and we used isospin symmetry to relate proton and neutron matrix elements. Note that the isoscalar matrix elements Δq inside g_0^q depend on the matching scale Q, such dependence is however canceled once the couplings $g_0^q(Q)$ are multiplied by the corresponding UV couplings $c_q(Q)$ inside the isoscalar currents $\hat{A}_\mu^q$. Non-singlet combinations such as g_A are instead protected by non-anomalous Ward identities[1]. For future convenience we set the matching scale $Q = 2$ GeV.

We can therefore write the EFT Lagrangian (6.33) directly in terms of the UV couplings as

$$\mathcal{L}_N = \bar{N}v^\mu D_\mu N + \frac{\partial_\mu a}{f_a}\left\{\frac{c_u - c_d}{2}(\Delta u - \Delta d)\bar{N}S^\mu \sigma^3 N \right.$$
$$\left. + \left[\frac{c_u + c_d}{2}(\Delta u + \Delta d) + \sum_{q=s,c,b,t} c_q \Delta q\right]\bar{N}S^\mu N\right\}. \quad (6.36)$$

We are thus left to determine the matrix elements Δq. The isovector combination can be obtained with high precision from β-decays [341]

$$\Delta u - \Delta d = g_A = 1.2723(23), \quad (6.37)$$

where the tiny neutron-proton mass splitting $m_n - m_p = 1.3$ MeV guarantees that we are within the regime of our effective theory. The error quoted is experimental and does not include possible isospin breaking corrections.

Unfortunately we do not have other low energy experimental inputs to determine the remaining matrix elements. Until now such information has been extracted from a combination of deep-inelastic-scattering data and semi-leptonic hyperon decays: The former suffer from uncertainties coming from the integration over the low-x kinematic region, which is known to give large contributions to the observable of interest; the latter are not really within the EFT regime, which does not allow a reliable estimate of the accuracy.

---

[1]This is only true in renormalization schemes which preserve the Ward identities.

Fortunately lattice simulations have recently started producing direct reliable results for these matrix elements. From [349–354] (see also [355, 356]) we extract[1] the following inputs computed at $Q = 2$ GeV in $\overline{\text{MS}}$

$$g_0^{ud} = \Delta u + \Delta d = 0.521(53)\,, \qquad \Delta s = -0.026(4)\,, \qquad \Delta c = \pm 0.004\,. \tag{6.38}$$

Notice that the charm spin content is so small that its value has not been determined yet, only an upper bound exists. Similarly we can neglect the analogous contributions from bottom and top quarks which are expected to be even smaller. As mentioned before, lattice simulations do not include isospin breaking effects, these are however expected to be smaller than the current uncertainties. Combining eqs. (6.37) and (6.38) we thus get:

$$\Delta u = 0.897(27)\,, \qquad \Delta d = -0.376(27)\,, \qquad \Delta s = -0.026(4)\,, \tag{6.39}$$

computed at the scale $Q = 2$ GeV.

We can now use these inputs in the EFT Lagrangian (6.36) to extract the corresponding axion-nucleon couplings:

$$\begin{aligned}
c_p &= -0.47(3) + 0.88(3)c_u^0 - 0.39(2)c_d^0 - 0.038(5)c_s^0 \\
&\quad - 0.012(5)c_c^0 - 0.009(2)c_b^0 - 0.0035(4)c_t^0\,, \\
c_n &= -0.02(3) + 0.88(3)c_d^0 - 0.39(2)c_u^0 - 0.038(5)c_s^0 \\
&\quad - 0.012(5)c_c^0 - 0.009(2)c_b^0 - 0.0035(4)c_t^0\,,
\end{aligned} \tag{6.40}$$

which are defined in analogy to the couplings to quarks as

$$\frac{\partial_\mu a}{2f_a} c_N \bar{N} \gamma^\mu \gamma_5 N\,, \tag{6.41}$$

and are scale invariant (as they are defined in the effective theory below the QCD mass gap). The errors in eq. (6.40) include the uncertainties from the lattice data and those from higher order corrections in the perturbative RG evolution of the axial current (the latter is only important for the coefficients of $c_{s,c,b,t}^0$). The couplings c_q^0 are those appearing in eq. (4.43) computed at the high scale $f_a = 10^{12}$ GeV. The effect of varying the matching scale to a different value of f_a within the experimentally allowed range is smaller than the theoretical uncertainties.

A few considerations are in order. The theoretical errors quoted here are dominated by the lattice results, which for these matrix elements are still in an early phase and the systematic uncertainties are not fully explored yet. Still the error on the final result

---

[1]Details in the way the numbers in eq. (6.38) are derived are given in appendix C.

is already good (below ten percent), and there is room for a large improvement which is expected in the near future. Note that when the uncertainties decrease sufficiently for results to become sensitive to isospin breaking effects, new couplings will appear in eq. (6.33). These could in principle be extracted from lattice simulations by studying the explicit quark mass dependence of the matrix element. In this regime the experimental value of the isovector coupling g_A cannot be used anymore because of different isospin breaking corrections to charged versus neutral currents.

The numerical values of the couplings we get are not too far off those already in the literature (see e.g. [341]). However, because of the caveats in the relation of the deep inelastic scattering and hyperon data to the relevant matrix elements the uncertainties in those approaches are not under control. On the other hand the lattice uncertainties are expected to improve in the near future, which would further improve the precision of the estimate performed with the technique presented here.

The numerical coefficients in eq. (6.40) include the effect of running from the high scale f_a (here fixed to 10^{12} GeV) to the matching scale $Q = 2$ GeV, which we performed at the NLLO order (more details in appendix D). The running effects are evident from the fact that the couplings to nucleons depend on all quark couplings including charm, bottom and top, even though we took the corresponding spin content to vanish. This effect has been neglected in previous analysis.

Finally it is interesting to observe that there is a cancellation in the model independent part of the axion coupling to the neutron in KSVZ-like models, where $c_q^0 = 0$,

$$c_p^{\text{KSVZ}} = -0.47(3) , \qquad c_n^{\text{KSVZ}} = -0.02(3) , \tag{6.42}$$

the coupling to neutrons is suppressed with respect to the coupling to protons by a factor $\mathcal{O}(10)$ at least, in fact this coupling still is compatible with 0. The cancellation can be understood from the fact that, neglecting running and sea quark contributions

$$c_n \sim \left\langle Q_a \cdot \begin{pmatrix} \Delta d & 0 \\ 0 & \Delta u \end{pmatrix} \right\rangle \propto m_d \Delta d + m_u \Delta u , \tag{6.43}$$

and the down-quark spin content of the neutron Δu is approximately $\Delta u \approx -2\Delta d$, *i.e.* the ratio m_u/m_d is accidentally close to the ratio between the number of up over down valence quarks in the neutron. This cancellation may have important implications on axion detection and astrophysical bounds.

In models with $c_q^0 \neq 0$ both the couplings to proton and neutron can be large, for example for the DFSZ axion models, where $c_{u,c,t}^0 = \frac{1}{3}\sin^2\beta = \frac{1}{3} - c_{d,s,b}^0$ at the scale $Q \simeq f_a$, we get

$$c_p^{\text{DFSZ}} = -0.617 + 0.435\sin^2\beta \pm 0.025 , \qquad c_n^{\text{DFSZ}} = 0.254 - 0.414\sin^2\beta \pm 0.025 . \tag{6.44}$$

A cancellation in the coupling to neutrons is still possible for special values of $\tan\beta$.

Part III

Conclusions

Chapter 7

Conclusions and outlook

Several experimental and theoretical arguments suggest the existence of physics beyond the standard model, and one of the most fascinating and challenging issues is the nature of dark matter. Many promising models extend the SM predicting the existence of stable and massive particles with the properties needed to accommodate observations. In this thesis we have analysed two viable dark matter candidates: we have focused on the neutralino in split SUSY scenarios and in supersymmetric models with Dirac gaugino masses, and on the QCD axion.

In the first part of this thesis we have presented supersymmetric searches at future hadron colliders and dark matter direct detection experiments. In particular, in the contest of split SUSY models, we have analysed the mass reach of several electroweakino searches for future hadron colliders, their implications for dark matter and the complementarity with direct detection experiments. Moreover, we have compared prospects of discovering or excluding models with Dirac and Majorana gauginos at a possible future 100 TeV collider, considering a neutralino-squark-gluino simplified model. Finally, we have considered neutralino dark matter in SUSY models with Dirac gauginos and the relations between searches at a 100 TeV collider, direct and indirect detection.

In Chapter 1 we have reviewed the motivations for physics beyond the standard model and we have introduced split SUSY models and SUSY models with Dirac gauginos.

In the second Chapter we have discussed some aspects of collider phenomenology. In particular, in section 2.1, we have studied scenarios where Wino NLSPs decay into leptons (or b-jets and leptons) and Bino LSP, with long-lived Winos in models of anomaly mediation and with Wino or higgsino LSP in GMSB models. The LHC excludes electroweakinos up to few hundred GeV, well below the interesting cases of pure Wino or higgsino dark matter. Electroweakinos collider searches are relevant, for example in low

scale gauge mediation models with universal gaugino masses and large $\tan\beta$ or in models of anomaly mediation. Indeed, in the first scenario the gluino is expected to be at the same scale or below the squarks (the Higgs mass fixes this scale to be around 10 TeV) that means a Wino around 3 TeV. Such Winos could be explored at a 100 TeV collider with less than 100 fb^{-1} of luminosity. In anomaly mediation the ratio between the gluino and the Wino mass is large, making the Wino searches more powerful: a 100 TeV collider with few ab^{-1} of luminosity could explore 3 TeV Winos ($m_{\tilde{g}} \gtrsim 20$ TeV).

In section 2.2 we have compared the reach of coloured states in SUSY models with Dirac or Majorana gluinos. Our results are summarised in figure 2.8. Differences between Majorana and Dirac gaugino models are pronounced for heavy gluinos compared to the squarks, where the sensitivity is significantly weaker in Dirac models.

A major shortcoming of the present work is the lack of NLO K factors for Dirac models, a topic that needs further work. In extending our analysis there are many other possible searches for colour superpartners, and different patterns of soft masses to be studied. Additionally, study of scenarios where the first two generation sfermions are heavy, but the gluino and stop are relatively light would be worthwhile. Moreover, it would also be interesting to pursue dedicated analysis of the possible signatures of the sgluon, or the other adjoint scalars. Searches for Dirac Winos and Binos with or without sfermions at comparable masses and with the gluino decoupled would also be relevant because Dirac gaugino models often predict gluinos significantly heavier than the squarks and the Winos. Collider signatures of electroweakinos in Dirac models have been discussed in [127, 357], and the reach of a 100 TeV collider for Majorana gauginos with associated production has been studied in [144]. However, we leave the case of models of Dirac electroweakinos at a 100 TeV collider for future work.

Furthermore, we have considered some aspects of model building, and the relation of these to the future collider searches in section 2.3. Although a proper calculation of the fine tuning of a model requires a full UV complete theory to be specified, we have estimated the typical tuning that will be probed in the Dirac and Majorana scenarios. Our analysis has been fairly independent of the details of particular models, and is expected to give a lower bound on the tuning of a theory with a given low scale spectrum. It would therefore be interesting to take a well motivated UV complete model, for example a theory of Dirac gluinos that avoids tachyonic states, and investigate whether its true tuning is close to our estimates.

Dark matter direct detection searches for the SUSY models considered in this thesis have been analysed in chapter 3. In section 3.1, we have studied split SUSY models with universal gaugino masses or anomaly mediation. In split SUSY models with universal gaugino masses the strongest mass reach comes from direct detection in the positive μ

scenario. In particular, the recent LUX results already exclude the Bino-higgsino scenario for any value of $\tan\beta$ (see figure 3.3), while the combination of direct detection experiments (after LZ), monojet and gluino searches at a 100 TeV collider will leave unexplored a narrow region with $\mu \gtrsim 870$ GeV and $M_1 \gtrsim 5$ TeV. On the other hand, in the negative μ case dark matter direct detection experiments are weaker, due to the suppression of the cross section (although large $\tan\beta$ scenarios have been recently ruled out by LUX). However, gluino and monojet searches may explore also the region where the neutrino background limits direct detection experiments. In this scenario, therefore, it would be possible to explore the entire parameter space where the (non-termal) neutralino dark matter candidate is an admixture of higgsino and Bino states (see figure 3.4).

In anomaly mediation models direct detection experiments and collider searches are complementary. Indeed searches on long-lived Winos set strong mass reach in regions where direct detection is weak. The interplay between gluino searches, long-lived Winos and direct detection may cover large area of the parameter space where the neutralino does not contribute to the whole dark matter. Gluino searches at a 100 TeV collider could be able to explore the whole parameter space in which the dark matter particle is a Bino/higgsino or Bino/Wino mixed state. Moreover, the Wino-higgsino dark matter scenario with large $\tan\beta$ is now excluded by the recent LUX data (see figure 3.7). On the other hand, the small $\tan\beta$ scenario is not excluded only for negative μ. In the case with positive μ, LZ may probe pure thermal Winos or higgsinos.

Furthermore, in section 3.2, we have examined the prospects for viable neutralino dark matter candidates in Dirac gaugino models. In R-symmetric Dirac gaugino models, strong constraints from direct detection experiments already rule out higgsino dark matter. The remaining electroweakino dark matter possibilities are Binos coannihilating with sleptons, and a mainly Bino neutralino coannihilating with the Winos. LHC searches already constrain the viable Bino candidates to be close in mass to the sleptons, and it will be hard for a future hadron collider to strengthen limits in this part of parameter space. However, for many well motivated patterns of soft terms, searches for coloured particles at such a collider can indirectly exclude this scenario. It would be interesting to study whether a future lepton collider could constrain this case directly. In contrast, the Dirac Bino-Wino case can be fully covered by direct searches. Notably, models with Dirac gluinos but a neutralino sector with R-symmetry broken can lead to many other dark matter scenarios. It would be worthwhile to consider the impact of a 100 TeV collider on such theories, as well as R-symmetric models with gravitino dark matter.

In the second part of this thesis, we have studied the QCD axion. In chapter 4 we have introduced the QCD axion as the solution of the strong CP problem, the different realisations of the Peccei-Quinn idea that produced a variety of axion models and the leading

7. Conclusions and outlook

order properties of the QCD axion. In chapter 5 we have discussed in more detail the QCD axion as the dark matter particle, reviewing the three different production mechanisms. Furthermore, we have studied the dependence of the axion mass and potential on the temperature, which affects the axion relic abundance today. While at low temperature such information can be extracted accurately using chiral Lagrangians at temperatures close to the QCD crossover and above perturbative methods fail. We also point out that instanton computations, which are believed to become reliable at least when QCD becomes perturbative have serious convergence problems, making them unreliable in the whole region of interest. Recent lattice result suggests large deviations from the instanton estimates [283], although other lattice simulations are in agreement [284–286]. We studied the impact that this uncertainty has on the computation of the axion relic abundance and the constraints on the axion parameter space. More dedicated non-perturbative computations are therefore required to reliably determine the axion relic abundance. Moreover, we have not considered contributions from topological defects that may dominate over the misalignment mechanism if inflation happens before the PQ breaking.

Finally, in chapter 6, we have discussed the laboratory searches and astrophysical bounds. The possible discovery of the QCD axion would lead to a precise determination of its mass. Therefore, in order to fully exploit such experimental result, precise theoretical determination of the zero temperature properties of the QCD axion are needed. We showed that several QCD axion properties, despite being determined by non-perturbative QCD dynamics, can be computed reliably with high accuracy. In particular we computed higher order corrections to the axion mass, its self-coupling, the coupling to photons, the full potential and the domain-wall tension, providing estimates for these quantities with percent accuracy. We also showed how lattice data can be used to extract the axion coupling to matter (nucleons) reliably, providing estimates with better than 10% precision. These results are important both experimentally, to assess the actual axion parameter space probed and to design new experiments, and theoretically, since in the case of a discovery they would help determining the underlying theory behind the PQ breaking scale.

Appendix

Appendix A

The MRSSM neutralinos

In this Appendix we briefly review the MRSSM. This has a superpotential

$$
\begin{aligned}
W & = W_{MSSM}^{\mu=0,A=0} + \mu_d \hat{R}_d \hat{H}_d + \mu_u \hat{R}_u \hat{H}_u \\
& + \Lambda_d \hat{R}_d \hat{T} \hat{H}_d + \Lambda_u \hat{R}_u \hat{T} \hat{H}_u + \lambda_d \hat{S} \hat{R}_d \hat{H}_d + \lambda_u \hat{S} \hat{R}_u \hat{H}_u \, ,
\end{aligned}
\tag{A.1}
$$

where $\hat{H}_u$ and $\hat{H}_d$ are MSSM-like Higgs doublets, and $\hat{R}_u$ and $\hat{R}_d$ are new inert Higgs doublets added to allow viable phenomenology while preserving an R-symmetry. The other new fields compared to the MSSM are a singlet $\hat{S}$, a SU(2)–triplet $\hat{T}$, and a SU(3)–octet $\hat{O}$.

The gauginos $\tilde{B}$, $\tilde{W}$ and $\tilde{g}$ can get, R-symmetry preserving, Dirac mass terms with the fermionic parts of the adjoint chiral supermultiplets $\tilde{S}$, $\tilde{T}$ and $\tilde{O}$

$$
\mathcal{L}_D \supset M_{D_1} \tilde{B} \tilde{S} + M_{D_2} \tilde{W} \tilde{T} + M_{D_3} \tilde{g} \tilde{O} + \text{h.c.} \, .
\tag{A.2}
$$

There are also new trilinear terms involving these extra adjoint chiral multiplets, with coupling constants $\Lambda_{u,d}$ and $\lambda_{u,d}$. Other important parameters are the soft masses for the scalar components of $\hat{H}_{u,d}$ and $\hat{R}_{u,d}$. MSSM like trilinear A terms are forbidden by the R-symmetry.

During EW symmetry breaking the two MSSM-like Higgs doublets get vacuum expectation values, and $\hat{R}_u$ and $\hat{R}_d$ do not. There are several important differences between the EW sectors of the MSSM and the MRSSM. In the MRSSM, the neutralino mass matrix in the basis $\left(\lambda_{\tilde{B}}, \tilde{W}^0, R_d^0, R_u^0\right), \left(\tilde{S}, \tilde{T}^0, \tilde{H}_d^0, \tilde{H}_u^0\right)$ is

$$
m_{\tilde{\chi}^0} = \begin{pmatrix} M_{D_1} & 0 & -\frac{1}{2}g_1 v_d & \frac{1}{2}g_1 v_u \\ 0 & M_{D_2} & \frac{1}{2}g_2 v_d & -\frac{1}{2}g_2 v_u \\ -\frac{1}{\sqrt{2}}\lambda_d v_d & -\frac{1}{2}\Lambda_d v_d & m_{R_d^0 \tilde{H}_d^0} & 0 \\ \frac{1}{\sqrt{2}}\lambda_u v_u & -\frac{1}{2}\Lambda_u v_u & 0 & m_{R_u^0 \tilde{H}_u^0} \end{pmatrix} \, ,
\tag{A.3}
$$

A. The MRSSM neutralinos

where

$$m_{R_d^0 \tilde{H}_d^0} = -\frac{1}{2}\Lambda_d v_T - \frac{1}{\sqrt{2}}\lambda_d v_s - \mu_d \tag{A.4}$$

$$m_{R_u^0 \tilde{H}_u^0} = -\frac{1}{2}\Lambda_u v_T + \frac{1}{\sqrt{2}}\lambda_u v_s + \mu_u \ . \tag{A.5}$$

The Dirac neutralinos are therefore composed of eight Weyl spinors coming from the neutral components of the Higgs doublets $H_{u,d}^0$, $R_{u,d}^0$, the gauginos $\tilde{B}$, $\tilde{W}^0$, and the adjoint singlet $\tilde{S}$ and triplet $\tilde{T}$. The four mass parameters M_{D_1}, M_{D_2} and $\mu_{u,d}$ give most of the mass to the neutralinos. There are four new couplings $\lambda_{u,d}$ and $\Lambda_{u,d}$, that arise from the superpotential terms in the second line of Eq. (A.1). Instead in the MSSM the gauginos have Majorana masses and there is only one higgsino parameter that give mass to two almost degenerate neutralinos.

The neutralino mass matrix is diagonalised by two unitary matrices $N_{ij}^{(k)}$, where $k = 1, 2$, $i, j = 1, ...4$. Conservation of electromagnetic charge and R-charge divides the eight two-component fermions from the Winos, higgsinos and R-fields into four sets that do not mix. This means that there are two chargino mass matrices. Acting on the basis $(\tilde{T}^-, \tilde{H}_d^-)$, $(\tilde{W}^+, \tilde{R}_d^+)$ we have a mass matrix

$$m_{\tilde{\chi}^+} = \begin{pmatrix} g_2 v_T + M_{D_2} & \frac{1}{\sqrt{2}}\Lambda_d v_d \\ \frac{1}{\sqrt{2}}g_2 v_d & -\frac{1}{2}\Lambda_d v_T + \frac{1}{\sqrt{2}}\lambda_d v_s + \mu_d \end{pmatrix}, \tag{A.6}$$

while on the basis $\left(\tilde{W}^-, R_u^-\right)$, $\left(\tilde{T}^+, \tilde{H}_u^+\right)$ the mass matrix is

$$m_{\tilde{\rho}^-} = \begin{pmatrix} -g_2 v_T + M_{D_2} & \frac{1}{\sqrt{2}}g_2 v_u \\ -\frac{1}{\sqrt{2}}\Lambda_u v_u & -\frac{1}{2}\Lambda_u v_T - \frac{1}{\sqrt{2}}\lambda_u v_s - \mu_u \end{pmatrix} . \tag{A.7}$$

Both of these matrices is diagonalised by two unitary matrices, so there are four independent rotations. The parameters M_{D_1}, M_{D_2}, μ_u and μ_d can chosen to be real and positive, because it is possible to rotate any phases into the scalar adjoint holomorphic masses and the parameters $\lambda_{u,d}$, $\Lambda_{u,d}$.

Appendix B

The dilute instanton gas approximation

The effective potential of the axion in the dilute instanton gas approximation is computed in terms of the single instanton contribution to the partition function Z_1

$$V_{\text{eff}}(T) = -2Z_1(T)\cos\theta. \tag{B.1}$$

Consequently, the mass of the axion in the DIGA computation is

$$m_a^2(T) = \frac{2}{f_a^2}Z_1(T). \tag{B.2}$$

The one loop contribution to the partition function Z_1 of a single instanton is given by

$$Z_1(T) = \int d\rho\, n(\rho, T) = \int d\rho\, n_G(\rho)\, n_f(m_f, \rho)\, n_T(\rho, T), \tag{B.3}$$

where ρ is the size of the instanton and $n(\rho, T)$ is the instanton density. The explicit calculation of $Z_1(T)$, performed by [293], can be factorised in a gauge (n_G), a fermion (n_f), and a finite temperature contribution (n_T). The gauge contribution of the instanton density is

$$n_G(\rho) = \frac{C_{N_c}}{\rho^5}\left(\frac{\pi}{\alpha_s(\mu)}\right)^{2N_c}(\mu\,\rho)^{\beta_0'(n_f)}\,e^{-\frac{2\pi}{\alpha_s(\mu)}}, \tag{B.4}$$

$$C_{N_c} = \frac{e^{N_c/6}\,\xi_1\,\xi_2^{-(N_c-2)}}{(N_c-2)!(N_c-1)!},$$

where N_c is the number of colours, $\xi_1 = 0.260156$, $\xi_2 = 1.33876$, the constant $e^{N_c/6}$ in C_{N_c} appears in the $\overline{\text{MS}}$ scheme, and

$$\beta_0'(n_f) = \beta_0(n_f) + \frac{\alpha_s(\mu)}{4\pi}\left[\beta_1(n_f) - 4N_c\beta_0(n_f) + 3n_f\frac{N_c^2-1}{N_c}\right],$$

B. The dilute instanton gas approximation

$$\beta_0(n_f) = \frac{11N_c - 2n_f}{3}, \qquad \beta_1(n_f) = 2\frac{153 - 19n_f}{3}.$$

The fermionic contribution in presence of n_f quarks with mass m_f is given by [358]

$$n_f(m_f, \rho) = \prod_{f=1}^{n_f} (m_f \rho)^{\frac{2}{3}} \exp\left(\frac{\frac{1}{3}\log m_f\rho + 2\alpha - (6\alpha + 2\beta)(m_f\rho)^2 + 2A_1(m_f\rho)^4 - 2A_2(m_f\rho)^6}{1 - 3(m_f\rho)^2 + B_1(m_f\rho)^4 + B_2(m_f\rho)^6 + B_3(m_f\rho)^8}\right),$$

(B.5)

where

$$\begin{aligned}
\alpha &= 0.145873, & \beta &= 0.05797, \\
A_1 &= -13.4138, & A_2 &= 2.64587, \\
B_1 &= 25\left(\frac{592955}{21609}A_2 + \frac{255}{49}A_1 + 9\alpha + 3\beta\right), & B_2 &= -75\left(\frac{85}{49}A_2 + A_1\right), & B_3 &= 75A_2.
\end{aligned}$$

Finally, the finite temperature contribution is

$$n_T(\rho, T) = \exp\left[-\frac{2(\pi\rho)^2}{g_s^2}m_D^2(T) - 12A(\rho, T)\left(1 + \frac{1}{6}(N_c - n_f)\right)\right], \qquad (B.6)$$

$$A(\rho, T) = -\frac{1}{12}\log\left(1 + \frac{(\pi\rho T)^2}{3}\right) + c_1\left(\frac{1}{1 + c_2(\pi\rho T)^{-\frac{3}{2}}}\right),$$

where $c_1 = 0.01289764$, and $c_2 = 0.15858$. The leading order Debye mass is given by

$$m_D^2(T) = \frac{1}{3}g_s^2(\mu)T^2\left(N_c + \frac{n_f}{2}\right), \qquad (B.7)$$

that receives $\mathcal{O}(1)$ corrections at NLO for temperatures around few GeV.

Appendix C

Input parameters and conventions

For convenience in table C.1 we report the values of the parameters used in this work. When uncertainties are not quoted it means that their effect was negligible and they have not been used.

In the following we discuss in more in details the origin of some of these values.

Quark masses

The value of $z = m_u/m_d$ has been extracted from the following lattice estimates:

$$z = \begin{cases} 0.52(2) & [240] \\ 0.50(2)(3) & [238] \\ 0.451(4)(8)(12) & [239] \end{cases} \tag{C.1}$$

which use different techniques, fermion formulations, etc. In [359] the extra preliminary result $z = 0.49(1)(1)$ is also quoted, which agrees with the results above. Some results are still preliminary and the study of systematics may not be complete. Indeed the spread from the central values is somewhat bigger than the quoted uncertainties. Averaging the results above we get $z = 0.48(1)$. Waiting for more complete results and a more systematic study of all uncertainties we used a more conservative error, $z = 0.48(3)$, which better captures the spread between the different computations.

Axion properties have a much weaker dependence on the strange quark mass which only enter at higher orders. For definiteness we used the value of the ratio

$$r \equiv \frac{2m_s}{m_u + m_d} = 27.4(1) \,, \tag{C.2}$$

from [359].

C. Input parameters and conventions

z	0.48(3)	$\bar{l}_3$	3(1)
r	27.4(1)	$\bar{l}_4$	4.0(3)
m_π	134.98	l_7	0.007(4)
m_K	498	L_7^r	$-0.0003(1)$
m_η	548	L_8^r	0.00055(17)
f_π	92.2	g_A	1.2723(23)
f_η/f_π	1.3(1)	$\Delta u + \Delta d$	0.52(5)
$\Gamma_{\pi\gamma\gamma}$	$5.16(18)\,10^{-4}$	Δs	$-0.026(4)$
$\Gamma_{\eta\gamma\gamma}$	$7.63(16)\,10^{-6}$	Δc	0.000(4)

Table C.1: Numerical input values used in the computations. Dimensionful quantities are given in MeV. The values of scale dependent low-energy constants are given at the scale $\bar{\mu} = 770$ MeV, while the scale dependent proton spin content Δq are given at $Q = 2$ GeV.

ChPT low energy constants

For the value of the pion decay constant we used the PDG [341] value:

$$f_\pi = 92.21(14) \text{ MeV},\tag{C.3}$$

which is free from the leading EM corrections present in the leptonic decays used for the estimates.

Following [337] the ratio f_η/f_π can be related to f_K/f_π, whose value is very well known, up to higher order corrections. Assuming the usual 30% uncertainty on the $SU(3)$ chiral estimates we get $f_\eta/f_\pi = 1.3(1)$.

For the NLO low energy couplings we used the usual conventions of [336, 337]. As described in the main text we used the matching of the 3 and 2 flavor Lagrangians to estimate the SU(2) couplings from the SU(3) ones. In particular we only need the values of $L_{7,8}^r$, which we took as

$$L_7^r \equiv L_7^r(\bar{\mu}) = -0.3(1) \cdot 10^{-3}, \qquad L_8^r \equiv L_8^r(\bar{\mu}) = 0.55(17) \cdot 10^{-3},\tag{C.4}$$

computed at the scale $\bar{\mu} = 770$ MeV. The first number has been extracted from the fit in [338] using the constraints for L_4^r in [339]. The second from [339]. A 30% intrinsic uncertainty from higher order 3-flavor corrections has been added. This intrinsic uncertainty is not present for the 2-flavor constants where higher order corrections are much smaller.

In the main text we used the values

$$\bar{l}_3 = 3(1), \qquad l_3^r(\bar{\mu}) = -\frac{1}{64\pi^2} \left(\bar{l}_3 + \log\left(\frac{m_\pi^2}{\bar{\mu}^2} \right) \right),$$

$$\bar{l}_4 = 4.0(3)\,, \qquad l_4^r(\bar{\mu}) = \frac{1}{16\pi^2}\left(\bar{l}_4 + \log\left(\frac{m_\pi^2}{\bar{\mu}^2}\right)\right),$$

extracted from 3-flavor simulations in [339].

From the values above and using the matching in [337] between the 2 and the 3 flavor theories we can also extract:

$$l_7 = 7(4)\,10^{-3}\,, \qquad h_1^r - h_3^r - l_4^r = -0.0048(14)\,. \tag{C.5}$$

Preliminary results using estimates from lattice QCD simulations [360] give $\bar{l}_3 = 2.97(19)(14)$, $\bar{l}_4 = 3.90(8)(14)$, $l_7 = 0.0066(54)$ and $L_8^r = 0.51(4)(12)\,10^{-3}$. The new results in [361] using partially quenched simulations give $\bar{l}_3 = 2.81(19)(45)$, $\bar{l}_4 = 4.02(8)(24)$ and $l_7 = 0.0065(38)(2)$. All these results are in agreement with the numbers used here.

Proton spin content

While the axial charge, which is equivalent to the isovector spin content of the proton, is very well known (see discussion around eq. (6.37)) the isosinglet components are less known.

To estimate $g^{ud} = \Delta u + \Delta d$ we use the results in [349–354]. In particular we used [353], whose value for $g_A = 1.242(57)$ is compatible with the experimental one, to estimate the connected contribution to g^{ud}. For the disconnected contribution, which is much more difficult to simulate, we averaged the results in [351, 352, 354] increasing the error to accommodate the spread in central values, which may be due to different systematics. Combining the results we get

$$g_{conn.}^{ud} + g_{disc.}^{ud} = 0.611(48) - 0.090(20) = 0.52(5)\,. \tag{C.6}$$

All the results provided here are in the $\overline{\text{MS}}$ scheme at the reference scale $Q = 2$ GeV.

The strange spin contribution only have the disconnected contribution, which we extract averaging the results in [349–352, 354]

$$g^s = \Delta s = -0.026(4)\,. \tag{C.7}$$

All the results mostly agree with each others but they are still preliminary or use heavy quark masses or coarse lattice spacing or only two dynamical quarks. For this reason the estimate of the systematic uncertainties is not yet complete and further studies are required.

Finally [351] also explored the charm spin contribution. They could not see a signal and thus their results can only be used to put an upper bound which we extracted as in table C.1.

Appendix D

Renormalization of axial couplings

While anomalous dimensions of conserved currents vanish it is not true for anomalous currents. This means that the axion coupling to the singlet component of the axial current is scale dependent:

$$\frac{\partial_\mu a}{2f_a} \sum_q c_q j_q^\mu = \frac{\partial_\mu a}{2f_a} \left[\sum_q \left(c_q - \frac{\sum_{q'} c_{q'}}{n_f} \right) j_q^\mu + \frac{\sum_{q'} c_{q'}}{n_f} j_{\Sigma q}^\mu \right] \tag{D.1}$$

$$\rightarrow \quad \frac{\partial_\mu a}{2f_a} \left[\sum_q \left(c_q - \frac{\sum_{q'} c_{q'}}{n_f} \right) j_q^\mu + Z_0(Q) \frac{\sum_{q'} c_{q'}}{n_f} j_{\Sigma q}^\mu \right] \tag{D.2}$$

where $Z_0(Q)$ is the renormalization of the singlet axial current $j_{\Sigma q}^\mu$. It is important to note that $j_{\Sigma q}^\mu$ only renormalizes multiplicatively, this is not true for the coupling to the gluon operator $(G\tilde{G})$ which mixes at one-loop with $\partial_\mu j_{\Sigma q}^\mu$ after renormalization (see e.g. [362]).

The anomalous dimension of $j_{\Sigma q}^\mu$ starts only at 2-loops and is known up to 3-loops in QCD [347, 363]

$$\frac{\partial \log Z_0(Q)}{\partial \log Q^2} = \gamma_A = \frac{n_f}{2} \left(\frac{\alpha_s}{\pi} \right)^2 + n_f \frac{177 - 2n_f}{72} \left(\frac{\alpha_s}{\pi} \right)^3 + \dots \tag{D.3}$$

The evolution of the couplings $c_q(Q)$ can thus be written as

$$c_q(Q) = c_q(Q_0) + \left(\frac{Z_0(Q)}{Z_0(Q_0)} - 1 \right) \frac{\langle c_q \rangle_{n_f}}{n_f}, \tag{D.4}$$

where we used the short hand notation $\langle \cdot \rangle_{n_f}$ for the sum of q over n_f flavors. Iterating the running between the high scale f_a and the low scale $Q = 2$ GeV across the bottom and

D. Renormalization of axial couplings

top mass thresholds we can finally write the relation between the low energy couplings $c_q(Q)$ and the high energy ones $c_q = c_q(f_a)$:

$$c_t(m_t) = c_t + \left(\frac{Z_0(m_t)}{Z_0(f_a)} - 1 \right) \frac{\langle c_q \rangle_6}{6} \,,$$

$$c_b(m_b) = c_b + \left(\frac{Z_0(m_b)}{Z_0(m_t)} - 1 \right) \frac{\langle c_q \rangle_5}{5} + \frac{Z_0(m_b)}{Z_0(m_t)} \left(\frac{Z_0(m_t)}{Z_0(f_a)} - 1 \right) \frac{\langle c_q \rangle_6}{6} \,,$$

$$c_{q=u,d,s,c}(Q) = c_q + \left(\frac{Z_0(Q)}{Z_0(m_b)} - 1 \right) \frac{\langle c_q \rangle_4}{4} + \frac{Z_0(Q)}{Z_0(m_b)} \left(\frac{Z_0(m_b)}{Z_0(m_t)} - 1 \right) \frac{\langle c_q \rangle_5}{5}$$

$$+ \frac{Z_0(Q)}{Z_0(m_t)} \left(\frac{Z_0(m_t)}{Z_0(f_a)} - 1 \right) \frac{\langle c_q \rangle_6}{6} \,, \tag{D.5}$$

where at each mass threshold we matched the couplings at LO. In eq. (D.5) we can recognize the contributions from the running from f_a to m_t with 6 flavors, from m_t to m_b with 5 flavors and the one down to Q with 4 flavors.

The value for $Z_0(Q)$ can be computed from eq. (D.3), at LLO the solution is simply

$$Z_0(Q) = Z_0(Q_0) \, e^{-\frac{6 n_f}{33 - 2 n_f} \frac{\alpha_s(Q) - \alpha_s(Q_0)}{\pi}} \,. \tag{D.6}$$

At NLLO the numerical values at the relevant mass scales are

$$Z_0(10^{12} \,\text{GeV}) = 0.984 \,, \quad Z_0(m_t) = 0.939(3) \,, \quad Z_0(m_b) = 0.888(15) \,, \quad Z_0(2 \,\text{GeV}) = 0.863(24) \,, \tag{D.7}$$

where the error is estimated by the difference with the LLO which should capture the order of magnitude of the 1-loop thresholds not included in the computation. For the computation above we used the $\overline{\text{MS}}$ values of the quark masses, i.e. $m_t(m_t) = 164$ GeV and $m_b(m_b) = 4.2$ GeV. The dependence of $Z_0(f_a)$ on the actual value of f_a is very mild, shifting $Z_0(f_a)$ by less than $\pm 0.5\%$ for $f_a = 10^{12 \pm 3}$ GeV.

Note that DFSZ models at high energy can be written so that the axion couples only through the quark mass matrix. In this case no running effect should be present above the first SM mass threshold (at the top mass). Indeed in this models, $\langle c_q \rangle_6 = \langle c_q^0 \rangle_6 - \text{tr}\, Q_a = 0$ and the renormalization effects from f_a to m_t cancel out.

Bibliography

[1] G. Grilli di Cortona, "Hunting electroweakinos at future hadron colliders and direct detection experiments," *JHEP* **05** (2015) 035, `arXiv:1412.5952 [hep-ph]`. iv, 60

[2] G. Grilli di Cortona, "Searching SUSY from below," *PoS* **PLANCK2015** (2015) 054, `arXiv:1510.07616 [hep-ph]`.

[3] G. Grilli di Cortona, E. Hardy, J. P. Vega, and G. Villadoro, "The QCD axion, precisely," *JHEP* **01** (2016) 034, `arXiv:1511.02867 [hep-ph]`.

[4] G. Grilli di Cortona, E. Hardy, and A. J. Powell, "Dirac vs Majorana gauginos at a 100 TeV collider," *JHEP* **08** (2016) 014, `arXiv:1606.07090 [hep-ph]`. iv

[5] S. L. Glashow, "Partial Symmetries of Weak Interactions," *Nucl. Phys.* **22** (1961) 579–588. 3

[6] S. Weinberg, "A Model of Leptons," *Phys. Rev. Lett.* **19** (1967) 1264–1266.

[7] A. Salam, "Weak and Electromagnetic Interactions," *Conf. Proc.* **C680519** (1968) 367–377. 3

[8] **ATLAS** Collaboration, G. Aad *et al.*, "Observation of a new particle in the search for the Standard Model Higgs boson with the ATLAS detector at the LHC," *Phys. Lett.* **B716** (2012) 1–29, `arXiv:1207.7214 [hep-ex]`. 3, 39

[9] **CMS** Collaboration, S. Chatrchyan *et al.*, "Observation of a new boson at a mass of 125 GeV with the CMS experiment at the LHC," *Phys. Lett.* **B716** (2012) 30–61, `arXiv:1207.7235 [hep-ex]`. 3, 39

[10] F. Englert and R. Brout, "Broken Symmetry and the Mass of Gauge Vector Mesons," *Phys. Rev. Lett.* **13** (1964) 321–323. 3

BIBLIOGRAPHY

[11] P. W. Higgs, "Broken Symmetries and the Masses of Gauge Bosons," *Phys. Rev. Lett.* **13** (1964) 508–509.

[12] G. S. Guralnik, C. R. Hagen, and T. W. B. Kibble, "Global Conservation Laws and Massless Particles," *Phys. Rev. Lett.* **13** (1964) 585–587. 3

[13] G. F. Giudice, "Naturally Speaking: The Naturalness Criterion and Physics at the LHC," `arXiv:0801.2562 [hep-ph]`. 4

[14] M. A. Luty, "2004 TASI lectures on supersymmetry breaking," in *Physics in D >= 4. Proceedings, Theoretical Advanced Study Institute in elementary particle physics, TASI 2004, Boulder, USA, June 6-July 2, 2004*, pp. 495–582. 2005. `arXiv:hep-th/0509029 [hep-th]`. 5

[15] G. 't Hooft, "Naturalness, chiral symmetry, and spontaneous chiral symmetry breaking," *NATO Sci. Ser. B* **59** (1980) 135. 5

[16] G. Bertone and D. Hooper, "A History of Dark Matter," `arXiv:1605.04909 [astro-ph.CO]`. 6

[17] F. Zwicky, "Die Rotverschiebung von extragalaktischen Nebeln," *Helvetica Physica Acta* **6** (1933) 110–127. 6

[18] K. C. Freeman, "On the disks of spiral and SO Galaxies," *Astrophys. J.* **160** (1970) 811. 6

[19] V. C. Rubin, N. Thonnard, and W. K. Ford, Jr., "Rotational properties of 21 SC galaxies with a large range of luminosities and radii, from NGC 4605 /R = 4kpc/ to UGC 2885 /R = 122 kpc/," *Astrophys. J.* **238** (1980) 471.

[20] A. Bosma, "21-cm line studies of spiral galaxies. 2. The distribution and kinematics of neutral hydrogen in spiral galaxies of various morphological types.," *Astron. J.* **86** (1981) 1825. 6

[21] **Planck** Collaboration, P. A. R. Ade *et al.*, "Planck 2015 results. XX. Constraints on inflation," `arXiv:1502.02114 [astro-ph.CO]`. 7, 103

[22] E. W. Kolb and M. S. Turner, eds., *THE EARLY UNIVERSE. REPRINTS*. 1988. 7

[23] S. Dodelson, *Modern Cosmology*. Academic Press, Amsterdam, 2003. http://www.slac.stanford.edu/spires/find/books/www?cl=QB981:D62:2003.

[24] D. S. Gorbunov and V. A. Rubakov, *Introduction to the theory of the early universe: Hot big bang theory*. World Scientific, Hackensack, 2011. http://www.DESY.eblib.com/patron/FullRecord.aspx?p=737614. 7

[25] K. Griest and M. Kamionkowski, "Unitarity Limits on the Mass and Radius of Dark Matter Particles," *Phys. Rev. Lett.* **64** (1990) 615. 9

[26] K. Griest and D. Seckel, "Three exceptions in the calculation of relic abundances," *Phys. Rev.* **D43** (1991) 3191–3203. 10

[27] J. Edsjo and P. Gondolo, "Neutralino relic density including coannihilations," *Phys. Rev.* **D56** (1997) 1879–1894, arXiv:hep-ph/9704361 [hep-ph]. 10

[28] S. Profumo, "Astrophysical Probes of Dark Matter," in *Proceedings, Theoretical Advanced Study Institute in Elementary Particle Physics: Searching for New Physics at Small and Large Scales (TASI 2012)*, pp. 143–189. 2013. arXiv:1301.0952 [hep-ph]. 10

[29] P. Fayet, "Supersymmetry and Weak, Electromagnetic and Strong Interactions," *Phys. Lett.* **B64** (1976) 159. 10

[30] P. Fayet, "Spontaneously Broken Supersymmetric Theories of Weak, Electromagnetic and Strong Interactions," *Phys. Lett.* **B69** (1977) 489.

[31] G. R. Farrar and P. Fayet, "Phenomenology of the Production, Decay, and Detection of New Hadronic States Associated with Supersymmetry," *Phys. Lett.* **B76** (1978) 575–579.

[32] P. Fayet, "Relations Between the Masses of the Superpartners of Leptons and Quarks, the Goldstino Couplings and the Neutral Currents," *Phys. Lett.* **B84** (1979) 416. 10

[33] M. J. G. Veltman, "The Infrared - Ultraviolet Connection," *Acta Phys. Polon.* **B12** (1981) 437. 10

[34] S. P. Martin, "A Supersymmetry primer," arXiv:hep-ph/9709356 [hep-ph]. [Adv. Ser. Direct. High Energy Phys.18,1(1998)]. 10, 11

BIBLIOGRAPHY

[35] J. Wess and J. Bagger, *Supersymmetry and supergravity*. 1992.

[36] S. Weinberg, *The quantum theory of fields. Vol. 3: Supersymmetry.* Cambridge University Press, 2013.

[37] M. Drees, R. Godbole, and P. Roy, *Theory and phenomenology of sparticles: An account of four-dimensional N=1 supersymmetry in high energy physics.* 2004.

[38] J. Terning, *Modern supersymmetry: Dynamics and duality.* 2006.

[39] H. Baer and X. Tata, *Weak scale supersymmetry: From superfields to scattering events.* Cambridge University Press, 2006.
http://www.cambridge.org/9780521290319. 11

[40] P. Fayet and J. Iliopoulos, "Spontaneously Broken Supergauge Symmetries and Goldstone Spinors," *Phys. Lett.* **B51** (1974) 461–464. 12

[41] P. Fayet, "Supergauge Invariant Extension of the Higgs Mechanism and a Model for the electron and Its Neutrino," *Nucl. Phys.* **B90** (1975) 104–124.

[42] L. O'Raifeartaigh, "Spontaneous symmetry breaking for chiral scalar superfields," *Nucl. Phys.* **B96** (1975) 331–352.

[43] K. A. Intriligator, N. Seiberg, and D. Shih, "Supersymmetry breaking, R-symmetry breaking and metastable vacua," *JHEP* **07** (2007) 017, arXiv:hep-th/0703281 [hep-th].

[44] A. H. Chamseddine, R. L. Arnowitt, and P. Nath, "Locally Supersymmetric Grand Unification," *Phys. Rev. Lett.* **49** (1982) 970.

[45] R. Barbieri, S. Ferrara, and C. A. Savoy, "Gauge Models with Spontaneously Broken Local Supersymmetry," *Phys. Lett.* **B119** (1982) 343.

[46] L. E. Ibanez, "Locally Supersymmetric SU(5) Grand Unification," *Phys. Lett.* **B118** (1982) 73–78.

[47] L. J. Hall, J. D. Lykken, and S. Weinberg, "Supergravity as the Messenger of Supersymmetry Breaking," *Phys. Rev.* **D27** (1983) 2359–2378.

[48] N. Ohta, "GRAND UNIFIED THEORIES BASED ON LOCAL SUPERSYMMETRY," *Prog. Theor. Phys.* **70** (1983) 542.

[49] J. R. Ellis, D. V. Nanopoulos, and K. Tamvakis, "Grand Unification in Simple Supergravity," *Phys. Lett.* **B121** (1983) 123–129.

[50] L. Alvarez-Gaume, J. Polchinski, and M. B. Wise, "Minimal Low-Energy Supergravity," *Nucl. Phys.* **B221** (1983) 495.

[51] M. Dine and W. Fischler, "A Phenomenological Model of Particle Physics Based on Supersymmetry," *Phys. Lett.* **B110** (1982) 227–231.

[52] C. R. Nappi and B. A. Ovrut, "Supersymmetric Extension of the SU(3) x SU(2) x U(1) Model," *Phys. Lett.* **B113** (1982) 175–179.

[53] L. Alvarez-Gaume, M. Claudson, and M. B. Wise, "Low-Energy Supersymmetry," *Nucl. Phys.* **B207** (1982) 96.

[54] M. Dine and A. E. Nelson, "Dynamical supersymmetry breaking at low-energies," *Phys. Rev.* **D48** (1993) 1277–1287, `arXiv:hep-ph/9303230 [hep-ph]`.

[55] M. Dine, A. E. Nelson, and Y. Shirman, "Low-energy dynamical supersymmetry breaking simplified," *Phys. Rev.* **D51** (1995) 1362–1370, `arXiv:hep-ph/9408384 [hep-ph]`.

[56] M. Dine, A. E. Nelson, Y. Nir, and Y. Shirman, "New tools for low-energy dynamical supersymmetry breaking," *Phys. Rev.* **D53** (1996) 2658–2669, `arXiv:hep-ph/9507378 [hep-ph]`.

[57] E. A. Mirabelli and M. E. Peskin, "Transmission of supersymmetry breaking from a four-dimensional boundary," *Phys. Rev.* **D58** (1998) 065002, `arXiv:hep-th/9712214 [hep-th]`.

[58] D. E. Kaplan, G. D. Kribs, and M. Schmaltz, "Supersymmetry breaking through transparent extra dimensions," *Phys. Rev.* **D62** (2000) 035010, `arXiv:hep-ph/9911293 [hep-ph]`.

[59] Z. Chacko, M. A. Luty, A. E. Nelson, and E. Ponton, "Gaugino mediated supersymmetry breaking," *JHEP* **01** (2000) 003, `arXiv:hep-ph/9911323 [hep-ph]`.

[60] M. Schmaltz and W. Skiba, "The Superpartner spectrum of gaugino mediation," *Phys. Rev.* **D62** (2000) 095004, `arXiv:hep-ph/0004210 [hep-ph]`.

BIBLIOGRAPHY

[61] M. Schmaltz and W. Skiba, "Minimal gaugino mediation," *Phys. Rev.* **D62** (2000) 095005, `arXiv:hep-ph/0001172 [hep-ph]`.

[62] C. Csaki, J. Erlich, C. Grojean, and G. D. Kribs, "4-D constructions of supersymmetric extra dimensions and gaugino mediation," *Phys. Rev.* **D65** (2002) 015003, `arXiv:hep-ph/0106044 [hep-ph]`.

[63] H. C. Cheng, D. E. Kaplan, M. Schmaltz, and W. Skiba, "Deconstructing gaugino mediation," *Phys. Lett.* **B515** (2001) 395–399, `arXiv:hep-ph/0106098 [hep-ph]`.

[64] L. Randall and R. Sundrum, "Out of this world supersymmetry breaking," *Nucl. Phys.* **B557** (1999) 79–118, `arXiv:hep-th/9810155 [hep-th]`. 55

[65] G. F. Giudice, M. A. Luty, H. Murayama, and R. Rattazzi, "Gaugino mass without singlets," *JHEP* **12** (1998) 027, `arXiv:hep-ph/9810442 [hep-ph]`. 12, 55

[66] L. Girardello and M. T. Grisaru, "Soft Breaking of Supersymmetry," *Nucl. Phys.* **B194** (1982) 65. 12

[67] P. Langacker, "Grand Unified Theories and Proton Decay," *Phys. Rept.* **72** (1981) 185. 14

[68] N. Arkani-Hamed and S. Dimopoulos, "Supersymmetric unification without low energy supersymmetry and signatures for fine-tuning at the LHC," *JHEP* **06** (2005) 073, `arXiv:hep-th/0405159 [hep-th]`. 14, 17

[69] G. F. Giudice and A. Romanino, "Split supersymmetry," *Nucl. Phys.* **B699** (2004) 65–89, `arXiv:hep-ph/0406088 [hep-ph]`. [Erratum: Nucl. Phys.B706,487(2005)].

[70] N. Arkani-Hamed, S. Dimopoulos, G. F. Giudice, and A. Romanino, "Aspects of split supersymmetry," *Nucl. Phys.* **B709** (2005) 3–46, `arXiv:hep-ph/0409232 [hep-ph]`. 14, 17, 55

[71] **ATLAS** Collaboration, G. Aad *et al.*, "Summary of the searches for squarks and gluinos using $\sqrt{s} = 8$ TeV pp collisions with the ATLAS experiment at the LHC," *JHEP* **10** (2015) 054, `arXiv:1507.05525 [hep-ex]`. 14, 15

[72] J. L. Feng, "Naturalness and the Status of Supersymmetry," *Ann. Rev. Nucl. Part. Sci.* **63** (2013) 351–382, `arXiv:1302.6587 [hep-ph]`. 14

[73] N. Craig, "The State of Supersymmetry after Run I of the LHC," in *Beyond the Standard Model after the first run of the LHC Arcetri, Florence, Italy, May 20-July 12, 2013*. 2013. `arXiv:1309.0528 [hep-ph]`. 14

[74] **ATLAS** Collaboration, G. Aad *et al.*, "Search for the electroweak production of supersymmetric particles in $\sqrt{s}$=8 TeV *pp* collisions with the ATLAS detector," *Phys. Rev.* **D93** no. 5, (2016) 052002, `arXiv:1509.07152 [hep-ex]`. 15, 16

[75] J. P. Vega and G. Villadoro, "SusyHD: Higgs mass Determination in Supersymmetry," *JHEP* **07** (2015) 159, `arXiv:1504.05200 [hep-ph]`. 16, 18, 40

[76] A. Arvanitaki, M. Baryakhtar, X. Huang, K. van Tilburg, and G. Villadoro, "The Last Vestiges of Naturalness," *JHEP* **1403** (2014) 022, `arXiv:1309.3568 [hep-ph]`. 16, 20

[77] **ATLAS** Collaboration, "Search for strong production of supersymmetric particles in final states with missing transverse momentum and at least three b-jets using $20.1fb^1$ of pp collisions at $\sqrt{(s)} = 8$ TeV with the ATLAS Detector.," *ATLAS-CONF-2013-061* (2013) . 17

[78] **ATLAS** Collaboration, "Search for direct production of the top squark in the all-hadronic ttbar + etmiss final state in 21 fb^{-1} of p-pcollisions at $\sqrt{s} = 8$ TeV with the ATLAS detector," *ATLAS-CONF-2013-024* (2013) .

[79] **CMS** Collaboration, "Search for supersymmetry using razor variables in events with b-jets in pp collisions at 8 TeV," *CMS-PAS-SUS-13-004* (2013) .

[80] **CMS** Collaboration, S. Chatrchyan *et al.*, "Search for top-squark pair production in the single-lepton final state in pp collisions at $\sqrt{s} = 8$ TeV," *Eur. Phys. J.* **C73** no. 12, (2013) 2677, `arXiv:1308.1586 [hep-ex]`.

[81] **CMS** Collaboration, S. Chatrchyan *et al.*, "Search for three-jet resonances in *pp* collisions at $\sqrt{s} = 7$ TeV," *Phys. Lett.* **B718** (2012) 329–347, `arXiv:1208.2931 [hep-ex]`.

[82] **ATLAS** Collaboration, G. Aad *et al.*, "Search for pair production of massive particles decaying into three quarks with the ATLAS detector in $\sqrt{s} = 7$ TeV *pp* collisions at the LHC," *JHEP* **12** (2012) 086, `arXiv:1210.4813 [hep-ex]`.

[83] **ATLAS** Collaboration, "Search for strongly produced superpartners in final states with two same sign leptons with the ATLAS detector using 21 fb^{-1} of proton-proton collisions at $\sqrt{s} = 8$ TeV.," *ATLAS-CONF-2013-007* (2013) .

[84] **ATLAS** Collaboration, "Search for massive particles in multijet signatures with the ATLAS detector in $\sqrt{s} = 8$ TeV pp collisions at the LHC," *ATLAS-CONF-2013-091* (2013) . 17

[85] G. D. Kribs and A. Martin, "Supersoft Supersymmetry is Super-Safe," *Phys.Rev.* **D85** (2012) 115014, arXiv:1203.4821 [hep-ph]. 17, 18, 31, 32, 39, 60

[86] P. Fayet, "MASSIVE GLUINOS," *Phys. Lett.* **B78** (1978) 417–420. 18

[87] J. Polchinski and L. Susskind, "Breaking of Supersymmetry at Intermediate-Energy," *Phys. Rev.* **D26** (1982) 3661.

[88] L. J. Hall and L. Randall, "U(1)-R symmetric supersymmetry," *Nucl. Phys.* **B352** (1991) 289–308. 18

[89] P. J. Fox, A. E. Nelson, and N. Weiner, "Dirac gaugino masses and supersoft supersymmetry breaking," *JHEP* **0208** (2002) 035, arXiv:hep-ph/0206096 [hep-ph]. 18, 20

[90] G. D. Kribs, E. Poppitz, and N. Weiner, "Flavor in supersymmetry with an extended R-symmetry," *Phys. Rev.* **D78** (2008) 055010, arXiv:0712.2039 [hep-ph]. 18

[91] S. D. L. Amigo, A. E. Blechman, P. J. Fox, and E. Poppitz, "R-symmetric gauge mediation," *JHEP* **01** (2009) 018, arXiv:0809.1112 [hep-ph]. 20

[92] L. M. Carpenter, "Dirac Gauginos, Negative Supertraces and Gauge Mediation," *JHEP* **1209** (2012) 102, arXiv:1007.0017 [hep-th]. 20

[93] K. Benakli and M. Goodsell, "Dirac Gauginos, Gauge Mediation and Unification," *Nucl.Phys.* **B840** (2010) 1–28, arXiv:1003.4957 [hep-ph]. 20, 21, 60

[94] K. Benakli and M. Goodsell, "Dirac Gauginos in General Gauge Mediation," *Nucl.Phys.* **B816** (2009) 185–203, arXiv:0811.4409 [hep-ph]. 20, 60

[95] C. Csaki, J. Goodman, R. Pavesi, and Y. Shirman, "The $m_D - b_M$ problem of Dirac gauginos and its solutions," *Phys. Rev.* **D89** no. 5, (2014) 055005, arXiv:1310.4504 [hep-ph]. 20

[96] L. M. Carpenter and J. Goodman, "New Calculations in Dirac Gaugino Models: Operators, Expansions, and Effects," *JHEP* **07** (2015) 107, `arXiv:1501.05653` `[hep-ph]`.

[97] A. E. Nelson and T. S. Roy, "New Supersoft Supersymmetry Breaking Operators and a Solution to the μ Problem," `arXiv:1501.03251 [hep-ph]`. 20

[98] D. S. M. Alves, J. Galloway, M. McCullough, and N. Weiner, "Goldstone Gauginos," *Phys. Rev. Lett.* **115** no. 16, (2015) 161801, `arXiv:1502.03819` `[hep-ph]`. 20

[99] D. S. M. Alves, J. Galloway, N. Weiner, and M. McCullough, "Models of Goldstone Gauginos," `arXiv:1502.05055 [hep-ph]`. 20

[100] R. Ding, T. Li, F. Staub, C. Tian, and B. Zhu, "Supersymmetric standard models with a pseudo-Dirac gluino from hybrid F - and D -term supersymmetry breaking," *Phys. Rev.* **D92** no. 1, (2015) 015008, `arXiv:1502.03614 [hep-ph]`. 20

[101] S. P. Martin, "Nonstandard supersymmetry breaking and Dirac gaugino masses without supersoftness," *Phys. Rev.* **D92** no. 3, (2015) 035004, `arXiv:1506.02105` `[hep-ph]`. 20

[102] K. Benakli, M. Goodsell, F. Staub, and W. Porod, "Constrained minimal Dirac gaugino supersymmetric standard model," *Phys. Rev.* **D90** no. 4, (2014) 045017, `arXiv:1403.5122 [hep-ph]`. 20, 21, 60

[103] P. J. Fox, G. D. Kribs, and A. Martin, "Split Dirac Supersymmetry: An Ultraviolet Completion of Higgsino Dark Matter," *Phys. Rev.* **D90** no. 7, (2014) 075006, `arXiv:1405.3692 [hep-ph]`. 21, 66

[104] G. Salam and A. Weiler, "Collider reach." `http://collider-reach.web.cern.ch.` 24

[105] G. Salam and A. Weiler, "Collider reach β." `https://gsalam.web.cern.ch/` `gsalam/talks/repo/2014-02-FHC-PU-collider-reach.pdf.` 24

[106] J. Debove, B. Fuks, and M. Klasen, "Model-independent analysis of gaugino-pair production in polarized and unpolarized hadron collisions," *Phys. Rev.* **D78** (2008) 074020, `arXiv:0804.0423 [hep-ph]`. 24

[107] A. D. Martin, W. J. Stirling, R. S. Thorne, and G. Watt, "Parton distributions for the LHC," *Eur. Phys. J.* **C63** (2009) 189–285, `arXiv:0901.0002 [hep-ph]`. 24

[108] **ATLAS** Collaboration, G. Aad *et al.*, "Search for direct production of charginos and neutralinos in events with three leptons and missing transverse momentum in $\sqrt{s} = 8$TeV *pp* collisions with the ATLAS detector," *JHEP* **04** (2014) 169, `arXiv:1402.7029 [hep-ex]`. 25, 31

[109] **ATLAS** Collaboration, "Search for chargino and neutralino production in final states with one lepton, two b-jets consistent with a Higgs boson, and missing transverse momentum with the ATLAS detector in 20.3 fb^{-1} of $\sqrt{s} = 8$ TeV *pp* collisions," *ATLAS-CONF-2013-093* (2013) . 25, 26, 31

[110] B. S. Acharya, K. Bożek, C. Pongkitivanichkul, and K. Sakurai, "Prospects for observing charginos and neutralinos at a 100 TeV proton-proton collider," *JHEP* **02** (2015) 181, `arXiv:1410.1532 [hep-ph]`. 24

[111] **CMS** Collaboration, V. Khachatryan *et al.*, "Searches for electroweak production of charginos, neutralinos, and sleptons decaying to leptons and W, Z, and Higgs bosons in pp collisions at 8 TeV," *Eur. Phys. J.* **C74** no. 9, (2014) 3036, `arXiv:1405.7570 [hep-ex]`. 25, 30, 31, 66

[112] **ATLAS** Collaboration, G. Aad *et al.*, "Search for Supersymmetry at the high luminosity LHC with the ATLAS experiment," *ATL-PHYS-PUB-2014-010* (2014) . 26

[113] S. Gori, S. Jung, L.-T. Wang, and J. D. Wells, "Prospects for Electroweakino Discovery at a 100 TeV Hadron Collider," *JHEP* **1412** (2014) 108, `arXiv:1410.6287 [hep-ph]`. 26

[114] H.-C. Cheng, B. A. Dobrescu, and K. T. Matchev, "Generic and chiral extensions of the supersymmetric standard model," *Nucl. Phys.* **B543** (1999) 47–72, `arXiv:hep-ph/9811316 [hep-ph]`. 27

[115] J. L. Feng, T. Moroi, L. Randall, M. Strassler, and S.-f. Su, "Discovering supersymmetry at the Tevatron in wino LSP scenarios," *Phys. Rev. Lett.* **83** (1999) 1731–1734, `arXiv:hep-ph/9904250 [hep-ph]`.

[116] T. Gherghetta, G. F. Giudice, and J. D. Wells, "Phenomenological consequences of supersymmetry with anomaly induced masses," *Nucl. Phys.* **B559** (1999) 27–47, `arXiv:hep-ph/9904378 [hep-ph]`. 27

[117] **ATLAS** Collaboration, G. Aad *et al.*, "Search for charginos nearly mass degenerate with the lightest neutralino based on a disappearing-track signature in pp collisions at $\sqrt{(s)}$=8âĂĽâĂĽTeV with the ATLAS detector," *Phys. Rev.* **D88** no. 11, (2013) 112006, `arXiv:1310.3675 [hep-ex]`. 27, 28, 31

[118] J. M. Campbell, R. K. Ellis, F. Maltoni, and S. Willenbrock, "Associated production of a Z Boson and a single heavy quark jet," *Phys. Rev.* **D69** (2004) 074021, `arXiv:hep-ph/0312024 [hep-ph]`. 27

[119] A. Haas, "Lhc susy searches: pulling out all the stops," talk given at the workshop on Frontiers of New Physics: Colliders and Beyond, June 23-27, ICTP, Trieste, Italy, 2014. `http://indico.ictp.it/event/a13203/session/1/contribution/3/material/0/0.pdf`. 28

[120] M. Low and L.-T. Wang, "Neutralino dark matter at 14 TeV and 100 TeV," *JHEP* **1408** (2014) 161, `arXiv:1404.0682 [hep-ph]`. 28, 54

[121] M. Cirelli, F. Sala, and M. Taoso, "Wino-like Minimal Dark Matter and future colliders," *JHEP* **10** (2014) 033, `arXiv:1407.7058 [hep-ph]`. [Erratum: JHEP01,041(2015)]. 28

[122] T. Cohen, T. Golling, M. Hance, A. Henrichs, K. Howe, *et al.*, "SUSY Simplified Models at 14, 33, and 100 TeV Proton Colliders," *JHEP* **1404** (2014) 117, `arXiv:1311.6480 [hep-ph]`. 28, 35, 36, 38

[123] **ATLAS** Collaboration, "Search for Diphoton Events with Large Missing Transverse Momentum in 8 TeV pp Collision Data with the ATLAS Detector," *ATLAS-CONF-2014-001* (2014) . 29, 31

[124] A. De Simone, R. Franceschini, G. F. Giudice, D. Pappadopulo, and R. Rattazzi, "Lopsided Gauge Mediation," *JHEP* **05** (2011) 112, `arXiv:1103.6033 [hep-ph]`. 30

[125] K. T. Matchev and S. D. Thomas, "Higgs and Z boson signatures of supersymmetry," *Phys. Rev.* **D62** (2000) 077702, `arXiv:hep-ph/9908482 [hep-ph]`. 30

[126] P. Meade, M. Reece, and D. Shih, "Prompt Decays of General Neutralino NLSPs at the Tevatron," *JHEP* **05** (2010) 105, `arXiv:0911.4130 [hep-ph]`. 30

BIBLIOGRAPHY

[127] S. Choi, M. Drees, A. Freitas, and P. Zerwas, "Testing the Majorana Nature of Gluinos and Neutralinos," *Phys.Rev.* **D78** (2008) 095007, `arXiv:0808.2410 [hep-ph]`. 31, 130

[128] M. Heikinheimo, M. Kellerstein, and V. Sanz, "How Many Supersymmetries?," *JHEP* **1204** (2012) 043, `arXiv:1111.4322 [hep-ph]`. 32

[129] G. D. Kribs and N. Raj, "Mixed Gauginos Sending Mixed Messages to the LHC," *Phys.Rev.* **D89** no. 5, (2014) 055011, `arXiv:1307.7197 [hep-ph]`. 31, 32

[130] **ATLAS** Collaboration, "Search for squarks and gluinos with the ATLAS detector in final states with jets and missing transverse momentum and 20.3 fb^{-1} of $\sqrt{s} = 8$ TeV proton-proton collision data," *ATLAS-CONF-2013-047* (2013) . 31

[131] **CMS** Collaboration, "Search for New Physics in the Multijets and Missing Momentum Final State in Proton-Proton Collisions at 8 TeV," *CMS-PAS-SUS-13-012* (2013) . 31

[132] J. Alwall, R. Frederix, S. Frixione, V. Hirschi, F. Maltoni, O. Mattelaer, H. S. Shao, T. Stelzer, P. Torrielli, and M. Zaro, "The automated computation of tree-level and next-to-leading order differential cross sections, and their matching to parton shower simulations," *JHEP* **07** (2014) 079, `arXiv:1405.0301 [hep-ph]`. 32, 35

[133] C. Borschensky, M. Krämer, A. Kulesza, M. Mangano, S. Padhi, T. Plehn, and X. Portell, "Squark and gluino production cross sections in pp collisions at $\sqrt{s} = 13, 14, 33$ and 100 TeV," *Eur. Phys. J.* **C74** no. 12, (2014) 3174, `arXiv:1407.5066 [hep-ph]`. 32

[134] G. D. Kribs and A. Martin, "Dirac Gauginos in Supersymmetry – Suppressed Jets + MET Signals: A Snowmass Whitepaper," `arXiv:1308.3468 [hep-ph]`. 32

[135] T. Plehn and T. M. P. Tait, "Seeking Sgluons," *J. Phys.* **G36** (2009) 075001, `arXiv:0810.3919 [hep-ph]`. 34, 39

[136] D. Goncalves-Netto, D. Lopez-Val, K. Mawatari, T. Plehn, and I. Wigmore, "Sgluon Pair Production to Next-to-Leading Order," *Phys.Rev.* **D85** (2012) 114024, `arXiv:1203.6358 [hep-ph]`. 34

[137] F. Staub, "SARAH 3.2: Dirac Gauginos, UFO output, and more," *Comput.Phys.Commun.* **184** (2013) pp. 1792–1809, `arXiv:1207.0906 [hep-ph]`. 35

[138] T. Sjostrand, S. Mrenna, and P. Z. Skands, "PYTHIA 6.4 Physics and Manual," *JHEP* **05** (2006) 026, `arXiv:hep-ph/0603175 [hep-ph]`. 35

[139] J. Anderson *et al.*, "Snowmass Energy Frontier Simulations," in *Community Summer Study 2013: Snowmass on the Mississippi (CSS2013) Minneapolis, MN, USA, July 29-August 6, 2013.* 2013. `arXiv:1309.1057 [hep-ex]`. 35

[140] **DELPHES 3** Collaboration, J. de Favereau, C. Delaere, P. Demin, A. Giammanco, V. Lemaître, A. Mertens, and M. Selvaggi, "DELPHES 3, A modular framework for fast simulation of a generic collider experiment," *JHEP* **02** (2014) 057, `arXiv:1307.6346 [hep-ex]`. 35

[141] A. Avetisyan *et al.*, "Methods and Results for Standard Model Event Generation at $\sqrt{s} = 14$ TeV, 33 TeV and 100 TeV Proton Colliders (A Snowmass Whitepaper)," in *Community Summer Study 2013: Snowmass on the Mississippi (CSS2013) Minneapolis, MN, USA, July 29-August 6, 2013.* 2013. `arXiv:1308.1636 [hep-ex]`. 35

[142] I. Hinchliffe, A. Kotwal, M. L. Mangano, C. Quigg, and L.-T. Wang, "Luminosity goals for a 100-TeV pp collider," *Int. J. Mod. Phys.* **A30** no. 23, (2015) 1544002, `arXiv:1504.06108 [hep-ph]`. 35, 38

[143] N. Arkani-Hamed, T. Han, M. Mangano, and L.-T. Wang, "Physics Opportunities of a 100 TeV Proton-Proton Collider," `arXiv:1511.06495 [hep-ph]`. 35, 38

[144] S. A. R. Ellis and B. Zheng, "Reaching for squarks and gauginos at a 100 TeV p-p collider," *Phys. Rev.* **D92** no. 7, (2015) 075034, `arXiv:1506.02644 [hep-ph]`. 35, 130

[145] W. Beenakker, R. Hopker, M. Spira, and P. M. Zerwas, "Squark and gluino production at hadron colliders," *Nucl. Phys.* **B492** (1997) 51–103, `arXiv:hep-ph/9610490 [hep-ph]`. 35

[146] W. Barletta, M. Battaglia, M. Klute, M. Mangano, S. Prestemon, L. Rossi, and P. Skands, "Working Group Report: Hadron Colliders," in *Community Summer Study 2013: Snowmass on the Mississippi (CSS2013) Minneapolis, MN, USA, July 29-August 6, 2013.* 2013. `arXiv:1310.0290 [physics.acc-ph]`. 36

[147] P. Z. Skands, "Soft-QCD and UE spectra in pp collisions at very high CM energies (a Snowmass white paper)," `arXiv:1308.2813 [hep-ph]`. 36

[148] T. Cohen, R. T. D'Agnolo, M. Hance, H. K. Lou, and J. G. Wacker, "Boosting Stop Searches with a 100 TeV Proton Collider," *JHEP* **1411** (2014) 021, `arXiv:1406.4512 [hep-ph]`. 38

[149] M. Papucci, J. T. Ruderman, and A. Weiler, "Natural SUSY Endures," *JHEP* **09** (2012) 035, `arXiv:1110.6926 [hep-ph]`. 39

[150] M. I. Gresham and M. B. Wise, "Color octet scalar production at the LHC," *Phys.Rev.* **D76** (2007) 075003, `arXiv:0706.0909 [hep-ph]`. 39

[151] S. Choi, M. Drees, J. Kalinowski, J. Kim, E. Popenda, *et al.*, "Color-Octet Scalars of N=2 Supersymmetry at the LHC," *Phys.Lett.* **B672** (2009) 246–252, `arXiv:0812.3586 [hep-ph]`.

[152] M. Martynov and A. Smirnov, "Colored scalar particles production in pp-collisions and possible mass limits for scalar gluons from future LHC data," *Mod.Phys.Lett.* **A23** (2008) 2907–2913, `arXiv:0807.4486 [hep-ph]`.

[153] S. Choi, J. Kalinowski, J. Kim, and E. Popenda, "Scalar gluons and Dirac gluinos at the LHC," *Acta Phys.Polon.* **B40** (2009) 2913–2922, `arXiv:0911.1951 [hep-ph]`.

[154] S. Choi, M. Drees, J. Kalinowski, J. Kim, E. Popenda, *et al.*, "Color-octet scalars at the LHC," *Acta Phys.Polon.* **B40** (2009) 1947–1956, `arXiv:0902.4706 [hep-ph]`.

[155] B. Fuks, "Beyond the Minimal Supersymmetric Standard Model: from theory to phenomenology," *Int.J.Mod.Phys.* **A27** (2012) 1230007, `arXiv:1202.4769 [hep-ph]`.

[156] S. Calvet, B. Fuks, P. Gris, and L. Valery, "Searching for sgluons in multitop events at a center-of-mass energy of 8 TeV," *JHEP* **04** (2013) 043, `arXiv:1212.3360 [hep-ph]`. 39

[157] U. Ellwanger, C. Hugonie, and A. M. Teixeira, "The Next-to-Minimal Supersymmetric Standard Model," *Phys. Rept.* **496** (2010) 1–77, `arXiv:0910.1785 [hep-ph]`. 40

[158] L. J. Hall, D. Pinner, and J. T. Ruderman, "A Natural SUSY Higgs Near 126 GeV," *JHEP* **04** (2012) 131, `arXiv:1112.2703 [hep-ph]`. 40

[159] E. Hardy, J. March-Russell, and J. Unwin, "Precision Unification in λ SUSY with a 125 GeV Higgs," *JHEP* **10** (2012) 072, `arXiv:1207.1435 [hep-ph]`. 40

[160] K. Benakli, M. D. Goodsell, and F. Staub, "Dirac Gauginos and the 125 GeV Higgs," *JHEP* **1306** (2013) 073, `arXiv:1211.0552 [hep-ph]`. 40, 60

[161] A. E. Nelson, N. Rius, V. Sanz, and M. Unsal, "The Minimal supersymmetric model without a mu term," *JHEP* **08** (2002) 039, `arXiv:hep-ph/0206102 [hep-ph]`. 41

[162] K. Benakli, M. D. Goodsell, and A.-K. Maier, "Generating mu and Bmu in models with Dirac Gauginos," *Nucl.Phys.* **B851** (2011) 445–461, `arXiv:1104.2695 [hep-ph]`. 41

[163] P. Diessner, J. Kalinowski, W. Kotlarski, and D. Stöckinger, "Exploring the Higgs sector of the MRSSM with a light scalar," `arXiv:1511.09334 [hep-ph]`. 41

[164] E. Bertuzzo, C. Frugiuele, T. Gregoire, and E. Ponton, "Dirac gauginos, R symmetry and the 125 GeV Higgs," `arXiv:1402.5432 [hep-ph]`. 41, 43, 65

[165] P. Dießner, J. Kalinowski, W. Kotlarski, and D. Stöckinger, "Higgs boson mass and electroweak observables in the MRSSM," *JHEP* **12** (2014) 124, `arXiv:1410.4791 [hep-ph]`. 41, 65

[166] E. Hardy, "Is Natural SUSY Natural?," *JHEP* **10** (2013) 133, `arXiv:1306.1534 [hep-ph]`. 43

[167] A. Arvanitaki and G. Villadoro, "A Non Standard Model Higgs at the LHC as a Sign of Naturalness," *JHEP* **02** (2012) 144, `arXiv:1112.4835 [hep-ph]`. 43

[168] S. Dimopoulos, K. Howe, and J. March-Russell, "Maximally Natural Supersymmetry," *Phys. Rev. Lett.* **113** (2014) 111802, `arXiv:1404.7554 [hep-ph]`. 43

[169] I. G. Garcia, K. Howe, and J. March-Russell, "Natural Scherk-Schwarz Theories of the Weak Scale," *JHEP* **12** (2015) 005, `arXiv:1510.07045 [hep-ph]`. 43

[170] A. Kusenko, P. Langacker, and G. Segre, "Phase transitions and vacuum tunneling into charge and color breaking minima in the MSSM," *Phys. Rev.* **D54** (1996) 5824–5834, `arXiv:hep-ph/9602414 [hep-ph]`. 44

[171] M. W. Goodman and E. Witten, "Detectability of Certain Dark Matter Candidates," *Phys. Rev.* **D31** (1985) 3059. 47

[172] J. Billard, L. Strigari, and E. Figueroa-Feliciano, "Implication of neutrino backgrounds on the reach of next generation dark matter direct detection experiments," *Phys. Rev.* **D89** no. 2, (2014) 023524, `arXiv:1307.5458 [hep-ph]`. 48, 49, 51, 63

[173] J. Cooley, "Overview of Non-Liquid Noble Direct Detection Dark Matter Experiments," *Phys. Dark Univ.* **4** (2014) 92–97, `arXiv:1410.4960 [astro-ph.IM]`. 48

[174] J. Hisano, K. Ishiwata, and N. Nagata, "A complete calculation for direct detection of Wino dark matter," *Phys. Lett.* **B690** (2010) 311–315, `arXiv:1004.4090 [hep-ph]`. 49, 50

[175] J. Hisano, K. Ishiwata, N. Nagata, and T. Takesako, "Direct Detection of Electroweak-Interacting Dark Matter," *JHEP* **07** (2011) 005, `arXiv:1104.0228 [hep-ph]`.

[176] J. Hisano, K. Ishiwata, and N. Nagata, "Direct Search of Dark Matter in High-Scale Supersymmetry," *Phys. Rev.* **D87** (2013) 035020, `arXiv:1210.5985 [hep-ph]`. 49, 50

[177] R. J. Hill and M. P. Solon, "Universal behavior in the scattering of heavy, weakly interacting dark matter on nuclear targets," *Phys. Lett.* **B707** (2012) 539–545, `arXiv:1111.0016 [hep-ph]`. 50

[178] R. J. Hill and M. P. Solon, "WIMP-nucleon scattering with heavy WIMP effective theory," *Phys. Rev. Lett.* **112** (2014) 211602, `arXiv:1309.4092 [hep-ph]`.

[179] R. J. Hill and M. P. Solon, "Standard Model anatomy of WIMP dark matter direct detection I: weak-scale matching," *Phys. Rev.* **D91** (2015) 043504, `arXiv:1401.3339 [hep-ph]`.

[180] R. J. Hill and M. P. Solon, "Standard Model anatomy of WIMP dark matter direct detection II: QCD analysis and hadronic matrix elements," *Phys. Rev.* **D91** (2015) 043505, `arXiv:1409.8290 [hep-ph]`. 50

[181] P. Gondolo, J. Edsjo, P. Ullio, L. Bergstrom, M. Schelke, and E. A. Baltz, "DarkSUSY: Computing supersymmetric dark matter properties numerically," *JCAP* **0407** (2004) 008, `arXiv:astro-ph/0406204 [astro-ph]`. 50

[182] P.Gondolo et al., "DarkSUSY Home Page." `http://www.darksusy.org`. 50

[183] A. Hryczuk, "The Sommerfeld enhancement for scalar particles and application to sfermion co-annihilation regions," *Phys. Lett.* **B699** (2011) 271–275, `arXiv:1102.4295 [hep-ph]`. 50

[184] **Planck** Collaboration, P. A. R. Ade *et al.*, "Planck 2013 results. XVI. Cosmological parameters," *Astron. Astrophys.* **571** (2014) A16, `arXiv:1303.5076 [astro-ph.CO]`. 50

[185] Manalaysay, Aaron (for the LUX Collaboration), "Dark-matter results from 332 new live days of LUX data." `http://luxdarkmatter.org/LUX_dark_matter/Talks_files/LUX_ NewDarkMatterSearchResult_332LiveDays_IDM2016_160721.pdf`. 51, 52, 56, 63

[186] D. C. Malling *et al.*, "After LUX: The LZ Program," `arXiv:1110.0103 [astro-ph.IM]`. 51, 63

[187] P. Cushman *et al.*, "Working Group Report: WIMP Dark Matter Direct Detection," in *Community Summer Study 2013: Snowmass on the Mississippi (CSS2013) Minneapolis, MN, USA, July 29-August 6, 2013.* 2013. `arXiv:1310.8327 [hep-ex]`. 51, 63

[188] LEP2 SUSY Working Group, Aleph, Delphi, L3 and Opal experiments webpage. `http://lepsusy.web.cern.ch/lepsusy/`. 54

[189] K. Hsieh, "Pseudo-Dirac bino dark matter," *Phys. Rev.* **D77** (2008) 015004, `arXiv:0708.3970 [hep-ph]`. 60

[190] R. Harnik and G. D. Kribs, "An Effective Theory of Dirac Dark Matter," *Phys.Rev.* **D79** (2009) 095007, `arXiv:0810.5557 [hep-ph]`.

BIBLIOGRAPHY

[191] G. Belanger, K. Benakli, M. Goodsell, C. Moura, and A. Pukhov, "Dark Matter with Dirac and Majorana Gaugino Masses," *JCAP* **0908** (2009) 027, `arXiv:0905.1043 [hep-ph]`.

[192] M. D. Goodsell and P. Tziveloglou, "Dirac Gauginos in Low Scale Supersymmetry Breaking," *Nucl.Phys.* **B889** (2014) 650–675, `arXiv:1407.5076 [hep-ph]`.

[193] M. D. Goodsell, M. E. Krauss, T. Müller, W. Porod, and F. Staub, "Dark matter scenarios in a constrained model with Dirac gauginos," *JHEP* **10** (2015) 132, `arXiv:1507.01010 [hep-ph]`. 60

[194] A. Belyaev, N. D. Christensen, and A. Pukhov, "CalcHEP 3.4 for collider physics within and beyond the Standard Model," *Comput. Phys. Commun.* **184** (2013) 1729–1769, `arXiv:1207.6082 [hep-ph]`. 60

[195] F. Staub, "SARAH 4 : A tool for (not only SUSY) model builders," *Comput. Phys. Commun.* **185** (2014) 1773–1790, `arXiv:1309.7223 [hep-ph]`. 60

[196] W. Porod and F. Staub, "SPheno 3.1: Extensions including flavour, CP-phases and models beyond the MSSM," *Comput. Phys. Commun.* **183** (2012) 2458–2469, `arXiv:1104.1573 [hep-ph]`. 60

[197] G. Belanger, F. Boudjema, A. Pukhov, and A. Semenov, "micromegas 3: A program for calculating dark matter observables," *Comput. Phys. Commun.* **185** (2014) 960–985, `arXiv:1305.0237 [hep-ph]`. 60

[198] **Planck** Collaboration, P. A. R. Ade *et al.*, "Planck 2015 results. XIII. Cosmological parameters," `arXiv:1502.01589 [astro-ph.CO]`. 60, 93

[199] J. Bramante, P. J. Fox, A. Martin, B. Ostdiek, T. Plehn, T. Schell, and M. Takeuchi, "Relic neutralino surface at a 100 TeV collider," *Phys. Rev.* **D91** (2015) 054015, `arXiv:1412.4789 [hep-ph]`. 60, 66

[200] A. Hryczuk, I. Cholis, R. Iengo, M. Tavakoli, and P. Ullio, "Indirect Detection Analysis: Wino Dark Matter Case Study," *JCAP* **1407** (2014) 031, `arXiv:1401.6212 [astro-ph.HE]`. 61

[201] M. R. Buckley, D. Hooper, and J. Kumar, "Phenomenology of Dirac Neutralino Dark Matter," *Phys.Rev.* **D88** (2013) 063532, `arXiv:1307.3561`. 61

[202] G. D. Kribs, A. Martin, and T. S. Roy, "Supersymmetry with a Chargino NLSP and Gravitino LSP," *JHEP* **01** (2009) 023, `arXiv:0807.4936 [hep-ph]`. 63, 64

[203] LEPSUSYWG, ALEPH, DELPHI, L3, and OPAL, "Note lepsusywg/02-04.1,". http://lepsusy.web.cern.ch/lepsusy/Welcome.html. 64

[204] LEPSUSYWG, ALEPH, DELPHI, L3, and OPAL, "Note lepsusywg/04-01.1,". http://lepsusy.web.cern.ch/lepsusy/Welcome.html. 65

[205] **ATLAS** Collaboration, G. Aad *et al.*, "Search for direct production of charginos, neutralinos and sleptons in final states with two leptons and missing transverse momentum in *pp* collisions at $\sqrt{s} = 8$ TeV with the ATLAS detector," *JHEP* **05** (2014) 071, arXiv:1403.5294 [hep-ex]. 65, 66

[206] L. Bergstrom, T. Bringmann, I. Cholis, D. Hooper, and C. Weniger, "New limits on dark matter annihilation from AMS cosmic ray positron data," *Phys. Rev. Lett.* **111** (2013) 171101, arXiv:1306.3983 [astro-ph.HE]. 66

[207] R. D. Peccei and H. R. Quinn, "CP Conservation in the Presence of Instantons," *Phys. Rev. Lett.* **38** (1977) 1440–1443. 71, 75, 76

[208] R. D. Peccei and H. R. Quinn, "Constraints Imposed by CP Conservation in the Presence of Instantons," *Phys. Rev.* **D16** (1977) 1791–1797. 75

[209] F. Wilczek, "Problem of Strong p and t Invariance in the Presence of Instantons," *Phys. Rev. Lett.* **40** (1978) 279–282.

[210] S. Weinberg, "A New Light Boson?," *Phys. Rev. Lett.* **40** (1978) 223–226. 76, 83

[211] J. E. Kim, "Weak Interaction Singlet and Strong CP Invariance," *Phys. Rev. Lett.* **43** (1979) 103. 78, 120

[212] M. A. Shifman, A. I. Vainshtein, and V. I. Zakharov, "Can Confinement Ensure Natural CP Invariance of Strong Interactions?," *Nucl. Phys.* **B166** (1980) 493–506. 72, 78, 120

[213] A. R. Zhitnitsky, "On Possible Suppression of the Axion Hadron Interactions. (In Russian)," *Sov. J. Nucl. Phys.* **31** (1980) 260. [Yad. Fiz.31,497(1980)]. 79, 120

[214] M. Dine, W. Fischler, and M. Srednicki, "A Simple Solution to the Strong CP Problem with a Harmless Axion," *Phys. Lett.* **B104** (1981) 199. 71, 79, 120

[215] J. Preskill, M. B. Wise, and F. Wilczek, "Cosmology of the Invisible Axion," *Phys. Lett.* **B120** (1983) 127–132. 71, 89, 96

BIBLIOGRAPHY

[216] L. F. Abbott and P. Sikivie, "A Cosmological Bound on the Invisible Axion," *Phys. Lett.* **B120** (1983) 133–136.

[217] M. Dine and W. Fischler, "The Not So Harmless Axion," *Phys. Lett.* **B120** (1983) 137–141. 89, 96

[218] F. W. Stecker and Q. Shafi, "The Evolution of Structure in the Universe From Axions," *Phys. Rev. Lett.* **50** (1983) 928.

[219] M. S. Turner, "Thermal Production of Not SO Invisible Axions in the Early Universe," *Phys. Rev. Lett.* **59** (1987) 2489. [Erratum: Phys. Rev. Lett.60,1101(1988)]. 88

[220] M. S. Turner and F. Wilczek, "Inflationary axion cosmology," *Phys. Rev. Lett.* **66** (1991) 5–8.

[221] Z. G. Berezhiani, A. S. Sakharov, and M. Yu. Khlopov, "Primordial background of cosmological axions," *Sov. J. Nucl. Phys.* **55** (1992) 1063–1071. [Yad. Fiz.55,1918(1992)]. 96

[222] D. H. Lyth and E. D. Stewart, "Axions and inflation: String formation during inflation," *Phys. Rev.* **D46** (1992) 532–538.

[223] E. Masso, F. Rota, and G. Zsembinszki, "On axion thermalization in the early universe," *Phys. Rev.* **D66** (2002) 023004, `arXiv:hep-ph/0203221 [hep-ph]`. 88, 96

[224] M. Beltran, J. Garcia-Bellido, and J. Lesgourgues, "Isocurvature bounds on axions revisited," *Phys. Rev.* **D75** (2007) 103507, `arXiv:hep-ph/0606107 [hep-ph]`.

[225] M. P. Hertzberg, M. Tegmark, and F. Wilczek, "Axion Cosmology and the Energy Scale of Inflation," *Phys. Rev.* **D78** (2008) 083507, `arXiv:0807.1726 [astro-ph]`.

[226] P. Graf and F. D. Steffen, "Thermal axion production in the primordial quark-gluon plasma," *Phys. Rev.* **D83** (2011) 075011, `arXiv:1008.4528 [hep-ph]`. 96

[227] A. Salvio, A. Strumia, and W. Xue, "Thermal axion production," *JCAP* **1401** (2014) 011, `arXiv:1310.6982 [hep-ph]`. 71, 88, 96

[228] M. Kuster, G. Raffelt, and B. Beltran, "Axions: Theory, cosmology, and experimental searches. Proceedings, 1st Joint ILIAS-CERN-CAST axion training, Geneva, Switzerland, November 30-December 2, 2005," *Lect. Notes Phys.* **741** (2008) pp.1–258. 71

[229] J. E. Kim and G. Carosi, "Axions and the Strong CP Problem," *Rev. Mod. Phys.* **82** (2010) 557–602, arXiv:0807.3125 [hep-ph]. 71

[230] S. Pokorski, *GAUGE FIELD THEORIES*. Cambridge University Press, 2005. http://www.cambridge.org/uk/catalogue/catalogue.asp?isbn=0521265371. 72

[231] S. Weinberg, "The U(1) Problem," *Phys. Rev.* **D11** (1975) 3583–3593. 72

[232] G. 't Hooft, "Computation of the Quantum Effects Due to a Four-Dimensional Pseudoparticle," *Phys. Rev.* **D14** (1976) 3432–3450. [Erratum: Phys. Rev.D18,2199(1978)]. 72

[233] G. 't Hooft, "Symmetry Breaking Through Bell-Jackiw Anomalies," *Phys. Rev. Lett.* **37** (1976) 8–11. 72

[234] W. A. Bardeen, "Anomalous Currents in Gauge Field Theories," *Nucl. Phys.* **B75** (1974) 246–258. 72

[235] V. Baluni, "CP Violating Effects in QCD," *Phys. Rev.* **D19** (1979) 2227–2230. 74

[236] R. J. Crewther, P. Di Vecchia, G. Veneziano, and E. Witten, "Chiral Estimate of the Electric Dipole Moment of the Neutron in Quantum Chromodynamics," *Phys. Lett.* **B88** (1979) 123. [Erratum: Phys. Lett.B91,487(1980)]. 74

[237] J. Pendlebury *et al.*, "Revised experimental upper limit on the electric dipole moment of the neutron," *Phys. Rev.* **D92** no. 9, (2015) 092003, arXiv:1509.04411 [hep-ex]. 74

[238] **RM123** Collaboration, G. M. de Divitiis, R. Frezzotti, V. Lubicz, G. Martinelli, R. Petronzio, G. C. Rossi, F. Sanfilippo, S. Simula, and N. Tantalo, "Leading isospin breaking effects on the lattice," *Phys. Rev.* **D87** no. 11, (2013) 114505, arXiv:1303.4896 [hep-lat]. 74, 113, 139

[239] **MILC** Collaboration, S. Basak *et al.*, "Electromagnetic effects on the light hadron spectrum," *J. Phys. Conf. Ser.* **640** no. 1, (2015) 012052, arXiv:1510.04997 [hep-lat]. 139

[240] R. Horsley *et al.*, "Isospin splittings of meson and baryon masses from three-flavor lattice QCD + QED," `arXiv:1508.06401 [hep-lat]`. 74, 113, 139

[241] M. A. B. Beg and H. S. Tsao, "Strong P, T Noninvariances in a Superweak Theory," *Phys. Rev. Lett.* **41** (1978) 278. 74

[242] H. Georgi, "A Model of Soft CP Violation," *Hadronic J.* **1** (1978) 155.

[243] R. N. Mohapatra and G. Senjanovic, "Natural Suppression of Strong p and t Noninvariance," *Phys. Lett.* **B79** (1978) 283–286. 74

[244] A. E. Nelson, "Naturally Weak CP Violation," *Phys. Lett.* **B136** (1984) 387–391. 74

[245] S. M. Barr, "A Natural Class of Nonpeccei-quinn Models," *Phys. Rev.* **D30** (1984) 1805.

[246] S. M. Barr, "A Survey of a New Class of Models of CP Violation," *Phys. Rev.* **D34** (1986) 1567.

[247] A. E. Nelson, "Calculation of θ Barr," *Phys. Lett.* **B143** (1984) 165–170. 74

[248] C. Vafa and E. Witten, "Parity Conservation in QCD," *Phys. Rev. Lett.* **53** (1984) 535. 75

[249] W. A. Bardeen, R. D. Peccei, and T. Yanagida, "CONSTRAINTS ON VARIANT AXION MODELS," *Nucl. Phys.* **B279** (1987) 401–428. 77

[250] Y. Asano, E. Kikutani, S. Kurokawa, T. Miyachi, M. Miyajima, Y. Nagashima, T. Shinkawa, S. Sugimoto, and Y. Yoshimura, "Search for a Rare Decay Mode K+ —> pi+ Neutrino anti-neutrino and Axion," *Phys. Lett.* **B107** (1981) 159. 77

[251] P. Di Vecchia and G. Veneziano, "Chiral Dynamics in the Large n Limit," *Nucl. Phys.* **B171** (1980) 253. 83

[252] H. Georgi, D. B. Kaplan, and L. Randall, "Manifesting the Invisible Axion at Low-energies," *Phys. Lett.* **B169** (1986) 73. 84

[253] L. Ubaldi, "Effects of theta on the deuteron binding energy and the triple-alpha process," *Phys. Rev.* **D81** (2010) 025011, `arXiv:0811.1599 [hep-ph]`. 85

[254] M. Archidiacono, S. Hannestad, A. Mirizzi, G. Raffelt, and Y. Y. Y. Wong, "Axion hot dark matter bounds after Planck," *JCAP* **1310** (2013) 020, `arXiv:1307.0615 [astro-ph.CO]`. 89

[255] O. Philipsen, "The QCD equation of state from the lattice," *Prog. Part. Nucl. Phys.* **70** (2013) 55–107, `arXiv:1207.5999 [hep-lat]`. 92

[256] S. Borsanyi, Z. Fodor, C. Hoelbling, S. D. Katz, S. Krieg, and K. K. Szabo, "Full result for the QCD equation of state with 2+1 flavors," *Phys. Lett.* **B730** (2014) 99–104, `arXiv:1309.5258 [hep-lat]`. 92

[257] D. H. Lyth and E. D. Stewart, "Constraining the inflationary energy scale from axion cosmology," *Phys. Lett.* **B283** (1992) 189–193. 93

[258] A. Vilenkin and A. E. Everett, "Cosmic Strings and Domain Walls in Models with Goldstone and PseudoGoldstone Bosons," *Phys. Rev. Lett.* **48** (1982) 1867–1870. 94, 95, 96

[259] P. Sikivie, "Of Axions, Domain Walls and the Early Universe," *Phys. Rev. Lett.* **48** (1982) 1156–1159. 94, 95, 96

[260] R. L. Davis, "Goldstone Bosons in String Models of Galaxy Formation," *Phys. Rev.* **D32** (1985) 3172.

[261] R. L. Davis, "Cosmic Axions from Cosmic Strings," *Phys. Lett.* **B180** (1986) 225–230. 95, 96

[262] R. L. Davis and E. P. S. Shellard, "DO AXIONS NEED INFLATION?," *Nucl. Phys.* **B324** (1989) 167–186.

[263] D. P. Bennett and F. R. Bouchet, "High resolution simulations of cosmic string evolution. 1. Network evolution," *Phys. Rev.* **D41** (1990) 2408.

[264] A. Dabholkar and J. M. Quashnock, "Pinning Down the Axion," *Nucl. Phys.* **B333** (1990) 815–832. 95, 96

[265] B. Allen and E. P. S. Shellard, "Cosmic string evolution: a numerical simulation," *Phys. Rev. Lett.* **64** (1990) 119–122.

[266] C. Hagmann and P. Sikivie, "Computer simulations of the motion and decay of global strings," *Nucl. Phys.* **B363** (1991) 247–280.

[267] R. A. Battye and E. P. S. Shellard, "Global string radiation," *Nucl. Phys.* **B423** (1994) 260–304, `arXiv:astro-ph/9311017 [astro-ph]`.

[268] R. A. Battye and E. P. S. Shellard, "Axion string constraints," *Phys. Rev. Lett.* **73** (1994) 2954–2957, `arXiv:astro-ph/9403018 [astro-ph]`. [Erratum: Phys. Rev. Lett.76,2203(1996)].

[269] E. P. S. Shellard and R. A. Battye, "On the origin of dark matter axions," *Phys. Rept.* **307** (1998) 227–234, `arXiv:astro-ph/9808220 [astro-ph]`.

[270] S. Chang, C. Hagmann, and P. Sikivie, "Studies of the motion and decay of axion walls bounded by strings," *Phys. Rev.* **D59** (1999) 023505, `arXiv:hep-ph/9807374 [hep-ph]`.

[271] M. Yamaguchi, M. Kawasaki, and J. Yokoyama, "Evolution of axionic strings and spectrum of axions radiated from them," *Phys. Rev. Lett.* **82** (1999) 4578–4581, `arXiv:hep-ph/9811311 [hep-ph]`.

[272] C. Hagmann, S. Chang, and P. Sikivie, "Axion radiation from strings," *Phys. Rev.* **D63** (2001) 125018, `arXiv:hep-ph/0012361 [hep-ph]`.

[273] T. Hiramatsu, M. Kawasaki, K. Saikawa, and T. Sekiguchi, "Axion cosmology with long-lived domain walls," *JCAP* **1301** (2013) 001, `arXiv:1207.3166 [hep-ph]`.

[274] M. Kawasaki, K. Saikawa, and T. Sekiguchi, "Axion dark matter from topological defects," *Phys. Rev.* **D91** no. 6, (2015) 065014, `arXiv:1412.0789 [hep-ph]`. 96

[275] L. Fleury and G. D. Moore, "Axion dark matter: strings and their cores," *JCAP* **1601** (2016) 004, `arXiv:1509.00026 [hep-ph]`.

[276] L. M. Fleury and G. D. Moore, "Axion String Dynamics I: 2+1D," *JCAP* **1605** no. 05, (2016) 005, `arXiv:1602.04818 [hep-ph]`. 94

[277] D. P. Bennett and F. R. Bouchet, "Evidence for a Scaling Solution in Cosmic String Evolution," *Phys. Rev. Lett.* **60** (1988) 257. 94, 95, 96

[278] G. Lazarides and Q. Shafi, "Axion Models with No Domain Wall Problem," *Phys. Lett.* **B115** (1982) 21–25. 95

[279] P. Sikivie, "AXIONS IN COSMOLOGY," in *Where are the elementary particles?*, pp. 1–40, Proc. Gif-sur-Yvette Summer School. 1983. 95

[280] A. Vilenkin, "Cosmic Strings and Domain Walls," *Phys. Rept.* **121** (1985) 263–315. 95, 96

[281] G. R. Vincent, M. Hindmarsh, and M. Sakellariadou, "Scaling and small scale structure in cosmic string networks," *Phys. Rev.* **D56** (1997) 637–646, `arXiv:astro-ph/9612135 [astro-ph]`. 95, 96

[282] P. Sikivie, "Axion Cosmology," *Lect. Notes Phys.* **741** (2008) 19–50, `arXiv:astro-ph/0610440 [astro-ph]`. [,19(2006)]. 96

[283] C. Bonati, M. D'Elia, M. Mariti, G. Martinelli, M. Mesiti, F. Negro, F. Sanfilippo, and G. Villadoro, "Axion phenomenology and θ-dependence from $N_f = 2 + 1$ lattice QCD," *JHEP* **03** (2016) 155, `arXiv:1512.06746 [hep-lat]`. 96, 99, 100, 101, 102, 132

[284] P. Petreczky, H.-P. Schadler, and S. Sharma, "The topological susceptibility in finite temperature QCD and axion cosmology," `arXiv:1606.03145 [hep-lat]`. 96, 101, 132

[285] J. Frison, R. Kitano, H. Matsufuru, S. Mori, and N. Yamada, "Topological susceptibility at high temperature on the lattice," `arXiv:1606.07175 [hep-lat]`.

[286] S. Borsanyi *et al.*, "Lattice QCD for Cosmology," `arXiv:1606.07494 [hep-lat]`. 96, 99, 100, 101, 102, 132

[287] J. O. Andersen, L. E. Leganger, M. Strickland, and N. Su, "Three-loop HTL QCD thermodynamics," *JHEP* **08** (2011) 053, `arXiv:1103.2528 [hep-ph]`. 96

[288] S. Borsanyi, M. Dierigl, Z. Fodor, S. D. Katz, S. W. Mages, D. Nogradi, J. Redondo, A. Ringwald, and K. K. Szabo, "Axion cosmology, lattice QCD and the dilute instanton gas," *Phys. Lett.* **B752** (2016) 175–181, `arXiv:1508.06917 [hep-lat]`. 96, 99

[289] J. Gasser and H. Leutwyler, "Light Quarks at Low Temperatures," *Phys. Lett.* **B184** (1987) 83. 97

[290] J. Gasser and H. Leutwyler, "Thermodynamics of Chiral Symmetry," *Phys. Lett.* **B188** (1987) 477. 97

[291] F. C. Hansen and H. Leutwyler, "Charge correlations and topological susceptibility in QCD," *Nucl. Phys.* **B350** (1991) 201–227. 97

BIBLIOGRAPHY

[292] P. Gerber and H. Leutwyler, "Hadrons Below the Chiral Phase Transition," *Nucl. Phys.* **B321** (1989) 387. 97

[293] D. J. Gross, R. D. Pisarski, and L. G. Yaffe, "QCD and Instantons at Finite Temperature," *Rev. Mod. Phys.* **53** (1981) 43. 98, 137

[294] A. D. Linde, "Infrared Problem in Thermodynamics of the Yang-Mills Gas," *Phys. Lett.* **B96** (1980) 289. 98

[295] A. K. Rebhan, "The NonAbelian Debye mass at next-to-leading order," *Phys. Rev.* **D48** (1993) 3967–3970, `arXiv:hep-ph/9308232 [hep-ph]`. 98

[296] P. B. Arnold and L. G. Yaffe, "The NonAbelian Debye screening length beyond leading order," *Phys. Rev.* **D52** (1995) 7208–7219, `arXiv:hep-ph/9508280 [hep-ph]`. 98

[297] K. Kajantie, M. Laine, J. Peisa, A. Rajantie, K. Rummukainen, and M. E. Shaposhnikov, "Nonperturbative Debye mass in finite temperature QCD," *Phys. Rev. Lett.* **79** (1997) 3130–3133, `arXiv:hep-ph/9708207 [hep-ph]`. 98

[298] O. Philipsen, "Debye screening in the QCD plasma," in *Strong and electroweak matter. Proceedings, Meeting, SEWM 2000, Marseille, France, June 13-17, 2000*, pp. 95–106. 2000. `arXiv:hep-ph/0010327 [hep-ph]`. `http://alice.cern.ch/format/showfull?sysnb=2227150`.

[299] **WHOT-QCD** Collaboration, Y. Maezawa, N. Ukita, S. Aoki, S. Ejiri, T. Hatsuda, N. Ishii, and K. Kanaya, "Heavy-quark free energy, debye mass, and spatial string tension at finite temperature in two flavor lattice QCD with Wilson quark action," *Phys. Rev.* **D75** (2007) 074501, `arXiv:hep-lat/0702004 [hep-lat]`. 98

[300] E. Berkowitz, M. I. Buchoff, and E. Rinaldi, "Lattice QCD input for axion cosmology," *Phys. Rev.* **D92** no. 3, (2015) 034507, `arXiv:1505.07455 [hep-ph]`. 99

[301] A. D. Linde, "Generation of Isothermal Density Perturbations in the Inflationary Universe," *Phys. Lett.* **B158** (1985) 375–380. 103

[302] J. Hamann, S. Hannestad, G. G. Raffelt, and Y. Y. Y. Wong, "Isocurvature forecast in the anthropic axion window," *JCAP* **0906** (2009) 022, `arXiv:0904.0647 [hep-ph]`. 103

[303] L. J. Rosenberg and K. A. van Bibber, "Searches for invisible axions," *Phys. Rept.* **325** (2000) 1–39. 105

[304] R. Bradley, J. Clarke, D. Kinion, L. J. Rosenberg, K. van Bibber, S. Matsuki, M. Muck, and P. Sikivie, "Microwave cavity searches for dark-matter axions," *Rev. Mod. Phys.* **75** (2003) 777–817.

[305] S. J. Asztalos, L. J. Rosenberg, K. van Bibber, P. Sikivie, and K. Zioutas, "Searches for astrophysical and cosmological axions," *Ann. Rev. Nucl. Part. Sci.* **56** (2006) 293–326.

[306] P. W. Graham, I. G. Irastorza, S. K. Lamoreaux, A. Lindner, and K. A. van Bibber, "Experimental Searches for the Axion and Axion-Like Particles," *Ann. Rev. Nucl. Part. Sci.* **65** (2015) 485–514, `arXiv:1602.00039 [hep-ex]`. 105

[307] P. Sikivie, "Experimental Tests of the Invisible Axion," *Phys. Rev. Lett.* **51** (1983) 1415–1417. [Erratum: Phys. Rev. Lett.52,695(1984)]. 105, 106

[308] H. Primakoff, "Photo-production of neutral mesons in nuclear electric fields and the mean life of the neutral meson," *Phys. Rev.* **81** no. 899, (Mar, 1951) 899–899. 105

[309] K. Zioutas *et al.*, "A Decommissioned LHC model magnet as an axion telescope," *Nucl. Instrum. Meth.* **A425** (1999) 480–489, `arXiv:astro-ph/9801176 [astro-ph]`. 105

[310] E. Armengaud *et al.*, "Conceptual Design of the International Axion Observatory (IAXO)," *JINST* **9** (2014) T05002, `arXiv:1401.3233 [physics.ins-det]`. 105, 109

[311] D. Budker, P. W. Graham, M. Ledbetter, S. Rajendran, and A. Sushkov, "Proposal for a Cosmic Axion Spin Precession Experiment (CASPEr)," *Phys. Rev.* **X4** no. 2, (2014) 021030, `arXiv:1306.6089 [hep-ph]`. 105, 107

[312] A. Arvanitaki and A. A. Geraci, "Resonantly Detecting Axion-Mediated Forces with Nuclear Magnetic Resonance," *Phys. Rev. Lett.* **113** no. 16, (2014) 161801, `arXiv:1403.1290 [hep-ph]`. 105, 108

[313] G. G. Raffelt, "Astrophysical axion bounds," *Lect. Notes Phys.* **741** (2008) 51–71, `arXiv:hep-ph/0611350 [hep-ph]`. [,51(2006)]. 105, 109

[314] R. Catena and P. Ullio, "A novel determination of the local dark matter density," *JCAP* **1008** (2010) 004, `arXiv:0907.0018 [astro-ph.CO]`. 106

[315] P. Salucci, F. Nesti, G. Gentile, and C. F. Martins, "The dark matter density at the Sun's location," *Astron. Astrophys.* **523** (2010) A83, `arXiv:1003.3101 [astro-ph.GA]`. 106

[316] S. De Panfilis, A. C. Melissinos, B. E. Moskowitz, J. T. Rogers, Y. K. Semertzidis, W. Wuensch, H. J. Halama, A. G. Prodell, W. B. Fowler, and F. A. Nezrick, "Limits on the Abundance and Coupling of Cosmic Axions at 4.5-Microev < m(a) < 5.0-Microev," *Phys. Rev. Lett.* **59** (1987) 839. 106

[317] W. Wuensch, S. De Panfilis-Wuensch, Y. K. Semertzidis, J. T. Rogers, A. C. Melissinos, H. J. Halama, B. E. Moskowitz, A. G. Prodell, W. B. Fowler, and F. A. Nezrick, "Results of a Laboratory Search for Cosmic Axions and Other Weakly Coupled Light Particles," *Phys. Rev.* **D40** (1989) 3153. 106

[318] C. Hagmann, P. Sikivie, N. S. Sullivan, and D. B. Tanner, "Results from a search for cosmic axions," *Phys. Rev.* **D42** (1990) 1297–1300. 106

[319] **ADMX** Collaboration, S. J. Asztalos *et al.*, "A SQUID-based microwave cavity search for dark-matter axions," *Phys. Rev. Lett.* **104** (2010) 041301, `arXiv:0910.5914 [astro-ph.CO]`. 106

[320] G. Rybka, A. Wagner, A. Brill, K. Ramos, R. Percival, and K. Patel, "Search for dark matter axions with the Orpheus experiment," *Phys. Rev.* **D91** no. 1, (2015) 011701, `arXiv:1403.3121 [physics.ins-det]`. 107

[321] D. Horns, J. Jaeckel, A. Lindner, A. Lobanov, J. Redondo, and A. Ringwald, "Searching for WISPy Cold Dark Matter with a Dish Antenna," *JCAP* **1304** (2013) 016, `arXiv:1212.2970 [hep-ph]`. 108

[322] D. A. Dicus, E. W. Kolb, V. L. Teplitz, and R. V. Wagoner, "Astrophysical Bounds on the Masses of Axions and Higgs Particles," *Phys. Rev.* **D18** (1978) 1829. 108

[323] H. Schlattl, A. Weiss, and G. Raffelt, "Helioseismological constraint on solar axion emission," *Astropart. Phys.* **10** (1999) 353–359, `arXiv:hep-ph/9807476 [hep-ph]`. 108

[324] **SNO** Collaboration, Q. R. Ahmad *et al.*, "Direct evidence for neutrino flavor transformation from neutral current interactions in the Sudbury Neutrino Observatory," *Phys. Rev. Lett.* **89** (2002) 011301, `arXiv:nucl-ex/0204008 [nucl-ex]`. 108

[325] J. N. Bahcall, A. M. Serenelli, and S. Basu, "New solar opacities, abundances, helioseismology, and neutrino fluxes," *Astrophys. J.* **621** (2005) L85–L88, `arXiv:astro-ph/0412440 [astro-ph]`.

[326] **SNO** Collaboration, B. Aharmim *et al.*, "Electron energy spectra, fluxes, and day-night asymmetries of B-8 solar neutrinos from measurements with NaCl dissolved in the heavy-water detector at the Sudbury Neutrino Observatory," *Phys. Rev.* **C72** (2005) 055502, `arXiv:nucl-ex/0502021 [nucl-ex]`. 108

[327] **CAST** Collaboration, M. Arik *et al.*, "New solar axion search using the CERN Axion Solar Telescope with ^{4}He filling," *Phys. Rev.* **D92** no. 2, (2015) 021101, `arXiv:1503.00610 [hep-ex]`. 109

[328] M. Koshiba, "Observational neutrino astrophysics," *Phys. Rept.* **220** (1992) 229–381. 109

[329] A. H. Corsico, O. G. Benvenuto, L. G. Althaus, J. Isern, and E. Garcia-Berro, "The Potential of the variable DA white dwarf G117 - B15A as a tool for fundamental physics," *New Astron.* **6** (2001) 197–213, `arXiv:astro-ph/0104103 [astro-ph]`. 110

[330] J. Isern and E. Garcia-Berro, "White dwarf stars as particle physics laboratories," *Nucl. Phys. Proc. Suppl.* **114** (2003) 107–110. [,107(2003)]. 110

[331] A. Ayala, I. Domínguez, M. Giannotti, A. Mirizzi, and O. Straniero, "Revisiting the bound on axion-photon coupling from Globular Clusters," *Phys. Rev. Lett.* **113** no. 19, (2014) 191302, `arXiv:1406.6053 [astro-ph.SR]`. 110

[332] A. Arvanitaki, S. Dimopoulos, S. Dubovsky, N. Kaloper, and J. March-Russell, "String Axiverse," *Phys. Rev.* **D81** (2010) 123530, `arXiv:0905.4720 [hep-th]`. 110

[333] A. Arvanitaki and S. Dubovsky, "Exploring the String Axiverse with Precision Black Hole Physics," *Phys. Rev.* **D83** (2011) 044026, `arXiv:1004.3558 [hep-th]`. 110

[334] M. Spalinski, "CHIRAL CORRECTIONS TO THE AXION MASS," *Z. Phys.* **C41** (1988) 87–90. 111, 112

[335] **TWQCD** Collaboration, Y.-Y. Mao and T.-W. Chiu, "Topological Susceptibility to the One-Loop Order in Chiral Perturbation Theory," *Phys. Rev.* **D80** (2009) 034502, `arXiv:0903.2146 [hep-lat]`. 111

[336] J. Gasser and H. Leutwyler, "Chiral Perturbation Theory to One Loop," *Annals Phys.* **158** (1984) 142. 112, 140

[337] J. Gasser and H. Leutwyler, "Chiral Perturbation Theory: Expansions in the Mass of the Strange Quark," *Nucl. Phys.* **B250** (1985) 465. 112, 117, 140, 141

[338] J. Bijnens and G. Ecker, "Mesonic low-energy constants," *Ann. Rev. Nucl. Part. Sci.* **64** (2014) 149–174, `arXiv:1405.6488 [hep-ph]`. 112, 140

[339] S. Aoki *et al.*, "Review of lattice results concerning low-energy particle physics," *Eur. Phys. J.* **C74** (2014) 2890, `arXiv:1310.8555 [hep-lat]`. 112, 140, 141

[340] D. B. Kaplan and A. V. Manohar, "Current Mass Ratios of the Light Quarks," *Phys. Rev. Lett.* **56** (1986) 2004. 113

[341] **Particle Data Group** Collaboration, K. A. Olive *et al.*, "Review of Particle Physics," *Chin. Phys.* **C38** (2014) 090001. 114, 122, 124, 140

[342] F.-K. Guo and U.-G. Meißner, "Cumulants of the QCD topological charge distribution," *Phys. Lett.* **B749** (2015) 278–282, `arXiv:1506.05487 [hep-ph]`. 114

[343] J. Bijnens, L. Girlanda, and P. Talavera, "The Anomalous chiral Lagrangian of order p**6," *Eur. Phys. J.* **C23** (2002) 539–544, `arXiv:hep-ph/0110400 [hep-ph]`. 116, 117

[344] J. F. Donoghue, B. R. Holstein, and Y. C. R. Lin, "Chiral Loops in pi0, eta0 —> gamma gamma and eta eta-prime Mixing," *Phys. Rev. Lett.* **55** (1985) 2766–2769. [Erratum: Phys. Rev. Lett.61,1527(1988)]. 116

[345] B. Ananthanarayan and B. Moussallam, "Electromagnetic corrections in the anomaly sector," *JHEP* **05** (2002) 052, `arXiv:hep-ph/0205232 [hep-ph]`. 117

[346] G. F. Giudice, R. Rattazzi, and A. Strumia, "Unificaxion," *Phys. Lett.* **B715** (2012) 142–148, `arXiv:1204.5465 [hep-ph]`. 120

[347] J. Kodaira, "QCD Higher Order Effects in Polarized Electroproduction: Flavor Singlet Coefficient Functions," *Nucl. Phys.* **B165** (1980) 129. 121, 143

[348] E. E. Jenkins and A. V. Manohar, "Baryon chiral perturbation theory using a heavy fermion Lagrangian," *Phys. Lett.* **B255** (1991) 558–562. 121

[349] **QCDSF** Collaboration, G. S. Bali *et al.*, "Strangeness Contribution to the Proton Spin from Lattice QCD," *Phys. Rev. Lett.* **108** (2012) 222001, `arXiv:1112.3354 [hep-lat]`. 123, 141

[350] M. Engelhardt, "Strange quark contributions to nucleon mass and spin from lattice QCD," *Phys. Rev.* **D86** (2012) 114510, `arXiv:1210.0025 [hep-lat]`.

[351] A. Abdel-Rehim, C. Alexandrou, M. Constantinou, V. Drach, K. Hadjiyiannakou, K. Jansen, G. Koutsou, and A. Vaquero, "Disconnected quark loop contributions to nucleon observables in lattice QCD," *Phys. Rev.* **D89** no. 3, (2014) 034501, `arXiv:1310.6339 [hep-lat]`. 141

[352] T. Bhattacharya, R. Gupta, and B. Yoon, "Disconnected Quark Loop Contributions to Nucleon Structure," *PoS* **LATTICE2014** (2014) 141, `arXiv:1503.05975 [hep-lat]`. 141

[353] A. Abdel-Rehim *et al.*, "Nucleon and pion structure with lattice QCD simulations at physical value of the pion mass," *Phys. Rev.* **D92** no. 11, (2015) 114513, `arXiv:1507.04936 [hep-lat]`. [Erratum: Phys. Rev.D93,no.3,039904(2016)]. 141

[354] A. Abdel-Rehim, C. Alexandrou, M. Constantinou, K. Hadjiyiannakou, K. Jansen, C. Kallidonis, G. Koutsou, and A. V. Avilés-Casco, "Disconnected quark loop contributions to nucleon observables using $N_f = 2$ twisted clover fermions at the physical value of the light quark mass," in *Proceedings, 33rd International Symposium on Lattice Field Theory (Lattice 2015)*. 2015. `arXiv:1511.00433 [hep-lat]`. 123, 141

[355] T. Bhattacharya, S. D. Cohen, R. Gupta, A. Joseph, H.-W. Lin, and B. Yoon, "Nucleon Charges and Electromagnetic Form Factors from 2+1+1-Flavor Lattice QCD," *Phys. Rev.* **D89** no. 9, (2014) 094502, `arXiv:1306.5435 [hep-lat]`. 123

[356] N. Yamanaka, H. Ohki, S. Hashimoto, T. Kaneko (JLQCD Collab.), "Nucleon axial and tensor charges with the overlap fermions," in *talk presented at Lattice 2015 on 15-07-2015*. 123

[357] S. Choi, D. Choudhury, A. Freitas, J. Kalinowski, J. Kim, *et al.*, "Dirac Neutralinos and Electroweak Scalar Bosons of N=1/N=2 Hybrid Supersymmetry at Colliders," *JHEP* **1008** (2010) 025, `arXiv:1005.0818 [hep-ph]`. 130

[358] G. V. Dunne, J. Hur, C. Lee, and H. Min, "Calculation of QCD instanton determinant with arbitrary mass," *Phys. Rev.* **D71** (2005) 085019, `arXiv:hep-th/0502087 [hep-th]`. 138

[359] F. Sanfilippo, "Quark Masses from Lattice QCD," *PoS* **LATTICE2014** (2015) 014, `arXiv:1505.02794 [hep-lat]`. 139

[360] R. Mawhinney [RBC and UKQCD Collaborations], "NLO and NNLO low energy constants for SU(3) chiral perturbation theory," in *talk given at Lattice 2015, Japan, July 2015.* 141

[361] P. A. Boyle *et al.*, "Low energy constants of SU(2) partially quenched chiral perturbation theory from N_f=2+1 domain wall QCD," *Phys. Rev.* **D93** no. 5, (2016) 054502, `arXiv:1511.01950 [hep-lat]`. 141

[362] G. Altarelli and G. G. Ross, "The Anomalous Gluon Contribution to Polarized Leptoproduction," *Phys. Lett.* **B212** (1988) 391. 143

[363] S. A. Larin, "The Renormalization of the axial anomaly in dimensional regularization," *Phys. Lett.* **B303** (1993) 113–118, `arXiv:hep-ph/9302240 [hep-ph]`. 143